VNiVERSiDAD D SALAMANCA
CAMPUS DE EXCELENCIA INTERNACIONAL

**PhD Thesis**

**2021**

# A study of the Water-Energy Nexus in power plants

Department of Chemical Engineering

Lidia Sánchez Guerras

VNiVERSiDAD D SALAMANCA

CAMPUS DE EXCELENCIA INTERNACIONAL

# A STUDY OF THE WATER–ENERGY NEXUS IN POWER PLANTS

Doctoral thesis dissertation for the degree of Doctor by the University of Salamanca by

LIDIA SÁNCHEZ GUERRAS

Salamanca 2021

VNiVERSiDAD D SALAMANCA
CAMPUS DE EXCELENCIA INTERNACIONAL

Dr. D. **Mariano Martín Martín**, Profesor titular de Ingeniería Química de la Universidad de Salamanca

Informa:

Que la memoria titulada "A study of the wáter-energy nexus in power plants" que para optar al Grado de Doctor en Ingeniería Química, Programa de Doctorado de "Ciencia y Tecnología Químicas" presenta Dª Lidia Sánchez Guerras, ha sido realizada bajo mi dirección en el Departamento de Ingeniería Química y Textil de la Universidad de Salamanca.

Considerando que constituye trabajo de tesis, se autoriza su presentación ante la Escuela de Doctorado de la Universidad de Salamanca.

Y para que así conste se firma el presente informe,

en Salamanca a 20 de mayo de 2021

**D. Mariano Martín Martín**

# *Agradecimientos*

En primer lugar, deseo expresar mi agradecimiento al director de mi tesis doctoral, el Doctor Mariano Martín Martín, por convencerme para adentrarme en esta aventura, así como por haberme dedicado su tiempo y brindado su apoyo cuando más lo necesitaba. Asimismo, agradezco sus reuniones semanales, donde discutíamos diversos temas y siempre me ha mostrado un gran respeto acerca de mis ideas aunque no estuviera totalmente de acuerdo con ellas. Gracias por potenciar mis habilidades y reforzar mis debilidades, gracias a ello he crecido a nivel profesional y a nivel personal.

También me gustaría darle las gracias al Departamento de Ingeniería Química de la Universidad de Salamanca, por cedernos otros espacios y darnos todas las facilidades a su disposición para que pudiéramos trabajar en un lugar seguro a lo largo de esta pandemia que nos está asolando. También me gustaría agradecer a los miembros del laboratorio de ingeniería química todos los buenos momentos que hemos vivido a lo largo de este periodo y todo el cariño y apoyo que he recibido de su parte.

Also, I would like to thank Doctor Mahmoud El-Halwagi and Prof. Debalina Sengupta from the University of Texas A&M for their valuable guidance throughout my internship. It has been a pleasure and a privilege to work with you and I would like to thank you for all. This opportunity allowed me to meet amazing people from all over the world as well as forge great friendships. The exchange allowed me to grow both professionally and personally, and I will never forget it.

Respecto a mis compañeros del grupo de investigación (Borja, Antonio, Edgar, Luceño, Manuel, Guillermo…) así como los estudiantes de intercambio (Cesar, Salvador, Gabriel, Javier…) y estudiantes de grado y máster daros las gracias a todos vosotros por ser como sois, por las charlas, por los consejos, por las discusiones, y por permitirme aprender de vosotros y ayudarme cuando lo he necesitado. Me gustaría hacer una mención especial a Salvador por todo el apoyo y facilidades que me brindó durante mi estancia en Estados Unidos, así como sus consejos.

I would like to special mention to Maryam Mohammadi for your advice, for helping me to practice English, and for that unforgettable week that we began our friendship.

También me gustaría dar las gracias a dos grandes amistades Ángela y Marisa, que se han preocupado por mi, que me han apoyado y me han hecho reír y olvidarme del mundo con un café.

Estas últimas líneas se las dedico a mi familia, a mi tía Chiqui y a mi tío Javi por su amparo cada vez que he tenido que ir a Madrid, así como su apoyo y su sinceridad. A mi tía Ana, así como a mi primo Miguel, por preocuparse cada vez que iba a La Robla y mostrarme su apoyo a lo largo de ese proyecto. A todos mis sobrinos (Marcos, Daniela, Hugo, Carmen, Laia y Luca), que con un abrazo los problemas son menos importantes y por esos momentos que vivimos juntos haciendo experimentos y lograba desconectarme del mundo. También me gustaría darles las gracias de corazón a dos de los pilares fundamentales de mi vida a mi abuela y a mi madre, por ayudarme a lo largo de toda mi vida y guiarme para convertirme en la persona que soy hoy en día. Asimismo, me gustaría darles las gracias por todo el apoyo, ayuda que he recibido en los últimos meses, que han sido tan duros para mí. Por último, y no por ello menos importante me gustaría darle las gracias a la parte de la familia que se elige y que se ha convertido en otro pilar muy importante de mi vida, a mi pareja Pedro que me ha ayudado a creer en mi misma y ha creído en mí cuando yo no lo he hecho. Gracias por tus interrupciones (a pesar de que me enfadara) para hacerme que descansara, comiera o simplemente para que me riese un rato, por esos paseos con los perros que me permitían desconectar para volver con más fuerzas y por todos los amaneceres. Gracias a todos por vuestro apoyo incondicional y creer en mí.

# TABLE OF CONTENT

## *Summary in Spanish.*



## *Chapter 1: Introduction*



## *Chapter 2: Objectives.*

## *Chapter 3: Optimal gas treatment and coal blending for reduced emissions in power plants: A case study in Northwest Spain.*



## *Chapter 4: Optimal Flue Gas Treatment for Oxy-Combustion-Based Pulverized Coal Power Plants.*

## *Chapter 5: On the water footprint in power production: Sustainable design of wet cooling towers.*

## *Supplementary material: On the water footprint in power production: Sustainable design of wet cooling towers.*



## *Chapter 6: Multi-layer approach for product portfolio optimization: Waste to added value products.*

## *Chapter 7: Conclusions*



## *Chapter 8: Other works.*

# *Resumen de los artículos*

En este epígrafe se muestra un breve resumen de los artículos publicados que conforman está tesis, como indica la normativa de la Universidad de Salamanca "*Procedimiento para la presentación de la Tesis Doctoral en la Universidad de Salamanca en el Formato de Compendio de Artículos / Publicaciones (Comisión de Doctorado y Posgrado, 15 de febrero de 2013)*".

## Artículo 1

*Título:* Optimal gas treatment and coal blending for reduced emissions in power plants: A case study in Northwest Spain.

*Autores*: Lidia S Guerras y Mariano Martín.

*Revista*: Energy

*DOI*: 10.1016/j.energy.2018.12.089

*Resumen:* En este trabajo se ha desarrollado un marco de toma de decisiones para el diseño de la sección de tratamiento de gases de combustión de una central eléctrica, que incluye operaciones de remoción de partículas, NOx y $SO_2$. Se ha aplicado a una central térmica de carbón en España para seleccionar las tecnologías óptimas y su secuencia. Se han desarrollado modelos sustitutos para los tratamientos. El problema corresponde a una programación no lineal entera mixta que incluye la eliminación de NOx catalítica y no catalítica, lo que permite varias asignaciones para la tecnología catalítica, precipitación electrostática y eliminación de $SO_2$ húmedo o seco. Se reformula como un problema no lineal para evaluar las oportunidades de bypass. La optimización sugiere el uso de precipitación electrostática, seguida de la eliminación catalítica de NOx y la eliminación de $SO_2$ seco. A continuación, también se ha resuelto un problema de mezcla de carbón para dos funciones objetivo. Cuando solo se consideran los costos de tratamiento, se recomienda el uso de carbón importado, pero un aumento del 4% en su precio puede cambiar la decisión por el uso de carbón nacional. Si la energía del carbón se agrega a la función objetivo, el carbón de alquitrán crudo se incluye en la mezcla y el carbón importado se usa para mantener las emisiones dentro de los límites. La oxidación forzada de piedra caliza es la tecnología seleccionada.

## Artículo 2

*Título:* Optimal Flue Gas Treatment for Oxy-Combustion-Based Pulverized Coal Power Plants

*Autores*: Lidia S Guerras y Mariano Martín.

*Revista*: Industrial & Engineering Chemistry Research

*DOI*: 10.1021/acs.iecr.9b04453

*Resumen:* La oxicombustión es reconocida como la tecnología más limpia que utiliza carbón como fuente de energía. La limpieza de los gases de combustión es esencial para un funcionamiento sostenible. En este trabajo se determina la selección óptima de las tecnologías de tratamiento de gases de combustión en centrales de oxicombustión. Se utiliza un procedimiento de dos etapas que combina heurística y programación matemática para evaluar las tecnologías involucradas, incluida la caldera, la desnitrificación, la precipitación electrostática, la eliminación de dióxido de azufre y la captura de carbono. Para el funcionamiento de la planta, se debe seleccionar la alimentación de carbón. Se resuelve un problema de mezcla extendido para evaluar el tipo de carbón que se comprará en función de su costo y composición. El procesamiento óptimo de los gases de combustión consiste en la precipitación electrostática, seguida de la eliminación de $SO_2$ seco y la purificación de $CO_2$ con zeolitas. No se requiere ningún método de desnitrificación específico debido a los bajos niveles de concentración de NOx generados en la oxicombustión. Esta hoja de flujo se utiliza para seleccionar uno entre una mezcla de tres tipos diferentes de carbón: alquitrán de hulla nacional, importado y crudo. Sin embargo, no se recomienda ninguna mezcla ya que se seleccionó alquitrán de hulla crudo. Aunque los costos de procesamiento son más altos, se ve compensado por el menor coste de la materia prima.

## Artículo 3

*Título:* On the water footprint in power production: Sustainable design of wet cooling towers*Autores*: Lidia S Guerras y Mariano Martín.

*Revista*: Applied Energy

*DOI*: 10.1016/j.apenergy.2020.114620

*Resumen:* Las plantas de energía renovable deben instalarse donde esté disponible el recurso principal. El clima afecta el diseño y la huella hídrica de estas plantas. Se estudian dos tipos de ciclos de potencia, un ciclo Rankine regenerativo, representativo de biomasa y plantas termosolares, y el ciclo combinado, correspondiente a procesos basados en biogás o gasificación. Las instalaciones se modelan en detalle unidad por unidad para calcular el rendimiento del ciclo, el trabajo del condensador, el consumo de agua y la geometría de la torre de enfriamiento húmedo de tiro natural para su diseño sostenible. Las regiones cálidas, apropiadas para instalaciones solares, y las regiones húmedas requieren torres más grandes y caras. Las áreas con alta disponibilidad solar también muestran un mayor consumo de agua, lo que representa un intercambio para un futuro sistema de energía basado en energías renovables. Además, también se han desarrollado pautas de diseño y modelos sustitutos para estimar el consumo de agua, el tamaño de la torre de enfriamiento y su costo en función del clima. Los sustitutos son útiles para el análisis de la huella hídrica de un sistema de energía de base renovable que sustituye al de base fósil.

## Artículo 4

*Título:* Multilayer Approach for Product Portfolio Optimization: Waste to Added-Value Products

*Autores*: Lidia S. Guerras, Debalina Sengupta, Mariano Martín, and Mahmoud M. El-Halwagi

*Revista*: ACS Sustainable Chemistry & Engineering.

*DOI*: 10.1021/acssuschemeng.1c01284

*Resumen:* Se ha desarrollado un procedimiento sistemático multicapa de varias etapas para la selección de la cartera de productos óptima a partir de biomasa residual como materia prima para sistemas que implican el nexo “wáter-energy-food”. Consiste en una metodología híbrida heurística, basada en métricas y optimización que evalúa el desempeño económico y ambiental de productos de valor agregado a partir de una materia prima en particular. La primera etapa preselecciona los productos prometedores. A continuación, se formula un problema de optimización de la superestructura para valorizar o transformar los residuos en el conjunto óptimo de productos. La metodología se ha aplicado dentro de la iniciativa “Waste to Power and Chemicals” para evaluar el mejor uso de los residuos de biomasa de la industria del aceite de oliva en alimentos, productos químicos y energía. La etapa heurística se basa en la revisión de la literatura para analizar los productos y técnicas factibles. A continuación, se han desarrollado y utilizado

métricas simples para preseleccionar productos que son prometedores. Finalmente, se utiliza un enfoque de optimización de la superestructura para diseñar la instalación que procesa hojas, astillas de madera y aceitunas en productos finales. La mejor técnica para recuperar fenoles del “alperujo”, un residuo sólido húmedo/subproducto del proceso, consiste en el uso de membranas, mientras que la técnica de adsorción se utiliza para la recuperación de fenoles de hojas y ramas de olivo. La inversión necesaria para procesar los residuos asciende a 110,2 millones de euros por 100 kt/año para la instalación de producción de aceitunas, mientras que el beneficio depende del nivel de integración. Si la instalación está adscrita a la producción de aceite de oliva, el beneficio generado oscila entre los 14,5 MM €/año (cuando los residuos se compran a precios de 249 € por tonelada de alperujo y 6 € por tonelada de hojas y ramas de olivo) y 34,3 MM €/año cuando el material de desecho se obtiene de forma gratuita.

# *Chapter 1.*

# *Introduction*

## 1. Motivation

The use of coal dates back to 5000 BC by the Chinese, but it was not until the industrial revolution that a huge demand of coal is created. During the industrial revolution, coal became the main energy source. One of the most important facts was the use of coal to feed the steam engine as well as the progress generated in the steel-making process. After the second world war, petroleum gained importance, becoming the main energy source. The energy consumption has been raising, due to the increase of population, the technological advancements that need more electrical energy, as well as the wider access to electricity in all countries. Fossil fuels as coal and oil are the major source of greenhouse gases in the production of energy. Figure 1.1 shows the percentage of energy consumption as a function of source.

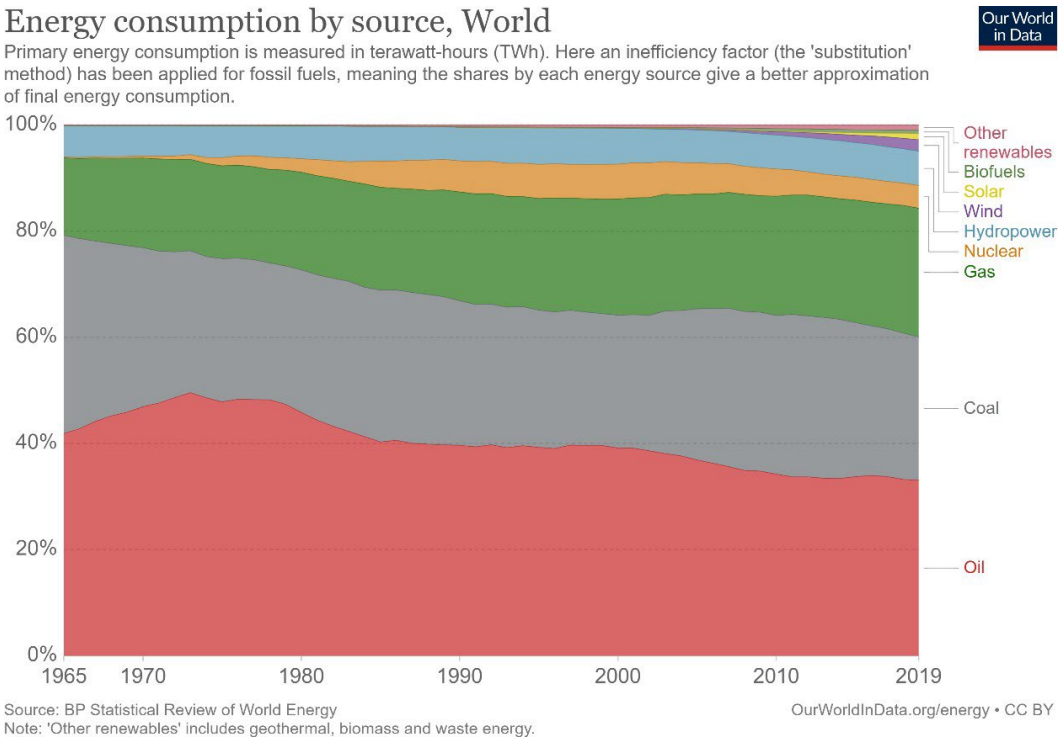


***Figure 1.*** Energy consumption by source, in the World (Our World in Data, 2021)

The generation of more energy produces more pollutants and as a result, more greenhouse gases are emitted which increase global warming. Carbon dioxide, methane, nitrous oxide, or fluorinated gases are the main greenhouse gases. These gases are not only produced in the generation of energy, but also, they are emitted during the production and transportation of coal, natural gas and oil, agricultural and industrial activities, combustion of fossil fuel, and solid waste.

In 1896, Svante Arrhenius was the first to study the relationship between global warming and fossil fuel combustion, but it was not until 1997 when the Kyoto Protocol is approved that society becomes aware of the actual issues. This protocol is an international treaty whereby members are committed to reducing greenhouse gas (GHGs) emissions. The global average temperature has increased by 1.2ºC since the late 19th century (NASA, 2021). Some of the consequences of global warming are the increase of the desert areas, the melting of the polar ice caps, the rising sea, the drying of surface water bodies, that may cause the extinction of more than one million species of animals and plants (Goel and Bhatt, 2012).

Despite coal is one of larger pollutant generators, currently, it is still one of the top primary energy sources in this world, being responsible for around 37% of the global electricity generated (Coal & Electricity, 2021). In the case of coal power plants, the main pollutants carbon dioxide, sulfur dioxide, nitrogen oxides, mercury, and ash are yielded. Over the last years, emissions of sulfur dioxide, nitrogen oxides, and ash have been reduced, due to the legislation applied.

The need for controlling the emissions at "La Robla" power plant, property of Naturgy, was the starting point of this thesis project as a way to help them address the issues and select the technologies from a systematic way. From that point, the beginning of this thesis emerged, corresponding to the first work, shown here as Chapter 3.

### *1.1. Environmental and human health effects of pollutants generated from coal power plants.*

**Sulfur dioxide** is a nonflammable, nonexplosive, and colorless gas. At a concentration larger than 3.0 ppm, the sulfur dioxide gas has a pungent, irritating odor (Miller, 2011). The environmental effects of sulfur dioxide, generated by coal combustion in power plants, can be impaired visibility, damage to materials, damage to vegetation, and deposition as acid rain.

Impaired visibility occurs when fine particles of sulfur dioxide in the atmosphere decrease the visual range by dispersion and absorption of light. In urban air, 5 to 20 percent of all suspended particulate matter can be sulfuric acid and other sulfates, so this fact generates a decrease in visibility (Miller, 2011). Sulfur compounds are responsible for major damage to materials. Sulfur dioxide is one of the most damaging. When the sulfur dioxide enters in contact with water and oxygen from the atmosphere, sulfuric acid is formed. This compound accelerates metal corrosion. It should be noted that temperature and relative

humidity has also an important influence on the rate of metal corrosion. It also damage plants. Usually sulfur dioxide enters leaves and the cells of the plants transforming from sulfite into sulfate. This generates the disruption of the cell structure and the death of the plants. Sulfur dioxide together with nitrogen oxides emissions are responsible for acid rain when they react with water and oxygen in the atmosphere,. Consequences of acid rain are acidification of the environment, destroying aqueous habitats, and damaging tree foliage and crops.

Talking about health effects, sulfur dioxide has an important role in the formation of small acidic particulates that can penetrate in human and animal lungs and be absorbed by the bloodstream (El Safty and Siha, 2013). It should be noted that there are not a lot of studies about the effects of individual pollutants given that sulfur oxides tend to happen in the same kinds of atmospheres as particulate matter and high humidity (Miller, 2011). Normally, it is difficult to define the specific cause, since maybe it can be one part of the pollutants in the atmosphere.

The term **nitrogen oxides** concerns nitric oxide (NO), and nitrogen dioxide ($NO_2$), being nitrogen dioxide the main compound in the group. Nitric oxide is a colorless gas, noncombustible, very toxic by inhalation and skin absorption, and has a slight odor (Nitric oxide, 2021). Nitric dioxide is a deep red-orange gas, not flammable, toxic by inhalation, and skin absorption (Nitrogen dioxide, 2021). In the event the nitrogen oxides are not removed after combustion, they are released and accumulate in the atmosphere, and damage the environment and human and animal health (Munawer, 2018). Regarding the effects on the environment, they include photochemical smog and visibility impairment, ground-level ozone, acid rain or acid depositions, acidification, and eutrophication of water and soils, damage to natural ecosystems, cultural heritage and crops, and damage to materials.

Photochemical smog is a brownish-yellow haze over urban areas, resulting from the combination of nitrogen oxides with other pollutants in the atmosphere as unburned hydrocarbons that react in the presence of sunlight (Cholakov, 2009). Besides nitrogen dioxide absorbs visible light at a concentration of 0.25ppmv which creates a reduction in visibility (Miller, 2011). Nitrogen oxides contribute 25 to 30% to acid rain (Cholakov, 2009), since they react with atmospheric moisture to form $NO_3^-$ and $H^+$

(i.e. nitric acid ($HNO_3$)). Nitric acid produces considerable corrosion of metal surfaces, damage to terrestrial systems, acidification of freshwater bodies, eutrophication, among others. The growth of the ozone level is due to the reaction between nitrogen oxides and volatile organic compounds ($VOC_s$)in presence of heat and sunlight.

Regarding health effects, nitrogen oxides can cause chronic obstructive pulmonary diseases, respiratory infections, and alterations in the lungs, if the exposition is long- therm.

**Particulate matter** consists of coal fly ash and coal dust (Munawer, 2018). The environmental problems are depositions, dumping site, and reduction of visibility.

The particulate matter is transferred through the atmosphere to form depositions and dumping sites causing serious problems to terrestrial and water ecosystems. They can be generated by the decrease the pH level of soil, and reduce the crops. Besides during the transportation of the particulate matter, since they are solid particles the visibility in the atmosphere is reduced.

Concerning health effects, there are a lot of consequences since the particulate matter can be made up of a large number of compounds responsible for different cancers, cardiovascular diseases, and reproductive disorders.

**Carbon dioxide** is colorless, odorless, nontoxic, and noncombustible (Carbon dioxide, 2021). Carbon dioxide generates harmful impacts on the environment in the form of global warming and greenhouse gases.

The effects of global warming concern people, animals, and the habitat resulting in phenomena such as the rising of sea level in some places, the increasing of desert areas in others or the drying of surface water bodies. These effects can cause the extinction of a lot of species of animals and plants (Goel and Bhatt, 2012). For that reason, in some parts of the world freshwater scarcity is becoming an important issue so it is very important to minimize pollutants emissions, to limit or even avoid global warming and therefore its consequences.

This fact, in the case of the production of electricity, is very significant since to produce energy water is required to cool. River water is employed usually, and some places nowadays do not have enough

water to produce the electricity demanded. This problem is not only for coal power plants, despite the low carbon technologies to produce electricity generate lower pollutants since these facilities still have a demand for water (IEA, 2020).

As a result of the decision from the European Commission to shut-down coal power plants, one of the affected was "La Robla" power plant, generating a slight change in the direction of the thesis. From this moment on, we started to analyze other problems from power plants, for try to minimize the pollutants emissions. In this point, the second work was developed analyzing on oxy-combustion power plants, corresponding to Chapter 4.

### *1.2. Water-Food-Energy nexus and circular economy.*

In 2008, the concept of water-energy-food nexus began to gain popularity, and along the time their own concept has been changing. Nowadays, there are two categories of definitions for this nexus. In the first category, this concept is known as the interlink between water, energy, and food; and not only the interactions among different sectors within the nexus system. While in the second category, this nexus is considered as an analysis approach to quantify the link between the nexus nodes (Zhang et al., 2018). This nexus allows a cross-sector coordination and promotes the sustainable development of each sector in the same work. The interlink between the different sectors is explained below, and a summary is shown in Figure 1.2.

*Water to food:* Water is essential for agriculture since a large number of crops need irrigation to grow up. Furthermore, the increase of population and a new healthy lifestyle results in a significant rise of demand for healthy food. It should be noted that to satisfy this growing demand, an increment of quantity of water is needed (Brears, 2015). Also, in the processing and preparation of food it is necessary the use of water such as to clean the crops, to boil the crops, and so on.

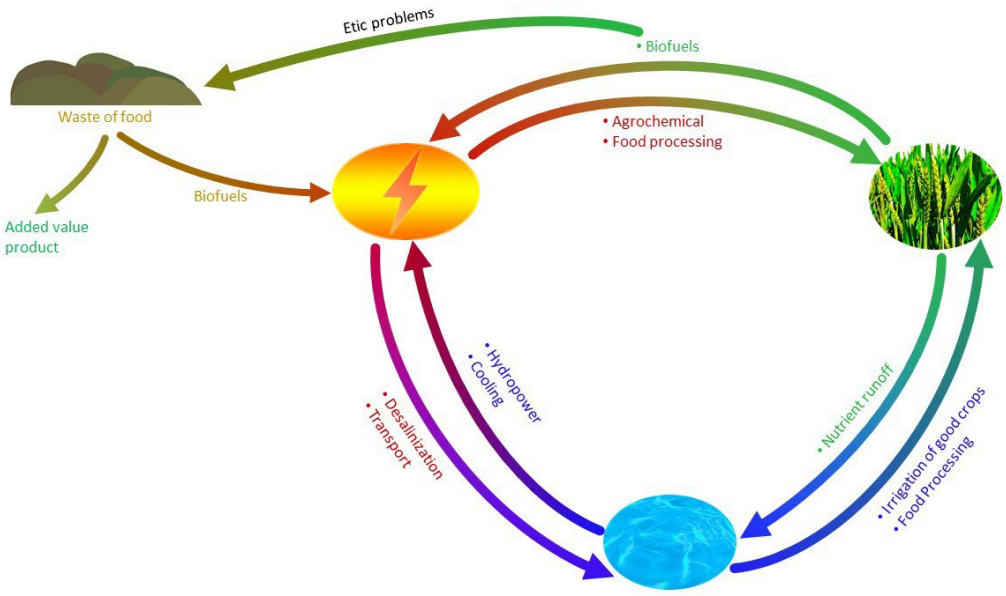


***Figure 1.2***. Water-Food-Energy nexus

*Food to water:* Agriculture production utilizes fertilizer and pesticides, creating major environmental changes as the pollution of water sources (Cai et al., 2018) or nutrient loading in waterways (Woo and Kumar, 2016).

*Water to energy*: Energy production and supply is highly dependent on water supplies. The energy production from traditional and emerging energy sources requires significant amount of water for both cooling systems and turbines systems (heating) (Cai et al., 2018).

*Energy to water:* Energy is required for water abstraction, distribution, and treatment (Zhang et al., 2018). The process of water abstraction consists of taking water from any sources for irrigation, industry, recreation, flood control, or treatment to produce drinking water. The distribution process involves the transport of water from one location to another such as pumping irrigation water, while the water treatment can be heating, desalinization, purification, and so on.

*Energy to food:* Energy is required for fertilizer production, agricultural machinery, food preservation, food processing, food transport, cooking, and pumping irrigation water (Sadeghi et al., 2020).

*Food to energy:* In this case, there is only one link between these sectors and consists of the use of some kinds of food such as cereals and grain, known as first generation biofuels, to the production of energy (Zhang et al., 2018).

The food to energy link has some ethical issues due to use of food for energy production when certain parts of the world do not have enough to feed their population. Another problem that this link generates is that certain cereals can be employed as raw materials for biofuels and which increases the market price and by this, a rise of the cost of some products in supermarkets. The solution to this ethical problem is provided by the circular economy, using the waste from the food to produce energy instead of the food itself. For maximizing the concept of circular economy, the added value products from the waste should be recovered.

As mentioned previously, both traditional power plants and non-traditional power plant has a high demand of water. In this regard, an analysis of water consumption in all kinds of power plants across to Spain is developed, corresponding to Chapter 5.

To complete the thesis, and contribute to the food - energy link an analysis of the circular economy in multi product power plants was elaborated based on the waste from olive oil production. In this study, added valued product are recovered and the remaining of the solid waste are burning to product energy. This study is explained in Chapter 6.

## 2. Background

Over the years, a large number of researches concerning flue gas from coal power plants have been developed. Pre-combustion, post-combustion, and during combustion studies are carried out to reduce the production of pollutants and eject them into the atmosphere. Usually, studies are based on different processes for the removal or reduction of one or two pollutants.

### *2.1. Gas treatment*

#### *2.1. Sulfur dioxide removal*

One of the most studied pollutants is the sulfur dioxide, and therefore there are a lot of types of investigations and technologies to remove it. The main advantage of sulfur dioxide is that a large number of sorbents can be employed as lime, limestone, ammonia, sodium carbonate, potassium carbonate, sodium hydroxide, potassium hydroxide, ammonium, amine, active carbon, and so one. This fact allows the development of a number of technologies to remove sulfur dioxide (Kohl and Nielsen, 1997).

The pre-combustion process to reduce the sulfur from the coal, consists of removing pyritic sulfur that contains the coal. Physical coal cleaning is not effective for remove all sulfur content. However, chemical coal cleaning processes can be used, although it is not used on a commercial scale. The advantage of the use of this technique is the elimination of traces of elements as antimony, arsenic, cobalt, and so on. The disadvantages of this technique are the increasing of the price coal, the decrease in the heating value due to the increasing of moisture content, and the low-sulfur content coal is recommended (Miller, 2015).

Post-combustion (PC) processes and during-combustion (DC) processes can be classified in two major groups: wet flue gas desulfurization (FGD) systems and dry and/ or semi-dry FGD systems. Figure 1.3 shows some of the most significant wet and dry FGD systems. Regarding the wet FGD systems are carried out post-combustion process while in the case of the dry and/ or semi-dry FGD systems some processes are developed post-combustion and other during the combustion, corresponding in Figure 1.3 as PC and DC.

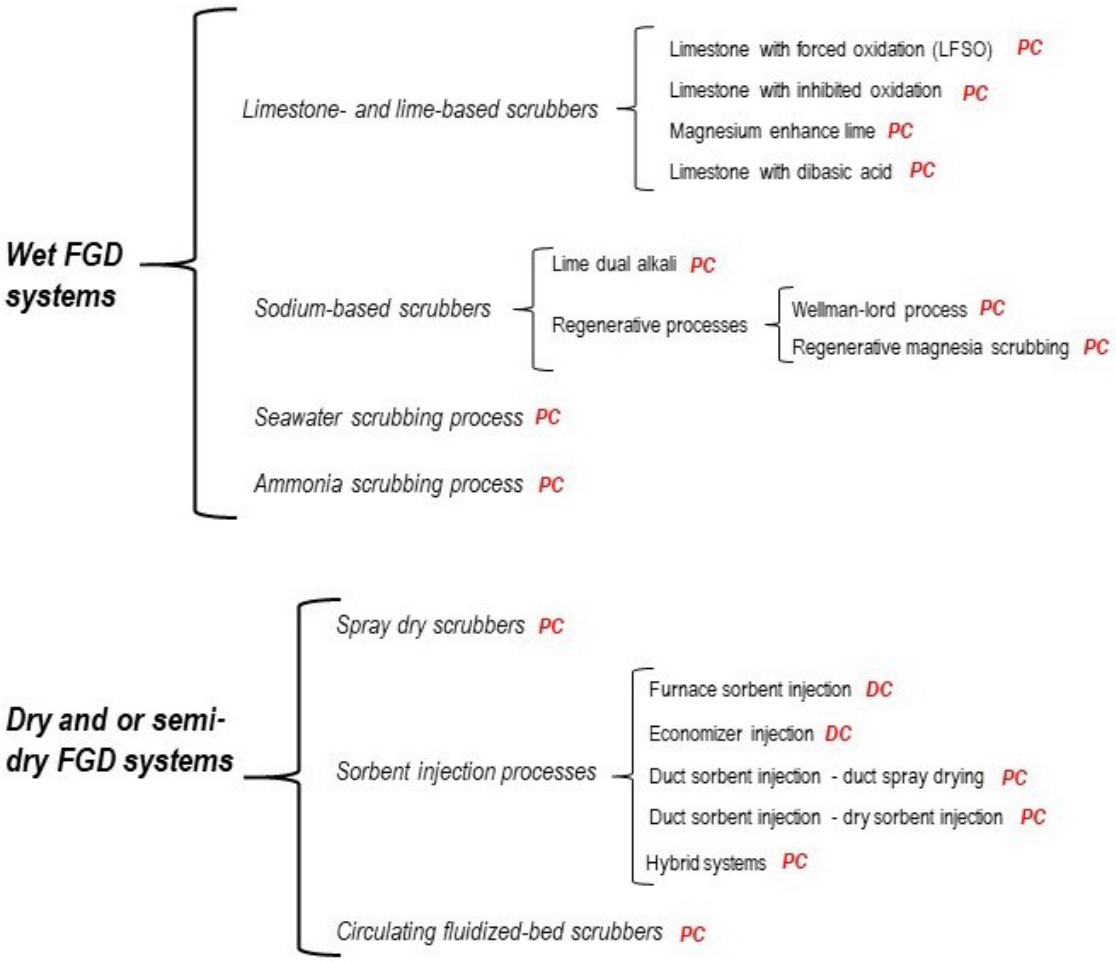


***Figure 1.3.*** Classification of some flue gas desulfurization technologies.

### *2.2. Nitrogen oxides removal*

NOx abatement and control technologies are a relatively complex issue. NOx cannot be easily removed or reduced, and there are not many alternatives as in the case of sulfur dioxide removal. The NOx removal technologies are implemented during the combustion and process post-combustion. Technologies of elimination of nitrogen before combustion (pre-combustion) are not considered because there are other sources of nitrogen that be able to react to form NOx, as will be explained in Chapter 3.

The principles or methods employed for NOx abatement are reducing peak temperature, drop-in residence time at peak temperature, chemical reduction of NOx, oxidation of NOx with subsequent absorption, removal of nitrogen, or using a sorbent (Clean Air Technology Center, 1999). They can be developed as modifications in the combustion process or applied in the post-combustion. Reducing peak temperature can be accomplished through different ways, as recirculation of flue gas reburning of natural gas, using low NOx burners, rendering out of service of some burners, and so on. The drop-in resistance time at the peak is achieved through injecting air, fuel, or steam into the boiler. The chemical reduction consists of adding a chemical to react with the NOx, for instance, the selective catalytic reduction to selective non-catalytic reduction. The oxidation of NOx technique raises the valence of the nitrogen ion to allow water to absorb it, generating $N_2O_5$, finally, a scrubber must be used to remove it. The use of sorbents for removed NOx can be applied in combustion chambers or ducts. The sorbent can generate adsorption or adsorption processes. Sorbents employed can be ammonia, powdered limestone, aluminum oxide, or carbon and some of them can remove other pollutants, like sulfur dioxide.

Two categories can be considered for NOx control technologies: primary control technologies and second control technologies. Primary control technologies reduce the production of NOx in the primary combustion zone, and they get through different modifications in the boiler. On the contrary, second control techniques reduce the NOx produced in the flue gas away from the primary combustion zone (Srivastava et al., 2005).

Primary control technologies consist of the use of low-NOx burners, carried out furnace air staging, attain a flue gas recirculation, fuel staging, and made a process optimization (Miller, 2015; Reddy, 2014). These technologies are easier to apply in the case of new boilers since they are adapted throughout of building of the boiler. In old boilers, techniques such as furnace air staging, fuel staging can be adapted or

in some cases change of low-NOx burners. The application of these techniques may cause some problems such as the rise of the amount of unburnt carbon, the generation of more quantity of CO, or the abatement of boiler efficiency. As a consequence, the implementation of these primary techniques needs to be accompanied by control systems into the boiler since these parameters (NOx, $O_2$, CO, unburnt carbon, and boiler efficiency) should be controlled (Power Line, 2020).

Two strategies have been developed for post-combustion control and are commercially available, the selective catalytic reduction (SCR) and selective non-catalytic reduction (SNCR). These techniques are explained in detail in Chapters 2 and 3. SCR technology was patented in the United States by Englehard Corporation in 1957 (Sorrels et al., 2019). This technology can achieve NOx reductions above 90% and has been widely used for over 30 years in commercial applications in western Europe especially Germany, Japan, the USA, and China (Reddy, 2014). SNCR technology was originally developed for oil and gas units in the 1970s but in the late 1990s, it was applied for coal power plants. This technique requires low capital for installation but on the contrary, it has relatively higher operating costs (Sorrels et al., 2019). The post-combustion techniques are explained in detail in Chapters 3 and 4.

### *2.3. Carbon dioxide capture*

In the seventies, the removal of carbon dioxide was considered for the first time, being pioneers in this field Marchetti in 1977 and Baes et al. in 1980. It was not until the 1990s that the topic gain support (Herzog, 2018). The carbon capture technology involves three main stages: carbon capture, transportation of the captured $CO_2$, and finally, $CO_2$ sequestration (Wilberforce et al., 2021). Nevertheless this thesis only focuses on the step of carbon capture. There are three general methods to carbon capture from electric power generation: pre-combustion $CO_2$ capture, oxy-combustion, and post-combustion $CO_2$ capture.

*Pre-combustion $CO_2$ capture* is based on the gasification of coal through partial oxidation, employing air or oxygen, to produce synthesis gas (syngas) rich in monoxide carbon and hydrogen. Carbon monoxide is reacted with steam in a catalytic reactor (shift converter), to generate dioxide carbon and more hydrogen. Then, the syngas is treated to removed acid gases in two steps: first sulfur dioxide and follow dioxide carbon. After that dioxide carbon is sent to a drying and compression unit. Clean syngas is fed in a gas turbine modified for firing syngas with high hydrogen content. Thus, electricity is produced similar to a

natural gas combined-cycle plant. In addition to that from the combustion turbine can be obtained additional electricity, employing a heat recovery steam generator as an integrated gasification combined cycle (IGCC) power plant.(Metz et al., 2005; Miller, 2015; Zhu and Frey, 2012). Spain hosts an IGCC power plant whose main source is coal with a production capacity of 350 MW (INITEC Energía, 2010).

In the strict sense, *oxy-fuel combustion* is not technically a capture technology, since its main goal is the generation of electricity. It should be noted that this process which coal combustion occurs in an oxygen-enriched environment, generates a flue gas comprised principally of $CO_2$. The process is based on the coal combustion with air and dioxide carbon, flue gas obtained is treated to clean and split different compounds. One part of dioxide carbon is sent to the boiler and the other part is storage (Goel et al., 2018). This methodology is explained widely in Chapter 4.

*Post-combustion $CO_2$ capture* is applied in flue gas combustion. These techniques can be applied in pulverized coal power plants (Maroto-Valer, 2010). These abatement techniques are described completely in Chapter 4.

### *2.4. Biomass as a source of power and chemicals*

The concept of biorefineries in the literature has evolved from simple bioethanol or biodiesel production facilities, single raw material -single main product, where byproducts where used to improve the tight economics, i.e. DDGS (Karuppiah et al., 2008) or glycerol (Martín and Grossmann, 2012a) to truly integrated plants (Bond et al., 2014; Cruz et al., 2014), where intermediates and final products are generated and the facilities show several production lines. The process to design such integrated biorefineries involves integration of several concepts such as circular economy, water-energy nexus, to encourage the use of waste and byproducts, the energy and water efficiency, catalysis and synthesis that allowed the further transformation of chemicals into added value ones, and process intensification. This process follows from the studies of many groups such as experimentalists in the catalyst, bioengineering and biological fields, but it is typically the process system engineering community the one with the skills to put together such integrated facilities. In between, second generation bioethanol plants, algae based biodiesel production can be considered steps of the evolution (Martín and Grossmann, 2013). Energy and fuels are no longer the aim of these facilities, see Figure 1.4. The reasons are diverse including cost, social expectations and efficiency

in the use of the natural resources. The initial one is the cost. Competing with crude based chemicals is hard since the use of biomass as raw material requires additional steps to obtain the actual raw material for the transformation, i.e. sugars or syngas. That is the reason for the development of integrated facilities, to take advantage of synergies and improve the economics obtaining multiple products. In addition, society does no longer easily accept the fact that the final use of biomass is just to burn it to obtain energy. This is part of the European strategy. More interesting uses for the biomass are to be found. Thus, added value products such as carotenoids (Psycha et al., 2014), platform chemicals such as levulinic acid (Alonso et al., 2013), furfural and either hydroxymethylfurfural (Torres et al., 2010), and/or dimethyl furfural (Martín and Grossmann, 2016), dioles (Huang et al., 2017), food supplements and polymers (García Prieto et al., 2017), essential oils (Dávila et al., 2015) and active principles for drugs enter in the portfolio of the biorefinery. These products also help in the economy of the biorefinery. In addition, waste use and valorization provides the opportunity to create a circular economy. Waste to power initiative is the one that has paved the way for waste to be recycled (www.eia.gov). Waste as raw material includes from lignocellulosic biomass such as wood chips, forest residues, etc., to manure, sludge or municipal solid waste. While lignocellulosic biomass has been widely addressed as a raw material, the rest are starting to gain attention. For years waste was devoted for the production of power via anaerobic digestion (León and Martín, 2016) or gasification of municipal solid waste (Niziolek et al., 2015). However it is also possible lo produce bulk and specialty chemicals. Using digestion as waste processing technology, the biogas produced contains all the ingredients for dry reforming so that it can be used for the production of methanol, ethanol, dimethyl ether or FT fluids (Hernández and Martín, 2016). In addition, the digestion of waste generates a residue rich in nutrients. The use of the nutrients to grow algae integrated with the production of methanol from the biogas allows the self-sufficient production of biodiesel from waste (Hernández and Martín, 2017). Furthermore, specialty chemicals such as essential oils can also be obtained (Dávila et al., 2015). The design of such integrated refineries involves concepts like circular economy, integration and intensification, and process system engineering tools have been developed to aid in the synthesis. Alternatively, for less diluted waste sources such as MSW (Niziolek et al., 2015) once a raw syngas is available, the synthesis possibilities are almost endless (Martín and Grossmann, 2013). The analysis and development on integrated biorefineries, rely on

the modelling of the units and the formulation of the problem as a simulation based or a superstructure-based approach.

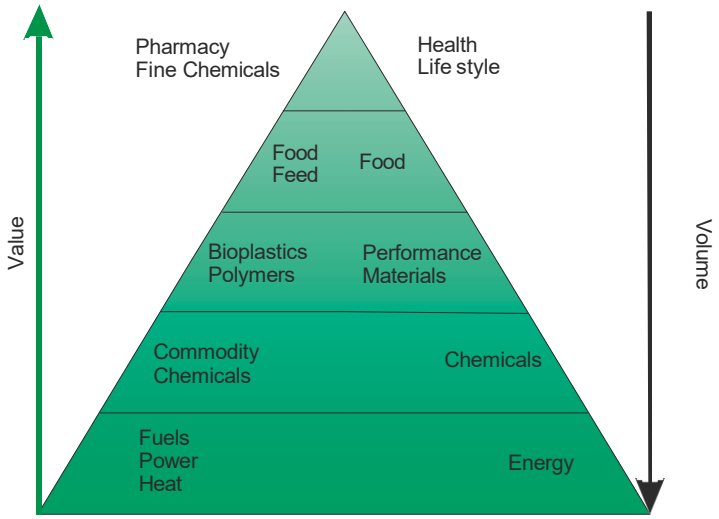


***Figure 1.4***. Pyramid of biomass related products

### *2.5. Water scarcity*

The term "water scarcity" refers to the lack of resources of freshwater to meet the water demand. Water scarcity is an important issue since other civilizations, without the current environmental problems, collapsed due to the prevalence of intense and prolonged droughts (Tzanakakis et al., 2020). All life on the planet depends on the availability of water, so that it becomes one of the most precious of resources. Water scarcity generates serious restrictions in terms of social integrity and economic development. In fact, many regions and countries around the world are affected (Angelakis et al., 2018). Of all the fresh water consumed, 15% is used for household purposes, 70% for agriculture and 15% within the industrial sector. Unfortunately, only 3% of the water on Earth is fresh water and two-thirds correspond to polar ice caps and glaciers (Jess and Wasserscheid, 2013). Due to population growth, the water necesities increase, as well as the energy and food requirements which in turn have other water needs. In this way, a large number of researches have focused on the exploitation of alternative water sources as recycled water, rainwater, and brackish water. Recycled water or also known as reclaimed water consists of the reuse of wastewater. If this water will be employed to drink it is called potable reuse or purified water. Recycled water can be used in several areas as domestic (bathing, showering, toilet, clothes washer, dishwasher, garden,...), agriculture (irrigation, cleaning food,...), or industrial (Salgot et al., 2018). Some companies as Coca-Cola, Frito-Lay, PepsiCo, or Intel have implemented industrial water reuse to address energy and sustainability goals. For example,

Coca-Cola company has installed several recycle and reclaim loops, allowing facilities to reuse processed water in cooling towers, boilers, or cleaning (Saeid Eslamian and Faezeh Eslamian, 2017).

## 3. Theoretical foundations.

### *3.1. Methodologies.*

Several approaches can be employed for the design of a transformation process or the development of the flowsheeting. These approaches can be classified into heuristic-based and mathematical optimization. The heuristic approaches are based on rules and known-how to improve decision making, while the mathematical programming consists of optimization techniques to select the configuration and parameter of the processing system (Grossmann, 1996).

#### *3.1.1. Heuristic-based approach.*

The implementation of heuristic methods is presented in the literature through two main approaches, Douglas hierarchy (Douglas, 1988), and the onion model (Smith, 2005). The Douglas hierarchy procedure consists of five stages. The first decision corresponds to determining if the process operates in continuous or batch. Then, feeds and products are evaluated through input-output in the structure. Next, the recycle structure and the reactor operations and conversion are analyzed. Subsequently, the separation systems are studied, and finally, the energy in the process is researched, allowing the reduction of consumption. As Figure 1.5 shows, the onion model begins in the analysis of the reactor, followed by the separation and the recycled system, based on the output stream from the reactor and its conversion. Then, the heat recovery is studied, followed by the assessment of the heating and cooling utilities. Finally, the treatment of water and other effluents is researched (Sánchez et al., 2020). In certain cases, the same operation can be developed by different processes. In this way, the best choice can be determined on industrial experience, collected in several books and usually called rules of thumb (Couper et al., 2012; Hall, 2012).

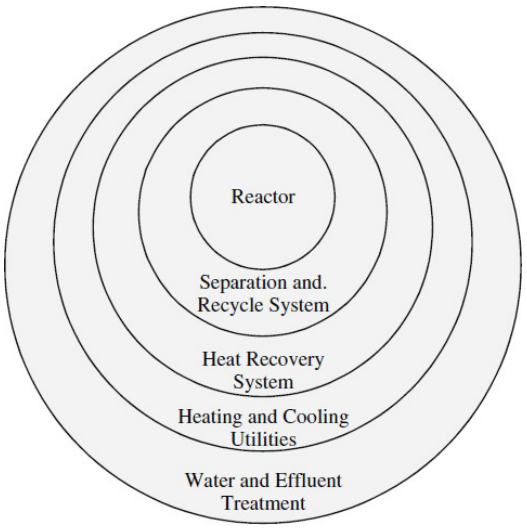


***Figure 1.5*** The onion model of process design (Smith, 2005)

### *3.1.2. Mathematical programming approach.*

Mathematical programming is also known as synthesis problem. Mathematical-based methods began to replace heuristic methods for solving more and more complex problems. The development of simultaneous design approaches based on superstructure optimization (Yee and Grossmann, 1990) or pinch localization approaches (Duran and Grossmann, 1986) generated a major shift in the field, as did the development of mathematical programming approach. The formulation of the synthesis problem should be carried out through three steps: modelling of the superstucutre flowsheet; problem formulation; and solution of the optimization model.

#### *3.1.2.1. Modeling techniques*

The modelling is based on algebraic models for the different process unit that flowsheet represent. Martin and Grossman presented a number of techniques to classify these different algebraic models. These classification is short cut methods, mechanistic methods, rules of thumb, dimensional analysis, surrogate models, or experimental correlations (Martín and Grossmann, 2012b;Martín and Martínez, 2013). These modeling techniques can be applied to the same problem.

The *short cut approach* is a simple represetantion of systems and it is based on basic first principles, that is mass and energy balance. The disadvantage of this method is that it is not easy to model non ideal or complex behaviour.

The *mechanistic models* are more complex than the previous one and they are sitll based on physical principles. They include equilibrium models, kinetic models, phase equilibrium or even rigorous models where it is employed the continuity, momentum and energy equations. Contrary to the previous one, the disadvantage of this methods is the complexity of the models finally developed.

*Rules of thumbs models* are based on experimental experience of the operation units. Usually operational data are limited and therefore their use too.

*Factorial design of experiment* considers the statistical analysis, allowing the systematic study of a large number of variables from experiments. This method is only available for the range of they have been obtained. In some occasion they can be generated scale up problems.

*Empirical correlation methods* are obtained from experimental studies and involve physical meaning and experimental background. Like the previous one, the method is only implemented for the range of they have been obtained and sometimes it is difficult to find the equation to represent the relation-ship between several variables.

*Neural networks* consist of statistical analysis too but in this case, require a large number of samplings and as a result, good fittings and predictions are obtained.

The *Kriging* model is developed through interpolation methods and a good representation of complex surfaces of response is obtained.

#### *3.1.2.2. Problem formulation*

The optimization problems are composed by objetive function (single or multiple), equations and constraints. In the case of these studies, a single objetive function is used. The general form of optimization problems is shown following (Grossmann et al., 2000):

$$\begin{aligned} &\min Z = f(x, y) \\ &st \qquad h(x, y) = 0 \\ &\qquad\quad g(\mathrm{x},\ \mathrm{y}) \leq 0 \\ &\qquad\quad x \in X; y \in Y \end{aligned} \tag{1}$$

Where f(x,y) is the single objective function such as cost, environmental index, amount of products, use of sources, ... ; h(x,y)=0 represents the performance of the system and can be mass and energy balance,

equilibrium equations, among others; g(x,y) are inequalities that some specifications or constraints for feaseble choices.

Optimization problems may be classified as a function of the type of variables (continue/integer/binary), the kind of objective function (single/multiple), or sort of constraints (linear/nonlinear). The classification is:

- *Linear*: the vector x is continuous and all funcions are linear.
- *Non-linear*: the variable x is continuous and at least one equation is nonlinear.
- *Mixed-integer linear:* The vector x is integer or binary but all functions are linear.
- *Mixed integer non-linear*: The vector x is integer or binary and at least one equation is nonlinear.

In order to develop a better classification of optimization problems, the concept of convexity must be clarified. An optimization problem is convex when all of the constraints and the objective functions are convex functions. While any optimization problem is non-convex whtna the objetive function or any of the constraints are non-convex. Figure 1.6 illustrates graphical the concept of convex and non-convex optimization problems.

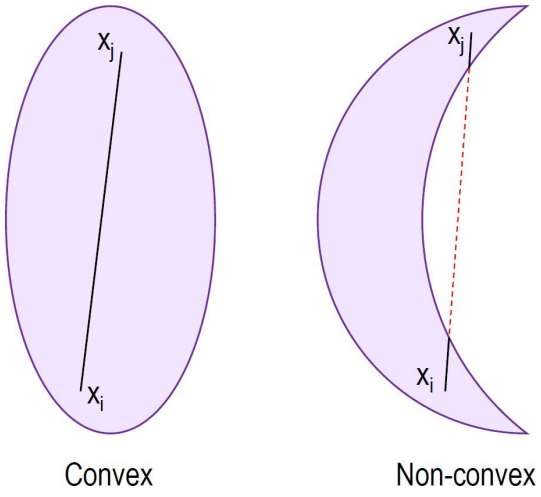


***Figure 1.6.*** Graphical representation convexity concepts.

In this way, the classification of optimization problems can be illustrated in Figure 1.7 as a function of the convexity property (Lin et al., 2012).

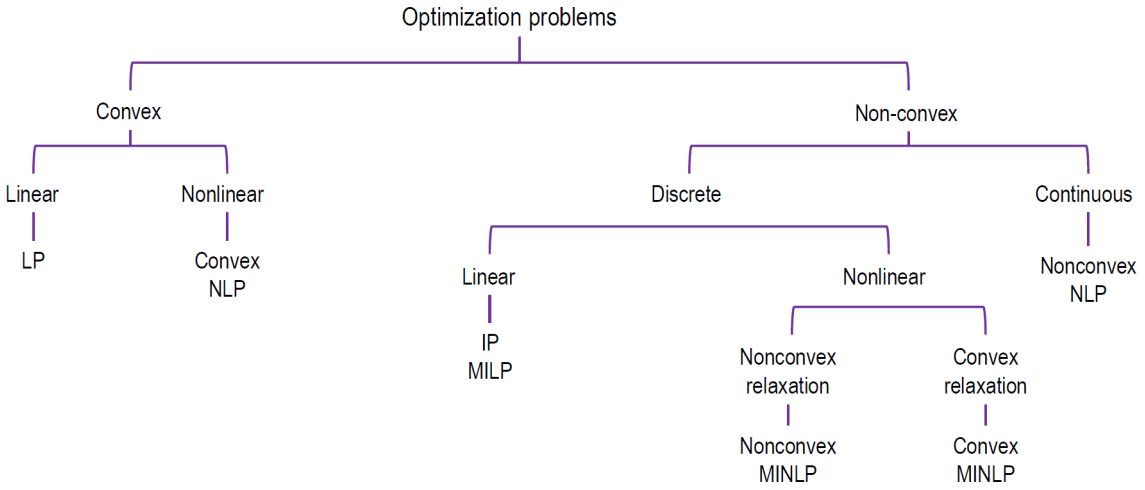


***Figure 1.7.*** Overview of problem types related to optimization problems.

## *3.2. Superstructures optimization*

### *3.2.1. General problem formulation*

A superstructure can be defined as a network of all possible alternatives to carry out a systematic design of chemical processes, to select the best option to define a flowsheet and a portfolio of products. Superstructure-based process synthesis was introduced by Umeda et al. (1972) and it is based on three sequential steps:

1. The postulation of a superstructure that consists of the set of all possible alternatives in the structure of the process.
2. Conversion of the superstructure into mathematical programming.
3. Apply mathematical optimization models to find the optimal structure solution.

Initially, the superstructure should capture all possible alternatives which generate limitations in the problems because in some cases several feasible or optimal process alternatives may be omitted. In view of theses limitations, the community has developed differents approaches to solvent it. One of them consists of automated superstructure generation methods, in which the superstructure is built from a set of alternatives via deterministic algorithmic procedures. Another case is evolutionary “superstructure-free” approaches where the superstructure is generated dynamically along with the research process, each superstructure is created by the algorithm instead of by the designer or the chemical process engineer. Over

time, several types of superstructure representations have been developed. Mencarelli et al. (2020) have been collected the main types of representations, generating a classification of ten cathegories:

1. State-task network
2. P-Graph representation;
3. State-equipment network representation;
4. State-space representation;
5. R-graph representation;
6. Generalized modular framework representation;
7. Group contribution based methodology;
8. Phenomena-building block approach;
9. Unit, port, conditioning stream representation
10. Building block-based superstructure

The conversion of a superstructure into mathematical programming is based on the mathematical representation of the real behavior of the process. For developed this conversion, the methods explained in previous section (3.1.2.2) are employed.

It should be noted that there is no single solution in the case of superstructure, as there are many factors that modify the optimal solutions (Sánchez et al., 2020). These factors can be the decision criterion or the type of objective function to be optimized, such as minimum energy consumption, production cost, environmental footprint, heat and water consumption or even maximizing process profit .

Superstructures have been applied in a lot of topics as bioethanol (Martín and Grossmann, 2011a), biodiesel (Gong and You, 2015; Martín and Grossmann, 2011b), hydrocabron refinery (Wang et al., 2013), water integration (Ahmetović and Grossmann, 2011), energy integration (Martín and Grossmann, 2012c), water and energy consumption (Baliban et al., 2013), water-energy nexus (Ahmetović and Kravanja, 2012), environmental impacts (Gebreslassie et al., 2013), or savety considerations (Peña-Lamas et al., 2018).

To complement the mathematical design of superstructures hybrid methods have been developed for process flowsheet sintesis. This methods includes the use of heuristics (Grossmann et al., 2000) as well as mathematical prescreaning approaches (Bertran et al., 2017).

### *3.2.2. Types of problems: Bleeding problem and pooling problem.*

Pooling and blending problems are an industrially relevant mathematical programming problem that arises in the petroleum refining industry. The importance of these problems on the industrial scale is due to the large amount of money that can be saved it as well as the improvement of some products. According to Misener and Floudas (2009), there are five classes of pooling problems as a function of mathematically modeling:

- *Standard pooling problem* is defined as a network flow problem over three set nodes: feed stocks, pooling or storage tanks, and final products. These nodes are called input, intermediate and output too, respectivelly. Flow rates are selected to maximize profit or minimize cost. The first algothm was introduced by Haverly in 1978.
- *Generalized pooling problem* increases the complexity of the problem by letting the flow rates between the intermediate pooling tanks and converting the network from a pre-determied structure into an optimally chosen configuration.
- *Extended pooling problem* was introduced by Gounaris and Floudas in 2007, incorporate Title 40 Code of Federal Regulations Part 80.45: Complex Emissions Model and associated legislative bounds into the constraint set. The problem maximizes profit as a standart pooling problem, adding as constraints the volatile organic, $NO_X$, and toxics emissions.
- *Non-linear blending:* The assumption that pooling problems can be simplified into linear blends is not always valid. Thus, this new group of blending problems appears because in the petroleum industry there are several non-linear characteristics such as the qualities of the fuels, including the vapor pressure, the octane number, among others.
- *Crude oil operations:* This type of pooling problem concerns at the front-end of a refinery. In this case, input nodes refer supply ships that arrive at a refinery, intermediate nodes are storage tanks and charging tanks, and the output nodes correspond crude distillation units.

Although this type of problems referred to refineries, over the years it has been extended to other areas within process engineering. Increasingly, these problems are being applied to the production of

formulated products such as polymers (Vaidyanathan and El-Halwagi, 1996), surfactants (Mattei et al., 2014), repellent lotions (Conte and Gani, 2011), detergents (Martín and Martínez, 2013), surfactant design (Martín and Martínez, 2015), among others. Another important application of growing interest is biorefineries. Hernandez et al. presented a methodology to evaluate the mixture of different types of waste including manure, sludge, urban food waste, and urban green waste for the production of syngas. Hovewer, simultaneous process and product design is still a challenge.

## 4. Conclusions

After carrying out the analysis of these environmental problems generated by energy production, the following conclusions were reached:

- Gas treatment technologies require detailed models to evaluate their performance. In addition not only a number of technologies are availabled in the market but also the amount of raw material purchased, coal type, is linked. The process design and coal blend selection is somehow a new type of extended pooling problem that companies need to solve on a daily basis.
- The location as well as the type of energy technology used to obtain the energy must be studied simultaneously, since it will affect water consumption. It is expected that the new plants will have a suitable location. For example, concentrated solar plants will be located in an area with a climate that negatively affects water consumption, opposite to the more flexible location form coal-fired power plants.
- With the need to introduce waste as a source of chemicals and energy, the use of biomass has to diversify towards value-added products so that only the waste is a source of energy. The simultaneous selection of products integrated with a power plant can provide the economic opportunity for the exploitation of biomass waste.

## 5. List of acronyms and abbreviations

GHGs: greenhouses gas.

SCR: selective catalytic reduction.

SNCR: selective non-catalytic reduction.

VOCs: volatile organic compounds.

## 6. References.

Ahmetović, E., Grossmann, I.E., 2011. Global superstructure optimization for the design of integrated process water networks. AIChE Journal 57, 434–457. https://doi.org/10.1002/aic.12276

Ahmetović, E., Kravanja, Z., 2012. Solution Strategies for the Synthesis of Heat-Integrated Process Water Networks, Chemical Engineering Transactions. https://doi.org/10.3303/CET1229170

Alonso, D.M., Wettstein, S.G., Mellmer, M.A., Gurbuz, E.I., Dumesic, J.A., 2013. Integrated conversion of hemicellulose and cellulose from lignocellulosic biomass. Energy Environ. Sci. 6, 76–80. https://doi.org/10.1039/C2EE23617F

Angelakis, A., Eslamian, S., Dalezios, N., 2018. Water scarcity management: part 1: methodological framework. International Journal of Global Environmental Issues 17, 1. https://doi.org/10.1504/IJGENVI.2018.10011706

Baes, C.F., Beall, S.E., Lee, D.W., 1980. The collection, disposal and storage of carbon dioxide., in: Interactions of Energy and Climate. Proceedings of an International Workshop Held in Münster, Germany, March 3–6, 1980. pp. 495–519.

Baliban, R.C., Elia, J.A., Floudas, C.A., 2013. Biomass to liquid transportation fuels (BTL) systems: process synthesis and global optimization framework. Energy Environ. Sci. 6, 267–287. https://doi.org/10.1039/C2EE23369J

Bertran, M.-O., Frauzem, R., Sanchez-Arcilla, A.-S., Zhang, L., Woodley, J.M., Gani, R., 2017. A generic methodology for processing route synthesis and design based on superstructure optimization. Computers & Chemical Engineering 106, 892–910. https://doi.org/10.1016/j.compchemeng.2017.01.030

Bond, J.Q., Upadhye, A.A., Olcay, H., Tompsett, G.A., Jae, J., Xing, R., Alonso, D.M., Wang, D., Zhang, T., Kumar, R., Foster, A., Sen, S.M., Maravelias, C.T., Malina, R., Barrett, S.R.H., Lobo, R., Wyman, C.E., Dumesic, J.A., Huber, G.W., 2014. Production of renewable jet fuel range alkanes and commodity chemicals from integrated catalytic processing of biomass. Energy Environ. Sci. 7, 1500–1523. https://doi.org/10.1039/C3EE43846E

Brears, R.C., 2015. The circular economy and the water-food nexus. Future of Food: Journal on Food, Agriculture and Society 3, 53–59.

Cai, X., Wallington, K., Shafiee-Jood, M., Marston, L., 2018. Understanding and managing the food-energy-water nexus – opportunities for water resources research. Advances in Water Resources 111, 259–273. https://doi.org/10.1016/j.advwatres.2017.11.014

Carbon dioxide, 2021. PubChem. URL https://pubchem.ncbi.nlm.nih.gov/compound/280

Cholakov, G., 2009. ©Encyclopedia of Life Support Systems (EOLSS): Pollution Control Technologies - Contents of Volume 1, Volume 2 and Volume 3.

Clean Air Technology Center, 1999. Nitrogen oxides (NOx). Why and how they are controlled. (Technical bulletin No. EPA-456/F-99-006R). Environmental Protection Agency.

Coal & Electricity, 2021. World coal association. URL https://www.worldcoal.org/coal-facts/coal-electricity/

Conte, E., Gani, R., 2011. Chemicals-Based Formulation Design: Virtual Experimentations, in: Pistikopoulos, E.N., Georgiadis, M.C., Kokossis, A.C. (Eds.), Computer Aided Chemical Engineering. Elsevier, pp. 1588–1592. https://doi.org/10.1016/B978-0-444-54298-4.50096-9

Couper, J.R., Penney, W.R., Fair, J.R., Walas, S.M., 2012. Chemical Process Equipment: Selection and design, 3th ed. Butterworth-Heinemann, Boston. https://doi.org/10.1016/B978-0-12-396959-0.00031-8

Cruz, V., Hernández, S., Martín, M., Grossmann, I., 2014. Integrated Synthesis of Biodiesel, Bioethanol, Isobutene, and Glycerol Ethers from Algae. Industrial & Engineering Chemistry Research 53, 14397–14407. https://doi.org/10.1021/ie5022738

Dávila, J.A., Rosenberg, M., Cardona, C.A., 2015. Techno-economic and Environmental Assessment of p-Cymene and Pectin Production from Orange Peel. Waste and Biomass Valorization 6, 253–261. https://doi.org/10.1007/s12649-014-9339-y

Douglas, J.M., 1988. Conceptual design of chemical processes, 1st ed. McGraw-Hill Education.

Duran, M.A., Grossmann, I.E., 1986. Simultaneous optimization and heat integration of chemical processes. AIChE Journal 32, 123–138. https://doi.org/10.1002/aic.690320114

El Safty, A., Siha, M., 2013. Environmental and health impact of coal use for energy production. Egyptian Journal of Occupational Medicine 37, 181–194. https://doi.org/10.21608/ejom.2013.783

García Prieto, C.V., Ramos, F.D., Estrada, V., Villar, M.A., Diaz, M.S., 2017. Optimization of an integrated algae-based biorefinery for the production of biodiesel, astaxanthin and PHB. Energy 139, 1159–1172. https://doi.org/10.1016/j.energy.2017.08.036

Gebreslassie, B.H., Slivinsky, M., Wang, B., You, F., 2013. Life cycle optimization for sustainable design and operations of hydrocarbon biorefinery via fast pyrolysis, hydrotreating and hydrocracking. Computers & Chemical Engineering 50, 71–91. https://doi.org/10.1016/j.compchemeng.2012.10.013

Goel, A., Bhatt, R., 2012. Causes and consequences of global warming. Int. J. LifeSc. Bt & Pharm. Res. 1, 27–31.

Goel, M., Sudhakar, M., Shahi, R.V., 2018. Carbon Capture, Storage and Utilization: A Possible Climate Change Solution for Energy Industry, 1st ed, CRC Press. Taylor &Francis group.

Gong, J., You, F., 2015. Value-Added Chemicals from Microalgae: Greener, More Economical, or Both? ACS Sustainable Chem. Eng. 3, 82–96. https://doi.org/10.1021/sc500683w

Grossmann, I., Caballero, J., Yeomans, H., 2000. Advances in mathematical programming for the synthesis of process systems. Latin American Applied Research 30.

Grossmann, I.E., 1996. Mixed-Integer Optimization Techniques for Algorithmic Process Synthesis, in: Anderson, J.L. (Ed.), Advances in Chemical Engineering. Academic Press, pp. 171–246. https://doi.org/10.1016/S0065-2377(08)60203-3

Hall, S., 2012. Rules of Thumb for Chemical Engineers, 5th ed. Butterworth-Heinemann, Oxford.

Haverly, C.A., 1978. Studies of the Behavior of Recursion for the Pooling Problem. SIGMAP Bull. 19–28. https://doi.org/10.1145/1111237.1111238

Hernández, B., Martín, M., 2017. Optimal Integrated Plant for Production of Biodiesel from Waste. ACS Sustainable Chem. Eng. 5, 6756–6767. https://doi.org/10.1021/acssuschemeng.7b01007

Hernández, B., Martín, M., 2016. Optimal Process Operation for Biogas Reforming to Methanol: Effects of Dry Reforming and Biogas Composition. Ind. Eng. Chem. Res. 55, 6677–6685. https://doi.org/10.1021/acs.iecr.6b01044

Herzog, H.J., 2018. Carbon capture, The MIT Press Essential Knowledge series.

Huang, K., Brentzel, Z.J., Barnett, K.J., Dumesic, J.A., Huber, G.W., Maravelias, C.T., 2017. Conversion of Furfural to 1,5-Pentanediol: Process Synthesis and Analysis. ACS Sustainable Chem. Eng. 5, 4699–4706. https://doi.org/10.1021/acssuschemeng.7b00059

INITEC Energía, 2010. IGCC, oxicombustión y otras plantas especiales [WWW Document]. INITEC Energía. URL http://www.initec-energia.es/section3.cfm?id=3&side=135&lang=sp

Introduction to the water-energy nexus, 2020. International Energy Agency. URL https://www.iea.org/articles/introduction-to-the-water-energy-nexus

Jess, A., Wasserscheid, P., 2013. Chemical Technology. An Integral Textbook. Wiley-VCH.

Karuppiah, R., Peschel, A., Grossmann, I.E., Martín, M., Martinson, W., Zullo, L., 2008. Energy optimization for the design of corn-based ethanol plants. AIChE Journal 54, 1499–1525. https://doi.org/10.1002/aic.11480

Kohl, A.L., Nielsen, R.B., 1997. Chapter 8 - Sulfur Recovery Processes, in: Kohl, A.L., Nielsen, R.B. (Eds.), Gas Purification (Fifth Edition). Gulf Professional Publishing, Houston, pp. 670–730. https://doi.org/10.1016/B978-088415220-0/50008-2

León, E., Martín, M., 2016. Optimal production of power in a combined cycle from manure based biogas. Energy Conversion and Management 89–99.

Lin, M.-H., Tsai, J.-F., Yu, C.-S., 2012. A Review of Deterministic Optimization Methods in Engineering and Management. Mathematical Problems in Engineering 2012, 756023. https://doi.org/10.1155/2012/756023

Marchetti, C., 1977. On geoengineering and the CO2 problem. Climatic Change 1, 59–68. https://doi.org/10.1007/BF00162777
Maroto-Valer, M.M. (Ed.), 2010. Developments and Innovation in Carbon Dioxide (CO2) Capture and Storage Technology, 1st ed. Woodhead Publishing.
Martín, M., Grossmann, I.E., 2016. Optimal Production of Furfural and DMF from Algae and Switchgrass. Ind. Eng. Chem. Res. 55, 3192–3202. https://doi.org/10.1021/acs.iecr.5b03038
Martín, M., Grossmann, I.E., 2013. On the Systematic Synthesis of Sustainable Biorefineries. Ind. Eng. Chem. Res. 52, 3044–3064. https://doi.org/10.1021/ie2030213
Martín, M., Grossmann, I.E., 2012a. Simultaneous Optimization and Heat Integration for Biodiesel Production from Cooking Oil and Algae. Ind. Eng. Chem. Res. 51, 7998–8014. https://doi.org/10.1021/ie2024596
Martín, M., Grossmann, I.E., 2012b. BIOpt: A library of models for optimization of biofuel production processes, in: Bogle, I.D.L., Fairweather, M. (Eds.), Computer Aided Chemical Engineering. Elsevier, pp. 16–20. https://doi.org/10.1016/B978-0-444-59519-5.50004-6
Martín, M., Grossmann, I.E., 2012c. Energy optimization of bioethanol production via hydrolysis of switchgrass. AIChE Journal 58, 1538–1549. https://doi.org/10.1002/aic.12735
Martín, M., Grossmann, I.E., 2011a. Energy optimization of bioethanol production via gasification of switchgrass. AIChE Journal 57, 3408–3428. https://doi.org/10.1002/aic.12544
Martín, M., Grossmann, I.E., 2011b. Process Optimization of FT-Diesel Production from Lignocellulosic Switchgrass. Ind. Eng. Chem. Res. 50, 13485–13499. https://doi.org/10.1021/ie201261t
Martín, M., Martínez, A., 2015. Addressing Uncertainty in Formulated Products and Process Design. Ind. Eng. Chem. Res. 54, 5990–6001. https://doi.org/10.1021/acs.iecr.5b00792
Martín, M., Martínez, A., 2013. A methodology for simultaneous process and product design in the formulated consumer products industry: The case study of the detergent business. Chemical Engineering Research and Design 91, 795–809. https://doi.org/10.1016/j.cherd.2012.08.012
Mattei, M., Kontogeorgis, G.M., Gani, R., 2014. A comprehensive framework for surfactant selection and design for emulsion based chemical product design. Fluid Phase Equilibria 362, 288–299. https://doi.org/10.1016/j.fluid.2013.10.030
Mencarelli, L., Chen, Q., Pagot, A., Grossmann, I.E., 2020. A review on superstructure optimization approaches in process system engineering. Computers & Chemical Engineering 136, 106808. https://doi.org/10.1016/j.compchemeng.2020.106808
Metz, B., Davidson, O., de Coninck, H., Loos, M., Meyer, L., 2005. IPCC Special Report on Carbon dioxide Capture and Storage. Policy Stud.
Miller, B., 2015. Fossil Fuel Emissions Control Technologies. Stationary Heat and power systems. Butterworth-Heinemann.
Miller, B.G. (Ed.), 2011. Clean Coal Engineering Technology. Butterworth-Heinemann, Boston.
Misener, R., Floudas, C.A., 2009. Advances for the pooling problem: Modeling, global optimization, and computational studies Survey. Applied and Computational Mathematics 8.
Munawer, M.E., 2018. Human health and environmental impacts of coal combustion and post-combustion wastes. Journal of Sustainable Mining 17, 87–96. https://doi.org/10.1016/j.jsm.2017.12.007
NASA, 2021. 2020 Tied for warmest year on redorc, NASA analysis shows. URL https://www.giss.nasa.gov/research/news/20210114/
Nitric oxide, 2021. PubChem. URL https://pubchem.ncbi.nlm.nih.gov/compound/145068
Nitrogen dioxide, 2021. . PubChem. URL https://pubchem.ncbi.nlm.nih.gov/compound/3032552
Niziolek, A.M., Onel, O., Hasan, M.M.F., Floudas, C.A., 2015. Municipal solid waste to liquid transportation fuels – Part II: Process synthesis and global optimization strategies. Computers & Chemical Engineering 74, 184–203. https://doi.org/10.1016/j.compchemeng.2014.10.007
Our World in Data, 2021. Energy consumption by source, World. URL www.OurWorldInData.org.
Peña-Lamas, J., Martinez-Gomez, J., Martín, M., María Ponce-Ortega, J., 2018. Optimal production of power from mid-temperature geothermal sources: Scale and safety issues. Energy Conversion and Management 165, 172–182. https://doi.org/10.1016/j.enconman.2018.03.048
Power Line, 2020. De-NOx Technologies. Primary and advanced emission control steps taken by TPPs. Power Line. URL https://powerline.net.in/2020/07/07/de-nox-technologies/

Psycha, M., Pyrgakis, K., Harvey, P., Ben-Amotz, A., Cowan, A., Kokossis, A., 2014. Design Analysis of Integrated Microalgae Biorefineries. Computer Aided Chemical Engineering 34, 591–596. https://doi.org/10.1016/B978-0-444-63433-7.50083-3

Reddy, P.J., 2014. Clean Coal Technologies for Power Generation, 1st ed. CRC Press.

Sadeghi, S.H., Sharifi Moghadam, E., Delavar, M., Zarghami, M., 2020. Application of water-energy-food nexus approach for designating optimal agricultural management pattern at a watershed scale. Agricultural Water Management 233, 106071. https://doi.org/10.1016/j.agwat.2020.106071

Saeid Eslamian, Faezeh Eslamian (Eds.), 2017. Handbook of Drought and Water Scarcity, Handbook of Drought and Water Scarcity. CRC Press. https://doi.org/10.1201/9781315226781

Salgot, M., Oron, G., Cirelli, G., Dalezios, N., Diaz, A., Angelakis, A., 2018. Criteria for Wastewater Treatment and Reuse under Water Scarcity. pp. 263–282. https://doi.org/10.1201/9781315226781-15

Sánchez, A., Hernández, B., Martín, M., 2020. Multiscale Analysis for the Exploitation of Bioresources, in: Process Systems Engineering for Biofuels Development. John Wiley & Sons, Ltd, pp. 49–83. https://doi.org/10.1002/9781119582694.ch3

Smith, R., 2005. Chemical process: design and integration. Wiley, New York.

Sorrels, J.L., Randall, D.D., Richardson-Fry, C., Schaffner, K.S., 2019. Chapter 1- Selective non-catalytic reduction. (No. Revised —4/25/2019). Environmental Protection Agency.

Srivastava, R.K., Hall, R.E., Khan, S., Culligan, K., Lani, B.W., 2005. Nitrogen oxides emission control options for coal-fired electric utility boilers. J Air Waste Manag Assoc. 55, 1367–88. https://doi.org/10.1080/10473289.2005.10464736

Torres, A.I., Daoutidis, P., Tsapatsis, M., 2010. Continuous production of 5-hydroxymethylfurfural from fructose: a design case study. Energy Environ. Sci. 3, 1560–1572. https://doi.org/10.1039/C0EE00082E

Tzanakakis, V.A., Paranychianakis, N.V., Angelakis, A.N., 2020. Water Supply and Water Scarcity. Water 12. https://doi.org/10.3390/w12092347

Umeda, T., Hirai, A., Ichikawa, A., 1972. Synthesis of optimal processing system by an integrated approach. Chemical Engineering Science 27, 795–804. https://doi.org/10.1016/0009-2509(72)85013-9

Vaidyanathan, R., El-Halwagi, M., 1996. Computer-Aided Synthesis of Polymers and Blends with Target Properties. Ind. Eng. Chem. Res. 35, 627–634. https://doi.org/10.1021/ie950072c

Wang, B., Gebreslassie, B.H., You, F., 2013. Sustainable design and synthesis of hydrocarbon biorefinery via gasification pathway: Integrated life cycle assessment and technoeconomic analysis with multiobjective superstructure optimization. Computers & Chemical Engineering 52, 55–76. https://doi.org/10.1016/j.compchemeng.2012.12.008

Wilberforce, T., Olabi, A.G., Sayed, E.T., Elsaid, K., Abdelkareem, M.A., 2021. Progress in carbon capture technologies. Science of The Total Environment 761, 143203. https://doi.org/10.1016/j.scitotenv.2020.143203

Woo, D.K., Kumar, P., 2016. Mean age distribution of inorganic soil-nitrogen. Water Resources Research 52, 5516–5536. https://doi.org/10.1002/2015WR017799

Yee, T.F., Grossmann, I.E., 1990. Simultaneous optimization models for heat integration—II. Heat exchanger network synthesis. Computers & Chemical Engineering 14, 1165–1184. https://doi.org/10.1016/0098-1354(90)85010-8

Zhang, C., Chen, X., Li, Y., Ding, W., Fu, G., 2018. Water-energy-food nexus: Concepts, questions and methodologies. J. Clean. Prod 195, 625–639. https://doi.org/10.1016/j.jclepro.2018.05.194

Zhu, Y., Frey, H.C., 2012. 4 - Integrated gasification combined cycle (IGCC) systems, in: Rao, A.D. (Ed.), Combined Cycle Systems for Near-Zero Emission Power Generation. Woodhead Publishing, pp. 129–161. https://doi.org/10.1533/9780857096180.129

# *Chapter 2*

# *0bjectives*

With 2030 agenda in mind, society faces challenges for the new energy system aiming at reducing emissions water footprint and supporting the development of a circular economy. In this context the contribution of this thesis focuses on analyzing the water energy food nexus from different perspectives.

- The first stage deals with the optimal design of the flue gas treatment in pulverized coal power facilities. The systematic analysis of the technologies available is developed towards defining the actual flowsheet and the operation conditions.
- The market decision of the selection of the raw material mix depends on the price and composition in terms sulfur, nitrogen, chlorine, and others. And extended blending problem is formulated as a tool for the simultaneous selection of technologies and coal mix.
- The trend towards a more sustainable operation let us to evaluate the flue gas treatment in oxy-combustion power plants and the corresponding blending problem.
- Together with flue gas water footprint is another challenge in power production. Water consumption depends on the thermodynamic cycle, the energy source (fuel; solar) and the location of the facility. To address all the challenges the systematic design of wet cooling towers is attempted developing surrogate models to evaluate cost and water consumption across climates and technologies.
- Waste is valuable resource towards energy and chemicals. Integrated facilities to produce added-value products and utilities are to be systematically design, selecting the portfolio of product and the reuse of waste to produce energy for the operation of the facility and the market. A general hybrid methodology is proposed to this task.

# *Chapter 3*

# Optimal gas treatment and coal blending for reduced emissions in power plants: A case study in Northwest Spain

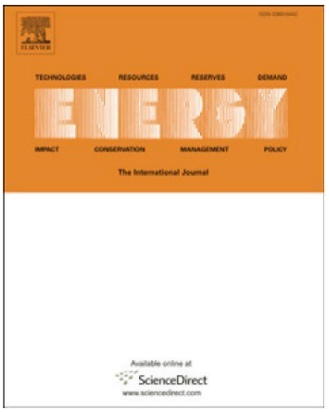


*Authors: **Lidia S Guerras** and Mariano Martín*

*DOI: doi.org/10.1016/j.energy.2018.12.089*

## Abstract

In this work a decision making framework for the design of the flue gas treatment section of a power plant has been developed, including particle, NOx and $SO_2$ removal operations. It has been applied to a coal based thermal power plant in Spain to select the optimal technologies and its sequence. Surrogate models for the treatments have been developed. The problem corresponds to a mixed integer non-linear programming one including catalytic and non-catalytic NOx removal, allowing various allocations for the catalytic technology, electrostatic precipitation and wet or dry $SO_2$ removal. It is reformulated as a nonlinear problem to evaluate bypass opportunities. The optimization suggests the use of electrostatic precipitation, followed by catalytic NOx removal and dry $SO_2$ removal. Next, a coal blending problem has also been solved for two objective functions. When only treatment costs are considered, the use of imported coal is recommended, but an increase of 4% in its price can change the decision into the use of national coal. If the energy within the coal is added to the objective function, crude tar coal is included in the blend and imported coal is used to maintain the emissions within limits. Limestone Forced Oxidation is the selected technology.

## 1. Introduction

Coal based power plants have been responsible for a fair share of the power production worldwide. However, current trends towards clean and sustainable energy have led to an effort towards reducing $SO_2$ and NOx emissions and water consumption. Modelling has been widely used to evaluate the performance of the facilities and the units. The different works have focused on one the he four main sections of the power plants: the boiler, the power cycle, the cooling units and the flue gas treatment section. Regarding the power island, most of the work in the literature evaluates the steady state operation of the thermal cycle (Sanpasertparnich and Aroonwilas, 2009), using specialized software such as "Power plant simulator" (KED, 2018), Cycle Tempo 5.0 (Kumar et al., 2016), or using commercial process simulators such as CHEMCAD (Martín and Martín, 2017) or ASPEN (Ong'iro et al., 1996). However, the actual operation of power plants is not in steady state. Their production is regulated to meet demand depending on the availability of renewable resources. Thus, the analysis of the dynamics has been presented in a number of studies (Weng et al., 1996), using specialized software (i.e. or ClaRaCSC (Brunnemann et al., 2012)) or commercial software such as SIMULINK, ThermoSysPro (El Hefni et al., 2011) or Apros 6 (Hentschel et al., 2017). Apart from the power produced, water scarcity and the water e energy nexus have attracted attention towards evaluating the water con- sumption involved in the cooling units. Power plants typically consume at least 1.8 L/kWh as a result of condensing the exhaust stream from the turbine, but the actual value depends on the plant location (Martín and Martín, 2017). The third section corresponds to emission control and includes the evaluation of the boiler operation. Two ap- proaches have been used to reduce emissions: i) the implementa- tion of measures to reduce the formation of those species by controlling the combustion at the boiler (Wang et al., 2018). ii) the installation of end of trail gas treatment. Most of the studies on boiler design are carried out to mitigate the production of pollutants by evaluating the temperature (Al-Abbas et al., 2012) and velocity profiles, the burner design (Safaei et al., 2014) and the excess of air (Li et al., 2018) and the composition of the oxidizer (Rahmanian et al., 2014). Furthermore, flue gas treatment has been widely addressed from an industrial perspective (Kikkawa et al., 2008) and the technologies are well estab- lished (Mitsubishi, 2017). However, the flue gas section has received less attention in the literature focusing on carbon capture. Several simulations of the carbon capture section of power plants using ASPEN plus can be found in the

literature for coal-based plants using MEA solutions (Alie et al., 2004), for IGCC technologies using amine solutions (Adams and Mac Dowell, 2016) or evaluating the $CO_2$ emissions of the co-firing of biomass with coal (Cebrucean et al., 2017). The difficulties in carbon capture from dilute streams have led to study oxycombustion systems. Two approaches to model oxycombustion power plants have been used, the use of process simulators (Xiong et al., 2011) and the development of equation-based models of the various units from the boiler to the air separation system to build a systematic framework for optimization (Dowling et al., 2014). Together with $CO_2$, the emission of NOx and $SO_2$ must be limited. There are several alternative denitrification (DeNOx) technologies such as catalytic or non- catalytic processes, as well as wet and dry systems for desulfur- ization (DeSOx). The removal yield and cost of each technology depends on the operating conditions and the addition of chemicals such as ammonia, CaO or $CaCO_3$ (NLWA, 2014). The actual selection of tech- nologies and their relative position in the treatment chain depends on the coal composition and emission limits. Apart from the in- dustrial experience and guidelines, no systematic study has addressed the optimal location of the DeNOx and DeSOx, the selection of the proper technologies or the operating conditions. The few studies that evaluate the production of NOx and $SO_2$ associated with power plants use empirical correlations to char- acterize the boiler and the fuel used. The abatement technologies are modeled using fixed removal ratios (Luo et al., 2012). The same group extended the work to perform a multiobjective optimization to account for environmental impact of the generation of power from fossil resources (Luo et al., 2014).

In this work, a framework is developed to select among different denitrification and desulfurization technologies and their relative position along the flue gas treatment chain of a power plant. It consists of a two-stage procedure. The first stage corresponds to the pre-screening of the technologies available based on industrial know-how. The second one consists of formulating a superstruc- ture model (Grossmann et al., 2000; Yeomans and Grossmann, 1999) of alternative technologies from the boiler to the discharge of the flue gas involving denitrifier, desulphurizer and particle removal. Surrogate models for each of the units are developed based on experimental and industrial data providing a flexible framework to evaluate and design the flue gas treatment process.

Once the plant is installed, it may have to process different coals. Price fluctuations in coal, supply agreements, social reasons and the ever-changing policies can result in the interest or need to process

different types of coal. Coal blending is a well-known topic aiming at selecting the proper mixture of coal types to meet sulfur content and optimize the combustion properties (Shih and Frey, 1995). However, the blending studies in the literature for different feedstocks either for coal (Shih and Frey, 1995), gasoline (Zhao and Wang, 2009), refrigerants (Churi and Achenie, 1997), detergents (Martín and Martínez, 2013), paints (Conte et al., 2011) are limited to the addition of process constraints on the composition of the feed to the mathematical formulation of the problem. Only lately, raw material blending and/or formulation have been coupled with process analysis and design (Ameri et al., 2018). Martín and Grossmann (2013) considered process and product formulation design in the context of algae growing for biodiesel FAEE produc- tion. Furthermore, biodiesel (FAME) has been produced from waste considering the NPK composition of digestate for optimal algae growing and the biogas composition for the optimal production of the methanol required for oil transesterification (Hernández and Martín, 2017). Hernández et al. (2017) presented a methodology to evaluate the mixture of waste for the production of syngas with the appropriate composi- tion for methanol, ethanol and FT-liquids production including the entire process model in the formulation. In this work we have extended this approach to formulate a coal blending problem that includes a detailed model of the technologies responsible for flue gas processing as a decision making tool to help select the coal blend.

The rest of the paper is organized as follows. Section 2 presents the details of the modelling including operating constraints for the different technologies and regulation constraints on the emissions. In section 3 the formulation is described and the model charac- teristics. In section 4 we present the results of the operation of the treatment process and the coal blending problem. Finally, section 5 draws some conclusions.

## 2. Process design

A section of coal-based power plants from the boiler to the disposal of flue gas is analyzed to compute the composition of the gas produced and the alternative technologies to remove ash, NOx, $SO_2$ and acids such as HF and HCl. The optimization of the flue gas treatment consists of two stages combining heuristics and super- structure optimization for the selection of the technologies and their location.

### *2.1. Heuristic based selection of technologies*

There are a number of technologies that have been proposed for particle, NOx and $SO_2$ removal. Particle removal can be carried out using gravity settling chambers, impingement separators, cyclone (centrifugal) separators, electrostatic precipitators (ESPs), fabric filters and wet collectors/scrubbers. Among them, ESPs are typi- cally used when very high efficiencies are required for removing fine particulate matter and very large volumes of gas are to be handled. Therefore, we disregard the rest (Miller, 2015). Three types of sources are identified for the production of NOx, namely, thermal, prompt (fixing $N_2$ from the atmosphere) and fuel nitrogen. Mostly, there are two types of technologies used in industry, those aimed at reducing their generation by modifying combustion characteristics, including low NOx burners, and those that treat the flue gas. We assume that the first measurements have already been included in the current design of the thermal plant and we focus on post combustion modifications that include catalytic (SCR) and non- catalytic (SNCR) abatement (Miller, 2015). There is also a large number of alternatives to remove $SO_2$ from a flue gas. They are commonly classified between wet and dry scrubbers. There is a large number of alternatives such as the use of limestone combined with natural or forced oxidation, the use of a mixture of MgO and CaO, the use of high e calcium lime, dual ealkali, dry scrubbing, dry injection, Wellmann-Lord and regenerable MgO (Miller, 2015). However, in industry, approximately 85% of the flue gas desulfurization units installed in the US are wet scrubbers, 12% are spray dry systems, and 3% are dry injection systems. The removal efficiencies of wet systems are higher than 90% while last dry designs can also reach 90% removal (EPA, 2003). Thus, for this work we have selected two alternatives: A wet removal system known as the Limestone Forced Oxidation (LFSO) and the dry removal using a Spray drier, Spray dry scrubbers (LSD). Therefore, for the superstructure we only focus on these two.

### *2.2. Process superstructure*

In a second stage a superstructure optimization model is formulated for the selection of flue gas treatment technologies by modelling each of the units. The flue gas generated in the boiler can be treated using a non-catalytic NOx removal unit within the boiler structure, selective non-catalytic reduction (SNCR). We allow the presence or absence of this technology by defining a split of the flue gas stream. The hot flue gas is later used to reheat up steam before it is sent to the medium pressure section of the turbine. Next,

the possibility of treating the flue gas using a selective catalytic reduction (SCR_1) as deNOx technology is considered. This technology operates within a range of temperatures. A heat exchanger is allocated before the catalytic reactor to adjust the temperature. However, it is possible that the SCR is not selected at that point of the flue gas treatment chain, thus a bypass is allowed. The subsequent treating step is the removal of particles. We allow the presence or absence of this technology by creating a divider that sends the flue gas to the electrostatic precipitator or through a bypass. The next treatment stage is the removal of $SO_2$. Three alternatives are allowed, a bypass, if the $SO_2$ concentration is already below limits, a wet and a dry removal technology. In the last two cases the flue gas must be cooled down before being fed to the absorption column and heat exchangers are placed before the treatment units. In the case of the dry removal technology, the solids are recovered, and the flue gas is sent to further treatment. Only a fraction of the liquid is reused, the rest is discarded. Finally, it may be interesting to locate the catalytic removal of NOx by the end of the trail (SRC_2). A bypass is also allowed in case the concentration of particles NOx and $SO_2$ is already within the limits. Otherwise, at this point the flue gas must be heated up before feeding the catalytic reactor using a heat exchanger. The concentrations of $SO_2$ and NOx must meet the legal limits at the end of the processing train. Figure 3.1 shows the superstructure of alternatives that is solved towards the optimal flue gas deNOx and de$SO_2$.

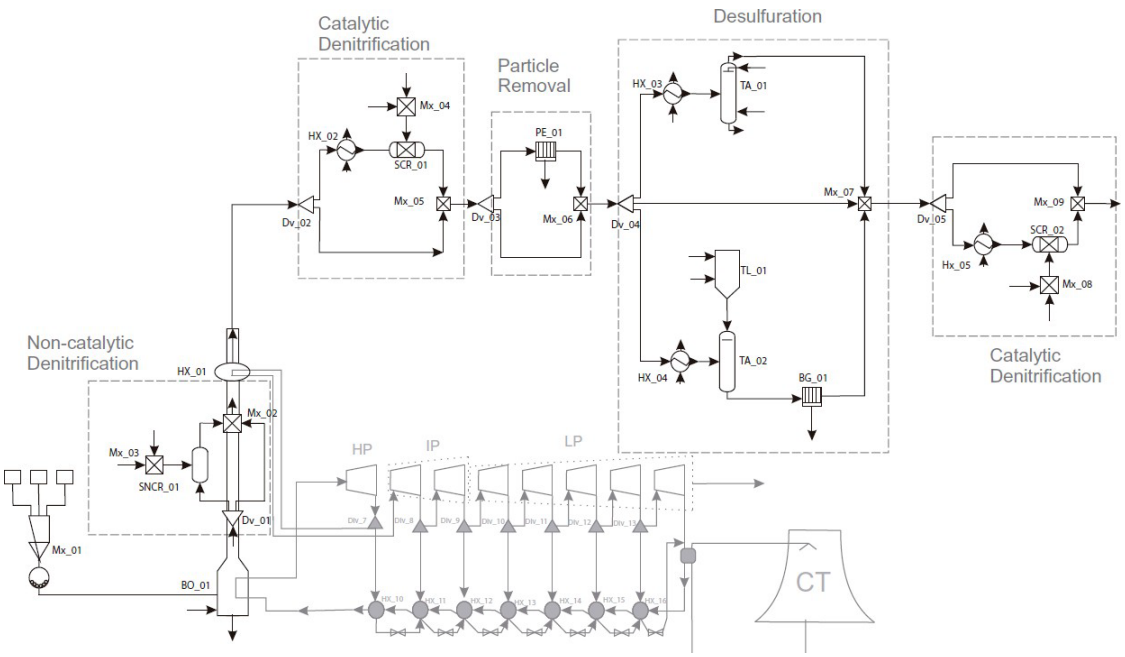


***Figure 3. 1***.- Superstructure for flue gas denitrification and desulfuration.

## 3. Superstructure model formulation

All the units involved in the process are modeled using exper- imental data, mainly for removal ratios as a function of process conditions, rules of thumb, thermodynamic and chemical equilibrium and mass and energy balances applied to the following list of species:

{C, CO, $CO_2$, $O_2$, S, $SO_2$, $N_2$, $Cl_2$, $F_2$, NO, $NO_2$, ash, $NH_3$, $H_2O$, CaO, $CaCO_3$, $CaSO_3$, $CaSO_4$, HCl, HF, $CaCl_2$, $CaF_2$, $H_2$}.

In this section we present the modelling issues of each of the main units. Splitters, triangles in Figure 3.1, and mixers, crossed squares in Figure 3.1, are modeled based on simple mass and energy balances. Stream mixing is assumed to be adiabatic and stream splitting is isothermal. Heat exchangers are modeled using a mass balance assuming no species change and an energy balance assuming no losses, using heat capacities as a function of the temperature in the form of polynomials (Martín, 2016). The rest of the units are modeled based also on mass and energy balances. However, along the following subsections we present the particularities of the models for the main units such as boiler, selective non-catalytic reduction of NOx, (SNCR), selective catalytic reduction of NOx (SCR), electrostatic precipitator, wet and dry systems for $SO_2$ removal.

### *3.1. Boiler model*

The operation of the boiler depends on the actual design of the boiler and the burners, the composition of the coal used, resulting in the energy generated and the composition of the gas. In this work we assume that the geometries of the boiler and of the burners are given and the implementation of measures to reduce NOx and $SO_2$ formation is already considered. Typically, within the boiler a temperature distribution is generated. The particular pro- file depends on the fuel and the fuel to air ratio. Thus, the gas composition is computed as a function of the temperature profile where atom balances and chemical equilibria must also hold. Experimental data or a detailed CFD model of the boiler can be used to compute the temperature profile. For proprietary issues, public data from the literature of an industrial air fired burner are used instead (Al-Abbas et al., 2012). To compute the species equilibrium, we divide the boiler into two parts, zone 1, the flame section, and zone 2, the upper one, see Figure 3.2. The temperature of each region is computed as an area average. To determine this temperature from the profile, each of the regions is

discretized using a grid. For zone 1, 6 subregions are considered, while for zone 2, that presents a more homogeneous temperature distribution, only 1 region has been used. We compute the equilibria in the lower section and later we recomputed the NO to $NO_2$ equilibrium in the cooler region.

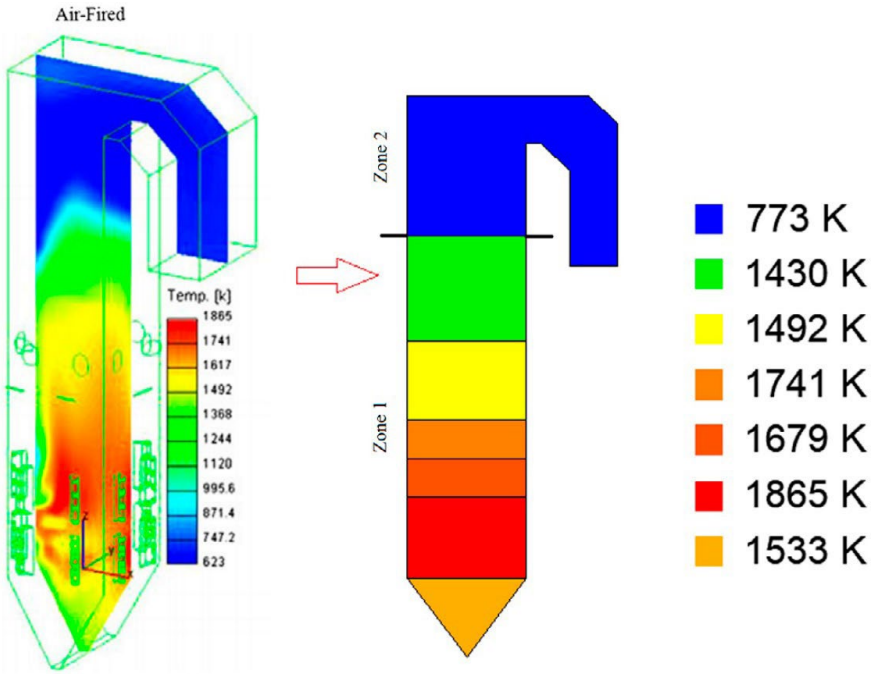


***Figure 3.2***. Temperature profile of an air fired coal burner. Zone 1: Flame section. Zone 2: Upper region, Experimental data from(Al-Abbas et al., 2012).

### *3.1.1. Flame section (zone 1)*

The average temperature is computed out of the spatial distribution of temperatures using eq. (1). The relative areas and their correspondent temperatures are computed from (Al-Abbas et al., 2012).

$$T = \sum_{area} a_i T_i \tag{1}$$

The 6 subregions of zone 1 represent, from bottom to top in Figure 3.2, areas of 13.3, 23.6, 31.8, 11.3, 12.2 and 7.6%. Using this temperature, we compute the equilibrium that generates the various species. The following species and equilibria are considered in the analysis.

*1. Carbon burning.* It is the source of energy in the process.

$$C + O_2 \rightarrow CO_2 \tag{2}$$

Experimental data at industrial scale shows that around 99% of the coal is burned into CO and $CO_2$. Thus, 1% unburned coal based on this rule of thumb is assumed. Out of it, 20% is slang while the rest,

80%, is dragged by the flue gas (La Robla, 2017). The actual ratio between CO and $CO_2$ depends on a number of other reactions such as Bouduard reaction (Martín, 2016). The equilibrium is given by the following equation:

$$C + CO_2 \longleftrightarrow 2CO \tag{3}$$

$$K = \frac{P_{CO}^2}{P_{CO_2}} \Rightarrow \log(K) = 9.1106 - \frac{8841}{T} \tag{4}$$

However, we use experimental data from the literature to impose a $CO_2$ to CO ratio of 1.198 (Dolman et al., 2008).

2. *NO production*.

It is produced following two reactions given by eq. (5):

$$\begin{aligned} &N_2 + O \underset{k_{-1}}{\overset{k_1}{\longrightarrow}} NO + N \\ &N + O_2 \underset{k_{-2}}{\overset{k_2}{\longrightarrow}} NO + O \\ &\overline{N_2 + O_2 \underset{}{\overset{K_{eq}}{\longrightarrow}} 2\,NO} \end{aligned} \tag{5}$$

The kinetic constants for the direct and indirect reactions for the two original ones are given as eq. (6) (Habib et al., 2008) and allow us to compute the equilibrium constants for each reaction and the overall production of NO.

$$\begin{aligned} k_1 &= 1.8 \cdot 10^8 \cdot \exp\left(-\frac{38{,}370}{T}\right) \\ k_{-1} &= 3.8 \cdot 10^7 \cdot \exp\left(-\frac{425}{T}\right) \\ K_1 &= \frac{k_1}{k_{-1}} \\ k_2 &= 1.8 \cdot 10^8 \cdot \exp\left(-\frac{4{,}680}{T}\right) \\ k_{-2} &= 3.8 \cdot 10^7 \cdot \exp\left(-\frac{20{,}820}{T}\right) \\ K_2 &= \frac{k_2}{k_{-2}} \end{aligned} \tag{6}$$

Due to numerical issues when using the individual equations, the individual kinetic constants in eq. (6) have been rearranged into a global equilibrium constant as follows, eq. (7):

$$K_{eq_{NO}} = K_1 \cdot K_2 = 22.44 \cdot \exp\left(-\frac{21{,}805}{T}\right) \quad (7)$$

3. *$NO_2$ production:* It follows the reaction below (Jess and Wasserscheid, 2013), eq. (8):

$$2NO + O_2 \underset{\longleftarrow}{\xrightarrow{K_{eq}}} 2NO_2 \quad (8)$$

$$K_{eq_{NO_2}} = 2.75369 \cdot 10^{20} \cdot T^{-6.95528} \quad (9)$$

Other nitrogen oxides can also be produced in the boiler, such as $N_2O_3$ and $N_2O_4$, but the concentrations are negligible in the flue gas (Clean Air Technology Center, 1999). Typically, NOx consists of 95% NO and 5% $NO_2$ (Mussatti et al., 2002).We use this proportion to validate the model results.

4. *Sulfur* combustion (Sarkar, 2015). We assume 100% conversion of the sulfur into $SO_2$ (La Robla, 2017)

$$S + O_2 \rightarrow SO_2 \quad (10)$$

5. *HCl* production (Shemwell et al., 2002) We assume 100% conversion (La Robla, 2017).

$$Cl_2 + H_2 \rightarrow 2\,HCl \quad (11)$$

6. *HF* production (Laird and Smith, 2017). We assume 100% conversion (La Robla, 2017)

$$F_2 + H_2 \rightarrow 2\,HF \quad (12)$$

Apart from the equilibria, the atom balances must also hold, eq.(13):

$$\begin{aligned}
&\sum_{in=\{C\}} n_c = \sum_{out=\{CO,CO_2,C,ash\}} n_c \\
&\sum_{in=\{N,N_2\}} n_N = \sum_{out=\{NO,NO_2,N_2\}} n_N \\
&\sum_{in=\{O_2,H_2O\}} n_O = \sum_{out=\{O_2,NO,NO_2,SO_2,H_2O\}} n_O \\
&\sum_{in=\{F\}} n_F = \sum_{out=\{HF\}} n_F \\
&\sum_{in=\{Cl\}} n_{Cl} = \sum_{out=\{HCl\}} n_{Cl} \\
&\sum_{in=\{H_2O\}} n_H = \sum_{out=\{HCl,HF,H_2O\}} n_H
\end{aligned} \tag{13}$$

#### *3.1.2. Upper section (zone 2)*

In this section an average temperature computed from the temperature profile is assumed to recompute the equilibrium using eqs. (8) and (9) again to determine the ratio between NO and $NO_2$ in the flue gas exiting the boiler. The composition of the gases provided by the model is validated by personal communication with the company. Finally, the excess of air, up to 30%, determines the efficiency of the combustion (Grassi et al., 1992):

$$\eta = 0.2473 \cdot \%_{excess,air} + 0.6016 \tag{14}$$

### *3.2. Electrostatic precipitator*

The electrostatic precipitator is in charge of removing the par- ticles in suspension. It provides them with an electric charge so that they are attracted by the walls. The removal efficiency depends on the particle size and the strength of the electric field (Gajbhiye et al., 2015; Nóbrega et al., 2004). The unburned coal is also removed at this point (La Robla, 2017). With the appropriate field generated, the efficiency is already close to 100% and thus the particle size is the yield defining parameter (Nazaroff and Alvarez-Cohen, 2000). The target is to reduce the particle concentration below 50 mg/$Nm^3$ (BOE, 2004).

The precipitator is modeled using a mass balance where only the solids are removed from the gas stream, a removal ratio and an energy balance, see eq. (15). The typical exit temperature is around 423 K (GasNatural Fenosa, 2015).

$$\eta(d) = f(size)$$
$$Particle_{Removal} = \sum \eta(d) n_{Particle}(d) \quad (15)$$
$$\eta = \frac{Particle_{Removal}}{Particle_{in}}$$

To compute the removal yield, η, the information on the performance of an electrostatic precipitator as a function of the particle size as presented by Nichols and McCain (1975) is used. We consider a particle size distribution discretized into 7 sizes, eq. (16). Most of the particles are of 10 mm, based on industrial experimental data (La Robla, 2017). Using the removal efficiency from the literature discretized per particle size (Nichols and McCain, 1975), the matrixes in eq. (16) are developed:

$$PSD\left(\varphi_{particle}\right) = \begin{pmatrix} 0.075 & 0 \\ 0.2 & 0 \\ 0.5 & 0 \\ 1.5 & 0 \\ 2 & 0 \\ 5 & 0.01 \\ 10 & 0.99 \end{pmatrix} \quad \eta\left(\varphi_{particle}\right) = \begin{pmatrix} 0.075 & 0.99 \\ 0.2 & 0.95 \\ 0.5 & 0.90 \\ 1.5 & 0.96 \\ 2 & 0.97 \\ 5 & 1 \\ 10 & 1 \end{pmatrix} \quad (16)$$

The estimation of the cost for the electrostatic precipitator is given by Miller (2015), where $Q_y$ is the volume of gas ($Nm^3$) processed in a year. The advantage of this type of cost functions is that if the technology is not selected, no flowrate is processed and, as a result, there is no cost associated.

$$Cost_{PE} = 2.85 \cdot \left(Q_y\right)_{24} + 8.50 \cdot \left(Q_y\right) \quad (17)$$

### *3.3. Denitrifier*

The limit for NOx concentration in the flue gas in the Spanish law is 600 mg/$Nm^3$ (BOE, 2004). Therefore, the concentration of NOx in the flue gas after processing must be below this limit.

#### *3.3.1. Selective catalytic reduction (SRC)*

The location for the denitrifier technology in the flue gas treatment chain depends on the source of the flue gas. Coal thermal plants generate flue gases that contain high concentration of dust. To process these kind of flue gases, the selective catalytic denitrifier (SCR), is typically located just after the boiler and

before the elec- trostatic precipitator (SRC_1) (Sorrels et al., 2016). Alternatively, tail end denitrifier technology can also be used (SRC_2). This option requires flue gas reheating. To provide generality to the superstructure we consider both alternatives for the location of the SCR technology. In both cases the reduction of NOx takes place using $NH_3$ following the reactions given by eq. (18). Before the SRC, the temperature must be adjusted using a heat exchanger so that the operating temperature ranges within 545-650 K (Mussatti et al., 2002). The ammonia is fed at 423 K with a composition of 99.5% ammonia and the rest dry air (Sorrels et al., 2015). An excess of ammonia with respect to the stoichiometric is used, typically 5% (Rosenberg and Oxley, 1993).

$$\begin{aligned} 4NO + 4NH_3 + O_2 &\rightarrow 4N_2 + 6H_2O \\ 2NO_2 + 4NH_3 + O_2 &\rightarrow 3N_2 + 6H_2O \end{aligned} \quad (18)$$

Oxygen is added using an air to ammonia ratio of 20:1, to work below flammability limits (Sorrels et al., 2016). The air is assumed to be atmospheric air with moisture. The removal yield, or the conversion of the reactions, is a function of the temperature as given by a figure in Rosenberg and Oxley (1993).We developed a correlation to predict the removal efficiency as a function of temperature as follows, eq. (19). Good fitting between the data and the equation is achieved:

$$\eta = 6.6537 \cdot 10^{-6} \cdot T(K)^3 - 1.523 \cdot 10^{-2} \cdot T(K)^2 + 11.43 \cdot T(K) - 2,731.8 \quad (19)$$

The SRC is modeled based on the stoichiometry of the reactions taking place, eq. (18), the conversion as a function of the operating temperature, eq. (19), a mass balance accounting for the fed of $NH_3$ and additional air, and an adiabatic energy balance (Martín, 2016).

The investment cost of this unit is estimated using the correlation from Miller (2015), eq. (20), where $m_{NOx}$ is tons processed in a year of NOx:

$$Cost_{SCR} = 5,000 \cdot \frac{1}{0.8} \left( m_{NOx} \cdot (1 - \eta_{SCR}) \right) \quad (20)$$

### *3.3.2. Selective non catalytic reduction (SNCR)*

The SNCR is actually installed within the boiler since it requires high operating temperatures. In our model the SNCR is located between zone 1 and zone 2. This region corresponds to the section of the boiler that produces overheated steam for the turbine. The operating temperature is the same as that

computed for the boiler. We can use ammonia or urea. However, the use of urea increases the production of $N_2O$ and ammonia is used instead. The chemical reactions for the reduction of the NOx are the same as those presented for the SCR technology, eq. (18). However, in this case the removal efficiency depends on the excess of ammonia (Sorrels et al., 2016). Ammonia is fed to the boiler with an air to ammonia ratio of 20:1, to avoid safety issues (Sorrels et al., 2016). The air is atmospheric humid air and ammonia is provided with the same composition as before, 99.5 ammonia and the rest dry air (Sorrels et al., 2016).

The SNRC is modeled based on the stoichiometry of the reactions taking place, eq.(18), accounting for the feed of $NH_3$ and additional air, the yield as a function of the excess of ammonia, eq.(21), and an adiabatic energy balance for streammixing because we neglect the reaction heat due to the small amount of NOx in the stream. An empirical model is developed to predict the removal yield, eq. (21), using experimental data in a figure by Dobrei. The removal efficiency is correlated versus the stoichiometric excess of ammonia, η. Good fitting between eq. (21) and the data is achieved.

$$NH_{3,excess} = 0.0267 \cdot \eta - 0.0202 \quad (21)$$

The investment cost is estimated using the information in Miller (2015), where mNOx is tons of NOx processed in a year.

$$Cost_{SCR} = 2,500 \cdot \frac{1}{0.8} \left( m_{NOx} \cdot (1 - \eta_{SCR}) \right) \quad (22)$$

### *3.4. Desulfuration*

The target for $SO_2$ in the flue gas exiting the treatment is 200 mg/Nm$^3$ according to the Spanish regulations (GasNatural Fenosa, 2015). LFSO and LSD operate at a reduced temperature. Thus, heat exchangers are used to adjust the temperature before treatment.

#### *3.4.1. Wet removal (LFSO)*

The optimal operating temperature is 323 K (Sargent and Lundy, 2003). Thus, a heat exchanger is needed to cool down the flue gas before feeding it to the absorber column. The mechanism for the removal of $SO_2$ using a wet process follows the reactions below, eq. (23), where $SO_2$ is treated with limestone and the product is oxidized to gypsum (Kohl and Nielsen, 1997).

$$
\begin{aligned}
&SO_2 + CaCO_3 + \frac{1}{2}H_2O \rightarrow CaSO_3 \cdot \frac{1}{2}H_2O \downarrow + CO_2 \\
&CaSO_3 \cdot \frac{1}{2}H_2O + \frac{1}{2}O_2 + \frac{3}{2}H_2O \rightarrow CaSO_4 \cdot 2H_2O \downarrow \\
&2HCl + CaCO_3 \rightarrow CaCl_2 \downarrow + H_2CO_3 \\
&2HF + CaCO_3 \rightarrow CaF_2 \downarrow + H_2CO_3 \\
&H_2CO_3 \rightarrow H_2O + CO_2
\end{aligned}
\qquad (23)
$$

To obtain gypsum, a 3 to 1 ratio of moles of $O_2$ to $SO_2$ is needed [60]. The removal efficiency depends on the ratio between the flue gas flowand the slurry containing the $CaCO_3$. Typically, a slurry 20% w/w of $CaCO_3$ is used (Zhong et al., 2008). Using the experimental data in Zhong et al. (2008), we developed a surrogate model to estimate the removal ratio as a function of the liquid to gas ratio given in liters per $Nm^3$ of gas, eq. (24). Good fitting with the experimental data is obtained.

$$\eta = -5.06993 \cdot 10^{-4} \left(\frac{L}{G}\right)^2 + 2.591958 \cdot 10^{-2} \cdot \left(\frac{L}{G}\right) + 0.653958042 \qquad (24)$$

The LSFO process is modeled using a mass balance based on the stoichiometry of the reactions shown above, eq. (23), the removal efficiency as a function of the (L/G) ratio, eq. (24), and an adiabatic energy balance to compute the exit temperature. The gas exits the unit saturated at the operating temperature. Antoine correlation is used to compute the moisture in the flue gas.

The investment cost of the technology is estimated by the $SO_2$ eliminated in tons per year (Miller, 2015) using eq. (25):

$$Cost_{LFSO} = 3,700 \cdot \left( \left( m_{SO_2} \right) \cdot \left( 1 - \eta_{LFSO} \right) \right) \qquad (25)$$

### *3.4.2. Dry removal (LSD)*

Dry removal uses a CaO slurry with 35% of water to the spray tower. The feed temperature must be between 393 K and 448 K. The reaction mechanism is as follows, eq. (26) (Hayton, 2015):

$$CaO + H_2O \rightarrow Ca(OH)_2$$
$$SO_2 + Ca(OH)_2 \rightarrow CaSO_3 \cdot \frac{1}{2} H_2O + \frac{1}{2} H_2O$$
$$SO_2 + Ca(OH)_2 + H_2O + \frac{1}{2} O_2 \rightarrow CaSO_4 \cdot 2H_2O \quad (26)$$
$$2HCl + Ca(OH)_2 \rightarrow CaCl_2 \downarrow + 2H_2O$$
$$2HF + Ca(OH)_2 \rightarrow CaF_2 \downarrow + 2H_2O$$

The typical molar ratio CaSO3 to CaSO4 is 9:1, because the absence of forced oxidation leads to a low yield of gypsum (Farber, 1986). The removal efficiency depends on the fraction of S in the coal and the stoichiometric molar ratio between Ca and S. A two-stage fitting procedure (Martín and Martín, 2013) is used to produce a general model considering both variables. A range of sulfur concentrations, %S, from 2.5 to 6% and Ca/S ratios of 0.7e1.5 are common and will be imposed as lower and upper bounds for these variables. Eq. (27) shows good fitting with the experimental data.

$$\eta = \left(-0.4554 \cdot (\%S) + 1.2451\right) + \left(0.3469 \cdot (\%S) + 0.6286\right) \cdot \left(\frac{Ca}{S}\right) + \left(-0.0243 \cdot (\%S) - 0.56325\right) \cdot \left(\frac{Ca}{S}\right)^2 \quad (27)$$

The LSD process is modeled using a mass balance based on the stoichiometry of the reactions shown above, eq. (26), the removal efficiency, eq. (27), and an adiabatic energy balance. The gas exits the unit saturated at the temperature, typically from 338 K to 448 K. Antoine correlation is used to compute the moisture in the flue gas. The investment cost of the technology is estimated as a function of the $SO_2$ eliminated in tons per year (Miller, 2015).

$$Cost_{LDS} = 4,400 \cdot \left( \left( m_{SO_2} \right) \cdot \left( 1 - \eta_{LFSO} \right) \right) \quad (28)$$

### *3.5. Solution procedure*

The optimization of the gas treatment chain presents several steps. After the pre-screening of technologies based on industrial experience, a model for a superstructure with the most used/promising ones is formulated. Surrogate models for all units are developed as presented along section 3.

We consider two steps in the solution of the mathematical problem, namely, technology selection and operation.

The first step corresponds to a design problem. We formulate the problem as a large non-linear programming (NLP) for the optimal selection of technologies for a fixed carbon feed to the boiler. Due to the complexity of the non-linear models we avoid the use of integer variables by allowing bypasses. The optimization uses an economic objective function since the aim is to be able to meet the current limits imposed by the legislation.We consider a typical mix of coals based on actual data of a particular day. The model is 4500 var and 4100 eqs, written in GAMS and solved using a multistart procedure with CONOPT. 3.0 as the preferred solver with eq.(29) as the objective function.

$$Cost_{Anual} = \frac{1}{3}\left(\text{Cost}_{SCR\_1} + \text{Cost}_{PE} + \text{Cost}_{LSD} + \text{Cost}_{LFSO}\right) + \text{Cost}_{NH3} + \text{Coste}_{CaCO3} \quad (29)$$

Once the technologies are installed in a facility, the market and/or political decisions are behind the selection of the coal or coal blend to be processed. Thus, the second step is the everyday problem that the managers of the plants must solve on the decision on the coal blend to burn. An extending blending problem is formulated for the optimal set of technologies to select on the optimal coal blend used including the detail models for the flue gas treatment technologies.

Two different objective functions are used. First, we consider the treatment costs. The model is slightly smaller than the entire superstructure, 3100 var and 2800 eqs. written in GAMS and solved using a multistart procedure with CONOPT. 3.0 as the preferred solver using eq. (30) as objective function.

$$Cost_{Anual} = \frac{1}{3}\left(\text{Cost}_{SCR\_1} + \text{Cost}_{PE} + \text{Cost}_{LSD} + \text{Cost}_{LFSO}\right) + \text{Cost}_{NH3} + \text{Cost}_{CaCO3} + \text{Cost}_{NatCoal} + \text{Cost}_{\text{ImpCoal}} + \text{Cost}_{\text{FuelCoal}} \quad (30)$$

Finally, the different heating values of the various coals provide another interesting tradeoff. Even though in this work the power island of the plant is not considered, in eq. (30) we add the benefit of the power produced by each coal type. Assuming 50% efficiency from thermal energy to power, based on the ratio of the actual power capacity of the plant (350-400 MW) and the thermal energy involved in the coal blends used (700-780 MW), and an electricity price of 0.07 V/kWh we reevaluate the blending problem. The size of the blending model remains the same, 3100 var and 2800 eqs. written in GAMS and solved with eq. (31) as objective function using a multistart procedure with CONOPT. 3.0 as the preferred solver.

$$Cost_{Anual} = \frac{1}{3}\left(Cost_{SCR\_1} + Cost_{PE} + Cost_{LSD} + Cost_{LFSO}\right) + Cost_{NH3} + Cost_{CaCO3} + \sum_{i \in coal} Cost_{coal} - P_{Electricity} \cdot \eta_{TtoE} \cdot \sum_{i \in coal} HHV_i \cdot Coal_i \quad (31)$$

## 4. Results

We consider the use of three types of coal, national, imported and crude tar coal. The compositions and the prices are presented in Table 3.1. A feed of 23 kg/s of coal or coal mixture is used as reference for a typical production capacity of around 350-400 MWe (La Robla, 2017). To compute the flue gas exiting the boiler, the temperature profile provided in the literature was used (Al-Abbas et al., 2012). Other examples from the literature have also been studied with average temperatures within 5% error (Ma et al., 2016). The resulting flue gas composition was corroborated with industry to validate the model (BOE, 2004; La Robla, 2017). This section is divided in two. The first one presents the process design problem. The second one presents an extended coal blending problem evaluating the selection of technologies as a function of the coal mixture.

***Table 3.1*** Coal composition and price

| | National[1] | Imported[2] | Crude coal tar[2] |
|---|---|---|---|
| $H_2O$ | 0.1357 | 0.0988 | 0.1038 |
| $C$ | 0.688493 | 0.705099 | 0.779552 |
| $H_2$ | 0.022585 | 0.030706 | 0.03033 |
| $O_2$ | 0.000165 | 0.000579 | 0.021109 |
| $S$ | 0.018631 | 0.004351 | 0.041942 |
| $N_2$ | 0.013844 | 0.018164 | 0.017093 |
| $Cl$ | 0.000140 | 0.00012 | 0.00004 |
| $F$ | 0.000072 | 0.000076 | 0.000017 |
| Ash | 0.12037 | 0.142105 | 0.006117 |
| Price (€/t) | 69.36 | 103.3 | 23.59 |
| PCS(kcal/kg) | 6,311 | 6,716 | 8,475 |

1: (Nichols and McCain, 1975) 2:(Sorrels et al., 2016)

### *4.1. Process design*

The superstructure in Figure 3.1 is applied to a particular case based on data provided from a power plant in the Northwestern of Spain, La Robla, using a coal blend of 26% national, 26% imported and the rest crude coal tar. This blend shows an availability of 717MW. The optimization of the superstructure in Figure 3.1 for this case, selects the use of selective catalytic reduction and dry removal of $SO_2$ using LSD. However, in some of the units there is a fraction of the total flow of flue gas that is not processed through

the units, but a bypass is suggested, see Table 3.2. The results are reported per thermal energy available in the coal or coal blend used in each case.

***Table 3.2*** Costs of the units selected by case

| Costs | PE (€/kW) | NOx Removal (€/kW) | $SO_2$ Removal (€/kW) | Total (M€/yr) |
|---|---|---|---|---|
| *Superstructure* | 10.691 | 142.633 | 200.651 | 94.5 |
| *Bypass not processed* | | 16% | 1% | |

The solution to the superstructure in Figure 3.1 involves the selection of PP followed by SCR and LSD. However, 16% of the flue gas is not fed to the SCR and it is suggested that 1% of the flow is not fed to the LSD. The decision on the installation of fractional bypasses to the desulphurizer and denitrifier is difficult to be implemented in industry. It is easier to process the entire flow of flue gas through the units. Therefore, instead of solving the mathematical model for the entire Figure 3.1, we consider four flowsheets consisting of the combination among the two deNOx and the two deSOx removal technologies, disregarding the use of the deNOx by the end of the processing train.

In Table 3.3 we compare the solution to the four main alternative flowsheets without the possibility of bypass. It is possible to see that the values of the objective function, column Total (MV/yr) in the table, are of the same order of magnitude as those in Table 3.2. Futhermore, the optimal solution involves the same technologies and in the same order as described in the solution of the complete superstructure given by Figure 3.1, SCR and LSD. The main operating conditions for the units are presented in Table 3.4.

***Table 3.3*** Costs of the units selected by case

| Costs | PE (€/kW) | NOx Removal (€/kW) | $SO_2$ Removal (€/kW) | Total (M€/yr) |
|---|---|---|---|---|
| *SCR_1 + LFSO* | 12.114 | 171.438 | 165.690 | 96 |
| *LFSO + SCR_2* | 11.735 | 228.015 | 165.690 | 135 |
| *SCR_1 + LSD* | 10.592 | 142.640 | 200.671 | 89 |
| *LSD + SCR_2* | 10.427 | 181.328 | 200.580 | 123 |

***Table 3.4*** Main operating conditions

| | Electrostatic Precipitator (PE) | NOx Removal | $SO_2$ Removal |
|---|---|---|---|
| *SCR_1 + LFSO* | Yield:100 | □ 72.667<br>T(K)= 580.457 | L/G: 15<br>□=0.929 |
| *LFSO + SCR_2* | Yield:100 | □ 83.263<br>T(K)= 608.5 | L/G:15<br>□ 0.929 |
| *SCR_1 + LSD* | Yield:100 | □ 89.240<br>T(K)= 638.446 | Ca/S= 0.949<br>□ =0.946 |
| *LSD + SCR_2* | Yield:100 | □ 74.241<br>T(K)= 583.9 | Ca/S=0.931<br>□=0.956 |

The differences in the objective function using LFSO or LSD are within 10% margin for the coal blend used in this case study. However, it is more interesting to use the catalytic removal of NOx before the electrostatic precipitator than any other alternative for the removal of NOx. Actually, the cost for the removal of NOx is the same no matter the location of the unit. The main difference is that by the end of the processing train the flue gas is already cold and thermal energy is required to heat up the flue gas, reducing the efficiency of the plant. In terms of the operating conditions, see Table 3.4, the removal ratio of NOx is always above 70% and the variability in the yield is related to the removal ratio required to meet the emission limits. In the case of the removal of $SO_2$, the optimal operation conditions are always the same for the technology no matter the option selected for the removal of NOx. Note that we do not claim global optimum.

### *4.2. Coal selection: blending problem*

The blending problem is analyzed considering a fixed flowsheet consisting of the SCR, PE and either LFSO or LSD. Four items are considered in this analysis: 1) Optimal blend as a function of the cost of processing the emissions. 2) Cost of the coals so that the national one is selected. 3) Cost of the technology for the selection of the national coal and 4) Optimal blend for maximum power production with emissions limitations. Taking into account that around 85% of the industrial plants already have LFSO technologies installed, including La Robla thermal plant, Leon (Spain), we will be considering this technology first for our evaluation of the optimal blend considering the three coals presented in Table 3.1. In a second case, the LSD technology is also evaluated following the same procedure.

Thus, we optimize first the coal selection among the national coal from Spain, the imported coal and crude coal tar, using eq. (30) as objective function. The flue gas treatment train consists of SCR followed by PE and the LFSO desulphurizer technology. The tradeoff corresponds to the coal cost versus its sulfur content. It turns out that the optimization selects the imported coal. No blend is selected. In spite of being the most expensive coal, see Table 3.5, the operating costs of the facility including the flue gas processing are the lowest. In Table 3.5 it is possible to see that the cost of the LFSO process for $SO_2$ removal is 4 times larger when using the national coal compared to the use of imported one mitigating the difference in the cost of the raw materials, which results in a small difference in the total operating cost.

***Table 3.5*** Cost for gas processing for the various coal types.

| | Coal (€/t) | SCR 1 (€/kW) | LFSO (€/kW) | TAC (M€) | €/ MWh | NOx remov (kg/s) | $SO_2$ remov (kg/s) |
|---|---|---|---|---|---|---|---|
| *National* | 69.36 | 153.123 | 138.204 | 116.849 | 410.4 | $6.45 \cdot 10^{-4}$ | 0.786 |
| *Imported* | 103.3 | 144.542 | 30.329 | 114.457 | 385.2 | $6.48 \cdot 10^{-4}$ | 0.184 |
| *Crude coal* | 23.59 | 128.011 | 231.683 | 132.132 | 352.8 | $7.24 \cdot 10^{-4}$ | 1.77 |

Based on these results, a sensitivity analysis was carried out to determine the critical price of the imported coal so that national coal was preferred. It turns out that for a price of imported coal from 107.4 V/t, national coal is preferred. Thus, for imported coal prices 4% above the current value, national coal can be competitive. The cost of the treatment technologies also evolves in time.

Apart from evaluating the critical cost for imported coal, the effect of the cost of the technology on the coal selection is also evaluated. By performing a sensitivity analysis, the cost for LFSO technology must decrease by 12.5% with respect to the base case provided by eq. (25) for national coal to be preferable. Thus, by technology development and optimization it would be attractive to use national coal. These two issues, coal price and treatment technology costs, have many social implications. Many families in the Northwest region of Spain live by the coal and related industries. After generations, the expertise is in coal industry and mining operations. Therefore, either the operators are trained otherwise, or we provide a more efficient and cost-efficient sulfur removal process. Alternatively, subsidies can be provided so that the economic advantage of using imported coal is mitigated. Note that these solutions are local, not global optimization is claimed and therefore further studies can be carried out.

The energy per kg of coal is inversely related to the sulfur content in these three coals. As a result, the crude coal tar, in spite of presenting large costs for desulfurization, is the one that shows the best cost per unit of power produced, as seen in Table 3.5. The blending problem is solved for a different objective function that includes the power produced as benefit, eq. (31). By solving the updated blending problem with eq. (31) as objective function, it turns out that the optimal blend consists of 25% imported coal and the rest crude coal tar. Table 3.6 summarizes the breakdown of the treatment cost and the total amount of $SO_2$ and NOx removed. Note that the power within the coal blend is 773MW, 7% larger that the base case used in the design study. Using this objective function, for national coal to be used the cost of imported coal must

be around twice its current cost. A more integrated approach including the evaluation of the power cycle is to be added.

***Table 3.6*** Cost for gas processing for mixed of coals using LFSO: Economic objective

| | N/I/C | PE(€/kW) | SCR 1 (€/kW) | LFSO (€/kW) | TAC (M€) | €/ MWh | NOx remov (kg/s) | $SO_2$ remov (kg/s) |
|---|---|---|---|---|---|---|---|---|
| *Mixed* | 0/25/75 | 10.280 | 91.880 | 193.941 | -100.12 | -281.6 | $4.925 \cdot 10^{-04}$ | 1.405 |

A similar study is carried out for considering the LSD technology for the removal of $SO_2$. The particular feature of this technology is its lower removal yield. The optimization of the blending problem using eq. (30) as objective function results in selecting imported coal. Table 3.7 shows the performance and the cost of processing the flue gas using LSD. Comparing Tables 3.5 and 3.7 it can be seen that the use of LFSO technologies is cheaper than using LSD technologies when particular coals are used. Furthermore, in spite of the lower cost of the crude coal tar, its larger content in sulfur does not allow meeting the environmental constraints. Again, for national coal to be used the cost of imported coal must be around twice its current cost and it is difficult that a decrease in the cost of the LSD technology makes the use of national coal preferable. Finally, the blending problem is solved again using eq. (31) to evaluate the trade-off between sulfur content and power production of the various coal types. The solution of the model suggests the use of a combination of 58% imported and the rest crude tar coal. This blend contains the same power that the original blend used in the design case study, 717MW. Note that no global optimum can be claimed. The main operating results are summarized in Table 3.8. The largest $SO_2$ removal yield achieved using the LFSO technology results in larger profit using this alternative. As a result, LFSO is the best technology among the two for a wider range of blending ratios.

***Table 3.7*** Cost for gas processing for the various coal types.

| | Coal (€/t) | SCR 1 (€/kW) | LSD (€/kW) | TAC (M€) | €/MWh | NOx remov (kg/s) | $SO_2$ remov (kg/s) |
|---|---|---|---|---|---|---|---|
| *National* | 69.36 | 158.984 | 167.593 | 125.693 | 450 | $6.69 \cdot 10^{-4}$ | 0.802 |
| *Imported* | 103.3 | 149.501 | 36.202 | 117.19 | 396 | $6.70 \cdot 10^{-4}$ | 0.184 |
| *Crude coal tar* | 23.59 | Does not meet environmental limits | | | | | |

***Table 3.8*** Cost for gas processing for mixed of coals using LSD: Economic objective

| | N/I/C | PE (€/kW) | SCR 1 (€/kW) | LSD (€/KkW) | TAC (M€) | €/MWh | NOx remov (kg/s) | $SO_2$ remov (kg/s) |
|---|---|---|---|---|---|---|---|---|
| *Mixed* | 0/58/42 | 10.721 | 141.372 | 153.297 | -69.967 | -212.110 | $7.031 \cdot 10^{-4}$ | 0.866 |

## 5. Conclusions

In this work we have developed a flexible framework for the optimal selection of flue gas treatment technologies. The extended framework allowed formulating a blending problem that includes process models to evaluate the selection of the coal and the critical prices resulting in a useful tool for decision makers in the power industry. The framework is based on a mathematical optimization approach that models each of the units using surrogate models based on first principles and industrial data developing a superstructure of alternative technologies, catalytic and non-catalytic NOx abatement, particle removal and $SO_2$ removal using wet and dry systems, aiming at minimum total annual cost for flue gas processing. Further CFD modelling of the boiler can be performed as a preliminary stage.

This general framework is used to evaluate the optimal gas treatment technologies in a power plant in Spain for particle, NOx and $SO_2$ removal the operating conditions as well as the limits that would allow selecting the use of local coal in terms of coal price and technology cost. The optimal train of operation consists of the use, in this order, of catalytic NOx removal, an electrostatic precipitator and LSD $SO_2$ removal. However, this solution is for a particular coal blend. Considering the most typical technology, LFSO, imported coal is the preferred raw material, but if its price increases by 4%, national coal becomes the raw material of choice. Alternatively, a 12.5% decrease in the cost of LFSO also suggests the use of national coal which means that it could be possible to maintain the local industry. If the energy available in the coal is also considered, crude tar coal is included in the blend up to 75% and the rest imported coal so that the $SO_2$ emissions are maintained within the legal limits. The larger removal yield from the LFSO provides flexibility and shows larger benefits when using this technology. Therefore, this is the technology of choice for general use.

## 6. List of acronyms and abbreviations

$Cost_i$: Cost of item i (V/unit)
K: Kinetic constant ($m^3$/mol s)
K: Equilibrium constant ($bar^n$)
ESP: Electrostatic precipitator
FAME: Fatty acid methyl ester
FT: Fischer - Tropsch

(L/G): In L of liquid solution per $m^3$ of gas

$m_i$: tons per year of contaminant (t/yr)

$n_i$: Molar flow of species I (mol/s)

$n_{Particle}(d)$: Number of particles of sized d

$NH_3$ excess: Molar excess of ammonia with respect to the stoichiometric one

NLP Non linear programming

NPK Nitrogen e Phosphorous-Potassium

$P_i$: Partial pressure of species i (bar)

$P_{Electricity}$: Electricity price (V/kWh)

PS: Particle size distribution

$Q_y$: Volume of gas ($Nm^3$) processed in a year ($Nm^3$/yr)

T: Temperature (K)

*Symbols*

$\eta_i$: Fraction of area of section i

$\eta_j$: Removal efficiency of technology j

$\eta_{TtoP}$: Thermal to power efficiency

$\phi$: Particle size (mm)

*Abbreviations*

BG: Filter

Div: Splitter

CT: Cooling tower

HP: High pressure turbine

HX: Heat Exchanger

LP: Lower pressure turbine

LSD: Spray dry scrubbers

LSFO: Limestone Forced Oxidation

MP: medium pressure turbine

Mx: Mixter

PE: Electrostatic precipitator

SRC: Selective catalytic reduction of NOx SRC_1 After boiler

SRC_2: After desulfurization

SNCR: Selective non-catalytic reduction of NOx TA Absorption tower

TL: Tank

## 7. References


Adams, T., Mac Dowell, N., 2016. Off-design point modelling of a 420MW CCGT power plant integrated with an amine-based post-combustion CO2 capture and compression process. Applied Energy 178, 681–702. https://doi.org/10.1016/j.apenergy.2016.06.087

Al-Abbas, A.H., Naser, J., Dodds, D., 2012. CFD modelling of air-fired and oxy-fuel combustion in a large-scale furnace at Loy Yang A brown coal power station. Fuel 102, 646–665. https://doi.org/10.1016/j.fuel.2012.06.028

Alie, C., Douglas, P., Croiset, E., 2004. Simulation and optimization of a coal-fired power plant with integrated CO2 capture using MEA scrubbing.

Ameri, M., Mokhtari, H., Mostafavi Sani, M., 2018. 4E analyses and multi-objective optimization of different fuels application for a large combined cycle power plant. Energy 156, 371–386. https://doi.org/10.1016/j.energy.2018.05.039

BOE, 2004. Real Decreto 430/2004, BOE 69, de 20 de marzo de 2004.

Brunnemann, J., Gottelt, F., Wellner, K., Renz, A., Thüring, A., Roeder, V., Hasenbein, C., Schulze, C., Schmitz, G., Eiden, J., 2012. Status of ClaRaCCS: Modelling and Simulation of Coal-Fired Power Plants with CO2 Capture. https://doi.org/10.3384/ecp12076609

Cebrucean, D., Cebrucean, V., Ionel, I., 2017. Modeling and Evaluation of a Coal Power Plant with Biomass Cofiring and CO2 Capture. pp. 31–55. https://doi.org/10.5772/67188

Churi, N., Achenie, L.E.K., 1997. The optimal design of refrigerant mixtures for a two-evaporator refrigeration system. Computers & Chemical Engineering 21, S349–S354. https://doi.org/10.1016/S0098-1354(97)87526-6

Clean Air Technology Center, 1999. Nitrogen oxides (NOx). Why and how they are controlled. (Technical bulletin No. EPA-456/F-99-006R). Environmental Protection Agency.

Conte, E., Gani, R., Ng, K.M., 2011. Design of formulated products: A systematic methodology. AIChE Journal 57, 2431–2449. https://doi.org/10.1002/aic.12458

Dobrei, G., n.d. Analysis of the measures for NOx emissions reduction resulting from fossil fuel burning at deva thermal power plant for compliance with the EU environmental standard. URL https://www.upet.ro/simpro/2014/proceedings/01%20-%20SAFETY%20AND%20ENVIRONMENT%20ENGINEERING/1.9.pdf Last accessed March 2018.

Dolman, H. (A. J.), Valentini, R., Freibauer, A., 2008. The Continental-Scale Greenhouse Gas Balance of Europe. https://doi.org/10.1007/978-0-387-76570-9

Dowling, A.W., Eason, J.P., Ma, J., Miller, D.C., Biegler, Lorenz.T., 2014. Coal Oxycombustion Power Plant Optimization Using First Principles and Surrogate Boiler Models. Energy Procedia 63, 352–361. https://doi.org/10.1016/j.egypro.2014.11.038

EL Hefni, B., Bouskela, D., Lebreton, G., 2011. Dynamic modelling of a combined cycle power plant with ThermoSysPro. https://doi.org/10.3384/ecp11063365

EPA, 2003. EPA. Air pollution control technology fact sheet. EPA. URL https://www3.epa.gov/ttn/catc/dir1/ffdg.pdf

Farber, P.S., 1986. Production and disposal of wastes from dry and wet flue-gas cleaning systems. Energy 11, 1347–1356. https://doi.org/10.1016/0360-5442(86)90071-X

Gajbhiye, N., Eswaran, V., Saha, A.K., Kumar, A., 2015. Numerical calculation of particle collection efficiency in an electrostatic precipitator. Sadhana 40, 863–873. https://doi.org/10.1007/s12046-015-0342-1

GasNatural Fenosa, 2015. Central térmica La Robla (Leaflet).

Grassi, G., Collina, A., Zibetta, H., 1992. Biomass for Energy, Industry and Environment: 6th EC Conference. Oxford: Elsevier.

Grossmann, I., Caballero, J., Yeomans, H., 2000. Advances in mathematical programming for the synthesis of process systems. Latin American Applied Research 30.

Habib, M.A., Elshafei, M., Dajani, M., 2008. Influence of combustion parameters on NOx production in an industrial boiler. Computers & Fluids 37, 12–23. https://doi.org/10.1016/j.compfluid.2007.04.006

Hayton, J., 2015. Thermal power plant. Elsevier, Amsterdam.

Hentschel, J., Zindler, H., Spliethoff, H., 2017. Modelling and transient simulation of a supercritical coal-fired power plant: Dynamic response to extended secondary control power output. Energy 137, 927–940. https://doi.org/10.1016/j.energy.2017.02.165

Hernández, B., León, E., Martín, M., 2017. Bio-waste selection and blending for the optimal production of power and fuels via anaerobic digestion. Chemical Engineering Research and Design 121, 163–172. https://doi.org/10.1016/j.cherd.2017.03.009

Hernández, B., Martín, M., 2017. Optimal Integrated Plant for Production of Biodiesel from Waste. ACS Sustainable Chem. Eng. 5, 6756–6767. https://doi.org/10.1021/acssuschemeng.7b01007

Jess, A., Wasserscheid, P., 2013. Chemical Technology. An Integral Textbook. Wiley-VCH.

KED. http://www.powerplantsimulator.com/. [Accessed March 2018].

Kikkawa, H., Ishizaka, H., Kai, K., Nakamoto, T., 2008. DeNOx, DeSOx, and CO2 removal technology for power plant 57, 174–178.

Kohl, A.L., Nielsen, R.B., 1997. Chapter 8 - Sulfur Recovery Processes, in: Kohl, A.L., Nielsen, R.B. (Eds.), Gas Purification (Fifth Edition). Gulf Professional Publishing, Houston, pp. 670–730. https://doi.org/10.1016/B978-088415220-0/50008-2

Kumar, P.R., Raju, V.R., Kumar, N.R., 2016. Simulation and parametric optimisation of thermal power plant cycles. Perspectives in Science 8, 304–306. https://doi.org/10.1016/j.pisc.2016.04.060

La Robla staff personal communication., 2017.

Laird, C., Smith, K., 2017. Results of dry sorbent injection testing to reduce HCl. Carmeuse Lime & Stone, Technology Center;

Li, Z., Miao, Z., Zhou, Y., Wen, S., Li, J., 2018. Influence of increased primary air ratio on boiler performance in a 660 MW brown coal boiler. Energy 152, 804–817. https://doi.org/10.1016/j.energy.2018.04.001

Luo, X., Hu, J., Zhao, J., Zhang, B., Chen, Y., Mo, S., 2014. Multi-objective optimization for the design and synthesis of utility systems with emission abatement technology concerns. Applied Energy 136, 1110–1131. https://doi.org/10.1016/j.apenergy.2014.06.076

Luo, X., Zhang, B., Chen, Y., Mo, S., 2012. Operational planning optimization of multiple interconnected steam power plants considering environmental costs. Energy 37, 549–561. https://doi.org/10.1016/j.energy.2011.10.049

Ma, J., Eason, J.P., Dowling, A.W., Biegler, L.T., Miller, D.C., 2016. Development of a first-principles hybrid boiler model for oxy-combustion power generation system. International Journal of Greenhouse Gas Control 46, 136–157. https://doi.org/10.1016/j.ijggc.2015.12.036

Martín, L., Martín, M., 2013. Optimal year-round operation of a concentrated solar energy plant in the south of Europe. Appl. Therm. Eng. 59, 627–633. https://doi.org/10.1016/j.applthermaleng.2013.06.031

Martín, M., Grossmann, I.E., 2013. Optimal engineered algae composition for the integrated simultaneous production of bioethanol and biodiesel. AIChE Journal 59, 2872–2883. https://doi.org/10.1002/aic.14071

Martín, M., Martínez, A., 2013. A methodology for simultaneous process and product design in the formulated consumer products industry: The case study of the detergent business. Chemical Engineering Research and Design 91, 795–809. https://doi.org/10.1016/j.cherd.2012.08.012

Martín, Mariano, Martín, Mónica, 2017. Cooling limitations in power plants: Optimal multiperiod design of natural draft cooling towers. Energy 135, 625–636. https://doi.org/10.1016/j.energy.2017.06.171

Martín, M.M., 2016. Industrial Chemical Process Analysis and Design. Elsevier, Boston. https://doi.org/10.1016/B978-0-08-101093-8.00012-4

Miller, B., 2015. Fossil Fuel Emissions Control Technologies. Stationary Heat and power systems. Butterworth-Heinemann.

Mitsubishi hitachi power systems, 2017. . Mitsubishi hitachi power systems. URL https://www.mhps.com/en/ products/category/flue_gas_desulfurization.html

Mussatti, D., Vatavuk, W., Klotz, W., Stallings, R., Srivastava, R., Hemmer, P., Straight, R., Turner, J., McKenna, J., Mycock, J., Nunn, A., Lawless, P., Tamamoto, T., Coy, D., Greiner, G., 2002. Air pollution control cost manual. (No. EPA 452/B-02-002.).

Nazaroff, W.W., Alvarez-Cohen, L., 2000. Environmental Engineering Science.

Nichols, G.B., McCain, J.D., 1975. Particulate collection efficiency measurements on three electrostatic precipitators. Final report, Jul 1973--Jul 1975. United States.

NLWA. North London heat and power project e flue gas treatment plant options. 2014. URL http://northlondonheatandpower.london/documents/141117_NLWA_Flue_Gas_Treatment_Technology_Options_Consultation_V1.pdf

Nóbrega, S.W., Falaguasta, M.C.R., Coury, J.R., 2004. A study of a wire-plate electrostatic precipitator operating in the removal of polydispersed particles. Brazilian Journal of Chemical Engineering 21, 275–284. https://doi.org/10.1590/S0104-66322004000200018

Ong'iro, A., Ugursal, V.I., Al Taweel, A.M., Lajeunesse, G., 1996. Thermodynamic simulation and evaluation of a steam CHP plant using ASPEN Plus. Applied Thermal Engineering 16, 263–271. https://doi.org/10.1016/1359-4311(95)00071-2

Rahmanian, B., Safaei, M.R., Kazi, S.N., Ahmadi, G., Oztop, H.F., Vafai, K., 2014. Investigation of pollutant reduction by simulation of turbulent non-premixed pulverized coal combustion. Applied Thermal Engineering 73, 1222–1235. https://doi.org/10.1016/j.applthermaleng.2014.09.016

Rosenberg, H.S., Oxley, J.H. [Battelle M.I., Columbus, OH (USA)], 1993. Selective catalytic reduction for NO[sub x] control of coal-fired power plants. United States.

Safaei, M.R., Rahmanian, B., Goodarzi, M., 2014. Investigation Of The Coal Diameter Effect On Pulverized Coal Combustion For Pollutant Reduction. J. Math. Comput. Sci. 12, 143–151. https://doi.org/10.22436/jmcs.012.02.06

Sanpasertparnich, T., Aroonwilas, A., 2009. Simulation and optimization of coal-fired power plants. Energy Procedia 1, 3851–3858. https://doi.org/10.1016/j.egypro.2009.02.187

Sargent, Lundy, L., 2003. Wet flue gas desulfurization technology evaluation project number 11311-000 prepared for national lime association.

Sarkar, D.K., 2015. Thermal Power Plant: Design and Operation. Elsevier, Amsterdam.

Shemwell, B.E., Ergut, A., Levendis, Y.A., 2002. Economics of an Integrated Approach to Control SO2, NOx, HCl, and Particulate Emissions from Power Plants. null 52, 521–534. https://doi.org/10.1080/10473289.2002.10470805

Shih, J.-S., Frey, H.C., 1995. Coal blending optimization under uncertainty. European Journal of Operational Research 83, 452–465. https://doi.org/10.1016/0377-2217(94)00243-6

Sorrels, J.L., Randall, D.D., Richardson-Fry, C., Schaffner, K.S., 2016. Selective Noncatalytic Reduction.

Sorrels, J.L., Randall, D.D., Richardson-Fry, C., Schaffner, K.S., 2015. Selective catalytic Reduction.

Wang, C., Liu, Y., Zheng, S., Jiang, A., 2018. Optimizing combustion of coal fired boilers for reducing NOx emission using Gaussian Process. Energy 153, 149–158. https://doi.org/10.1016/j.energy.2018.01.003

Weng, C.-K., Ray, A., Xiaowen, D., 1996. Modelling of power plant dynamics and uncertainties for robust control synthesis. Applied Mathematical Modelling 20, 501–512. https://doi.org/10.1016/0307-904X(95)00169-K

Xiong, J., Zhao, H., Chen, M., Zheng, C., 2011. Simulation Study of an 800 MWe Oxy-combustion Pulverized-Coal-Fired Power Plant. Energy Fuels 25, 2405–2415. https://doi.org/10.1021/ef200023k

Yeomans, H., Grossmann, I.E., 1999. A systematic modeling framework of superstructure optimization in process synthesis. Computers & Chemical Engineering 23, 709–731. https://doi.org/10.1016/S0098-1354(99)00003-4

Zhao, X., Wang, Y., 2009. Gasoline Blending Scheduling Based on Uncertainty, in: 2009 International Conference on Computational Intelligence and Natural Computing. pp. 84–87. https://doi.org/10.1109/CINC.2009.206

Zhong, Y., Gao, X., Huo, W., Luo, Z., Ni, M., Cen, K., 2008. A model for performance optimization of wet flue gas desulfurization systems of power plants. Fuel Processing Technology 89, 1025–1032. https://doi.org/10.1016/j.fuproc.2008.04.004

# *Chapter 4*

# Optimal Flue Gas Treatment for Oxy-Combustion-Based Pulverized Coal Power Plants

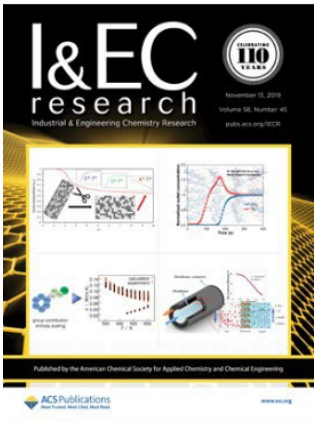


*Authors:* ***Lidia S Guerras*** *and Mariano Martín*

*DOI:* 10.1021/acs.iecr.9b04453

## Abstract

Oxy-combustion is recognized as the cleanest technology which uses coal as an energy source. Flue gas clean-up is essential for sustainable operation. In this work, the optimal selection of the flue gas treatment technologies in oxy-combustion power plants is determined. A two-stage procedure combining heuristics and mathematical programming is used to evaluate the technologies involved including the boiler, denitrification, electrostatic precipitation, sulfur dioxide removal, and carbon capture. For plant operation, the coal feed has to be selected. An extended blending problem is solved to evaluate the coal type to be purchased based on its cost and composition. The optimal flue gas processing consists of electrostatic precipitation, followed by dry $SO_2$ removal, and $CO_2$ purification using zeolites. No specific denitrification method is required due to the low concentration levels of NOx generated in oxy-combustion. This flowsheet is used to select one among a mixture of three different types of coal: national, imported, and crude coal tar. However, no mixture is recommended as crude coal tar was the one selected. Even though the processing costs are higher, it is outweighed by the lower cost of the raw material.

## 1.- Introduction

In spite of the penetration of renewable sources in the energy mix, coal still contributes to 40% of the world's total power production (The World Bank, 2014). Although several countries have issued regulations to reduce and even to eliminate coal in the power production sector, in the following years, it will still be an important resource. To reduce $CO_2$ emissions aiming at meeting the climate change targets of the Paris Agreement, carbon capture technologies have gained interest (Bui et al., 2018; National Energy Technology laboratory., 2018) but the need to find uses of $CO_2$ (Davis and Martín, 2014; Martín, 2016) and the issues related to its storage present important challenges to the implementation (Koytsoumpa et al., 2018; Martín, 2014). One carbon capture technology for a more environmentally friendly use of coal as a source of power is oxy-combustion (Lockwood, 2017; Nemitallah et al., 2017). The advantages behind oxy-combustion lie in the fact that the coal is burned with pure oxygen instead of air. Therefore, instead of being diluted with nitrogen, $CO_2$ is the accompanying gas allowing a high concentration. This stream can be better treated for the recycle of the $CO_2$ reducing the NOx formation. However, impurities such as $SO_2$ are generated in the gas, even though the removal efficiency is expected to be larger (Global CCS Institute., 2019).

Work on oxy-combustion has been extensive in the last decade, particularly on evaluating the combustion efficiency (Li et al., 2019), including simulations of the boiler (Donato et al., 2010), CFD models at different scales (Perrone et al., 2018), and its numerical optimization (Zebian et al., 2012). The general opinion is that oxy-combustion is the most promising alternative to the use of coal combustion for the production of power (Deng et al., 2012). A comprehensive review on oxy fuel combustion can be found in the work by Nemitallah et al. (2017) However, most of the work dealing with the flue gas treatment in oxy-combustion has focused on $CO_2$ capture for its recycle while the entire process of flue gas processing has not received the same attention (Duan et al., 2019). The literature on oxy-combustion discusses the need for particulate and sulfur control (Davidson and Santos, 2010), but no systematic analysis is carried out for the flue gas treatment and $CO_2$ recycle.

In this work, a two-stage optimization approach is used for the design of the flue gas treatment in oxy-combustion power plant facilities. The aim is to purify the stream for recycle and/or reuse of $CO_2$. A

hybrid approach is used (Guerras and Martín, 2019) where a prescreening of the technologies is carried out in a first stage. Next, a superstructure of alternatives is formulated by developing surrogate models of all the technologies to select the most promising flue gas processing chain for oxycombustion facilities. The rest of the work is organized as follows: Section 2 presents the details of the modeling including operating constraints for the different technologies and regulation constraints on emissions. In Section 3, a systematic procedure for the selection of the flue gas processing technologies is described together with the model characteristics. In Section 4, the results of the operation of the treatment process and the coal blending problem are presented. Finally, Section 5 draws some conclusions.

## 2.- Process design

Over the last few years, a large variety of treatments have been developed for $CO_2$, $SO_2$, NOx, and particle removal. A two stage procedure is considered for the design of the flue gas treatment in oxy-combustion facilities. In this section, the flowsheet design for the processing of the oxy-combustion flue gas treatment is presented as well as its use to formulate an extended blending problem as a tool for the selection of the coal blend to be purchased.

### *2.1. Design Procedure.*

The optimization of the gas treatment chain in oxy-combustion plants follows several steps as in a previous work (Guerras and Martín, 2019). First, the process flowsheet for the gas treatment is designed. This step consists of two stages. The first stage in the design of the flue gas processing consists of a thorough literature review to preselect a number of technologies for the removal of each one of the pollutants. The preselection of methods is based on the analysis of the alternatives that are predominantly employed at the industrial scale. In oxy-combustion boilers, it should be noted that the NOx generated originates from the impurities within the coal, and thus, they are in small amounts (Riaza et al., 2012). Typically selective catalytic reduction (SCR) and selective noncatalytic reduction are the more common methods for NOx abatement (Guerras and Martín, 2019; Miller, 2015). Based on a previous work, the selective noncatalytic reduction is not considered although it is employed in some cases at the industrial scale (Guerras and Martín, 2019). In the last few years, several methods have been developed for the removal of $SO_2$, HF, and

HCl. They are classified into wet, dry, and semi-dry. It should be noted that each class includes a number of methods like lime spray drying (LSD), limestone forced oxidation (LFSO), limestone natural oxidation, Mg−O-lime process, Wellman−Lord process, high-calcium lime process, among others (Elliott et al., 1989; Miller, 2015, 2005). However, the raw material cost and the yield lead to the selection of LFSO and LSD. These processes represent above 85 and 12% of the industrial practice, respectively (EPA, 2003). It should be noted that, on the one hand, LFSO shows larger efficiency than LSD, resulting in a more flexible technology. However, on the other hand, the LSD adopts a more simple technology (Jurczyk et al., 2016). Regarding $CO_2$ capture, over the last few years, the number of alternatives has been increasing (Wang et al., 2017). Nowadays, methods have been developed to remove carbon dioxide are physical and chemical solvents (particularly monoethanolamine, MEA), membranes, adsorption onto solids, pressure/vacuum swing adsorption (PSA), and cryogenic separation (Miller, 2015). In the literature, several reviews presenting the alternative technologies are available (Wang et al., 2017). However, few are the studies that present the cost of carbon capture in the operation of a power plant (Herzog, 2018). Lately, also life cycle assessment comparing the technologies has been presented (Cuéllar-Franca and Azapagic, 2015). Based on the results and comments of these works, a selection of technologies is considered in this work. Chemical solvent methods are widely used at the industrial scale, in particular, amine-based liquid solvent systems. They are widely studied and tested at the industrial scale, presenting large $CO_2$ recovery, but the energy consumption in the solvent regeneration stage is high, resulting in large environmental impact (Cuéllar-Franca and Azapagic, 2015). Physical solvents are highly efficient for concentrated $CO_2$ streams (Wang et al., 2017). However, membranes (Martín-Hernández et al., 2020) and physical solvents (GPSA, 2012) require operation at high pressure. The large flow of flue gas prevents from selecting these alternatives. Carbonation is gaining attention due to the high removal yields (Fennell and Anthony, 2015; Wang et al., 2017). Finally, adsorbent beds such as pressure swing adsorption (PSA) systems require low energy and show high performance (Hauchhum and Mahanta, 2014). The main advantage of PSA is the relative low cost and energy efficiency (Hauchhum and Mahanta, 2014; Leung et al., 2014; Mondal et al., 2012; Siqueira et al., 2017). Therefore, carbonation, absorption in amine solutions, and adsorption in zeolite beds are the preselected methods for carbon capture (Bui et al., 2018; Elliott et al., 1989; Miller, 2015, 2005). In this way, the prescreening of the treatment methods results in the selection of the electrostatic precipitator, for

particles removal, SCR, for NOx removal, lime spray drying (LSD) process and LFSO for sulfur removal process, and finally carbonation/calcination cycle, amine absorption, and PSA systems with zeolites for carbon dioxide removal. The second stage consists of the development of a superstructure of promising alternative technologies. The units that constitute the superstructure are modeled one by one using experimental data from the literature, first principles, and industrial data. The optimization of the superstructure selects the flue gas treatment technologies. Starting the description at the boiler, its configuration as well as the nozzles (Donato et al., 2010; Li et al., 2019; Nemitallah et al., 2017; Perrone et al., 2018) determine the performance of the oxycombustion. This performance can be represented by the temperature profile within the boiler is responsible for the flue gas composition. Noncatalyzed reduction was not selected in a previous work (Guerras and Martín, 2019), and therefore, only catalytic reduction is preselected to process the flue gas. Next, an electrostatic precipitator is used to remove particulates. Subsequently, the first of the $CO_2$ capture technologies is allocated. A system consisting of a carbonator and a calcinator is used to capture $CO_2$ using CaO and producing $CaCO_3$. It is a process that must take place at a high temperature, and therefore, it is allocated first downstream. A bypass is allowed in case this technology is not selected. The clean $CO_2$ recovered after the decomposition of the $CaCO_3$ is sent to Mx_07 for its reuse. The gases, including $O_2$ and other traces, are sent to Mx_05 for further treatment. After the carbonator-calciner looping system, the $SO_2$ removal technologies are used including the wet and dry $SO_2$ removal methods. A bypass is also allowed in case there is no need for these techniques. Finally, the amine absorption and the zeolite adsorption processes are placed in parallel with a bypass in case $CO_2$ was already captured in the carbonator-calciner system. The $CO_2$ captured is recycled. A purge is allowed and an additional feed of $CO_2$ is also possible.

The purge is intended to be further used as a source of $CO_2$ within the carbon capture and utilization initiative including the production of chemicals such as methane, methanol, and so forth. Each flue gas treatment unit is modeled in detail to formulate a superstructure of alternatives. In this section, the models developed for each of the treatment units are described. The following section “Superstructure Modeling” presents the modeling issues of the gas treatment units. The superstructure is used to define the optimal selection of flue gas treatments before recycling it to the boiler. The problem formulation becomes a large nonlinear programming (NLP) problem. The flue gas may not be treated in all technologies depending on

its purity and processing costs. Thus, bypasses are allowed and the problem is defined using continuous variables instead of integer ones. The main aim is the recycle of the carbon dioxide to the boiler to guarantee the cleaning of the flue gas at a minimum cost.

### *2.2. Extended Blending Problem.*

Once the optimal flue gas treatments are installed in the facility, the coal selection problem is evaluated. This is a typical problem in power plants because they have to select the coal to buy based on market price for minimum flue gas treatment costs. The formulation of the problem includes the flowsheet of the treatment technologies while freeing the flows of the different coal types available to be selected.

## 3. Superstructure modelling

The process model including all the technologies constitutes a superstructure of alternatives, see Figure 4.1. In this section, the modeling approach for the different units is presented including the assumptions and the source of the information. The superstructure is based on the selection or nonselection of the different processes described before. For that, splits are used to allow the use of different processes. In this way, to allow the selection of two or more processes, splitters are used, where the stream can be sent to one or several units.

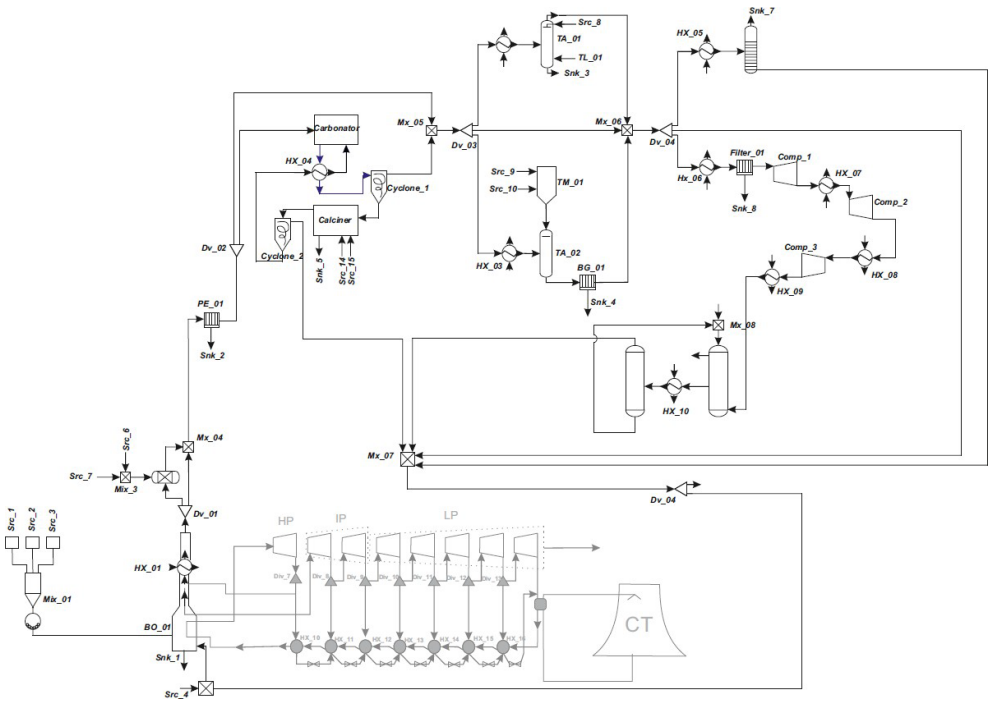


***Figure 4.1.*** Superstructure for oxy-combustion flue gas processing.

*3.1. Boiler Model.*

Pulverized coal is burned in the boiler. The composition of the flue gas is computed by determining the equilibrium of the gases assuming two main zones: flame zone and upper region. Each of the zones is modeled similarly considering the average temperature and the equilibria among the chemical species for the production of CO and $CO_2$, as well as for NO and $NO_2$. For S, $Cl_2$, and $F_2$, a complete conversion is assumed. In the following lines, the equations that model this unit are described. The main difference between coal-fired boilers and oxy-combustion boilers is the inert gas used. In the case of oxy-combustion boiler instead of using nitrogen, carbon is used. The principal advantages are the low generation of NOx and the reusage of carbon dioxide.

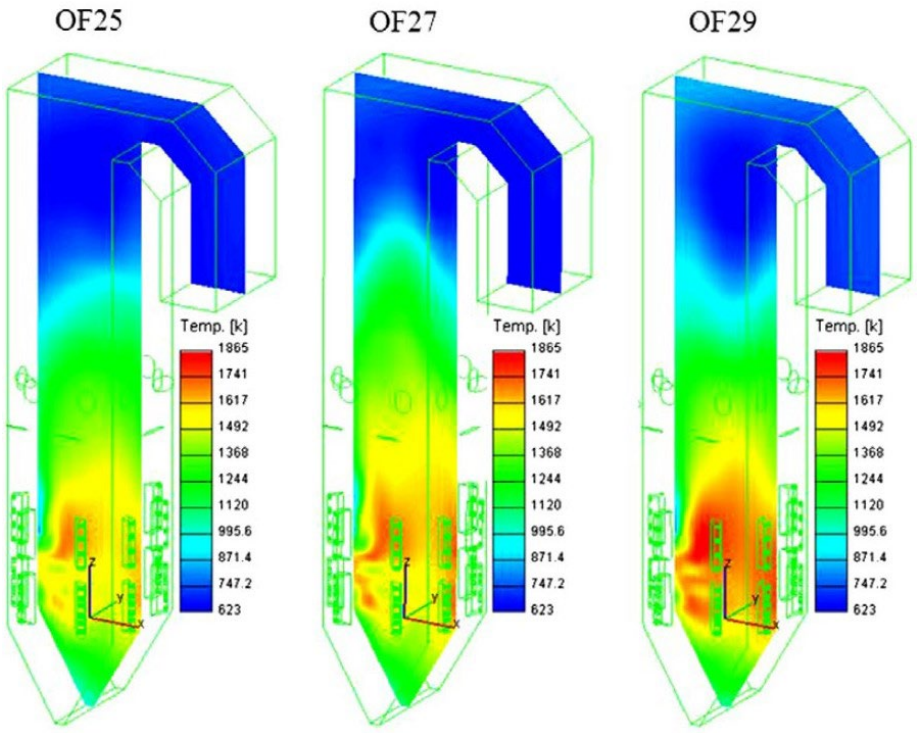


***Figure 4.2.*** Temperature profiles for oxy-combustion industrial boilers.(Al-Abbas et al., 2012 with permission).

The average temperature of each zone is computed from temperature profiles, see Figure 4.2, as in previous work (Guerras and Martín, 2019). Given that different $O_2$ to $CO_2$ ratios can be used, the temperature profiles vary. In Figure 4.2, these profiles are shown where $O_2/CO_2$ volume ratios of OF25, OF27, and OF29 correspond to 25/75, 27/73, and 29/71, respectively. The average temperature is computed out of the spatial distribution of temperatures using eq 1. The relative areas and their correspondent temperatures are taken from (Al-Abbas et al., 2012)

$$T = \sum_{area} a_i T_i \quad (1)$$

Table 4.1 shows the area sectors and their temperatures for the three cases in Figure 4.2, with regards to zone 2, the flame zone. In the upper zone, due to the more homogeneous temperature distribution, a unique division is assumed. A corresponds to the fraction of area and T indicates the temperature in Kelvin.

***Table 4.1.*** Temperature distribution in Zone 1: Flame zone

| | OF 5 | | OF27 | | OF29 | |
|---|---|---|---|---|---|---|
| | A | T (K) | A | T(K) | A | T(K) |
| Zone 1 | | 747.2 | | 747.2 | | 747.2 |
| Zone 2 | 0.0524 | 871.4 | 0.0784 | 912.8 | 0.1270 | 912.8 |
| | 0.0429 | 995.6 | 0.0421 | 912.8 | 0.0259 | 995.6 |
| | 0.0310 | 933.5 | 0.0619 | 1120 | 0.0198 | 995.6 |
| | 0.0310 | 1000 | 0.1858 | 1368 | 0.2590 | 1430 |
| | 0.1830 | 1244 | 0.0867 | 1492 | 0.0288 | 1368 |
| | 0.1088 | 1369 | 0.1288 | 1554.5 | 0.0288 | 1492 |
| | 0.0429 | 1461.0 | 0.0322 | 1409.3 | 0.0576 | 1492.0 |
| | 0.0381 | 1430.5 | 0.0322 | 1057.8 | 0.0288 | 1617 |
| | 0.0143 | 1430.5 | 0.0607 | 1741 | 0.0302 | 1120 |
| | 0.0306 | 1057.8 | 0.1586 | 1617 | 0.1914 | 1741 |
| | 0.2959 | 1554.5 | 0.0334 | 1679 | 0.0345 | 1617 |
| | 0.0272 | 1670 | 0.0991 | 1492 | 0.0604 | 1679 |
| | 0.1020 | 1399.0 | 1 | | 0.1079 | 1500.0 |
| | 1 | | | | | 1 |

Using the average temperature in each zone, the equilibrium that generates the various species is computed. The following species and equilibria are considered in the analysis.

a) *Carbon equilibria*: Reactions 2 and 3 show the combustion of carbon and the Bouduard equilibrium. Using this to model the $CO_2$ to CO ratio does not result in the industrial data. Therefore, experimental data are used. A value of 11,412 from the literature is assumed (Hu and Yan, 2012).

$$C + O_2 \rightarrow CO_2 \quad (2)$$

$$C + CO_2 \longleftrightarrow 2CO \quad (3)$$

A correlation is developed based on the data in the literature (Hu and Yan, 2012) to predict the unburned coal for oxy-combustion as a function of the percentage of oxygen, see eq 4.

$$C_{Unburned} = -1.0625 \cdot y_{O_2} + 0.3611 \quad (4)$$

20% of the unburned carbon corresponds to slag while the rest, 80%, is dragged by the flue gas (La Robla, 2017).

b) *NO production:* it is modeled based on the equations provided in eq 5. The equilibrium constant is computed based on the kinetic constants as given in eq 6 (Guerras and Martín, 2019).

$$\begin{aligned} &N_2 + O \underset{k_{-1}}{\overset{k_1}{\rightleftarrows}} NO + N \\ &N + O_2 \underset{k_{-2}}{\overset{k_2}{\rightleftarrows}} NO + O \\ &\overline{N_2 + O_2 \underset{}{\overset{K_{eq}}{\rightleftarrows}} 2\,NO} \end{aligned} \quad (5)$$

$$K_{eq_{NO}} = K_1 \cdot K_2 = 22.44 \cdot \exp\left(-\frac{21{,}805}{T}\right) \quad (6)$$

c) *$NO_2$ production:* it is modeled using eq 7 (Jess and Wasserscheid, 2013), where the equilibrium constant is given in eq 8

$$2NO + O_2 \underset{}{\overset{K_{eq}}{\rightleftarrows}} 2NO_2 \quad (7)$$

$$K_{eq_{NO_2}} = 2.75369 \cdot 10^{20} \cdot T^{-6.95528} \quad (8)$$

It is assumed that no other nitrogen oxides are present because typically their concentrations are negligible (Clean Air Technology Center., 1999). To verify that the model reports reasonable results, an industrial reported ratio of 95% of NO and 5% $NO_2$ (Mussatti et al., 2002) is expected.

d) *Sulfur combustion*:(Sarkar, 2015) 100% conversion of the sulfur into $SO_2$ is assumed (La Robla, 2017):

$$S + O_2 \rightarrow SO_2 \quad (9)$$

e) *HCl production*: (Shemwell et al., 2002) 100% conversion is assumed (La Robla, 2017):

$$Cl_2 + H_2 \rightarrow 2\,HCl \quad (10)$$

f) *HF production*: (Laird and Smith, 2017) 100% conversion is assumed (La Robla, 2017)

$$F_2 + H_2 \rightarrow 2\,HF \quad (11)$$

Apart from the equilibria, the atom balances must also hold, without accounting for the inert $CO_2$.

*Carbon balance*

$$(n_C)_{Inlet} = (n_{CO_2} + n_{CO} + n_C)_{Outlet}$$

*Hydrogen balance:*

$$\left[2\cdot(n_{H_2}) + 2\cdot(n_{H_2O})\right]_{inlet} = \left[2\cdot(n_{H_2}) + 2\cdot(n_{H_2O}) + (n_{HCl}) + (n_{HF})\right]_{Outlet}$$

*Oxygen balance:*

$$\left[2\cdot n_{O_2} + n_{H_2O}\right]_{Inlet} = \left[2\cdot n_{O_2} + n_{H_2O} + 2\cdot n_{CO_2} + n_{CO} + 2\cdot n_{NO_2} + n_{NO} + 2\cdot n_{SO_2}\right]_{Outlet}$$

*Nitrogen balance*

$$\left[2\cdot n_{N_2}\right]_{Inlet} = \left[2\cdot n_{N_2} + n_{NO_2} + n_{NO}\right]_{Outlet}$$

*Sulphur balance*

$$\left[n_S\right]_{Inlet} = \left[n_{SO_2}\right]_{Outlet}$$

*Chlorine balance:*

$$\left[2\cdot n_{Cl_2}\right]_{Inlet} = \left[n_{HCl}\right]_{Outlet}$$

*Fluorine balance:*

$$\left[2\cdot n_{F_2}\right]_{Inlet} = \left[n_{HF}\right]_{Outlet}$$

g) An excess of oxygen is recommended to improve the combustion yield. The reference is the $O_2$ required to burn C to $CO_2$. According to Hu and Yan (2012), values of 1.01 and 1.05 are considered as lower and upper bound.

### *3.2. Denitrifier*

Two main methods that are commonly considered for the removal of NOx from flue gas are: catalytic (SCR) and noncatalytic reduction. In this case, only SCR is evaluated based on previous results (Guerras and Martín, 2019). The removal of nitrogen oxides is based on the chemical equations below, in the presence of ammonia and oxygen:

$$4NO + 4NH_3 + O_2 \rightarrow 4N_2 + 6H_2O$$
$$2NO_2 + 4NH_3 + O_2 \rightarrow 3N_2 + 6H_2O \quad (12)$$

This unit is modeled using mass and energy balances as well as empirical correlations for the yield and rules of thumb for the feed ratios. The mass balance follows the stoichiometry of the reactions in eq 12. The oxygen to ammonia ratio used is 20:1, to avoid flammability issues, and the oxygen is fed as atmospheric humid air. In a previous work (Guerras and Martín, 2019), the conversion of the reactions was fit from the experimental data in Rosenberg and Oxley (1993) to eq 13.

$$\eta_{SCR} = 6.6537 \cdot 10^{-6} \cdot T(K)^3 - 1.523 \cdot 10^{-2} \cdot T(K)^2 + 11.43 \cdot T(K) - 2,731.8 \quad (13)$$

The temperature of the gas exiting the reactor is computed using an adiabatic energy balance (Martín, 2016). The investment cost of this unit is estimated using the correlation from Miller (2015), eq 14, where $m_{NOx}$ corresponds to the tons of NOx processed in a year.

$$Cost_{SCR} = 5,000 \cdot \frac{1}{0.8} \left( m_{NOx} \cdot (1 - \eta_{SCR}) \right) \quad (14)$$

### *3.3. Desulfuration*

The removal of the $SO_2$ is a major issue in oxy-combustion flue gas treatment because NOx concentration is expected to be well below that of air-fired boilers. Two methods are evaluated: wet removal (LFSO) and dry removal (lime spray drying, LSD).

#### *3.3.1. LFSO.*

The wet removal of $SO_2$ is based on the reactions that can be seen in eq 15 where a slurry of $CaCO_3$ is fed to a gas liquid contactor operating at 323 K (Sargent and Lundy, 2003) and the product is oxidized with air to gypsum (Kohl and Nielsen, 1997). The model for this unit is based on the mass balance

given by the stoichiometry of these set of reactions. The feed ratio of $O_2$ to $SO_2$ used is 3:1 (Kohl and Nielsen, 1997), and the slurry contains 20% w/w of $CaCO_3$. In a previous work (Guerras and Martín, 2019), an empirical model was developed using experimental data reported by Zhong et al. (2008) to predict the removal of $SO_2$ as a function of the liquid to gas ratio (in liters per $Nm^3$) as presented in eq 16. The exit gas temperature is computed using an adiabatic energy balance, and the gas exits the contact equipment saturated.

$$\begin{aligned}
&SO_2 + CaCO_3 + \frac{1}{2}H_2O \rightarrow CaSO_3 \cdot \frac{1}{2}H_2O \downarrow + CO_2 \\
&CaSO_3 \cdot \frac{1}{2}H_2O + \frac{1}{2}O_2 + \frac{3}{2}H_2O \rightarrow CaSO_4 \cdot 2H_2O \downarrow \\
&2HCl + CaCO_3 \rightarrow CaCl_2 \downarrow + H_2CO_3 \\
&2HF + CaCO_3 \rightarrow CaF_2 \downarrow + H_2CO_3 \\
&H_2CO_3 \rightarrow H_2O + CO_2
\end{aligned} \tag{15}$$

$$\eta_{LFSO} = -5.06993 \cdot 10^{-4} \cdot \left(\frac{L}{G}\right)^2 + 2.591958 \cdot 10^{-2} \cdot \left(\frac{L}{-}\right) + 0.653958042 \tag{16}$$

The investment cost of the method is estimated by the $SO_2$ eliminated in tons per year (Miller, 2015) using eq 17

$$Cost_{LFSO} = 3,700 \cdot \left( \left( m_{SO_2} \right) \cdot \left( 1 - \eta_{LFSO} \right) \right) \tag{17}$$

### *3.3.2. LSD.*

The dry removal method treats the flue gas with a slurry 35% in CaO operating within 393 and 448K. The mechanisms of the removal process (Hayton, 2015) can be seen in eq 18. The stoichiometry of the reactions allows computing the performance of this unit. Because of the absence of forced oxidation, the molar ratio $CaSO_3$ to $CaSO_4$ is 9:1. The removal yield of $SO_2$ is estimated using a model developed from experimental data (Martín and Martín, 2013) reported in a previous work (Guerras and Martín, 2019) as a function of the fraction of S in the coal and the molar ratio between Ca and S, see eq 19. The common range of sulfur concentrations, %S, and Ca/S ratios for the use of this correlation are from 2.5 to 6% and 0.7 to

1.5, respectively. The exit temperature of the gases is computed assuming an adiabatic energy balance. The gas exits saturated.

$$\begin{aligned} &CaO + H_2O \rightarrow Ca(OH)_2 \\ &SO_2 + Ca(OH)_2 \rightarrow CaSO_3 \cdot \frac{1}{2} H_2O + \frac{1}{2} H_2O \\ &SO_2 + Ca(OH)_2 + H_2O + \frac{1}{2} O_2 \rightarrow CaSO_4 \cdot 2H_2O \\ &2HCl + Ca(OH)_2 \rightarrow CaCl_2 \downarrow + 2H_2O \\ &2HF + Ca(OH)_2 \rightarrow CaF_2 \downarrow + 2H_2O \end{aligned} \quad (18)$$

$$\eta_{LSD} = \left(-0.4554 \cdot (\%S) + 1.2451\right) + \left(0.3469 \cdot (\%S) + 0.6286\right) \cdot \left(\frac{Ca}{S}\right) + \left(-0.0243 \cdot (\%S) - 0.56325\right) \cdot \left(\frac{Ca}{S}\right)^2 \quad (19)$$

The investment cost of the method is estimated based on $SO_2$ eliminated in tons per year (Miller, 2015).

$$Cost_{LDS} = 4,400 \cdot \left( \left( m_{SO_2} \right) \cdot \left( 1 - \eta_{LFSO} \right) \right) \quad (20)$$

### *3.4. Particle Removal.*

The electrostatic precipitator is modeled using a mass balance to the particles. The removal ratio is computed based on the particle size, see eq 21, using the experimental results reported by Nichols and McCain (1975). Seven diameter sizes are considered 0.075, 0.2, 0.5, 1.5, 2, 5, and 10 μm with removal ratios of 0.99, 0.95, 0.9, 0.96, 0.97, 1, and 1, respectively. Together with the mass balance, an energy balance is also performed. The exit temperature is typically 423K (GasNatural Fenosa, 2015).

$$\begin{aligned} &\eta(d) = f(size) \\ &Particle_{\text{Removal}} = \sum \eta(d) n_{Particle}(d) \\ &\eta_{PE} = \frac{Particle_{\text{Removal}}}{Particle_{in}} \end{aligned} \quad (21)$$

The estimation cost for the electrostatic precipitator is reported by Miller, (2015), where $H_y$ is the volume of gas ($Nm^3$) processed in a year. The advantage of this type of cost functions is that if the method is not selected, no flowrate is processed and, as a result, there is no cost associated.

$$Cost_{PE} = 2.85 \cdot \left(H_y\right) + 8.50 \cdot \left(H_y\right) \quad (22)$$

*3.5. Carbon Capture.*

After a prescreening of technologies, three alternatives are considered based on their application to power plants such as carbonation (Fennell and Anthony, 2015), amine absorption (GPSA, 2012), and PSA systems (Hasan et al., 2012). The gas purified is recycled to the boiler.

*3.5.1. Amines.*

Among the different amines, MEA has been traditionally used for power plants (Stec et al., 2015). To compute the flow of amine fed to the gas liquid contactor, a mass balance is performed, eq 23, where the molar ratio of $CO_2$ recovered per mol of amine (MR) and the MEA concentration ($MEA_{conc}$) are given in Table 4.2. 95% removal of $CO_2$, $CO_{2eff}$, is assumed (Zhang and Chen, 2013).

$$\frac{\mathrm{MW}_{MEA}}{MEA_{\mathrm{conc}}} \cdot \left( \frac{\mathrm{CO2}_{\mathrm{eff}} \cdot \mathrm{fc}_{CO_2}}{\mathrm{MW}_{CO_2}} \right) \cdot \left( \frac{1}{MR} \right) = \mathrm{fc}_{MEA} \quad (23)$$

The gas may need to be compressed. The compressors are modeled assuming polytropic behavior. The efficiency of the compression stages is assumed to be 0.85, and the polytropic coefficient is assumed to be 1.4 (Wallas, 1990). The absorption process is exothermic, and the column must be continuously cooled. The cooling needs are computed using eq 24 based on the amount of $CO_2$ absorbed by the amine and the heat reaction

$$\mathrm{Q}_{(\mathrm{Col1})} = \Delta H_{react,a\,\mathrm{min}\,e} \cdot \mathrm{CO2}_{\mathrm{eff}} \cdot fc_{CO_2} \quad (24)$$

The loaded amine flow is sent to regeneration in a distillation column. Rules of thumb from the literature (GPSA, 2012), see Table 4.2, are used to compute the energy involved in heating the amine flow ($q_{amine}$) before being fed to the column, eq 25, as well as the energy required by the reboiler and the cooling needs for the condenser eq 26.

$$Q_{(Feed)} = F_{Feed} \cdot q_{A\,\mathrm{min}\,e} \quad (25)$$

$$\mathrm{Q}_{(Cond)} = F_{Cond} \cdot q_{A\,\mathrm{min}\,e}$$
$$\mathrm{Q}_{(\mathrm{Re}b)} = F_{\mathrm{Re}b} \cdot q_{A\,\mathrm{min}\,e} \quad (26)$$

According to the literature, the inlet temperature to column 2, $T_{col2}$, is equal to 93 °C, with the bottom temperature, $T_{bottoms}$, of 125 °C while at the condenser, $T_{top}$, is assumed to be 54 °C. The factors $F_i$ in eqs 25−27 are given in Table 4.2. The MEA solution recovered from the bottom is recycled back to the gas-liquid contactor. From the reboiler, the regenerated amine is cooled down heating up the feed to the column. Next, a heat exchanger is used to adjust the temperature to 29 °C. Equation 27 computes the cooling needs. The make-up and the recycled solution are mixed adiabatically and fed to the gas−liquid contactor.

$$Q_{(Feed-Col1)} = F_{Cooler} \cdot q_{A\min e} \tag{27}$$

The cost correlations, for the investment, eq 28, and for the operating costs, eq 29, are given by empirical correlations developed using data from the literature (David and Herzog, 2019). The experimental data reported by David and Herzog (2019) show the operation of a facility with and without the carbon capture technology. Based on these data, the contribution of the amine absorption to the capital and operating costs is computed based on the thermal energy generated at the boiler by burning the coal and the actual flow of $CO_2$ fed to the process, see eqs 28 and 29.

$$Capital_{Cost} = \left( 623 \frac{\$}{kW} \right) \cdot (\text{Pot}_{CO_2}) \cdot (F_{CO_2\ In}) \tag{28}$$

$$Operation_{Cost} = \left( \frac{5.5}{1000} \frac{\$}{kWh} \right) \cdot (\text{Pot}_{CO_2}) \cdot (F_{CO_2\ In}) \tag{29}$$

The parameter $Pot_{CO2}$ is related to the power generated per kilogram of coal used where $F_{CO2}$ is the carbon dioxide fed into the process.

***Table 4.2.*** $CO_2$ capture using alkali solutions (GPSA, 2012)

| | MEA |
|---|---|
| *Gas pickup mol/mol amine* | 0.33 |
| *Solution concentration (wt %)* | 15-25 (0.2) |
| *Heat of reaction (BTU/lb $CO_2$)* | 620-700 |
| *MR* | 0.35 |
| *Density* | 1.018 |
| *Cost (€/kg)* | 1.3 |
| *Molecular Weight* | 61.08 |
| *Reboiler (BTU/hr)* | 72000 GPM |
| *Condenser (BTU/hr)* | 30000 GPM |
| *Amine feed to distillation (BTU/hr)* | 45000 GPM |
| *Amine cooler (BTU/hr)* | 15000·GPM |

*3.5.2. Zeolites.*

The PSA system is modeled to compute the absorbent bed required and the vessel that contains it. The bed of zeolites is designed based on the amount of $CO_2$ to be captured, considering the adsorption equilibrium between the $CO_2$ and the material. The adsorption yield of the $CO_2$ on the zeolite bed is computed based on experimental adsorption equilibrium data. The large model of the superstructure suggested the development of a surrogate model of the adsorption capacity, q, in mol per kg of the zeolite 13X, based on the operating temperature and the $CO_2$ partial pressure, $P_{CO2}$. The range of operation is from 0.2 to 1 atm and 25 to 60°C (Hauchhum and Mahanta, 2014).

$$q = (2\cdot 10^{-5}T^2 - 0.0025T - 1.1968)P_{C_2}^2 + (0.0027\cdot T + 2.1451)\cdot P_{CO_2} + (-0.035T + 3.9061) \quad (30)$$

The breakthrough curve for the zeolite determines the operating time and the size of the bed. It shows that the operating time must be below 20 min so that the exit gas contains only traces of $CO_2$. An operating time around 15 min is selected ($\tau$ = 15 min) because in the flue gas, there exist more components although in small proportions. In this way, the purity of the $CO_2$ is guaranteed. The yield, $\eta$, is assumed to be 95%. Thus, the mass of the zeolite bed required is given by eq 31.

$$m_{Zeolite} = \frac{1}{q}\frac{fc_{CO_2}\cdot 1000}{MW_{CO_2}}\eta\cdot\tau \quad (31)$$

In order to recycle high purity $CO_2$, the tails of the desorption curve must be cut. The order of desorption is $N_2$, NOx, $CO_2$, $SO_2$, $O_2$, and $H_2O$. Therefore, the traces of $N_2$ and NOx will be removed before recycling as well as the traces of $SO_2$, $O_2$, and $H_2O$ (Zhang et al., 2009).

The estimation of the cost of the PSA system consists of the vessel and the adsorbent bed, eqs 37 and 38. The vessel is sized as follows (Martín and Grossmann, 2011). The volume of the bed is computed using the apparent density of the zeolite.

$$V_{zeolites} = 1.1\cdot\frac{m_{zeolites}}{\rho_{Bed}\cdot 0.454}{0.3048^3} \quad (32)$$

The bed is to be installed in a vessel. Assuming L/D equal to 3 the diameter becomes:

$$D_{vessel} = \left(\frac{V_{zeolites}}{3\cdot\pi}\right)^{1/3} \quad (33)$$

$$L_{Vessel} = 3 \cdot D_{Vessel} \tag{34}$$

The thickness of the vessel is computed using a correlation developed in the work by Martín and Grossmann (2011).

$$Thickness = 0.023 + 0.003 \cdot D_{vessel} \tag{35}$$

The cost of the vessel is computed by the weight of metal. Thus, the material of the vessel is computed as:

$$Weight_{Vessel} = \rho_{steel} \cdot \left( \pi \cdot \left( \left( \frac{D_{vessel}}{2} + Thickness \right)^2 - \left( \frac{D_{vessel}}{2} \right)^2 \right) \cdot L_{Vessel} + \frac{4}{3} \cdot \pi \cdot \left( \left( \frac{D_{vessel}}{2} + Thickness \right)^3 - \left( \frac{D_{vessel}}{2} \right)^3 \right) \right) \tag{36}$$

Finally, the investment cost of the vessel (Almena and Martín, 2016).

$$Cost_{Vessel} = 56.181 \cdot (Weight_{Vessel})^{0.878} \tag{37}$$

The zeolites can be regenerated only a number of times. It is a complex issue since their adsorption capacity decays over time (Hauchhum and Mahanta, 2014). The cost of the operation is assumed to that of the bed that is to be bought over the plant lifetime.

$$Cost_{Zeolite\_Bed} = C_Z \cdot m_{Zeolite} \cdot \mathrm{N^o}_{Beds} \tag{38}$$

### 3.5.3. Carbonation.

Carbonation/calcination is a looping system to regenerate the absorbent. Even though it is a closed cycle, losses and efficiency decay results in the need to feed a make-up of solids (Abanades, 2002). Besides, secondary reactions such as sulfonation occur. This reaction also represents $SO_2$ removal (Manovic and Anthony, 2010). It is possible to use either $CaCO_3$ or CaO as adsorbents. However, $CaCO_3$ is the one of choice as it is the cheapest.

The system operates as follows: the flue gas is fed to the carbonator where carbon dioxide is removed. The product stream consisting of gases and solids is fed to a heat exchanger, Hx_4, where it is used to heat up the recycled adsorbent. Next, in cyclone 1, the solids are recovered from the stream and

the gas is sent to further treatment. The solids must be regenerated in the calciner. This stage consists of the decomposition of the $CaCO_3$ recovering the CaO and $CO_2$. The solids, CaO, are separated from the stream in cyclone 2, while the $CO_2$ can be reused in the boiler. The solids are heated up before being fed to the carbonator.

#### *3.5.3.1. Carbonator.*

This unit is responsible for the removal of $CO_2$, $SO_2$, HCl, and HF following eq 39 that is used to compute the mass balance to this unit. The flue gas and regenerated solids enter the carbonator.

$$CaSO_3 + \frac{1}{2}O_2 + SO_2 \rightarrow CaSO_4$$
$$CaO + CO_2 \rightarrow CaCO_3$$
$$2HCl + CaO \rightarrow CaCl_2 + H_2O \quad (39)$$
$$2HF + CaO \rightarrow CaF_2 + H_2O$$

The sulfonation and carbonation reactions are competitive. Because $SO_2$, HCl, and HF can be considered traces in the gas flow compared to the proportion of $CO_2$, it is assumed that these reactions will have a 100% conversion. The operating temperature must be higher than 600 °C but lower than 680 °C (Abanades, 2002). The range shows a significant effect on the $CO_2$ uptake in the diffusion-controlled stage. In the pilot plants, the operation temperature is around 650 °C, and hence this temperature is used in the carbonator (Ortiz et al., 2017). The efficiency of the carbon capture of this technology is computed using the correlation reported by Abanades (2002), eq 40.

$$\eta_{carbonator} = \frac{1 + \frac{F^0}{F_R}}{\left(\frac{F_0}{F_R}\right) + \left(\frac{F_{CO_2}}{F_R}\right)} \cdot \left[\frac{f \cdot \left(\frac{F_0}{F_R}\right)}{\left(\frac{F_0}{F_R}\right) + 1 - f} + b\right] \quad (40)$$

The parameters b and f are constants with values of 0.782 and 0.174, respectively. The $F_R/F_{CO2}$ ratio is limited by the experimental conditions. This ratio is limited between the values of 2 and 5. Another constraint is that the $F_0/F_R$ ratio, which represents the ratio between the fresh and regenerated sorbent, should be within the range of 0 and 0.05.

The stream exiting the carbonator is fed to the cyclone (cyclone_1). In the cyclone, the solids are recovered and fed to the calciner for their regeneration.

#### *3.5.3.2. Calcination.*

The calciner is used to regenerate the CaO from $CaCO_3$. High temperatures are needed for the decomposition of the $CaCO_3$ (Abanades, 2002; Ortiz et al., 2017; Romeo et al., 2008). In this work, a temperature of 950 °C is used. Thereby, the regeneration yield obtained is assumed to be 100% (Ortiz et al., 2017). This unit can be considered as a furnace because the operation consists of combustion with carbon and oxygen. The ratio between both is paramount for the operation and typically takes a value of 2.49 (Ortiz et al., 2017). The set of reactions that take place in this unit are shown in eq 41, which are used to compute the mass balance to the unit.

$$CaCO_3 \rightarrow CaO + CO_2$$
$$CaSO_3 + \frac{1}{2}O_2 + SO_2 \rightarrow CaSO_4 + CO_2$$
$$Cl_2 + H_2 \rightarrow 2HCl \quad (41)$$
$$F_2 + H_2 \rightarrow 2HF$$
$$S + \frac{1}{2}O_2 \rightarrow SO_2$$

Taking into account that the sorbent collects impurities and losses activity, a purge Sink_3 is considered, $F_0$ in eq 40, to remove a small fraction of the sorbent. Sorbent make-up is fed to the unit, Src_08, equal to the amount deactivated by the impurities, $F_0$. The cost correlations to compute the investment and operation costs of this technology are given by eqs 42 and 43 (Abanades et al., 2007).

$$Capital_{Cost} = 675 \cdot (\mathrm{Pot}_{CO_2}) \cdot (F_{CO})_{In} \quad (42)$$

$$Operation_{Cost} = 0.023 \cdot (\mathrm{Pot}_{CO_2}) \cdot (\mathrm{F}_{CO})_{In} \quad (43)$$

The clean stream is recycled back to the boiler, with a purity above 99.9%, to dilute the mixture instead of using the nitrogen in the air.

*3.6. Problem Formulation.*

Two mathematical problems are formulated: one for the design of the flowsheet, the second stage in the process design problem, and the extended blended problem, that is a tool for industry to select the coal blend to purchase for the sustainable operation of their facility. The process design problem consists of an NLP describing the flowsheet shown in Figure 4.1 including the models of the boiler, the denitrifier, the carbon capture, and $SO_2$ removal techniques described in the previous section. The objective function is given by eq 44.

$$Cost_{Total} = \frac{1}{3}\left(\sum_i Cost_i\right) + \sum_i Cost_{Operation_i} \quad (44)$$

where the term $cost_i$ refers to the investment cost to each unit, that is annualized, and $cost_{operationi}$ corresponds to the operation cost.

Because the oxy-combustion of coal can be carried out with different carbon dioxide and oxygen concentrations and the main effect of varying oxygen concentration is the flue gas composition (Mussatti et al., 2002), the effect of the oxygen concentration on the selection of flue gas treatment is also analyzed. In this case study, data from the literature is used for the temperature profiles inside the boiler for oxygen concentrations of 25, 27, and 29% (Al-Abbas et al., 2012). In all three cases, the superstructure consists of 4,815 equations and 5,422 variables. It is written in GAMS and is solved using the multistart procedure with CONOPT 3.0 as the preferred solver.

The extended blending problem requires an alternative objective function to add the cost of the coal. The problem also includes the models for the boiler, the denitrifier, the carbon capture, and $SO_2$ removal techniques. The objective function becomes:

$$Cost_{Total} = \frac{1}{3}\left(\sum_i Cost_i\right) + \sum_i Cost_{Operation_i} + \sum_k Cost_k \quad (45)$$

where the term $cost_k$ is the cost of imported coal, national coal, and crude coal tar. In this step, the optimal blending of coal is selected to be of minimum cost based on flue gas treatment and coal costs. The blending model consists of 4,818 equations and 5,425 variables. It is written in GAMS and is solved using the multistart procedure with CONOPT 3.0 as the preferred solver.

## 4. Results

Three types of coal, national, imported, and crude coal tar, are considered for the study with a composition as shown in Table 4.3. In all cases, a feed of 23 kg/s of coal or coal mixture is used to generate around 350−400 MWe. Similar to previous works (Guerras and Martín, 2019), an efficiency of the thermal cycle of 50% is used.

***Table 4.3*** Coal composition and price

| | National | Imported | Crude coal tar |
|---|---|---|---|
| $H_2O$ | 0.1357 | 0.0988 | 0.1038 |
| $C$ | 0.688493 | 0.705099 | 0.779552 |
| $H_2$ | 0.022585 | 0.030706 | 0.03033 |
| $O_2$ | 0.000165 | 0.000579 | 0.021109 |
| $S$ | 0.018631 | 0.004351 | 0.041942 |
| $N_2$ | 0.013844 | 0.018164 | 0.017093 |
| $Cl$ | 0.00014 | 0.00012 | 0.00004 |
| $F$ | 0.000072 | 0.000076 | 0.000017 |
| Ash | 0.12037 | 0.142105 | 0.006117 |
| Price ($/t) | 77.68 | 97.91 | 22.36 |
| HHV (kJ/kg) | 26411.535 | 28106.46 | 35467.875 |

### *4.1. Process Design.*

The first study corresponds to the design of the process that treats the flue gas. The flowsheet is extracted from the superstructure in Figure 4.1 by solving the NLP problem formulated in a previous section. To evaluate the robustness of the solution, three cases of the study with various oxygen concentrations in the boiler are considered. In these studies, a coal blend of 26% national, 26% imported, and the rest crude coal tar is used, generating around 717 MW, based on a typical composition used in a power plant.

Three oxygen concentrations in the boiler, 25, 27, and 29%, are evaluated. The model is optimized for each one of all of them. In all cases, the solution found shows the same flowsheet. The gas treatment chain consists of the electrostatic precipitator, to remove the particles, LSD, to remove sulfur, and the PSA system based on zeolites 13X to clean the carbon dioxide stream. This solution is important due to the fact that the selection of technologies is robust with the oxygen feed to the boiler providing certain general processing chain. Analyzing the solution, the electrostatic precipitator is employed in all cases because the flue gas always contains ash and unburned coal that must be removed before further processing. The

presence of these species in the gas flow affect other units in particular the bed of the PSA system, poisoning it. In addition, one on the characteristics of oxy-combustion is the low levels of NOx production. Due to this feature, it is not necessary to use any denitrification technique because the traces of NOx will be removed by adsorption in the zeolites. The superstructure allows bypasses. Thus, the LSD process is selected over the LFSO as the main technology to remove sulfur while the zeolites only deal with the traces of $SO_2$ remaining. In this way, the use of LFSO, a technique with a larger removal efficiency but also more expensive, is not selected. This result is similar to the one shown in previous work for conventional coal-based facilities (Guerras and Martín, 2019). However, note that most facilities use LFSO techniques for their flexibility in dealing with a wider range of sulfur contents (EPA, 2003). The recovery and purification of $CO_2$ is carried out using zeolites over MEA or the calcinator/combustion system. The PSA system is simpler and requires less energy. Moreover, it presents a high carbon capture yield as well as it serves as a trap for traces of NOx and $SO_2$. In all three cases, the solution suggests a bypass at the sulfur removal section that takes a value of around 10%, which means that around 90% is fed in the LSD process to remove sulfur. Table 4.4 summarizes the results of the cost per unit of power It is possible to see that the cost decreases with the concentration of oxygen because lower $CO_2$ must be recycled. Note that the air separation unit cost is not included in the analysis. In addition, the LSD cost drops abruptly from 25 to 27% oxygen concentration and remains almost constant for 29%. Note that NLP is solved obtaining a local solution and no global solution is claimed. It can also be seen a decrease in the cost of $CO_2$ capture as the amount of $CO_2$ in the stream is lower due to the oxygen concentration.

***Table 4.4.*** Costs per power generated of the units selected from the different alternatives

| | *OF25* | *OF27* | *OF29* |
|---|---|---|---|
| *PE cost ($/kW)* | 10.86 | 10.34 | 9.89 |
| *LSD cost ($/kW)* | 361.09 | 291.02 | 292.36 |
| *Zeolites adsorption cost ($/kW)* | 25.19 | 23.93 | 22.86 |
| *CaO cost ($/ kW·year)* | 14.41 | 11.62 | 11.68 |
| *Investment cost ($/kW)* | 397.14 | 325.30 | 325.11 |
| *Operation cost ($/ kW·year)* | 38.86 | 34.87 | 33.89 |
| *Total annual cost ($/kW)* | 171.23 | 143.30 | 142.26 |

### *4.2. Blending Problem: Coal Selection.*

In the previous section, the optimal technologies for flue gas treatment were determined. It is important to notice that industry does not use partial bypasses to the flue gas treatment units because it is

easier to feed the entire flow to the unit. Thus, the flowsheet is fixed as the one shown in Figure 4.3 to select the coal blend to be purchased. The bypass is avoided by fixing the flowrate of that stream to 0. Similar to the previous section, the study is carried out for three different initial concentrations of oxygen to determine the optimal coal blend. The same three types of coal, national coal, imported coal, and crude coal tar, are used. However, in this case, the amount of each type of coal is not fixed, only the total feed of coal mixture that is 23 kg/s.

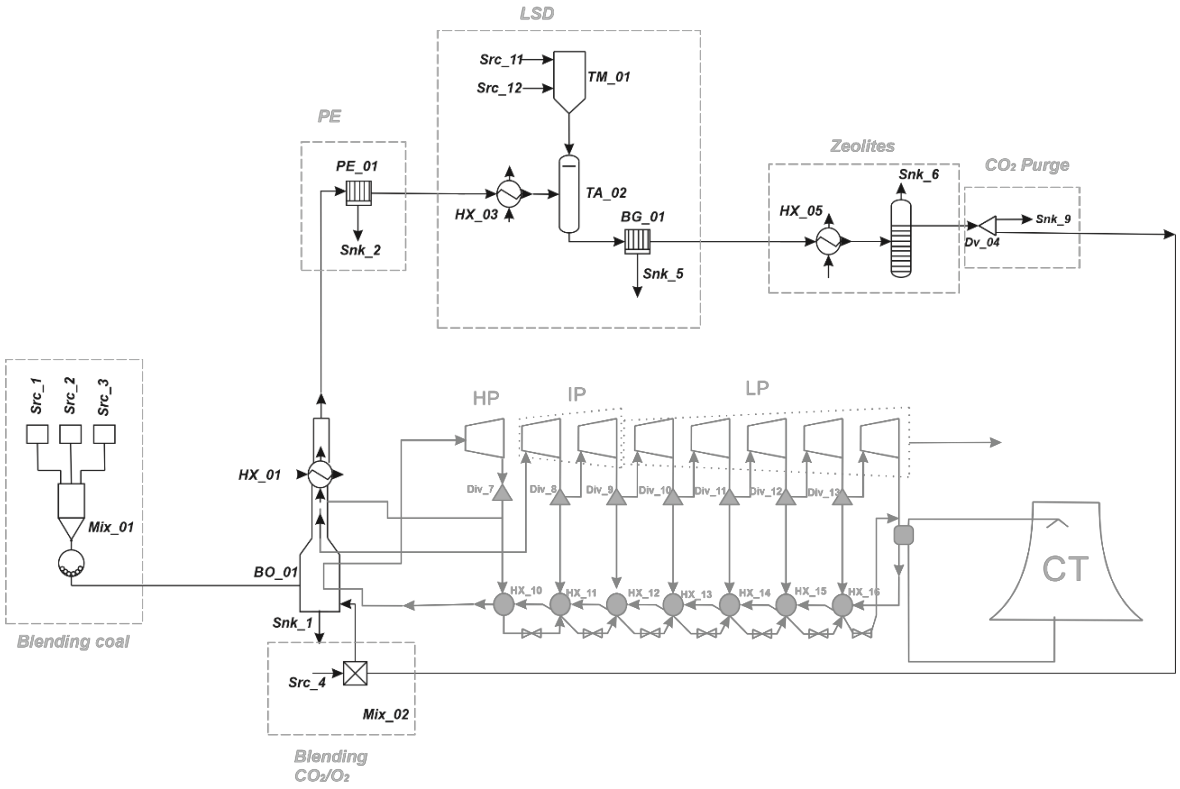


***Figure 4.3.*** Process flow diagram of the blending problem.

The optimization of the extended blending problem solves an NLP problem to define the amount of each coal type to be purchased, see previous section. The trade-offs that the three coals present are related to their price and sulfur content. On the one hand, crude coal tar is cheaper, has the highest energy content, but contains the largest amount of sulfur. On the other hand, the imported coal is the most expensive. However, the sulfur content in the lowest expecting lower processing cost and an intermediate energy content. Finally, the national coal shows an intermediate price and sulfur content while the energy content is the lowest. In principle, the trade-offs have a nontrivial solution as to which coal blend to use. However, by solving the extended blending problem, no mixture of coal is selected in spite of the trade-offs. The selection of crude coal tar is due to the fact that it is far cheaper than the other coals. Furthermore, if the

coal prices per unit of power generated are evaluated, see Table 4.5, it can be seen that the crude coal tar generates higher power than the others. Thus, if the blending problem is analyzed based on the coal cost and the coal heating values, the same result will be obtained.

However, in Spain, the use of national coal is encouraged for social reasons to support the economy of certain regions. The coal-based power plants are allocated in regions where mining exploitations are also in operation extracting national coal representing a social issue, the self-consumption of national coal. Therefore, because no coal blend is suggested, Table 4.5 compares the processing costs of the three coal types for the three oxygen concentrations for further insights. The results obtained show that the coal of choice is crude tar, followed by national and imported, regardless of the oxygen composition of the combustion gas. The price of the imported coal is a deterrent to be selected, in spite of the fact that the treatment cost using the LSD is 3 to 5 times lower than the processing of the crude coal tar. The largest investment cost corresponds to the removal of sulfur. Furthermore, the lower ash content in the crude coal tar reduces its processing costs around 20% compared to the other coals. In addition, in spite of the larger production of $CO_2$ as a consequence of the higher carbon content, the larger power production out of the crude coal tar results in lower carbon capture cost per unit of power. Note that the investment in the flue gas processing is far lower for the imported coal, one-half of that of the crude coal tar and one-third of the national coal. However, the cost of coal per year outweighs the savings in annualized investment, resulting in selecting the crude coal tar over the other two. Note that the national coal is the second best overall, but it requires the largest investment due to the sulfur content and the low yield to power. While the results point to the crude coal tar, from the company perspective, the risk in funding the flue gas treatment is large for the national and the crude coal tar.

Evaluating the effect of the concentration of oxygen in the processing costs, on average, the higher the oxygen concentration the lower the costs, but the decrease is not as high as selecting one coal type or another. On the one hand, the cost of the PE and the zeolites depends on the oxygen to $CO_2$ ratio, decreasing the cost with the oxygen fraction in the gas. On the other hand, the LSD costs depend on types of coal, and its sulfur content, but it does not depend on the oxygen concentration in the flue gas. Again, it should be noted that the air separation unit is not included in the total processing cost.

***Table 4.5.*** Coal for gas processing for the various coal types.

| | | PE Cost ($/kW) | LSD Cost ($/kW) | Zeolites Cost ($/kW) | CaO Cost ($/ kW·year) | Coal Cost ($/ kW·year) | Investment Cost ($/kW) | Operation Cost ($/ kW·year) | TAC ($/kW·year) |
|---|---|---|---|---|---|---|---|---|---|
| OF25 | National | 12.10 | 334.19 | 27.94 | 13.39 | 135.33 | 374.23 | 41.78 | 301.86 |
| | Imported | 11.70 | 72.03 | 26.83 | 4.46 | 251.32 | 110.56 | 31.70 | 319.87 |
| | Crude Coal Tar | 10.01 | 210.47 | 23.38 | 8.39 | 45.48 | 243.86 | 32.36 | 159.13 |
| OF27 | National | 11.52 | 334.19 | 27.44 | 13.39 | 135.33 | 372.26 | 40.31 | 299.72 |
| | Imported | 11.14 | 72.03 | 25.49 | 4.46 | 251.32 | 108.67 | 30.29 | 317.83 |
| | Crude Coal Tar | 9.52 | 210.47 | 22.22 | 8.39 | 45.48 | 242.20 | 31.11 | 157.33 |
| OF29 | National | 11.03 | 338.03 | 25.36 | 13.54 | 135.33 | 374.42 | 39.20 | 299.33 |
| | Imported | 10.67 | 72.03 | 24.36 | 4.46 | 251.32 | 107.05 | 29.08 | 316.08 |
| | Crude Coal Tar | 7.84 | 181.44 | 18.29 | 7.23 | 39.21 | 207.57 | 25.91 | 134.30 |

## 5. Conclusions

In this work, a flexible framework is developed for the evaluation of the optimal flue gas processing from oxycombustion power plant facilities. A systematic approach is used to optimally select the methods following a two-stage procedure including heuristic and mathematical optimization steps. After the preselection of promising technologies, a superstructure is developed, where the boiler, the electrostatic precipitator, dry and wet $SO_2$ removal, NOx catalytic removal, and $CO_2$ purification using carbonation/calcination cycle, zeolites, and amines are modeled using first principles, experimental and industrial data, and rules of thumb. Three different ratios of carbon dioxide and oxygen are studied. Once the processing technologies are selected, an extended blending problem is formulated for the selection of the coal blend to be purchased based on the coal composition and price.

At the design stage, for a typical coal mix in a power plant in Spain, dry $SO_2$ removal, no NOx removal method, and zeolite beds for $CO_2$ purification are selected. The treatment cost increases when the oxygen concentration decreases but the selection of technologies holds good. It should be noted that the air separation unit is not included in the cost. Finally, this framework is used to evaluate the best coal blend formulating an extended blending problem that includes detailed yield models for the operation of all the treatment units. The tradeoffs between sulfur content, price, and yield to power result in the fact that no coal blend is selected due to the low cost of the crude coal tar, in spite of larger flue gas processing costs.

## 6. List of acronyms and abbreviations

b: constant parameter

$C_{Unburned}$: unburned coal (kg/s)

Ca/S: calcium to sulphur molar ratio Q

$Cost_i$: Cost of item i ($/unit)

$CO_{2eff}$: Removal efficiency of $CO_2$ in amines

$D_{Vessel}$: Diameter of the vessel (m)

F: Total flow (kmol/s)

f: constant parameter, 0.174

$fc_{CO2}$: Mass flow of $CO_2$ (kg/s)

$F_0$ : Solid flow to fresh sorbent (mol/s)

$F_R$ : Solid flow to regenerative sorbent (mol/s)

$F_{CO_2}$ : Carbon dioxide feed into the system (mol/s).

$fc_i$: Flow of component i (kg/s)

$H_y$: volume of gas ($Nm^3$/year)

K: Equilibrium constant ($bar^n$)

$L_{Vessel}$: Height of the vessel (m)

L/G: liquid to gas ratio (L/$Nm^3$).

$m_i$: tons per year of contaminant (t/yr)

$m_{zeolites}$: Amount of zeolites (kg)

$MEA_{conc}$: MEA concentration

$MW_i$: Molecular weight of component i (kg/kmol)

MR: Molar ratio

$N^o_{Neds}$: Number of beds

$P_{CO2}$: carbon dioxide partial pressure (atm)

$Pot_{CO2}$: Power generated by carbon used (kwh/kg)

q. Zeolite adsorption capacity (mol/kg)

$q_{unit,amine}$: Experimental value of the thermal energy consumed in amine processing unit. See table 2.

$Q_{(unit)}$: Thermal energy involved in unit (kW)

T: temperature (K)

Thickness. Thickness of the vessel (m)

$V_{zeolites}$: volume of zeolite ($m^3$)

$Weight_{vessel}$: Weight of the vessel (kg)

$y_{O2}$: Percent of oxygen

$\Delta H_{reac}$: Heat of reaction (kJ/kg)

$\tau$: Residence time (s)

$\eta_{unit}$: removal efficiency per unit

$\rho_{steel}$: Density of steel ($kg/m^3$)

$\rho_{bed}$: Density of zeolite bed ($kg/m^3$)

%S: sulfur concentrations feed boiler (%)

## 7. References

Abanades, J.C., 2002. The maximum capture efficiency of CO2 using a carbonation/calcination cycle of CaO/CaCO3. Chemical Engineering Journal 90, 303–306. https://doi.org/10.1016/S1385-8947(02)00126-2

Abanades, J.C., Grasa, G., Alonso, M., Rodriguez, N., Anthony, E.J., Romeo, L.M., 2007. Cost Structure of a Postcombustion CO2 Capture System Using CaO. Environ. Sci. Technol. 41, 5523–5527. https://doi.org/10.1021/es070099a

Al-Abbas, A.H., Naser, J., Dodds, D., 2012. CFD modelling of air-fired and oxy-fuel combustion in a large-scale furnace at Loy Yang A brown coal power station. Fuel 102, 646–665. https://doi.org/10.1016/j.fuel.2012.06.028

Almena, A., Martín, M., 2016. Technoeconomic Analysis of the Production of Epichlorohydrin from Glycerol. Ind. Eng. Chem. Res. 55, 3226–3238. https://doi.org/10.1021/acs.iecr.5b02555

Bui, M., Adjiman, C.S., Bardow, A., Anthony, E.J., Boston, A., Brown, S., Fennell, P.S., Fuss, S., Galindo, A., Hackett, L.A., Hallett, J.P., Herzog, H.J., Jackson, G., Kemper, J., Krevor, S., Maitland, G.C., Matuszewski, M., Metcalfe, I.S., Petit, C., Puxty, G., Reimer, J., Reiner, D.M., Rubin, E.S., Scott, S.A., Shah, N., Smit, B., Trusler, J.P.M., Webley, P., Wilcox, J., Mac Dowell, N., 2018. Carbon capture and storage (CCS): the way forward. Energy Environ. Sci. 11, 1062–1176. https://doi.org/10.1039/C7EE02342A

Clean Air Technology Center., 1999. Nitrogen Oxides (NOx), Why and How They Are Controlled. (No. EPA-456/F-99-006R).

Cuéllar-Franca, R.M., Azapagic, A., 2015. Carbon capture, storage and utilisation technologies: A critical analysis and comparison of their life cycle environmental impacts. Journal of CO2 Utilization 9, 82–102. https://doi.org/10.1016/j.jcou.2014.12.001

David, J., Herzog, H.J., 2019. The Cost of Carbon Capture 6.

Davidson, R.M., Santos, S.O., 2010. Oxyfuel Combustion of Pulverized Coal (No. CCC/168). IEA Clean Coal Centre.

Davis, W., Martín, M., 2014. Optimal year-round operation for methane production from CO2 and water using wind energy. Energy 69, 497–505. https://doi.org/10.1016/j.energy.2014.03.043

Deng, H., Yi, H., Tang, X., Yu, Q., Ning, P., Yang, L., 2012. Adsorption equilibrium for sulfur dioxide, nitric oxide, carbon dioxide, nitrogen on 13X and 5A zeolites. Chemical Engineering Journal 188, 77–85. https://doi.org/10.1016/j.cej.2012.02.026

Donato, F., Favini, B., Giamazzi, E., Picchia, F.R., Arcidiano, N., Cecere, D., Creta, F., 2010. Numerical Modelling of Pulverized Coal Oxy-Combustion (No. Report RdS/2010/30).

Duan, Y., Duan, L., Wang, J., Anthony, E.J., 2019. Observation of simultaneously low CO, NOx and SO2 emission during oxy-coal combustion in a pressurized fluidized bed. Fuel 242, 374–381. https://doi.org/10.1016/j.fuel.2019.01.048
Elliott, T.C., Chen, K., Swanekamp, R.C., 1989. Standard handbook of powerplant engineering. New York, NY (USA); McGraw Hill Book Co., United States.
EPA, 2003. EPA. Air pollution control technology fact sheet. EPA. URL https://www3.epa.gov/ttn/catc/dir1/ffdg.pdf
Fennell, P., Anthony, B., 2015. Calcium and Chemical Looping Technology for Power Generation and Carbon Dioxide (CO2) Capture; Elsevier.
GasNatural Fenosa, 2015. Central térmica La Robla (No. Leaflet).
Global CCS Institute., 2019. Global CCS Institute. URL https://hub.globalccsinstitute.com
GPSA, 2012. Engineering Data Book, 13th ed.
Guerras, L.S., Martín, M., 2019. Optimal gas treatment and coal blending for reduced emissions in power plants: A case study in Northwest Spain. Energy 169, 739–749. https://doi.org/10.1016/j.energy.2018.12.089
Hasan, M.M.F., Baliban, R.C., Elia, J.A., Floudas, C.A., 2012. Modeling, Simulation, and Optimization of Postcombustion CO2 Capture for Variable Feed Concentration and Flow Rate. 2. Pressure Swing Adsorption and Vacuum Swing Adsorption Processes. Ind. Eng. Chem. Res. 51, 15665–15682. https://doi.org/10.1021/ie301572n
Hauchhum, L., Mahanta, P., 2014. Carbon dioxide adsorption on zeolites and activated carbon by pressure swing adsorption in a fixed bed. International Journal of Energy and Environmental Engineering 5, 349–356. https://doi.org/10.1007/s40095-014-0131-3
Hayton, J., 2015. Thermal power plant. Elsevier, Amsterdam.
Herzog, H.J., 2018. Carbon capture, The MIT Press Essential Knowledge series.
Hu, Y., Yan, J., 2012. Characterization of flue gas in oxy-coal combustion processes for CO2 capture. Applied Energy 90, 113–121. https://doi.org/10.1016/j.apenergy.2011.03.005
Jess, A., Wasserscheid, P., 2013. Chemical Technology. An Integral Textbook. Wiley-VCH.
Jurczyk, M., Mikus, M., Dziedzic, K., 2016. Flue gas cleaning in municipal Waste-to-Energy plants - Part 2. Presented at the Infrastructure and Ecology of Rural Areas, p. 1309−1321. https://doi.org/10.14597/INFRAECO.2016.4.2.096
Kohl, A.L., Nielsen, R.B., 1997. Chapter 8 - Sulfur Recovery Processes, in: Kohl, A.L., Nielsen, R.B. (Eds.), Gas Purification (Fifth Edition). Gulf Professional Publishing, Houston, pp. 670–730. https://doi.org/10.1016/B978-088415220-0/50008-2
Koytsoumpa, E.I., Bergins, C., Kakaras, E., 2018. The CO2 economy: Review of CO2 capture and reuse technologies. J. Supercrit. Fluids 132, 3–16. https://doi.org/10.1016/j.supflu.2017.07.029
La Robla staff personal communication., 2017.
Laird, C., Smith, K., 2017. Results of dry sorbent injection testing to reduce HCl. Carmeuse Lime & Stone, Technology Center;
Leung, D.Y.C., Caramanna, G., Maroto-Valer, M.M., 2014. An overview of current status of carbon dioxide capture and storage technologies. Renewable and Sustainable Energy Reviews 39, 426–443. https://doi.org/10.1016/j.rser.2014.07.093
Li, S., Xu, Y., Gao, Q., 2019. Measurements and modelling of oxy-fuel coal combustion. Proceedings of the Combustion Institute 37, 2643–2661. https://doi.org/10.1016/j.proci.2018.08.054
Lockwood, T., 2017. A Compararitive Review of Next-generation Carbon Capture Technologies for Coal-fired Power Plant. Energy Procedia 114, 2658–2670. https://doi.org/10.1016/j.egypro.2017.03.1850
Manovic, V., Anthony, E.J., 2010. Competition of Sulphation and Carbonation Reactions during Looping Cycles for CO2 Capture by CaO-Based Sorbents. J. Phys. Chem. A 114, 3997–4002. https://doi.org/10.1021/jp910536w
Martín, L., Martín, M., 2013. Optimal year-round operation of a concentrated solar energy plant in the south of Europe. Appl. Therm. Eng. 59, 627–633. https://doi.org/10.1016/j.applthermaleng.2013.06.031
Martín, M., 2014. Carbon Capture, How and then What? J Adv Chem Eng. https://doi.org/10.4172/2090-4568.1000e102

Martín, M., Grossmann, I.E., 2011. Energy optimization of bioethanol production via gasification of switchgrass. AIChE Journal 57, 3408–3428. https://doi.org/10.1002/aic.12544
Martín, M.M., 2016. Industrial Chemical Process Analysis and Design. Elsevier, Boston. https://doi.org/10.1016/B978-0-08-101093-8.00012-4
Martín-Hernández, E., Guerras, L.S., Martín, M., 2020. Optimal technology selection for the biogas upgrading to biomethane. Journal of Cleaner Production 267, 122032. https://doi.org/10.1016/j.jclepro.2020.122032
Miller, B., 2015. Fossil Fuel Emissions Control Technologies. Stationary Heat and Power Systems., 1st ed. Elsevier.
Miller, B.G., 2005. Coal Energy Systems. Academic Press, Burlington. https://doi.org/10.1016/B978-012497451-7/50001-2
Mondal, M.K., Balsora, H.K., Varshney, P., 2012. Progress and trends in CO2 capture/separation technologies: A review. Energy 46, 431–441. https://doi.org/10.1016/j.energy.2012.08.006
Mussatti, D., Vatavuk, W., Klotz, W., Stallings, R., Srivastava, R., Hemmer, P., Straight, R., Turner, J., McKenna, J., Mycock, J., Nunn, A., Lawless, P., Tamamoto, T., Coy, D., Greiner, G., 2002. Air pollution control cost manual. (No. EPA 452/B-02-002.).
National Energy Technology laboratory., 2018. Proceedings of the 2018 NETL CO2 Capture Technology Project Review Meeting. National Energy Technology laboratory. URL https://netl.doe.gov/events/conference-proceedings/2018capture
Nemitallah, M.A., Habib, M.A., Badr, H.M., Said, S.A., Jamal, A., Ben-Mansour, R., Mokheimer, E.M.A., Mezghani, K., 2017. Oxy-fuel combustion technology: current status, applications, and trends. International Journal of Energy Research 41, 1670–1708. https://doi.org/10.1002/er.3722
Nichols, G.B., McCain, J.D., 1975. Particulate collection efficiency measurements on three electrostatic precipitators. Final report, Jul 1973--Jul 1975. United States.
Ortiz, C., Valverde, J.M., Chacartegui, R., Benítez-Guerrero, M., Perejón, A., Romeo, L.M., 2017. The Oxy-CaL process: A novel CO2 capture system by integrating partial oxy-combustion with the Calcium-Looping process. Applied Energy 196, 1–17. https://doi.org/10.1016/j.apenergy.2017.03.120
Perrone, D., Castiglione, T., Klimanek, A., Morrone, P., Amelio, M., 2018. Numerical simulations on Oxy-MILD combustion of pulverized coal in an industrial boiler. Fuel Processing Technology 181, 361–374. https://doi.org/10.1016/j.fuproc.2018.09.001
Riaza, J., Gil, M.V., Álvarez, L., Pevida, C., Pis, J.J., Rubiera, F., 2012. Oxy-fuel combustion of coal and biomass blends. Energy 41, 429–435. https://doi.org/10.1016/j.energy.2012.02.057
Romeo, L.M., Abanades, J.C., Escosa, J.M., Paño, J., Giménez, A., Sánchez-Biezma, A., Ballesteros, J.C., 2008. Oxyfuel carbonation/calcination cycle for low cost CO2 capture in existing power plants. Energy Conversion and Management 49, 2809–2814. https://doi.org/10.1016/j.enconman.2008.03.022
Rosenberg, H.S., Oxley, J.H. [Battelle M.I., Columbus, OH (USA)], 1993. Selective catalytic reduction for NOx control of coal-fired power plants. United States.
Sargent, Lundy, L., 2003. Wet flue gas desulfurization technology evaluation project number 11311-000 prepared for national lime association.
Sarkar, D.K., 2015. Thermal Power Plant: Design and Operation. Elsevier, Amsterdam.
Shemwell, B.E., Ergut, A., Levendis, Y.A., 2002. Economics of an Integrated Approach to Control SO2, NOx, HCl, and Particulate Emissions from Power Plants. null 52, 521–534. https://doi.org/10.1080/10473289.2002.10470805
Siqueira, R.M., Freitas, G.R., Peixoto, H.R., Nascimento, J.F. do, Musse, A.P.S., Torres, A.E.B., Azevedo, D.C.S., Bastos-Neto, M., 2017. Carbon Dioxide Capture by Pressure Swing Adsorption. Energy Procedia 114, 2182–2192. https://doi.org/10.1016/j.egypro.2017.03.1355
Stec, M., Tatarczuk, A., Więcław-Solny, L., Krótki, A., Ściążko, M., Tokarski, S., 2015. Pilot plant results for advanced CO2 capture process using amine scrubbing at the Jaworzno II Power Plant in Poland. Fuel 151, 50–56. https://doi.org/10.1016/j.fuel.2015.01.014
The World Bank, 2014. The World Bank. Electricity Production from Coal Sources. The World Bank. URL https://data.worldbank.org/indicator/eg.elc.coal (accessed 5.18.21).
Wallas, S.M., 1990. Chemical Process Equipment. Selection and Design, Series in Chemical Engineering. Butterworth-Heinemann, Boston.

Wang, Y., Zhao, L., Otto, A., Robinius, M., Stolten, D., 2017. A Review of Post-combustion CO2 Capture Technologies from Coal-fired Power Plants. Energy Procedia 114, 650–665. https://doi.org/10.1016/j.egypro.2017.03.1209

Zebian, H., Gazzino, M., Mitsos, A., 2012. Multi-variable optimization of pressurized oxy-coal combustion. Energy 38, 37–57. https://doi.org/10.1016/j.energy.2011.12.043

Zhang, J., Xiao, P., Li, G., Webley, P.A., 2009. Effect of flue gas impurities on CO2 capture performance from flue gas at coal-fired power stations by vacuum swing adsorption. Energy Procedia 1, 1115–1122. https://doi.org/10.1016/j.egypro.2009.01.147

Zhang, Y., Chen, C.-C., 2013. Modeling CO2 Absorption and Desorption by Aqueous Monoethanolamine Solution with Aspen Rate-based Model. Energy Procedia 37, 1584–1596. https://doi.org/10.1016/j.egypro.2013.06.034

Zhong, Y., Gao, X., Huo, W., Luo, Z., Ni, M., Cen, K., 2008. A model for performance optimization of wet flue gas desulfurization systems of power plants. Fuel Processing Technology 89, 1025–1032. https://doi.org/10.1016/j.fuproc.2008.04.004

# Chapter 5

# On the water footprint in power production: Sustainable design of wet cooling towers.

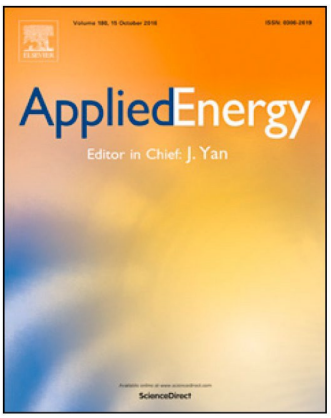


*Authors:* ***Lidia S Guerras*** *and Mariano Martín*

*DOI:* doi.org/10.1016/j.apenergy.2020.114620

## Abstract

Renewable based power plants must be installed where the main resource is available. The weather affects the design and the water footprint of these plants. Two types of power cycles, a regenerative Rankine cycle, representing biomass and solar thermal plants, and the combined cycle, corresponding to biogas or gasification based processes, are studied. The facilities are modeled unit by unit in detail to compute the cycle yield, the condenser duty, the water consumption and the natural draft wet cooling tower geometry for its sustainable design. Hot regions, appropriate for solar facilities, and humid regions require larger and more expensive towers. Areas with high solar availability also show larger consumption of water presenting a tradeoff for a future renewable based power system. In addition, design guidelines and surrogate models to estimate water consumption, cooling tower size and its cost as a function of the climate have also been developed. The surrogates are useful for the analysis on the water footprint of a renewable based power system that substitutes the fossil based one.

## 1. Introduction

The Water-Energy (WE) nexus has become an important criterion for the analysis of the sustainable growth of society (Tsolas et al., 2018). This nexus is of paramount importance in the power industry due to the strong link between water consumption and electricity production (Gjorgiev and Sansavini, 2018; Nouri et al., 2019). Most power plants use wet cooling towers as the technology of choice because of their efficiency (Dehaghani and Ahmadikia, 2017; Luceño and Martín, 2018), but their operation relies on the availability of water. These units cool down the water used in condensing the exhaust steam from the turbine at the expense of evaporating a fraction of it. Cooling towers play a key role in the cleaner production of power to avoid thermal load released to rivers (Gjorgiev and Sansavini, 2018;Harte and Krätzig, 2002), but the make-up water represents the consumption of water in the production of electricity. On average, Rankine based power plants consume around 2 L/kWh in their operation on average (Delgado and Herzog, 2012; Harte and Krätzig, 2002; Macknick et al., 2011; Torcellini et al., 2003; Zhai and Rubin, 2010), while combined cycles are more efficient, presenting consumptions of around 1 L/kWh (Maulbetsch and DiFilippo, 2006). The current trend towards a more sustainable energy system results in the penetration of resources such as biomass, solar and wind into the energy mix (Ali and Kumar, 2017). The main issue related to the use of renewable resources is that the location of the facilities that transform them into electricity is highly dependent on the availability of the resources. In most cases the weather conditions are not the most appropriate for the operation of cooling technologies and, in particular, cooling towers. In a future where water scarcity is also a major concern (Wan et al., 2016), the analysis of the water footprint of the emerging power system is an important index for its sustainability (Peer and Sanders, 2018).

Different dry cooling systems are being studied recently aiming at dealing with the water consumption on power plants, and in particular in concentrated solar power plants (CSP). Among these designs it is important to highlight the A-frames, air cooler condensers with a bundle of pipes in the form of an A (Kröger, 2004). While these systems are interesting for solar applications, they use up to 10% of the power from the facility to condense the exhaust (Luceño and Martín, 2018). Alternatively, natural draft dry cooling towers (NDDCT) can also be used. They are similar to wet cooling towers but within the structure a heat exchanger is built (Tanimizu and Hooman, 2013). Its operation relies on convective heat transfer

(Busch et al., 2002). Although, NDDCT operation does not consume water, it is highly dependent on the weather conditions (Li et al., 2017) and particularly on the crossflow wind (du Preez and Kröger, 1993). It has been proved that for hot days pre wet cooling is recommended (Zhang et al., 2017). Thus, the high efficiency of wet cooling towers, the fact that the power industry is used to operate them (Dehaghani and Ahmadikia, 2017) and the recent findings that show that even under scarce water availability wet cooling towers are competitive and offer a sustainable performance versus dry cooling (Luceño and Martín, 2018) encourages improving the sustainability and efficiency of these units towards their implementation within renewable based power facilities.

The design of natural draft wet cooling towers (NDWCT) is an area that combines the structural design of the unit and the unit operation of water cooling. As a result, two lines or work have been pursued, either structural analysis or the performance of the tower. On the one hand, studies have focused on the structural design of the tower (Gould and Kratzig, 1999) presenting new designs (Busch et al., 2002), the evolution of cooling tower sizing over time (Lang and Strauß, 2011) as well as the estimation of the cost of the unit from the mechanical and structural points of view (Buys and Kröger, 1989; Kloppers and Kröger, 2004). On the other hand, the evaluation of the gas-liquid contact responsible for water cooling has been studied experimentally (Lemouari et al., 2009) and theoretically (Kloppers and Kröger, 2005) evaluating the performance (EPA, 1970), optimizing it (Williamson et al., 2008), presenting design rules (Kreith and Goswami, 2005) as well as current efforts to evaluate their operation within concentrated solar power (CSP) plants (Xu et al., 2011), performing sensitivity analysis on the operation (Qi et al., 2007) as well as economic (Ifaei et al., 2016b, p. 1) and environmental analysis (Ifaei et al., 2016a, p. 2) of the tower, to optimize their performance when used for CSP plants (Sun et al., 2019). Simulation (Queiroz et al., 2012) and mathematical optimization (Martín and Martín, 2013) approaches have been used to improve the performance of the tower analyzing the transport phenomena involved in the operation, including the systematic comparison of various fillings (Gao et al., 2016; Serna-González et al., 2010). However, to the best of our knowledge, design of NDWCT considering structural and gas-liquid contact simultaneously has not been addressed. In addition, to achieve the goal of sustainable power production the use of renewable resources to produce electricity is not enough. The sustainable design of the cooling technologies is also to be addressed. A sustainable design must take into account the simultaneous analysis of the structure,

responsible for use of material, and the unit cost, and the gas-liquid contact, linked to the performance and the consumption of water. However, typically the estimation of the cost of cooling towers is based on the heat load rejected alone (Matches, 2020; Sinnott and Towler, 2016), while the size of the tower is a function of the weather (Martín and Martín, 2017). For instance, the tower size for the same cooling load is almost twice in the northwestern of Spain compared to the south east (Sun et al., 2019). Therefore, the cost estimation methods available in the literature (Matches, 2020; Sinnott and Towler, 2016) do not capture the effect of the location of the unit that is paramount for the design of the future power system towards reducing its environmental impact, including the water footprint. In addition, the analysis of water consumption has received less attention. Over the years research has focused on evaluating the operation of the cooling towers at different seasons (Jagadeesh and Reddy, 2013) and climatic zones (Ludovisi and Garza, 2015), including the effect of climate change on the future design of the towers (Ayoub et al., 2018), monitoring their efficiency over time (Krahé et al., 2016) and defining a methodology to evaluate that performance (Smrekar et al., 2011), presenting profiles of data on the water withdrawal and consumption (Peck and Smith, 2017), reporting average values for the consumption (Byers et al., 2014) and evaluating the crosswind effect on the temperature profile experimentally (Gao et al., 2014) and on their operation (Li et al., 2019). The systematic evaluation of the operation of cooling towers resulted in rules of thumb (Khamis Mansour and Hassab, 2014), surrogate models (ASHRAE, 1983) and the development of simplified models to estimate the evaporative loses (Qureshi and Zubair, 2006; Vengateson, 2017; Zhang et al., 2018). Only lately, due to the concerns on future water availability have led to computing the consumption of water related to the operation of the cooling tower (Martín and Martín, 2017; Nouri et al., 2019), comparing its performance with air cooling as a water saving alternative (IEA, 2010). However, the effect of the location of the unit on the water footprint due to the weather conditions has not been evaluated nor an easy method to compute is available.

In this work an integrated mathematical formulation is developed to provide design guidelines for the design of sustainable natural draft wet cooling towers and to estimate their water footprint as a function of the power plant location. The study provides process data on the water footprint when substituting the power produced by current facilities by renewable-based resources so as to be able to select the cooling system based on performance and cost comparing dry and wet cooling alternatives. These results are

needed to evaluate the future energy system where a range of resources will contribute to meet the power demand and whose availabilities are highly location dependent. To achieve that, the entire power facility is considered in the analysis. Two thermodynamic cycles are evaluated to cover all possible sources of energy in thermal plants, the Rankine and combined cycles. The facilities are modeled in detail from a process perspective to compute the power production, the cooling needs, the water consumption and the tower structure. Due to the effect of weather conditions on the design and water consumption of the tower, real data of an entire country are used. Spain is considered as a case study because it is in a vulnerable situation regarding water availability, presenting regions with moderate availability together with others where desertification is becoming an issue (IEA , 2010). The model is used for a variety of climate regions such as arid ones in the South West, continental, Mediterranean, Cantabrican and Atlantic climates and validated against industrial data. This study also allows developing surrogate models for the quick prediction of the water consumption and the estimation of the cooling tower sizing and cost as a function of the location. The rest of the paper is organized as follows. In Section 2 the methodology for the sustainable design of cooling towers and the location effect on their water footprint is presented and the development of surrogates for conceptual design. Section 3 shows the details of the modelling of the entire facility, from the power island to the cooling section, including mass and energy balances, thermodynamics, rules of thumb and geometric constraints. In Section 4 the main results are discussed. Finally, Section 5 draws some conclusions.

## 2. Methodology

NDWCTs are widely used as cooling technology for thermal plants due to their efficiency (Luceño and Martín, 2018). However, their design must address the structure and water use simultaneously to improve the environmental footprint of the future energy systems, whose location is linked to the availability of the resources. This work aims at designing sustainable cooling towers and also, once installed, evaluating their water footprint across weather conditions. The analysis presented in this work, as described in Section 2.1 of the methodology, evaluates the water footprint and the cooling tower design associated to the two main thermal cycles implemented in power plants, regenerative Rankine and combined cycle. The analysis of each of the cycles is based on a detailed first principle model of the entire power plant. This model will be developed and validated versus industrial data to represent the cooling tower, including structural and gas-

liquid contact features, as well as the thermodynamic cycles. The model itself will be described in Section 3. Aiming at the optimal sustainable design of the unit and consumption of water, a mathematical optimization framework is formulated. An objective function that considers sustainable parameters of the cooling tower is developed, as presented in Section 2.2, including the models described in Section 3 as constraints. The design of the cooling tower is a different problem compared to the evaluation of the water consumption. The first problem aims at the sustainable design of the cooling tower as a function of the location, and it is discussed in Section 2.3. The second one, presented in Section 2.4, addresses the effect of the weather conditions on the water consumption. Finally, for easy use of the results of this work, Section 2.5 presents the approach used to develop surrogate models to easily estimate the tower size, its cost and water consumption as a function of the facility location.

Two main results are expected from this work, the geometric design of the tower and the water consumption when a particular facility is located at a region. To present the variability in the water consumption and tower design under different weather conditions, the model is evaluated in different climate regions across Spain. The regions are selected so that all the climates are represented in the study. Figure 5.1 shows the map of the climatic regions of Spain. To be representative of cold and warm regions, 10 different provinces within the main climatic areas are considered, from arid in the southeast, to oceanic in the northwest including Mediterranean hot, to Mediterranean mild in the cost, from the continental, to the steppe, covering the places where current fossil based plants are located. Furthermore, the location of current nuclear, coal and natural gas facilities, as provided by the Spanish national electric network, is considered for the selection of the locations evaluated (Electrical Network of Spain, 2018). The selected locations are represented by stars in Figure 5.1.

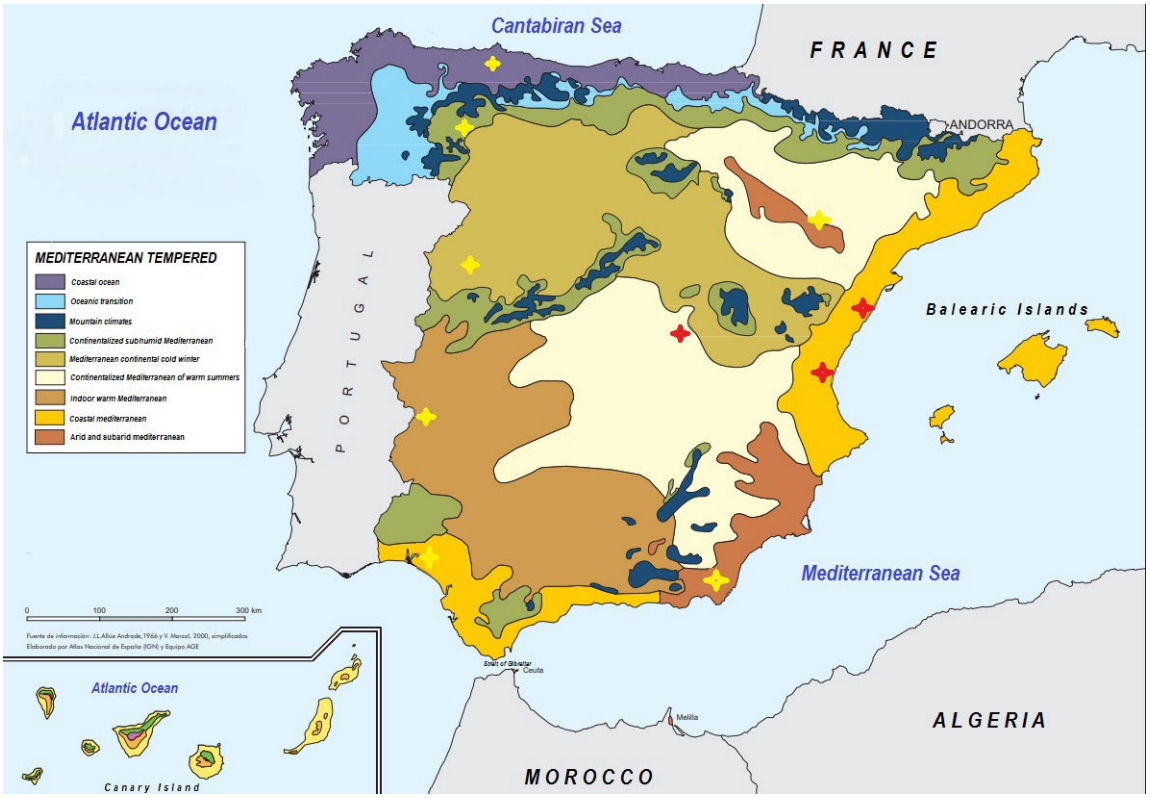


***Figure 5.1.*** Climatic regions and locations evaluated. Adapted with permission from (IGN, 2019).

### *2.1. Models structure of the thermodynamic cycles*

This study considers two different cycles to represent most of the thermal power facilities no matter the energy source. The regenerative Rankine Cycle, from now on P1, consists of the mass, energy balances and thermodynamic properties described in Sections 3.1 and 3.3, see supplementary material for the full set of equations. This cycle represents the operation of a conventional coal, any fossil fuel as well as concentrated solar (CSP's) and biomass power plants. This model is written in GAMS® with around 220 equations and similar number of variables. For the combined cycle, P2, the model includes the gas treatment and the gas turbine while the Rankine cycle is modified so that the energy source is the hot flue gas from the gas turbine, as presented in Sections 3.2 and 3.3. A combined cycle can be used with natural gas, shale gas, syngas or biogas. Furthermore, it can easily be extended to biomass or coal by integrating a gasifier into the process. The model is larger, around 778 eqs. and 971 var., and it is also written in GAMS®.

### *2.2. Objective function*

For the sustainable design of cooling towers, a number of criteria must be considered including costs and environmental impact. The Renewable Process Synthesis Index Metric (REPSIM) (Martín, 2016)

is used to develop an objective function so as to simultaneously account for the emissions saved when substituting current coal based facilities, the emissions due to water consumption, both translated into cost using the carbon tax and the investment cost of the materials such as the shell of the cooling tower and the heat exchanger of the cooling system. Thus, the objective function becomes Eq. (1).

$$Cost = C_{TAX}\left(-W_{total}\cdot CO_{2_{Power}}\cdot\tau + Water_{C}\cdot CO_{2_{Water}}\tau\right) + \frac{1}{3}\left(C_{Shell}\cdot Volume_{Shell} + C_{Wood}\,Volume_{Filling} + C_{HX}\right) \quad (1)$$

The emissions due to the cooling tower shell and its packing can also be computed. However, since the emissions due to the material are also related to the volume of concrete, as well as its cost, it is decided not to consider both to avoid double counting of the volume of the material in the objective function. The emissions and costs due to the different items are taken from the literature as well as the carbon tax, see Table 5.1.

***Table 5.1***. Parameters of the emissions and cost objective function(Katimber, n.d.; Kloppers and Kröger, 2004; Olivier et al., 1999)

| | $CO_2$ Emissions | Cost | |
|---|---|---|---|
| *Power* | 0.632 kg/kWh | 50 €/t Carbon Tax | |
| *Water Consumption* | 0.3 kg/m$^3$ | 50 €/t Carbon tax | |
| *Concrete Shell* | 0.41 kg/ L | 200 €/m$^3$ | (Khamis Mansour and Hassab, 2014; Zhang et al., 2017) |
| *Tower filling* | 1.33 kg/L | 25€/m$^3$ | (ASHRAE, 1983; Zhang et al., 2017) |

### *2.3. Cooling tower design problem.*

The design of a unit consists of defining the features so that it is flexible to operate over time. Therefore, the sustainable design of the cooling tower is performed optimizing P1 and P2 using Eq. (1) as objective function following a worst case scenario approach over the time horizon of a year. The worst case corresponds to the month with the most complex conditions for the tower to operate, typically the one with the lowest temperatures and largest humidity, resulting in the need for a larger tower size. The tower height and the materials cost are evaluated as a function of the plant production capacity, the pressure, temperature and humidity. The problems are solved using a multi-start optimization procedure with CONOPT as the preferred solver. The model is validated versus industrial data. To evaluate the effect of the production capacity on the tower size and cost, different power plant sizes for the 10 locations are considered. For the regenerative Rankine cycle 6 plant capacities are used from 40 to 450 MW. For the combined cycle, a more efficient cycle, 5 plant sizes from 100 to 450 MW are used.

### *2.4. Water consumption evaluation*

The water consumption of the optimal cooling tower installed under different weather conditions is evaluated by solving P1 and P2 using Eq. (1) as objective function. The problems are solved using a multi-start optimization procedure with CONOPT as preferred solver. In this case, for both cycles, the power production capacity is fixed to 350 MW, the typical size of a thermal group in coal based power plants in Spain (Vidal and Martín, 2015). The model is also validated versus industrial facilities data. Next, the actual weather data of the 10 locations over the entire year on a monthly basis generate a data set of 120 points, each considered as an independent design condition. Each thermodynamic cycle is evaluated over the data set to evaluate the effect of pressure, temperature and humidity on the consumption of water. Note that alternatively, we could have used a Monte Carlo approach to generate the set of combinations of the independent variables. However, by using real data, the results are expected to be more representative and allow presenting the water consumption across Spain to see the effect of the location of the facility on the use of water.

### *2.5. Surrogate model development*

The use of the detailed models given by P1 or P2 may not be easy for early stage analysis and conceptual design. The data obtained from the optimization of the cases described along the previous two paragraphs are used to develop surrogate models for quick estimation of the tower geometry, its cost and the water consumption as a function of the weather conditions and the power plant capacity. The fitting is carried out suggesting a non-linear multivariable model that is adjusted to the results of the detailed model minimizing the error of estimation using a reduced gradient method in GAMS®. These correlations can be implemented within the current tools (Matches, 2020; Sinnott and Towler, 2016) to estimate the performance and the cost of the NDWCT.

## 3. Process model

This section is divided into the evaluation of the power islands of two different thermodynamic cycles, regenerative Rankine, and combined cycle, and the detailed design for the cooling tower. P1 defined

in the Section 2 consists of the models described in Sections 3.1 and 3.3 while P2 includes the processes depicted in Sections 3.2 and 3.3.

### *3.1. Rankine cycle analysis*

The Rankine cycle is modeled unit by unit as presented in Figure 5.2. Mass and energy balances and detailed thermodynamics are used, see supplementary material for the modelling details. Here, only the major assumptions are presented. The source of energy can be a fuel, where a boiler is used, or a solar field. For a regenerative Rankine cycle two stages are considered, production of superheated steam and steam reheating. In case a fuel is used, both steps take place within the boiler. However, in the case of CSP plants, a series of heat exchanges are used to heat up, evaporate and overheat the steam and another heat exchanger is used for the regenerative section of the cycle. The overheated steam is fed to the turbine. This unit is modeled as consisting of high, medium and low pressure sections. The pressure range of operation for each section of the turbine is taken from the literature. In the literature the high pressure turbine typically operates from 40 to 126 bar (Ghobeity et al., 2011; Xu et al., 2011). Thus, a range from 90 bar to 125 bar for the steam being fed to the turbine is considered. The high pressure superheated steam is expanded into a medium pressure. A range from 11 to 35 bar is allowed based on data from the literature (Morin et al., n.d.; Xu et al., 2011). A fraction of the stream is used as an extraction to reheat up the condensed steam and the rest is expanded in the low pressure turbine. This last pressure ranges from 0.05 bar to 0.31 bar (Palenzuela et al., 2011; Walas, 1990). It is also an optimization variable within the range of 0.05 to 0.35 bar. This stream can contain a small amount of vapor, up to 8%. Each turbine, low, medium and high pressure, is modeled similarly considering a non-ideal isentropic expansion. The expansion of the steam in the different turbines is assumed to have an isentropic efficiency of 0.9 (León and Martín, 2016). The enthalpies and entropies are computed using surrogate models as a function of the pressure and temperature developed in previous works (León and Martín, 2016; Martín and Martín, 2017). The total energy obtained in the system to be optimized is the sum of the ones generated at the three bodies of the turbine.

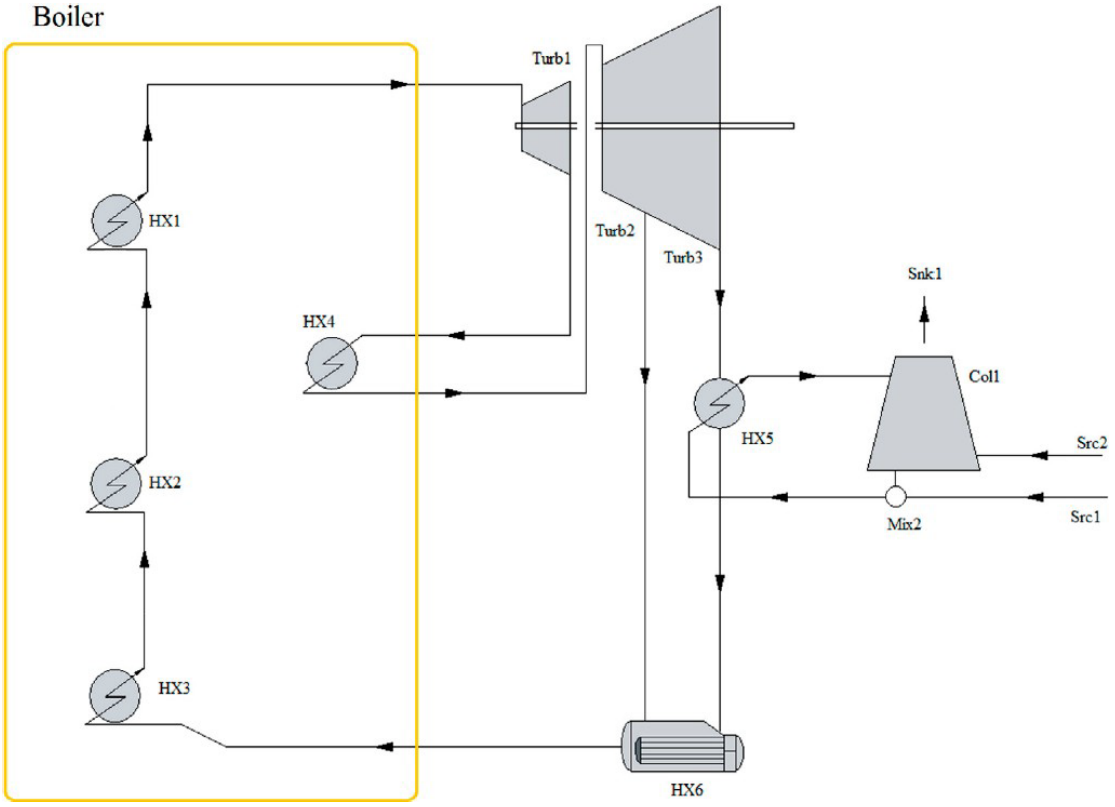


***Figure 5.2***. Flowsheet of the facility based on a regenerative Rankine cycle.

### *3.2. Combined cycle analysis*

From a gas fuel, the process consists of a treatment stage to remove sulphur hydride and other traces of undesirable species including ammonia, particles or $CO_2$. Next a gas turbine is used. The model for the gas turbine consists of four sections. The compression stages of air and fuel, a combustion chamber and a final gas expansion. Multistage compression with intercooling are used to model both assuming polytropic compressors, Eqs. (2)–(3). The polytropic coefficient, z, is taken to be 1.4 based on an offline simulation using CHEMCAD®. The efficiency of the compressor ($\eta_c$) is assumed to be 85% (Moran and Shapiro, 2003). A maximum gas pressure of 40 bar is considered.

$$T_{out/compresor} = T_{in/compressor} + T_{in/compressor}\left[\left(\frac{P_{out/compressor}}{P_{in/compressor}}\right)^{\frac{z-1}{z}} - 1\right]\frac{1}{\eta_c} \quad (2)$$

$$W_{(Compressor)} = (F)\cdot\frac{R\cdot z\cdot\left(T_{in/compressor}\right)}{((MW)\cdot(z-1))}\frac{1}{\eta_c}\left[\left(\frac{P_{out/compressor}}{P_{in/compressor}}\right)^{\frac{z-1}{z}} - 1\right] \quad (3)$$

The combustion chamber is modeled as an adiabatic furnace based on the stoichiometry of the combustion of the species with an excess of air. The excess is used to control the final temperature before expansion so that it is below 1600 °C, the typical upper bound for gas turbines. Complete combustion of all the species is assumed. The model is flexible so that not only natural gas but also biogas or syngas can be used, in case syngas is produced via biomass gasification.

$$Q_{(Furnace)} = \sum_h \Delta H_f(h)\Big|_{T(Furnace,GasTurb)}\Big|_{(Furnace,GasTur)} - \sum_h \Delta H_f(h)\Big|_{T(Compres\,2,Furnace)}\Big|_{(Compres\,2,Furnace)} - \sum_h \Delta H_f(h)\Big|_{T(Compres3,Furnace)}\Big|_{(Compres3,Furnace)} \quad (4)$$

The hot gas is expanded in a turbine to obtain power. This last section of the gas turbine is modeled as a polytropic expansion, with z equal to 1.3, computed offline with CHEMCAD®, and with an efficiency of 85% (Moran and Shapiro, 2003). The exhaust gas is used within a regenerative Rankine cycle that is modeled similarly to the one described in Section 3.2, but for the heat source that corresponds to the hot flue gas that generates the steam in HX8, HX19 and HX4 and overheats the expanded steam from the high pressure turbine in HX5. The rest is the same as for the previous case. Figure 5.3 shows the flowsheet used to model the combine cycle plant.

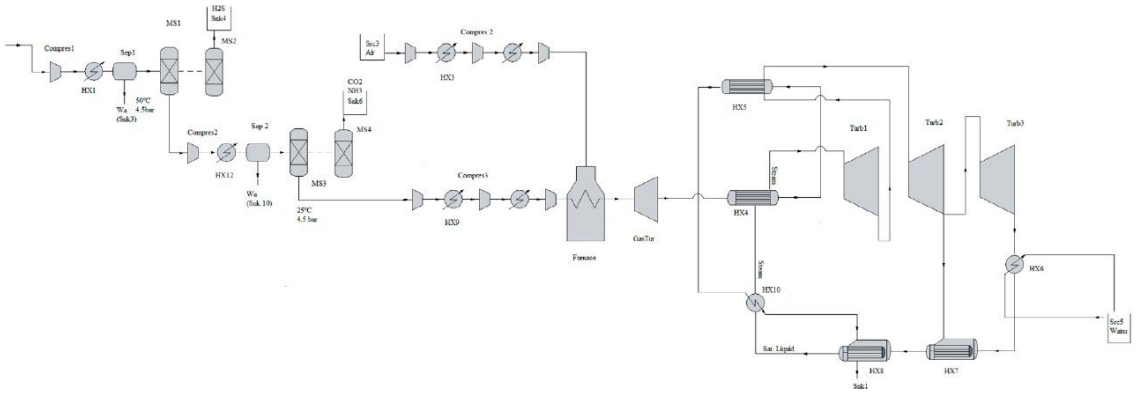


***Figure 5.3.*** Scheme of the flowsheet for a combined cycle.

### *3.3. Cooling tower design*

The operation of the cooling tower depends on the gas-liquid contact provided by the packing. An analysis of the mass and energy transfer in this region is performed to evaluate its design. Further details of the model can be found in the supplementary material and in previous work (Martín and Martín, 2017). The height of the packing is computed as given by Eq. (5), that is developed based on an energy balance to the packing.

$$P_{Height} = \frac{f_{air}}{k_y A S} \int_{h_1}^{h_2} \frac{dh}{h_i - h} \quad (5)$$

Mickley's method is used to solve the performance of the tower as described in previous work (Martín and Martín, 2017). The operating line is determined by an energy balance between the air and the water flows, resulting in Eq. (6).

$$\frac{H_2 - H_1}{t_{L,2} - t_{L,1}} = \frac{f_{Wa}}{f_{air}} = \frac{L}{V} \quad (6)$$

The water flow, $f_{Wa}$, that is used to condense the exhaust steam from the turbine, is calculated from the energy balance to HX5, see supplementary material. The cooling water is heated up at most 8–10°C across the heat exchanger, based on rules of thumb (Cheremisinoff and Cheremisinoff, 1981; Coulson and Richardson, 1999; Geankoplis, 2003).

$$8 \leq \left( t_{L,in} - t_{L,out} \right) \leq 10 \quad (7)$$

where $t_{L,in}$ is the temperature of the water to be cooled and $t_{L,out}$ the final temperature of the water. The operation of the cooling tower requires a minimum flow of air, typically from 1.3 to 1.5 times the minimum given by the profile of the humid air enthalpy (Palenzuela et al., 2011), calculated based on the inlet and outlet conditions of the air and water.

The water flow is cooled because a fraction is evaporated. Rules of thumb are used (Perry and Green, 1997) to establish the lower bound of the water losses of the system, $F_E$, that determines the water make-up to the system and the humidity of the air exiting the cooling:

$$F_E \geq 1.8 \cdot 0.00085 \cdot f_{Wa} \left( t_{L,in} - t_{L,out} \right) \quad (8)$$

The temperature of the air leaving the tower is calculated as the final temperature of the profile along the cooling tower. The Lewis relationship, Eq. (9), based on an energy balance (Geankoplis, 2003), relates the operation line with the equilibrium line determining the temperature of the air.

$$\frac{H_i - H}{T_i - t_L} = -\frac{h_L}{k_y} \quad (9)$$

Even though the ideal operation suggests that the slope (-hL/ky) is -inf, it typically ranges between -3 and -10. The profile of the air temperature is computed as the ratio of the change on enthalpy and temperature as it exchanges moisture with the liquid flow Eq. (10).

$$\frac{(H_i - H)}{(T_i - T_g)} = \frac{dH}{dT_g} \tag{10}$$

The mass transfer coefficient, ky, is computed using the correlation given by Coulson and Richardson (1999) assuming that the contact area provided by the fillings is constant and equal to 250 m2/m3, where $G_{flux}$ and $L_{flux}$ are the cross sectional flows and S the specific contact area.

$$k_y = \left(\frac{2.95}{S}\right) \cdot (G_{flux})^{0.72} \cdot (L_{flux})^{0.26} \tag{11}$$

The specific flows across the contact region are computed per the gas and liquid flows and the actual area

$$A = \left(\frac{\pi}{4}\right) \cdot D_{base}^{2} \tag{12}$$

$$G_{flux} = \frac{f_{air}}{A}; \tag{13}$$

$$L_{flux} = \frac{f_{Wa}}{A} \tag{14}$$

To compute the column diameter, a bound related to the height of the packing is added,

$$D_{Base} \geq 5 \cdot P_{Height}; \tag{15}$$

The design of the structure of the cooling tower aims to provide enough driving force to allow the air flow across the tower. The driving force, $\Delta P_{Generated}$, is given by buoyancy, Eq. (16).

$$\Delta P_{Generated} = T_{Height} \cdot g \cdot (\rho_{g,in} - \rho_{g,out}); \tag{16}$$

where $T_{height}$ is the total height of the tower, g is gravity and $\rho_g$ the air density. Assuming ideal gases, the air density across the tower is computed as follows:

$$\rho^g = \left(\frac{1}{M_{air}} + \frac{Y}{M_{water}}\right) \frac{RT_g}{p} \tag{17}$$

The driving force generated by the parabolic structure must be enough to counterbalance the pressure drop generated across the support of the tower, the contraction as the air enters the structure, the packing, the pressure drop generated by the water spray generated to cooldown the water and that of the mist eliminator (Buys and Kröger, 1989; Kloppers and Kröger, 2004), see Eq. (18).

$$\Delta P_{Loss} = \left(N_{Mist} + N_{Support} + N_{Contraction} + N_{Spray} + N_{Packing}\right)\rho_{air}\frac{v_{air}^2}{2}$$

$$where:$$

$$N_{Contraction} = 0.167\left(\frac{D_{base}}{h_c}\right)^2 \qquad (18)$$

$$0.02 \cdot D_{base} \le h_c \le 0.12 \cdot D_{base}$$

$$N_{Spray} = 0.16 \cdot h_c \cdot \left(\frac{f_{Wa,in}}{f_{air,in}}\right)^{1.32}$$

$$N_{Packing} = P_{Height} \cdot 2.36\left(\frac{L_{flux}}{3.391}\right)^{1.1} \cdot \left(\frac{G_{flux}}{3.391}\right)^{-0.64}$$

The driving force should be, at least, 10% larger that the pressure drop across the tower.

$$1.1 \cdot \Delta P_{Loss} \le \Delta P_{Generated} \qquad (19)$$

The geometry of the cooling tower is that of a hyperboloid (Dehaghani and Ahmadikia, 2017), see Figure 5.4. Thus, the dimensions involved in the pressure drop must comply with that geometry where each section of the hyperboloid, $Z_H$ and $Z_u$, is computed using eq (20) where di is the diameter at $Z_i$, $d_t$ is the largest diameter.

$$\frac{d_i^2}{d_t^2} - \frac{Z_i^2}{b^2} = 1 \qquad \forall i \in \{u, H\} \qquad (20)$$

The total height of the tower, THeight, is given by adding the three sections in Figure 5.4, where $h_c$ is the height of the opening for the air fed to the CT.

$$T_{Height} = Z_H + Z_u + h_c \qquad (21)$$

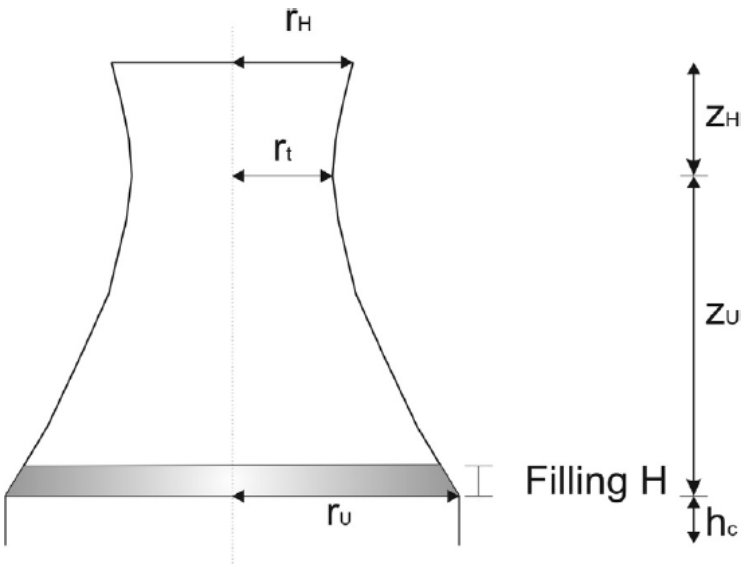


***Figure 5.4***. Scheme of the structure of the cooling tower.

Further constraints based on rules of thumb are imposed to avoid unstable designs (Kloppers and Kröger, 2004). Almási (1981) suggested typical ratios for the dimensions of the shell as shown in Eq. (21).

$$\begin{aligned} &0.55\cdot D_{base} \le 2\cdot r_t \le 0.65\cdot D_{base} \\ &0.61\cdot D_{base} \le 2\cdot r_H \le 0.73\cdot D_{base} \\ &1.25\cdot D_{base} \le CT_{Height} \le 1.5\cdot D_{base} \\ &1.1\cdot D_{base} \le Z_u + Z_h \le 1.3\cdot D_{base} \\ &0.92\cdot D_{base} \le Z_u \le 1.02\cdot D_{base} \end{aligned} \tag{22}$$

Diameter ratio to prevent cold inflow around 0.58 is recommended (Serna-González et al., 2010). The volume of the concrete in the tower shell can be approximated by

$$V_{Shell} = \frac{\pi}{2}\left(2\cdot r_u + 2\cdot r_H\right)\cdot t_s \cdot T_{Height} \tag{23}$$

where $t_s$ is the thickness of the cooling tower shell and it is computed based on data from actual columns where $t_{ratio}$ is 0.0023.

$$t_s = t_{ratio}\, D_{Base} \tag{24}$$

The capital cost of the tower shell is approximated by Eq. (25).

$$C_s = V_{Shell}\cdot C_{conc} \tag{25}$$

where $C_{conc}$ is the cost of concrete per unit volume, which includes the cost of construction.

The cost of the fill is given by

$$C_{fill} = V_{fi} \cdot C_{fi} = \left(\frac{\pi}{4}\right) \cdot D_{base}^{2} \cdot P_{Height} \cdot C_{fi} \quad (26)$$

where Cfi is the cost per cubic meter of fill. See the Table 5.1. A detailed implementation of the CT model can be found in (Sun et al., 2019).

### *3.4. Water consumption*

The water lost by the operation of a cooling tower is related to the recycle ratio, known as cycles of concentration (COC). Industrial practice uses COC's from 3 to 7 (Fatigati, 2006). A value of 6 is assumed for the calculations. The water lost is due to the blow down losses, $F_B$, the evaporation losses, $F_E$ and the drift. $F_D$. Drift is expected to be negligible in newly designed towers. $F_B$ losses is computed as a function of the $F_E$ as follows

$$F_B = F_E / (C.O.C - 1) \quad (27)$$

Thus, the lost waster is computed by Eq. (28)

$$F_M = F_E + F_B \quad (28)$$

## 4. Results

The results section is divided into three major subsections. First, major operating characteristics of the power cycles are presented, Section 4.1 that will help present the different water consumption and cooling tower size for the two thermodynamic cycles. Next, in Section 4.2 the design problem is addressed, by presenting the geometric features of the cooling towers required across different climates are presented and validated versus real plant data. In addition, the effect of the weather conditions on the tower height, the characteristic variable of the cooling tower, and on the cost is evaluated and validated. Finally, surrogate models are developed for quick estimation of both. The final section of the results focuses on the water-energy nexus, Section 4.3. The effect of the weather conditions on the consumption of water is analyzed and once validated, surrogate models are developed as a function of temperature, humidity and pressure.

### *4.1. Operation of the renewable based thermodynamic cycles*

In Section 2, the thermodynamic cycles, regenerative Rankine and combined cycle, that are used for power production in thermal plants from not only renewable resources but also fossil resources are described. Their performance determines the cooling needs. The major results of the operation of both cycles are reported in this section in the form of cooling requirements. Table 5.2 shows the cooling load required per kW of power produced and, in the case of the combined cycle, the contribution of each of the two turbines towards the power plant operation, steam turbine production corresponds to 45% of the total power obtained in the combined cycle. It is important to note that the energy integrated within the combined cycle reduces the cooling needs almost by half. This fact will not only determine the tower size but also the consumption of water related to that particular cycle and raw material as it will be presented in the following sections. In addition, it is fairly straight forward to use the models presented in Section 2 to compute the power-to-feed ratio. Table 5.3 shows the operation of the Rankine and the combined cycle from different renewable resources. The power produced per kg of raw material using the Rankine cycle is computed based on the LHV of the biomass/biowaste. Alternatively, biomass can be used within an Integrated Gasification Combined cycle (IGCC) scheme via the production of biosyngas from biomass. Using the model developed by Vidal and Martín (2015), the syngas composition and flowrate per kg of biomass used can be calculated. Biosyngas composition can be fed to the model described in Section 2 for the combined cycle to compute the yield to power, see Table 5.3. Note that the use of biosyngas is more efficient than using directly the biomass, due to the water decomposition within the process to generate hydrogen. Instead of syngas or natural gas, biogas without upgrading can also be used as raw material for the combined cycle. The composition of the biogas before upgrading is computed from (León and Martín, 2016). By optimizing the model presented in this paper, it is possible to compute the power obtained per kg of waste, see Table 5.3. These ratios represent the operation of power facilities based on renewable resources that together with the water consumption provide the basis for the capabilities of using waste and biomass in the transition of the power industry. For further information of CSP plants we refer to previous work (Martín and Martín, 2013, 2017).

***Table 5.2.*** Thermodynamic cycle cooling needs

| Definition | |
|---|---|
| *Cooling rate to power (Rankine Cycle / Solar CSP)* | 1.18<br>1.37 * |
| *Cooling rate to power (Combined Cycle)* | 0.56 |
| *Cooling rate to power Including gas turbine cooling (Combined Cycle)* | 0.67 |
| *Steam turbine contribution (Combined Cycle)* | 0.45 |

*(Kloppers and Kröger, 2005)

***Table 5.3.*** Renewable based power plant yields

| Raw material | Rankine | Combined cycle |
|---|---|---|
| *Biomass* | 6757 kJ/kg of wet biomass | Syngas comp. ($CO_2$=0.013; CO=0.898; $H_2$=0.089)<br>7663 kJ/kg wet biomass |
| *Biogas* | NA | Biogas comp. (Wa=0.12; $CO_2$=0.47; $CH_4$=0.385; $N_2$=0.02; $O_2$=0.006; $NH_3$=0.000)<br>3023 kJ/kg food waste |

## *4.2. Sustainable design of cooling towers*

### *4.2.1. Geometric design across climates*

Cooling tower sizing and costing in typically based on cooling load (Matches, 2020). However, the weather conditions play an important role on the operation and also on the water-energy nexus (Martín and Martín, 2013). For tower sizing, as described in Section 2.3, the worst-case scenario is used at the 10 different places. Evaluating summer and winter, it turned up that January was the most challenging month in terms of the operation of the cooling tower due to the cold weather and high humidity of the air. The tower size across Spain is computed. Analyzing the results, several conclusions can be drawn. It was found that the major tower dimensions can be related to the tower height that can be used as characteristic variable of the tower size. Using it as a reference, a number of ratios between geometric variables are computed representing the main tower features. Table 5.4 shows the results. These ratios held in all designs. It is possible to see that the tower height is suggested to be 25% larger than the base diameter. Another interesting feature is the ratio between the base and the top diameters. Typically, the top diameter is 60% that of the base. In addition to the geometric ratios, the effect of the climate on the tower size is represented in Figure 5.5. As it was expected, the tower size increases with the production capacity, since larger cooling needs are to be removed, see also Table 5.2. However, it is more interesting to see the effect of the site,

given by the temperature, humidity and pressure, on the tower height. In general, larger towers are required towards the South-East. The lower the relative humidity and the higher the temperature, the larger the tower size. Evaluating the tower cost as a function of the site, the trends and conclusions are similar to those presented for the tower height because the tower size can be represented by its height as shown in Table 4.4. Note that CSP facilities are being built to the South and South-East because of the high solar incidence. The location of CSP plants shows a tradeoff between power produced and the cost in cooling facilities (Ludovisi and Garza, 2015; Martín and Martín, 2013).

***Table 5.4.*** Major rules for cooling tower design (40-450 MW)

| Definition | |
|---|---|
| *Tower height to Base diameter* | 1.25 |
| *Tower height to entrance height* | 10.41 |
| *Base diameter to Opening diameter* | 1.64 |
| *$Z_h$ to tower height* | 0.13 |
| *$Z_u$ to tower height* | 0.77 |

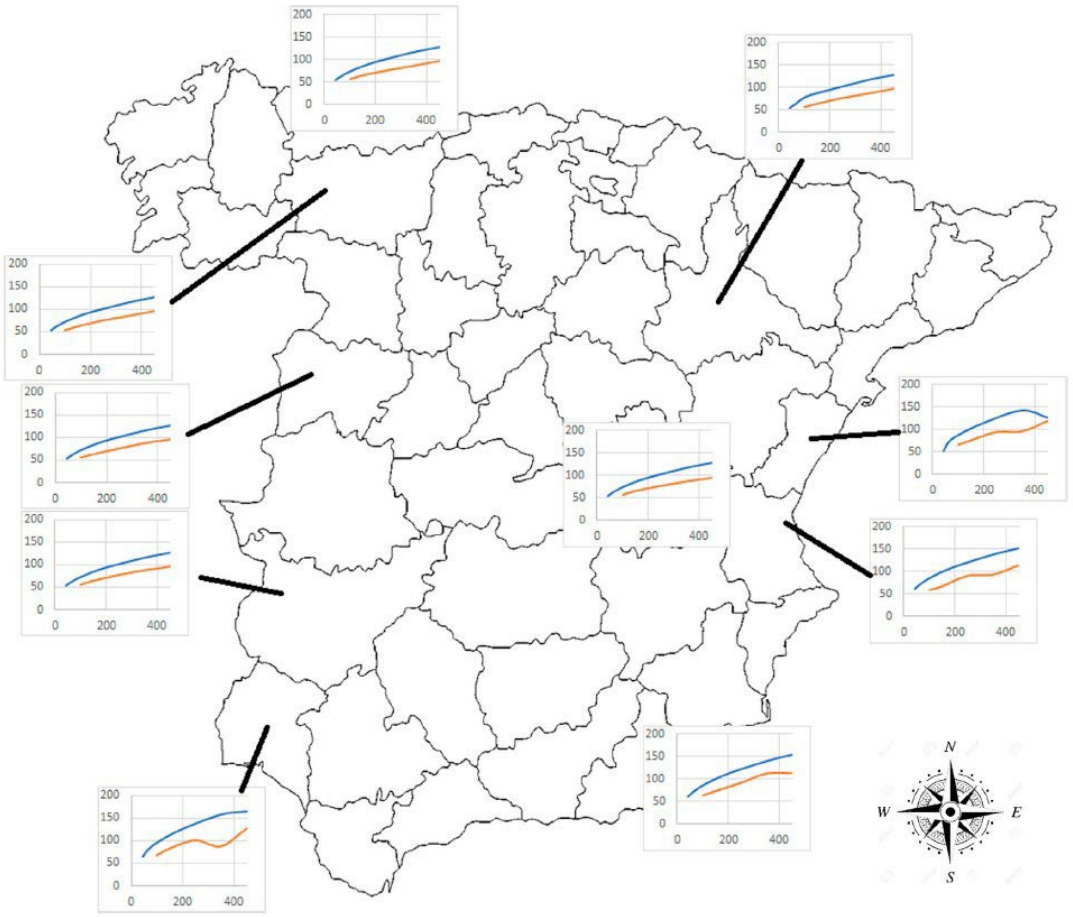


***Figure 5.5.*** Tower size (Height (m)) across the climatic regions por different production capacities (MW). Blue: Rankine; Red: Combined cycle.

The geometric ratios presented in Table 5.2 are compared with two industrial towers whose geometry is reported in detail in the literature (Gould and Kratzig, 1999). The height to diameter and the top to bottom diameter ratios are 1.38 and 1.72 for the Gundremmingen tower in Germany and 1.48 and 1.53 for the 200m tall project. Both ratios are close to the ones reported in Table 5.2 of 1.25 and 1.64, validating the model results. However, a more sustainable design shows values in between the values of the two industrial towers. With regards to the heights of the difference sections of the tower, the optimization reports values of 0.13 and 0.77 respectively. For the Gundremmingen tower the values are 0.22 and 0.70, while for 200 m tall one, ratios of 0.3 and 0.64 are reported. The bottom section is always larger than the top one, but a more sustainable design suggests a taller lower section.

### *4.2.2. Simplified models for tower sizing and costing*

The results show that the tower size depends on the weather as it was presented in Figure 5.5. To provide with information at an early stage and for conceptual level design, surrogate models are developed to estimate tower size and cost as a function of the production capacity of the facility and the weather conditions. Since the tower can be characterized by its height, see Table 5.4, the tower sizing can be carried out by developing a surrogate model of the tower height as a function of the power plant capacity, the pressure, the temperature and the humidity. The rest of the dimensions are computed from the ratios presented in Table 5.4. This surrogate model can be implemented in any design tool, i.e. (Matches, 2020; Sinnott and Towler, 2016) for conceptual tower design and costing. Note that the Rankine and the combined cycles have several differences and show different tower sizes. Therefore, two sets of surrogate models have been developed, one set per cycle, to characterize the tower height and its cost. In the case of the regenerative Rankine cycle, Eq. (29) shows the correlation developed, while for the combined cycle, the correlation is presented in Eq. (30), where the temperature (T) is in Celsius (3.2–11.38 °C), the relative humidity (H = 0.64–0.82) is given as a fraction, the pressure (p = 0.89–1) is in atm and Power ranges from 40 to 450 MW.

$$T_{Height}(m) = (-4.896\cdot10^{-5}\cdot T^2 - 5.027\cdot10^{-2}\cdot \mathrm{H}^2 + 1.698\cdot10^{-3}\cdot p^2 - 7.840\cdot10^{-3}\cdot T\cdot H + 2.3175\cdot10^{-3}\cdot T\cdot p + 0.467823\cdot H\cdot p + 4.6155\cdot10^{-3}\cdot T - 0.3066\cdot H - 0.3842\cdot p + 0.2837)\cdot Power^2 + (1.5485\cdot10^{-2}\cdot T^2 + + 21.8527\cdot H^2 - 32.4850\cdot p^2 + 3.5460\cdot T\cdot H + 0.1973\cdot T\cdot p - 210.8925\cdot H\cdot p - 3.1559\cdot T + + 139.613\cdot H + 223.761\cdot p - 148.1987)\cdot Power + (-1.9657T^2 - 1336.49058\cdot H^2 - 2991.472\cdot p^2 + - 178.296\cdot T\cdot H + 215.8447\cdot T\cdot p + 10534.978\cdot H\cdot p - 34.1144\cdot T - 6522.0254\cdot H - 4220.9457\cdot p + + 4712.888)$$

(29)

To validate the detailed model presented in Section 2 and Eq. (29), the two cooling towers of the La Robla power plant and the three ones corresponding to Andorra power plant are used. The two towers of the La Robla power plant serve two different groups of 284 MW and 370 MW each. The plant is located in the North-West of Spain, close to the city of León. The technical leaflet shows 100 m per tower ("Central Térmica La robla," 2019). Note that the height reported is the same but one of the groups has almost 25% larger production capacity. This correlation assigns 117 m and 128 m for the design condition of January. For the Andorra power plant, located in Teruel, the literature reports 107 m high and 81 m base diameter per group of 350 MW ("Central térmica de Andorra," 2019). Eq. (29) overestimates again the height, 130 m, but the industrial tower matches the ratio between tower height and diameter given in Table 5.2. The overestimation may be due to the fact that in Eq. (19) the draft must be 10% larger than the pressure drop together with the fact that the packing of the towers is not reported and it can be different than the one used in the model.

$$T_{Height}(m) = (4.231\cdot10^{-5}\cdot T^2 + 0.223\cdot H^2 - 0.6739\cdot p^2 + 9.371\cdot10^{-3}\cdot T\cdot H + 4.962\cdot10^{-3}\cdot T\cdot p - 0.25301\cdot H\cdot \mathrm{p} + - 1.2649\cdot10^{-2}\cdot T - 0.1701\cdot H + 1.4425\cdot p - 0.5751)\cdot \mathrm{Power}^2 + (-1.1214\cdot10^{-2}\cdot T^2 - 131.094\cdot H^2 + 581.498\cdot p^2 + - 6.6526\cdot T\cdot H - 6.7797\cdot T\cdot p + 220.124\cdot H\cdot p + 11.7415\cdot T + 41.4477\cdot H - 1221.983\cdot p + 520.181)\cdot \mathrm{Power} + (1.4349\cdot T^2 + 10677.289\cdot H^2 - 53566.636\cdot p^2 + 647.774876\cdot T\cdot H + 761.9941\cdot T\cdot p - 24850.89112755\cdot H\cdot p + - 1223.0867\cdot T + 2420.4049\cdot H + 114991.986\cdot p - 50867.282)$$

(30)

Eq. (30) is used to estimate the height of the tower of the Elcogas power plant. It is a combined cycle facility with a production capacity of 350 MW that had a natural draft cooling tower of 86 m of diameter and 122 m high (Europapress, 2018). For the design conditions of January at Puerto Llano, Ciudad Real (Spain), Eq. (30) predicts a tower size of 142 m. As in the case of the Rankine cycle, the correlation overestimates the size to make sure there is enough draft. Similarly, correlations for the cost estimation of

the cooling towers for the two different cycles are developed so that they can be used in conceptual design and/or implemented in current tools, i.e. (Geankoplis, 2003; Matches, 2020; Sinnott and Towler, 2016; Wallas, 1990). The tower cost is estimated using Eq. (25) as presented in Section 2. For the regenerative Rankine the surrogate model is shown in Eq. (31), where the variable "Power" is given in kW and the rest of the variables are computed within the same ranges presented for Eqs. (29) and (30). Figure 5.6 shows the fitting of the optimization results. The fitting is good, the correlation between the estimated and the computed values, $R^2$, is 0.9, but there are a few points with an error beyond 20%. Note that the cost estimated corresponds to the unit alone as given by Dehaghani and Ahmadikia (2017).

$$Cost_{Tower}\ (€) = (655.3\cdot T^2 - 177564\cdot H^2 + 5926519\cdot p^2 - 5753\cdot T\cdot H - 104650\cdot T\cdot p - 288982\cdot \mathrm{H}\cdot p + 95792\cdot T + 635954\cdot \mathrm{H} - 10319667\cdot p + 4307004)\cdot \mathrm{Power} + (10544\cdot \mathrm{T}^2 + 20745600\cdot H^2 - 73074990\cdot p^2 + 2457264\cdot T\cdot H - 130129\cdot T\cdot p - 132420969\cdot \mathrm{H}\cdot p - 1981510\cdot T + 74203328\cdot \mathrm{H} + 243931768\cdot p - 137298587) \quad (31)$$

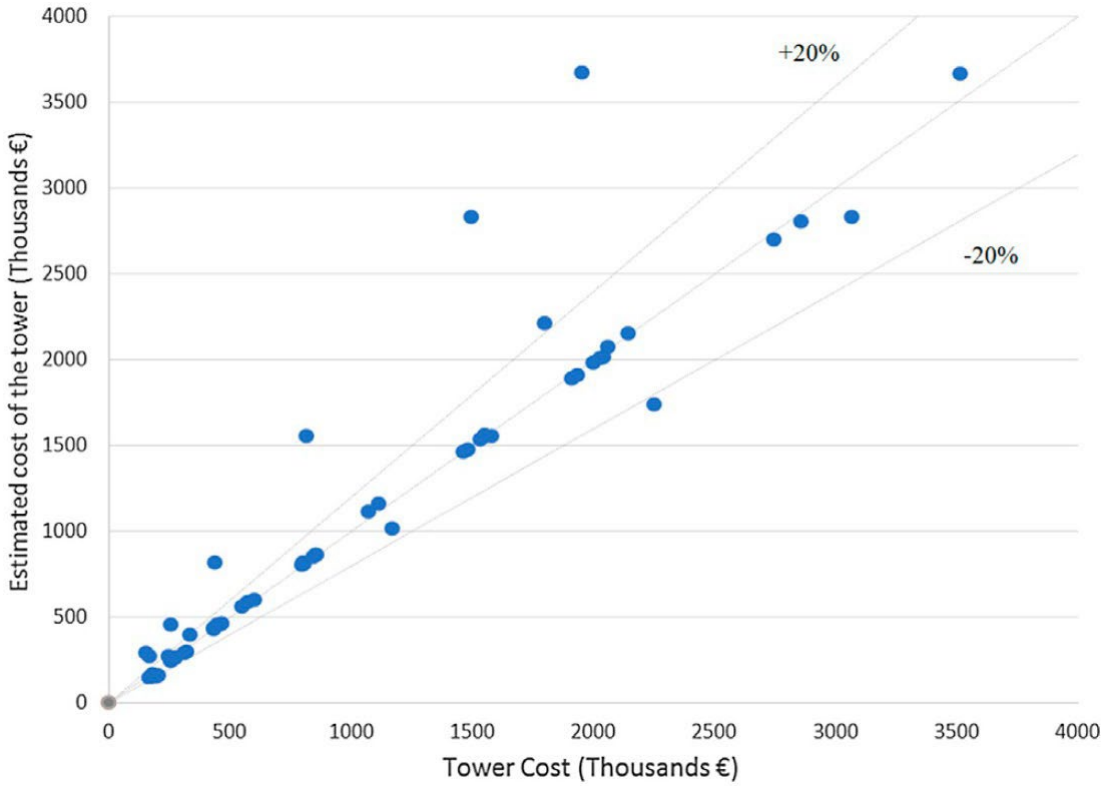


***Figure. 5.6.*** Fitting of the effect of weather on cooling tower costs. Rankine cycle.

A similar analysis is carried out for combined cycle based power facilities. To capture the plant production capacity, Eq. (32) is developed, and Figure 5.7 shows the fitting. In this case the fitting is better,

with almost all values within 20%. The correlation between the estimated and the computed values, $R^2$, is 0.92.

$$Cost_{Tower}(€) = (0.5175 \cdot T^2 + 2067 \cdot H^2 - 7474 \cdot p^2 + 114.5 \cdot T \cdot H + 56.05 \cdot T \cdot p - 4327 \cdot H \cdot p - 150.1 \cdot T + 62.05 \cdot H + 17136 \cdot p - 7602.8) \cdot Power^2 + (-344.6 \cdot T^2 - 1009868 \cdot H^2 + 2865079 \cdot p^2 - 51263 \cdot T \cdot H - 1084 \cdot T \cdot p + 1930691 \cdot H \cdot p + 46334 \cdot T + 112221 \cdot H - 6932563 \cdot p + 3075848) \cdot Power + (30585 \cdot T^2 + 77946022 \cdot H^2 - 249464395 \cdot p^2 + 4797070 \cdot T \cdot H + 397748 \cdot T \cdot p - 196626463 \cdot H \cdot p - 4596664 \cdot T + 29509822 \cdot H + 624161048 \cdot p - 290537291) \quad (32)$$

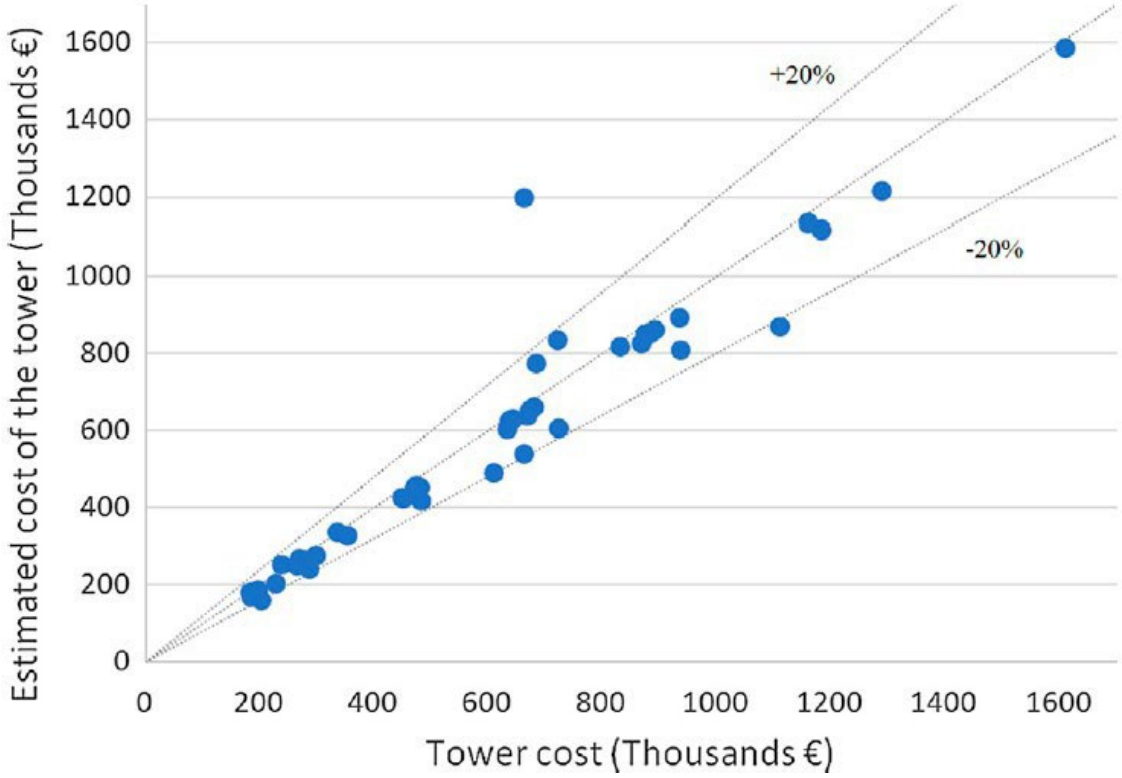


***Figure. 5.7.*** Fitting of the effect of weather on cooling tower costs. Combined cycle.

The cost of the construction of the unit includes the civil engineering, excavation, tunnels, electrics, etc. The value computed from Eqs. (31)–(32) only corresponds to the material as given by (Buys and Kröger, 1989). However, to compute the investment cost of the cooling tower, a ratio from the literature is used. It is reported that the direct cost of the project is around 10 times that of the tower itself (McDowell, 2018; US Nuclear regulatory commission, 1976). Using this correction, for the average value of each capacity within the range 40–450 MW the cost is compared with the updated values from the ones estimated from Matche (2020) and from the EPA (EPA, 2000). In the supplementary material it is possible to see that while Matche (2020) underestimates the costs, the correlation from the EPA consistently reports higher values. The

average values for each capacity computed by the correlations are consistently in between. Note that neither of the estimations from the literature can cope with the effect of the weather conditions nor it is possible to know the exact weather conditions for which the towers estimated with the literature correlations are designed.

### *4.3. Water consumption in renewable based plants.*

#### *4.3.1. Water consumption across weather conditions*

Apart from the structural design of the tower and its costing, water consumption is a major issue in the power industry (Gjorgiev and Sansavini, 2018; Lee et al., 2018; Nouri et al., 2019; Scanlon et al., 2013; Stillwell et al., 2011; Tsolas et al., 2018). Computing the consumption of water allows evaluating the water-energy nexus in the power industry as a function of the location of the facility as a first stage to evaluate the water footprint of any power system. The model described in Section 3 is used to determine the consumption of water for the two cycles, the regenerative Rankine and the combined cycle, for a set of weather conditions including air temperature, humidity and pressure. To validate the models water consumption data from 18 towers from thermal power plants from the literature, 12 coal based groups and 6 using natural gas, located in US (Xia et al., 2017), South Africa (Delgado and Herzog, 2012) Spain (Sesma-Martín, 2019) and China (Jiang and Ramaswami, 2015; Xia et al., 2017) are compared with the ones predicted the model, see Table S1 in the supplementary material for the actual values. Using the average weather for each of the locations and Eqs. (33)–(34), the water consumption is estimated and compared with the ones reported. Note that the cycles of concentration (COC) must be corrected in some cases since the model in this work used 6. It is important to highlight that in some cases the COC value is not reported and the same value as in the model is assumed. Figure 5.8 shows good agreement between the predicted and the reported ones in the case of combined cycle, while in the case of the Rankine cycle the values are underestimated unless drift is considered, blue symbols in the Figure. Note that while combined cycle facilities are newer, most coal based ones are older. More efficient cooling towers are expected for newer facilities. In addition, in the model description it was assumed that the drift was expected to be negligible. Using a parameter estimation approach, the average drift of all the towers is 0.006 of the water flow fed to the column, see orange cycles in Figure 5.8, with a $R^2$ of 0.85. It is a value lower than the one suggested by the rules of thumb (Perry and

Green, 1997), around 0.01, but still not negligible. Note that even thought it is not a good value, the results are within 15% error using generic settings for the cooling towers. Alternatively, the model can be used to simulate a particular tower by using a parameter estimation approach as long as detailed data of its operation is provided including packing features and profiles of its operation.

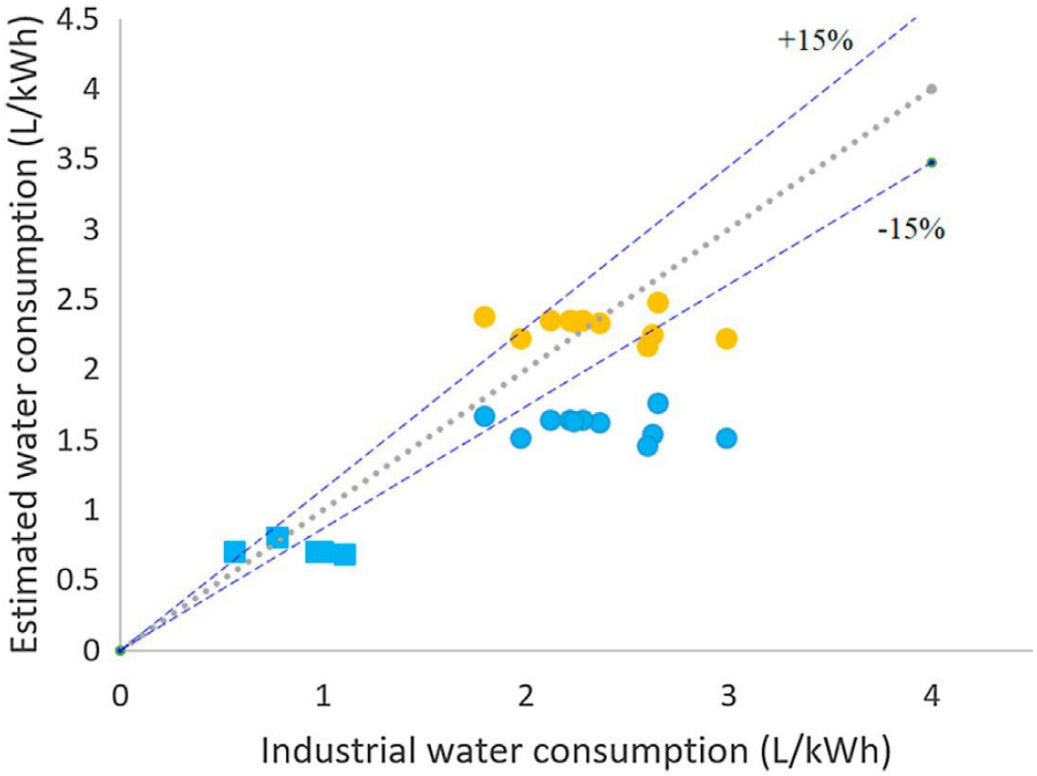


***Figure 5.8.*** Comparison between average water consumption and estimated one for different locations. Square: Combined cycle; Circle: Rankine. Blue: No drift; Orange: Drift.

Using the 10 locations and considering the weather of each month as an independent design condition, both cycles are studied for a fixed power production capacity of 350 MW. Drift is considered negligible. Figure 5.9 presents the water consumption across different weather conditions in Spain. The integrated design of the combined cycle results in a reduction of water consumption almost by half with respect to the regenerative Rankine one, see Table 5.2. In terms of the effect of the weather conditions, the consumption of water increases to the South-East due to the humidity and temperature of the places. The higher the temperature, the larger the consumption of water. But humidity also plays a role. As a result, the water footprint of a power system where biomass thermal plants and CSP facilities have a high share is determined by the availability of the biomass, the solar incidence and the water to be consumed while operating the facility. Avoiding the Mediterranean coast will reduce water consumption, because of the high

humidity coupled with high temperatures. Also at the North, characterized by high humidity, water consumption increases. Note, however, that water consumption must be relative to its availability, as exposed in the literature (Martín, 2016).

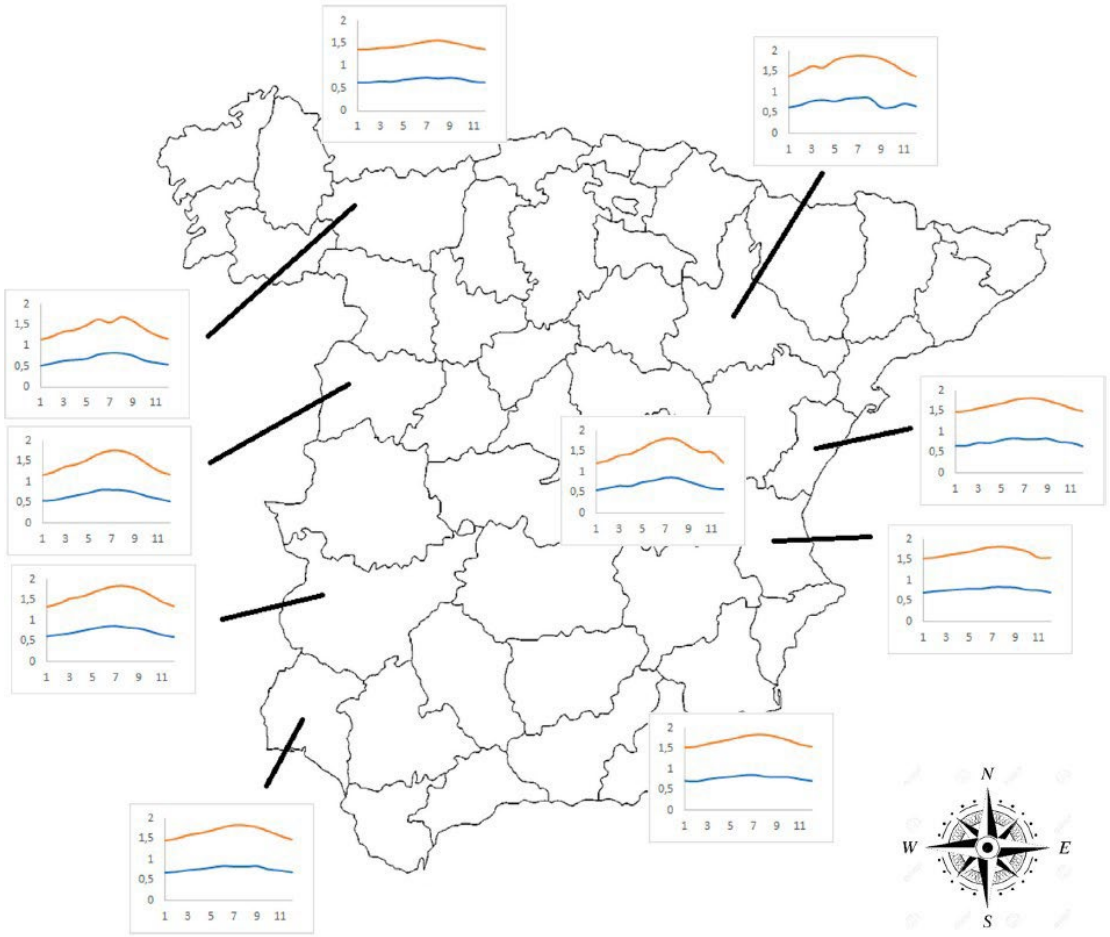


***Figure 5.9.*** Water consumption (L/kWh) across the climatic regions for 350 MW over the design conditions. Blue: Rankine; Red: Combined cycle. (For interpretation of the references to colour in this figure legend, the reader is referred to the web version of this article.)

The results showed in Figure 5.9 for the Rankine cycle range from 1 to 2 L/kWh, within the ones reported in the literature. In particular, while typical values from 1.8 L/kWh (Stillwell et al., 2011) to 2.6 L/kWh (Macknick et al., 2011) are reported in the literature for coal thermal plants, values of 2.7 L/kWh and 3.2 L/kWh (Stillwell et al., 2011) are shown for nuclear and CSP plants respectively confirming the variability of the model results and the fact that CSP facilities are located in regions where they require larger consumption of water as well as the lower efficiency of the thermodynamic cycle. Furthermore, it can be seen that when a particular region is analyzed, see the state of Texas, the water consumption varies from location to location from 0.54 to 5.87 L/kWh (Stillwell et al., 2011) with an average value of 2.1 L/kWh

(Stillwell et al., 2011). With regards to the combined cycle, the consumption of water is around 0.8 L/kWh, see Figure 5.9. In the literature values of 1 L/kWh are found for combined cycles (Maulbetsch and DiFilippo, 2006; Stillwell et al., 2011). In particular, for natural gas combined cycles values in the range of 0.7 L/kWh (Stillwell et al., 2011) to 1.4 L/kWh (Macknick et al., 2011) are reported, for an average value of 1 L/kWh, while for integrated gasification combined cycle values of 1.3±0.4 L/kWh are shown in the literature (Stillwell et al., 2011). For the state of Texas the average water consumption from combined cycle plants is 0.9 L/kWh (Scanlon et al., 2013). In the literature the results for US consumption of water in the thermal production of electricity is 1.25 L/kWh on average, with a range from 0.7 for combined cycles to 2.0 for steam turbine when using cooling towers (Lee et al., 2018). Thus, the results obtained in this work are within the ranges reported validating the model. Note that in the case of the combined cycle, only the stream from the steam turbine is condensed and both, the gas and the steam turbines, are responsible for the production of power.

#### *4.3.2. Surrogate models for water consumption*

The interactions between the variables prevent from a simple representation of the effect of the variables on the consumption of water. Using the set of results, surrogate models to estimate the water consumption as a function of the weather conditions of the site for both cycles are developed. As in the case of tower sizing, the aim is to provide easy to use models that can be useful in conceptual design, i.e. (Sinnott and Towler, 2016). For the regenerative Rankine cycle, the surrogate model to compute the water consumption is given by Eq. (33), where the range of application is for the temperature, 3.2-32.4 °C, for the pressure, 0.89–1 atm, and for the humidity, 0.41-0.83. The good fitting can be seen in Figure 5.10, with a correlation between the values estimated by the surrogate model and the computed ones by the detail one, $R^2$, is 0.94.

$$\begin{aligned} Water_{consumption}\ (L/\mathrm{kW h}) = &-2.297\cdot 10^{-4}\cdot T^2 + 0.798\cdot H^2 + 7.090\cdot p^2 \\ &+2.200\cdot 10^{-2}\cdot T\cdot H + 2.993\cdot 10^{-2}\cdot T\cdot p - 0.515\cdot H\cdot p + \\ &-1.533\cdot 10^{-2} T - 1.417\cdot H - 12.574\cdot p + 7.6256 \end{aligned} \quad (33)$$

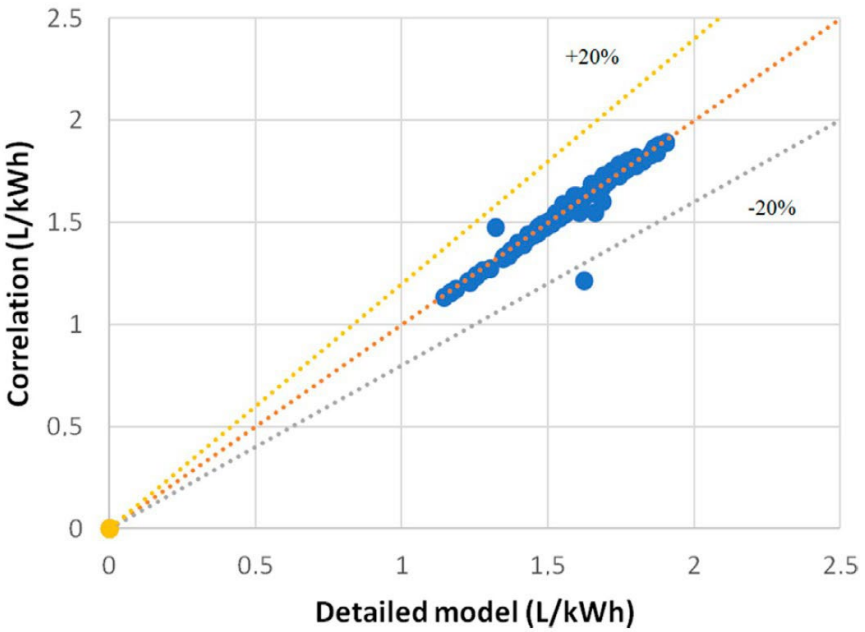


***Figure 5.10.*** Water consumption fitting. Rankine cycle.

Similarly, for the combined cycle, the correlation given by Eq. (34) is developed. The fitting is also good, as it can be seen in Figure 5.11, with a correlation between the values estimated by the surrogate model and the computed ones by the detail one, $R^2$, of 0.92.

$$\begin{aligned} Water_{consumption}\ (\mathrm{L/kWh}) = & -4.75\cdot10^{-4}T^2 + 1.255\cdot H^2 + 8.083\cdot p^2 \\ & +3.453\cdot10^{-3}\cdot T\cdot H + 5.833\cdot10^{-2}\cdot T\cdot p + 1.292\cdot H\cdot p + \\ & -3.447\cdot10^{-2}T - 3.255\cdot H - 16.555\,p + 9.690 \end{aligned} \tag{34}$$

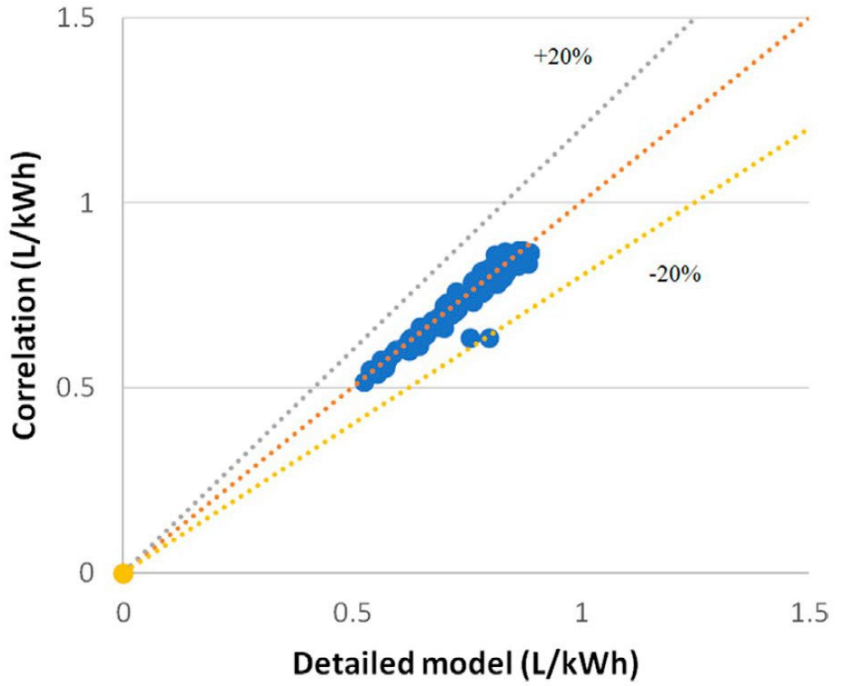


***Figure 5.11.*** Water consumption fitting. Combined cycle.

## 5. Conclusions

In this work a mathematical optimization framework is developed to conceptually compute the geometry of wet cooling towers and the water consumption rates for the sustainable design of the new power system where different energy sources and thermodynamic cycles are used. As a case study Spain has been used, a country very sensitive to water stress issues.

The optimal sustainable design of the tower results in the development of design guidelines in terms of geometric ratios that reduce material use and tower cost, maintaining tower performance and reducing water consumption. The geometry is validated versus actual towers; however, a higher lower section of the paraboloid is suggested from the analysis. Moreover, water consumption has been validated versus industrial data. Using the validated model, the operation of cooling towers across different climate areas is analyzed. It was shown that for the same production capacity, larger towers are to be installed to the South-East, where high temperatures and sometimes also moderate to high humidity are found. As a result of the weather conditions higher water footprint is reported also to the South-East. A large scale analysis comparing different cooling technologies would be needed to decide on the selection of the location of new facilities and their cooling system.

The analysis also allowed developing surrogate models to compute the water consumed, the tower size and its cost as a function of the humidity, the temperature and the atmospheric pressure for different power plant sizes. These correlations are useful to estimate the water stress of the energy transition from current fossil and nuclear based power to renewable one as well as to evaluate the water footprint of the next power production system where solar energy will play a key role.

## 6. List of acronyms and abbreviations

$A_{HX}$ : Area of the heat exchanger ($m^2$)
A(Wa): Antoine constant
B(Wa): Antoine constant
Cp: Heat capacity (kcal/kg ºC)
C(Wa): Antoine constant
$f_{air}$ : Flow of air (kg/s)
$fc_{(components)}$: Flow of components (kg/s)
$f_{Wa}$: Flow of water (kg/s)
g: Gravity ($m/s^2$)
$h_{liquid}$: Liquid enthalpy (kcal/kg)

$h_{steam}$: Steam enthalpy (kcal/kg)
H: Humid air enthalpy (kcal/kg)
$k_y$ : Resistance to mass transfer (kg /$m^2$s)
$L_{flux}$: Flow of water per unit area (kg/$m^2$s)
$M_i$: Molar weight of species I (kg/kmol)
p: Pressure (bar)
$P_{v, sa}$: Vapor pressure (mmHg)
$Q_{(unit)}$: Energy at unit (kW)
R: Gas constant (atm·L/mol·K)
S: Specific contact area ($m^{-1}$)
s: Entropy enthalpy (kcal/kg ºC)
t : Air temperature (ºC)
T: Water temperature across the cooling tower (ºC)
$T_{(unit)}$: Stream temperature (ºC)
$W_{(unit)}$: Energy unit (kW)

*Subindex*
i: Interphase conditions
in: Inlet
L: Liquid bulk
g: gas bulk
out: Outlet.
sat: Saturation condition
Wa: Component Water

*Symbols*
ρ: Air density (kg/$m^3$)
η: isentropic efficiency

*Units:*
CT: Cooling tower
HX: Heat exchanger
Turb: Turbine
Spl: Splitter
Furnace
Boiler

## 7. References

Adapated to IGN (National Geographic Institute) URL https://www.ign.es/espmap/mapas_clima_bach/pdf/Clima_Mapa_01_texto.pdf

Ali, B., Kumar, A., 2017. Development of water demand coefficients for power generation from renewable energy technologies. Energy Conversion and Management 143, 470–481. https://doi.org/10.1016/j.enconman.2017.04.028

Almási, J., 1981. Approximate determination of cooling tower dimensions. Periodica Polytechnica Civil Engineering 25, 95–110. https://doi.org/N/A

ASHRAE (Archives American Society of Heating)., 1983. Equipment Guide, Chapter 3, American Society of Heating, Refrigerating, and Air-Conditioning Engineers, INC. USA.

Ayoub, A., Gjorgiev, B., Sansavini, G., 2018. Cooling towers performance in a changing climate: Techno-economic modeling and design optimization. Energy 160, 1133–1143. https://doi.org/10.1016/j.energy.2018.07.080

Busch, D., Harte, R., Krätzig, W.B., Montag, U., 2002. New natural draft cooling tower of 200 m of height. Engineering Structures 24, 1509–1521. https://doi.org/10.1016/S0141-0296(02)00082-2

Buys, J.D., Kro¨ger, D.G., 1989. Cost-Optimal Design of Dry Cooling Towers Through Mathematical Programming Techniques. Journal of Heat Transfer 111, 322–327. https://doi.org/10.1115/1.3250680
Byers, E.A., Hall, J.W., Amezaga, J.M., 2014. Electricity generation and cooling water use: UK pathways to 2050. Global Environmental Change 25, 16–30. https://doi.org/10.1016/j.gloenvcha.2014.01.005
Central térmica de Andorra, 2019. Wikipedia. URL https://es.wikipedia.org/wiki/Central_t%C3%A9rmica_de_Andorra.
Central Térmica La robla, 2019. Union Fenosa. URL http://www.unionfenosa.es/webuf/wcm/ connect/430b6200495cc71ebd17fd8205e0cb4d/folleto_tecnico_central_termica_ de_la_robla.pdf
Cheremisinoff, N.P., Cheremisinoff, P.N., 1981. Cooling Towers Selection, Design And Practice. Ann Arbor Science Publishers, Michigan.
Coulson, J., Richardson, J., 1999. Chemical engineering. Butterworth-Heinemann, UK.
Dehaghani, S.T., Ahmadikia, H., 2017. Retrofit of a wet cooling tower in order to reduce water and fan power consumption using a wet/dry approach. Applied Thermal Engineering 125, 1002–1014. https://doi.org/10.1016/j.applthermaleng.2017.07.069
Delgado, A., Herzog, H.J., 2012. A simple model to help understand water use at power plants 21.
du Preez, A.F., Kröger, D.G., 1993. Effect of wind on performance of a dry-cooling tower. Heat Recovery Systems and CHP 13, 139–146. https://doi.org/10.1016/0890-4332(93)90033-R
Electrical Network of Spain, 2018. URL www.ree.es
EPA, 2000. Detailed Information on Technologies/Development of Unit Costs (No. §316(b) EEA Appendix A for New Facilities).
EPA, 1970. A method for predicting the performance of natural draft cooling towers. Pacific Northwestern Water Laboratory;
Europapress, 2018. La torre de refrigeración de Elcogas, demolida tras detonar 466 microcargas de dinamita. Wikipedia. URL https://www.europapress.es/castillalamancha/ noticia-torre-refrigeracion-elcogas-demolida-detonacion-466- microcargas-dinamita-20180628162541.html.
Fatigati, M., 2006. Conserving Water in Ethanol Plants. Presented at the Western Region BBI Biofuels Workshop, San Diego CA.
Gao, M., Sun, F., Turan, A., 2014. Experimental study regarding the evolution of temperature profiles inside wet cooling tower under crosswind conditions. International Journal of Thermal Sciences 86, 284–291. https://doi.org/10.1016/j.ijthermalsci.2014.07.010
Gao, M., Zhang, L., Wang, N., Shi, Y., Sun, F., 2016. Influence of non-uniform layout fillings on thermal performance for wet cooling tower. Applied Thermal Engineering 93, 549–555. https://doi.org/10.1016/j.applthermaleng.2015.09.054
Geankoplis, C., 2003. Transport processes and separation process principles (includes unit operations) fourth edition, 3rd ed. Prentice Hall, Upper Saddle River: New Jersey. U.S.A.
Ghobeity, A., Noone, C.J., Papanicolas, C.N., Mitsos, A., 2011. Optimal time-invariant operation of a power and water cogeneration solar-thermal plant. Solar Energy 85, 2295–2320. https://doi.org/10.1016/j.solener.2011.06.023
Gjorgiev, B., Sansavini, G., 2018. Electrical power generation under policy constrained water-energy nexus. Applied Energy 210, 568–579. https://doi.org/10.1016/j.apenergy.2017.09.011
Gould, P.L., Kratzig, W.B., 1999. Chapter 14: Cooling tower structures, in: Wai-Fah, C. (Ed.), Chapter 14: Cooling Tower Structures. CRC Press, Boca Raton.
Harte, R., Krätzig, W.B., 2002. Large-scale cooling towers as part of an efficient and cleaner energy generating technology. Thin-Walled Structures 40, 651–664. https://doi.org/10.1016/S0263-8231(02)00018-6
IEA (International Energy Agency)., 2010. Water for energy: Is energy becoming a thirstier resource?. URL https://www.iea.org/media/publications/weo/WEO_2012_Water_ Excerpt.pdf
Ifaei, P., Ataei, A., Yoo, C., 2016a. Thermoeconomic and environmental analyses of a low water consumption combined steam power plant and refrigeration chillers-Part 2: Thermoeconomic and environmental analysis. Energy Conversion and Management 123, 625–642. https://doi.org/10.1016/j.enconman.2016.06.030
Ifaei, P., Rashidi, J., Yoo, C., 2016b. Thermoeconomic and environmental analyses of a low water consumption combined steam power plant and refrigeration chillers – Part 1: Energy and

economic modelling and analysis. Energy Conversion and Management 123, 610–624. https://doi.org/10.1016/j.enconman.2016.06.036
Jagadeesh, T., Reddy, K.S., 2013. Performance Analysis of the Natural Draft Cooling Tower in Different Seasons. IOSR-Journal Mech Civ Eng 7, 19–23. https://doi.org/10.9790/1684-0751923
Jiang, D., Ramaswami, A., 2015. The `thirsty' water-electricity nexus: field data on the scale and seasonality of thermoelectric power generation's water intensity in China. Environmental Research Letters 10, 024015. https://doi.org/10.1088/1748-9326/10/2/024015
Katimber, n.d. URL http://www.kaltimber.com/blog/2017/6/19/how-much-co2-is-storedin- 1-kg-of-wood/
Khamis Mansour, M., Hassab, M.A., 2014. Innovative correlation for calculating thermal performance of counterflow wet-cooling tower. Energy 74, 855–862. https://doi.org/10.1016/j.energy.2014.07.059
Kloppers, J.C., Kröger, D.G., 2005. A critical investigation into the heat and mass transfer analysis of counterflow wet-cooling towers. International Journal of Heat and Mass Transfer 48, 765–777. https://doi.org/10.1016/j.ijheatmasstransfer.2004.09.004
Kloppers, J.C., Kröger, D.G., 2004. Cost optimization of cooling tower geometry. Engineering Optimization 36, 575–584. https://doi.org/10.1080/03052150410001696179
Krahé, D., Beisheim, B., Engell, S., 2016. Decision support for energy-efficient cooling tower operation using weather forecasts. Chemical Engineering Transactions 52, 1009–1014. https://doi.org/10.3303/CET1652169
Kreith, F., Goswami, D., 2005. The CRC handbook of mechanical engineering., 2nd ed. CRC Press, Boca Raton.
Kröger, D.G., 2004. Air-cooled heat exchangers and cooling towers: thermal-flow performance evaluation and design, vol. II. Tulsa: Pennwell: Oklahoma;
Lang, C., Strauß, J., 2011. Natural Draft Cooling Tower Design and Construction in Germany - Past (since 1965), Present and Future 8.
Lee, U., Han, J., Elgowainy, A., Wang, M., 2018. Regional water consumption for hydro and thermal electricity generation in the United States. Applied Energy 210, 661–672. https://doi.org/10.1016/j.apenergy.2017.05.025
Lemouari, M., Boumaza, M., Kaabi, A., 2009. Experimental analysis of heat and mass transfer phenomena in a direct contact evaporative cooling tower. Energy Conversion and Management 50, 1610–1617. https://doi.org/10.1016/j.enconman.2009.02.002
León, E., Martín, M., 2016. Optimal production of power in a combined cycle from manure based biogas. Energy Conversion and Management 89–99.
Li, X., Duniam, S., Gurgenci, H., Guan, Z., Veeraragavan, A., 2017. Full scale experimental study of a small natural draft dry cooling tower for concentrating solar thermal power plant. Applied Energy 193, 15–27. https://doi.org/10.1016/j.apenergy.2017.02.032
Li, X., Gurgenci, H., Guan, Z., Wang, X., Xia, L., 2019. A review of the crosswind effect on the natural draft cooling towers. Applied Thermal Engineering 150, 250–270. https://doi.org/10.1016/j.applthermaleng.2018.12.147
Luceño, J.A., Martín, M., 2018. Two-step optimization procedure for the conceptual design of A-frame systems for solar power plants. Energy 165, 483–500. https://doi.org/10.1016/j.energy.2018.09.177
Ludovisi, D., Garza, I.A., 2015. Water Consumption of Cooling Towers in Different Climatic Zones of the U. S., in: POWER2015. ASME 2015 Power Conference. https://doi.org/10.1115/POWER2015-49201
Macknick, J., Newmark, R., Heath, G., Hallett, K.C., 2011. Review of Operational Water Consumption and Withdrawal Factors for Electricity Generating Technologies (No. NREL/TP-6A20-50900, 1009674). National Renewable Energy Laboratory:, USA. https://doi.org/10.2172/1009674
Martín, L., Martín, M., 2013. Optimal year-round operation of a concentrated solar energy plant in the south of Europe. Appl. Therm. Eng. 59, 627–633. https://doi.org/10.1016/j.applthermaleng.2013.06.031
Martín, M., 2016. RePSIM metric for design of sustainable renewable based fuel and power production processes. Energy 114, 833–845. https://doi.org/10.1016/j.energy.2016.08.031
Martín, Mariano, Martín, Mónica, 2017. Cooling limitations in power plants: Optimal multiperiod design of natural draft cooling towers. Energy 135, 625–636. https://doi.org/10.1016/j.energy.2017.06.171

Matches, 2020. Cost of filter under pressure. Matches. URL https://www.matche.com/equipcost/Vessel.html (accessed 10.26.20).
Maulbetsch, J.S., DiFilippo, M.N., 2006. Cost and Value of Water Use at Combined-Cycle Power Plants. California Energy Commission.
McDowell, B., 2018. Comprehensive Technical Feasibility and Cost Evaluation Study. Alcoa Warrick Power Plant (No. Project No. 85014;).
Moran, M.J., Shapiro, H.N., 2003. Fundamentals of Engineering Thermodynamics, 1th ed. John Wiley & Sons.
Morin, G., Richter, P., Nitz, P., n.d. New method and software for multi-variable technoeconomic design optimization of CSF plants.
Nouri, N., Balali, F., Nasiri, A., Seifoddini, H., Otieno, W., 2019. Water withdrawal and consumption reduction for electrical energy generation systems. Applied Energy 248, 196–206. https://doi.org/10.1016/j.apenergy.2019.04.023
Olivier, J.G.J., Bouwman, A.F., Berdowski, J.J.M., Veldt, C., Bloos, J.P.J., Visschedijk, A.J.H., van der Maas, C.W.M., Zandveld, P.Y.J., 1999. Sectoral emission inventories of greenhouse gases for 1990 on a per country basis as well as on 1°×1°. Environmental Science & Policy 2, 241–263. https://doi.org/10.1016/S1462-9011(99)00027-1
Palenzuela, P., Zaragoza, G., Alarcón-Padilla, D.C., Guillén, E., Ibarra, M., Blanco, J., 2011. Assessment of different configurations for combined parabolic-trough (PT) solar power and desalination plants in arid regions. Energy 36, 4950–4958. https://doi.org/10.1016/j.energy.2011.05.039
Peck, J.J., Smith, A.D., 2017. Quantification and regional comparison of water use for power generation: A California ISO case study. Energy Reports 3, 22–28. https://doi.org/10.1016/j.egyr.2016.11.002
Peer, R.A.M., Sanders, K.T., 2018. The water consequences of a transitioning US power sector. Applied Energy 210, 613–622. https://doi.org/10.1016/j.apenergy.2017.08.021
Perry, R.H., Green, D.W. (Eds.), 1997. Perry's chemical engineers' handbook, 7th ed. ed. McGraw-Hill, New York.
Qi, X., Liu, Z., Li, D., 2007. Performance characteristics of a shower cooling tower. Energy Conversion and Management 48, 193–203. https://doi.org/10.1016/j.enconman.2006.04.021
Queiroz, J.A., Rodrigues, V.M.S., Matos, H.A., Martins, F.G., 2012. Modeling of existing cooling towers in ASPEN PLUS using an equilibrium stage method. Energy Conversion and Management 64, 473–481. https://doi.org/10.1016/j.enconman.2012.03.030
Qureshi, B.A., Zubair, S.M., 2006. Prediction of Evaporation Losses in Wet Cooling Towers. null 27, 86–92. https://doi.org/10.1080/01457630600846372
Scanlon, B.R., Reedy, R.C., Duncan, I., Mullican, W.F., Young, M., 2013. Controls on Water Use for Thermoelectric Generation: Case Study Texas, U.S. Environ. Sci. Technol. 47, 11326–11334. https://doi.org/10.1021/es4029183
Serna-González, M., Ponce-Ortega, J.M., Jiménez-Gutiérrez, A., 2010. MINLP optimization of mechanical draft counter flow wet-cooling towers. Chemical Engineering Research and Design 88, 614–625. https://doi.org/10.1016/j.cherd.2009.09.016
Sesma-Martín, D., 2019. The River's Light: Water Needs for Thermoelectric Power Generation in the Ebro River Basin, 1969–2015. Water 11. https://doi.org/10.3390/w11030441
Sinnott, R., Towler, G., 2016. Chemical Engineering Design:Principles, practice and economics of plant and process design., Chemical Engineering Series. Elsevier, Butterworth-Heinemann, Oxford.
Smrekar, J., Kuštrin, I., Oman, J., 2011. Methodology for evaluation of cooling tower performance - Part 1: Description of the methodology. Energy Conversion and Management 52, 3257–3264. https://doi.org/10.1016/j.enconman.2011.05.005
Stillwell, A., King, C., Webber, M., Duncan, I., Hardberger, A., 2011. The Energy-Water Nexus in Texas. Ecology and Society 16. https://doi.org/10.5751/ES-03781-160102
Sun, Y., Guan, Z., Gurgenci, H., Wang, J., Dong, P., Hooman, K., 2019. Spray cooling system design and optimization for cooling performance enhancement of natural draft dry cooling tower in concentrated solar power plants. Energy 168, 273–284. https://doi.org/10.1016/j.energy.2018.11.111
Tanimizu, K., Hooman, K., 2013. Natural draft dry cooling tower modelling. Heat and Mass Transfer 49, 155–161. https://doi.org/10.1007/s00231-012-1071-1

Torcellini, P., Long, N., Judkoff, R., 2003. Consumptive Water Use for U.S. Power Production (No. NREL/TP-550-33905, 15005918). https://doi.org/10.2172/15005918

Tsolas, S.D., Karim, M.N., Hasan, M.M.F., 2018. Optimization of water-energy nexus: A network representation-based graphical approach. Applied Energy 224, 230–250. https://doi.org/10.1016/j.apenergy.2018.04.094

US Nuclear regulatory commission, 1976. Office of Nuclear reactor regulation. Dradt Enviromental statement for selection of the preferred closed cycle cooling system at INDIAN (No. point unit no 2).

Vengateson, U., 2017. Cooling Towers: Evaporation Loss and Makeup Water. Chemical Engineering.

Vidal, M., Martín, M., 2015. Optimal coupling of a biomass based polygeneration system with a concentrated solar power facility for the constant production of electricity over a year. Computers & Chemical Engineering 72, 273–283. https://doi.org/10.1016/j.compchemeng.2013.11.006

Wallas, S.M., 1990. Chemical Process Equipment. Selection and Design, Series in Chemical Engineering. Butterworth-Heinemann, Boston.

Wan, L., Wang, C., Cai, W., 2016. Impacts on water consumption of power sector in major emitting economies under INDC and longer term mitigation scenarios: An input-output based hybrid approach. Applied Energy 184, 26–39. https://doi.org/10.1016/j.apenergy.2016.10.013

Williamson, N., Behnia, M., Armfield, S.W., 2008. Thermal optimization of a natural draft wet cooling tower. International Journal of Energy Research 32, 1349–1361. https://doi.org/10.1002/er.1456

Xia, L., Li, J., Ma, W., Gurgenci, H., Guan, Z., Wang, P., 2017. Water Consumption Comparison Between a Natural Draft Wet Cooling Tower and a Natural Draft Hybrid Cooling Tower—An Annual Simulation for Luoyang Conditions. Heat Transfer Engineering 38, 1034–1043. https://doi.org/10.1080/01457632.2016.1216975

Xu, C., Wang, Z., Li, X., Sun, F., 2011. Energy and exergy analysis of solar power tower plants. Applied Thermal Engineering 31, 3904–3913. https://doi.org/10.1016/j.applthermaleng.2011.07.038

Zhai, H., Rubin, E.S., 2010. Performance and cost of wet and dry cooling systems for pulverized coal power plants with and without carbon capture and storage. Energy Policy 38, 5653–5660. https://doi.org/10.1016/j.enpol.2010.05.013

Zhang, G., He, S., Zhang, Z., Xu, Y., Wang, R., 2017. Economic Analyses of Natural Draft Dry Cooling Towers Pre-cooled Using Wetted Media. Procedia Engineering 205, 423–430. https://doi.org/10.1016/j.proeng.2017.10.393

Zhang, H., Feng, X., Wang, Y., 2018. Comparison and evaluation of air cooling and water cooling in resource consumption and economic performance. Energy 154, 157–167. https://doi.org/10.1016/j.energy.2018.04.095

# Suplementary material

## On the water footprint in power production: Sustainable design of wet cooling towers.

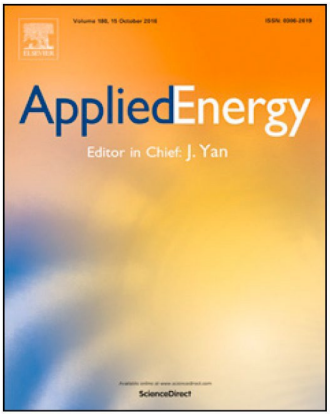


*Authors: Lidia S Guerras and Mariano Martín*

*DOI:* doi.org/10.1016/j.apenergy.2020.114620

## S1.-Modelling details Rankine Cycle

First, mass and energy balances are formulated to the set of heat exchangers that transfer the energy from the fuel or the Sun into the water to produce the steam that is fed to the power cycle. This can happen in a boiler or from the heat transfer fluid used to produce steam in the case of CSP plants. In the case of using a boiler the energy provided by the fuel (biomass, syngas, etc) provides the energy to generated superheated steam at heat exchangers HX1-HX3, while the reheater corresponds to HX4, eq. (1).

In case of CSP plants, HX1-HX3 generate superheated steam while HX4 corresponds to the regenerative section of the cycle.

$$\eta_{Fuel} \cdot E_{fuel} = Q_{(Boiler)} = Q_{(HX1)} + Q_{(HX2)} + Q_{(HX3)} + Q_{(HX4)} \quad (1)$$

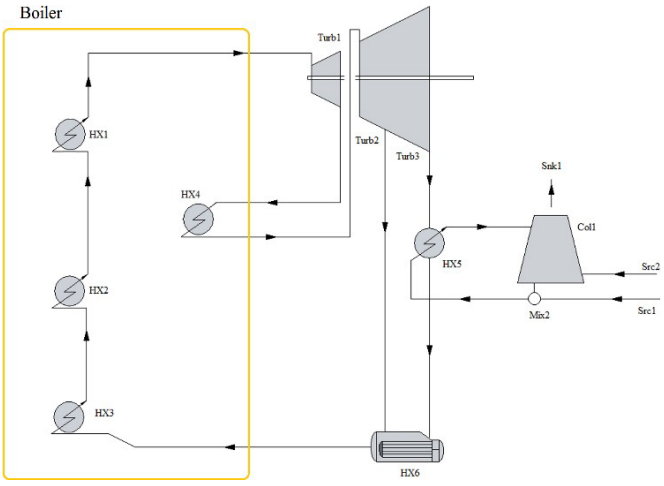


Figure1.-Flowsheet of the facility based on a regenerative Rankine cycle

HX1 is used to represent the heat up of the saturated steam at the operating pressure of the high pressure turbine. The entalphy and entrophy of the different water streams in the different aggregation states (compressed liquid, saturated liquid, saturated vapor and superheated steam) were correlated as a function of the pressure and temperature (Martín and Martín, 2013). The correlations can be found in the appendix of León and Martín (2016). Thus, a fraction from the energy provided either from the solar energy, the burning of fuels, corresponds to the energy transferred to generate superheated steam in HX1 as eq. (2):

$$Q_{(HX1)} = fc_{(Wa,HX2,HX1)} \cdot \left( h_{steam,(HX1,Turbine1)} - h_{steam,(HX2,HX1)} \right) \quad (2)$$

To ensure saturation conditions, the temperature at the inlet of heat exchanger 1, HX1, is that given by Antoine equation:

$$P_{\text{turb1}} \cdot 760 = e^{\left( A(\text{Wa}) - \left( \frac{B(\text{Wa})}{C(\text{Wa}) + T_{(\text{HX2,HX1})}} \right) \right)} \quad (3)$$

Water evaporation takes place at HX2, that is modelled using eqs. (4)-(5)

$$Q_{(\text{HX2})} = fc_{(\text{Wa,HX3,HX2})} \cdot \left( h_{\text{steam,(HX2,HX1)}} - h_{\text{liq,(HX3,HX2)}} \right) \quad (4)$$

$$fc_{(\text{Wa,HX3,HX2})} = fc_{(\text{Wa,HX2,HX1})} \quad (5)$$

Finally, the energy from the source is also used to heat up the compressed liquid stream already at Pturb1 from HX6. HX3 is modelled using mass and energy balances given by eqs (6)-(8)

$$Q_{(\text{HX3})} = fc_{(\text{Wa,HX6,HX3})} \cdot \left( h_{\text{liq,(HX3,HX2)}} - h_{\text{liq,(HX6,HX3)}} \right) \quad (6)$$

$$fc_{(\text{Wa,HX6,HX3})} = fc_{(\text{Wa,HX3,HX2})} \quad (7)$$

$$fc_{(\text{Wa,HX1,Turbine1})} = fc_{(\text{Wa,HX2,HX1})} = fc_{(\text{Wa,HX3,HX2})} \quad (8)$$

The superheated steam is sent from HX1 to the high pressure turbine. In the literature the high pressure turbine typically operates from 40 to 126 bar (Ghobeity et al., 2011; Xu et al., 2011). Thus, a range from 90 bar to 125 bar for the steam being fed to the turbine is considered. The high pressure superheated steam is expanded into a medium pressure. A range from 11 to 35 bar is allowed based on data from the literature (Morin et al., n.d.; Xu et al., 2011). The turbine is modelled as a system of high, medium and low pressure turbines that are modelled similarly. The expansion of the steam in the different turbines is assumed to have an isentropic efficiency of 0.9 (Wallas, 1990). Therefore, the stream exiting the first body can be calculated using eqs. (9)-(10)

$$\eta = \frac{h_{\text{steam,(Turbine1,HX4)}} - h_{\text{steam,(HX1,Turbine1)}}}{h_{steam,(isoentropy)} - h_{\text{steam,(HX1,Turbine1)}}} \quad (9)$$

Where

$$h_{steam,(isoentropy)} = f\left( p_{(\text{Turbine1,HX4})}, T^{*}_{(\text{Turbine1,HX4})} \right) \quad (10)$$

T* represents the isoentropic temperature after the expansion. And the entropy of the expansion is computed as follows:

$$s_{steam,(HX1,Turbine1)} = f\left(p_{(HX1,Turbine1)}, T_{(HX1,Turbine1)}\right) = f(p_{(Turbine2,HX4)}, T^{*}_{(Turbine1,HX4)}) \quad (11)$$

To enforce that the output of the turbine is superheated steam eqs. (12)-(13) are used.

$$p_{turb2} \cdot 760 = e^{\left(A(Wa) - \frac{B(Wa)}{(C(Wa)+T_{turb1min})}\right)} \quad (12)$$

$$T_{(Turbine1,HX4)} > T_{turb1min}; \quad (13)$$

The energy that is obtained at the high pressure turbine is given by eq. (14):

$$W_{(Turbine1)} = fc_{(Wa,HX1,Turbine1)} \cdot \left(h_{steam,(HX1,Turbine1)} - h_{steam(Turbine1,HX4)}\right) \quad (14)$$

A regenerative Rankine cycle is used (Martín and Martín, 2013). The stream as superheated vapor is heated up again in HX4. Next, the superheated steam is fed to the medium pressure turbine. HX4 is modeled using eq. (15).

$$Q_{(HX4)} = fc_{(Wa,Turbine1,HX4)} \cdot \left(h_{steam,(HX4,Turbine2)} - h_{steam,(Turbine1,HX4)}\right) \quad (15)$$

In the medium pressure turbine, the steam is expanded into a lower pressure. Part of the stream is sent to HX6, an extraction. The stream splitter after the second body of the turbine is modelled by eq. (16):

$$fc_{(Wa,HX4,Turbine2)} = fc_{(Wa,Turbine2,HX6)} + fc_{(Wa,Turbine2,Turbine3)} \quad (16)$$

The flow sent to HX6 is used to reheat the liquid obtained after condensing the exhaust of the low pressure turbine. The rest of the flow is used in the low pressure turbine where it is expanded to the exhaust pressure. This stream can contain a small amount of vapor, up to 8%. This last pressure ranges from 0.05 bar to 0.31 bar (Morin et al., n.d.; Palenzuela et al., 2011). It is an optimization variable within the range of 0.05 to 0.35 bar.

$$Q_{(HX5)} = fc_{(Wa,Turbine3,HX5)} \cdot \left(h_{liq,(HX5,HX6)} - h_{steam(Turbine3,HX5)}\right) \quad (17)$$

The energy from HX5, eq. (17) is removed from the system using a cooling tower, see section 2.3. The stream exiting HX6 must be liquid so that it is compressed using a pump up to $P_{turb1}$. To enforce eq. (18) is added:

$$T_{(HX6,HX3)} \leq T_{turb2min} \quad (18)$$

Where $T_{turb2min}$ is the saturated temperature at the pressure of the exhaust if the second body of the turbine calculated using Antonine correlation. The total energy obtained in the system to be optimized is the sum of the ones generated at the three bodies of the turbine named as Turbine1-3:

$$W_{total} = W_{(Turbine1)} + W_{(Turbine2)} + W_{(Turbine3)} \quad (19)$$

## S2.-Cost correlations validation

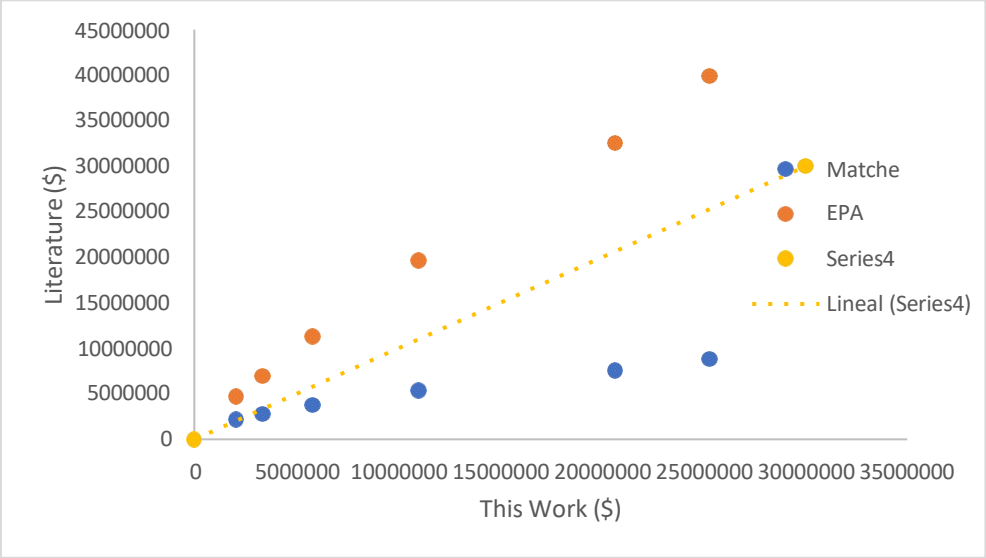


***Figure S1.*** Comparison between cost correlations to estimate tower cost

## S3.-Water consumption validation

The temperatures, humidifies are computed as the averages in the region from national weather services such as AEMET (Spain), http://www.weathersa.co.za/ (South Africa), https://www.accuweather.com/en/cn/china-weather etc and the pressure is given as a function of the altitude of the place

$$P=e^{(-29.91*9.8*Altitude/(8314*(Temperature+273.15)))} \quad (20)$$

***Table S1.*** Data from CT's for validation

| Rankine Cycle | | | | | | | | | |
|---|---|---|---|---|---|---|---|---|---|
| **Place** | Reference | T (ºC) | H (%) | P (bar) | Altitude (m) | Data (L/kWh) | Adj. Data (L/kWh) COC | | |
| | | | | | | | | No Drift | Drift |
| *Pittsburgh* | (Xia et al., 2017) | 11 | 0.57 | 0.95 | 416 | 2.0 | 20.625 | 1.506 | 2.285 |
| *Louyang* | (Xia et al., 2017) | 13 | 0.48 | 0.98 | 144 | 1.8 | 1.875 | 1.658 | 2.437 |
| *Arnot* | (Delgado and Herzog, 2012) | 14.5 | 0.5 | 0.81 | 1692 | 2.074 | 2.364 | 1.613 | 2.392 |
| *Duvha* | (Delgado and Herzog, 2012) | 16 | 0.5 | 0.81 | 1700 | 2.005 | 2.286 | 1.633 | 2.411 |
| *Hendrina* | (Delgado and Herzog, 2012) | 26 | 0.45 | 0.82 | 1655 | 2.327 | 2.653 | 1.757 | 2.536 |
| *Matla* | (Delgado and Herzog, 2012) | 16 | 0.5 | 0.81 | 1700 | 1.994 | 2.273 | 1.633 | 2.411 |
| *Lethabo* | (Delgado and Herzog, 2012) | 16 | 0.5 | 0.81 | 1700 | 1.819 | 2.074 | 1.633 | 2.411 |
| *Tutuka* | (Delgado and Herzog, 2012) | 15.2 | 0.5 | 0.81 | 1690 | 1.915 | 2.183 | 1.622 | 2.401 |
| *China* | (Jiang and Ramaswami, 2015) | 13.4 | 0.58 | 0.83 | 1545 | | 2.625 | 1.532 | 2.311 |
| *US (Pitt weather)* | (Jiang and Ramaswami, 2015) | 11 | 0.57 | 0.95 | 416 | | 2.990 | 1.506 | 2.285 |
| *Aliaga* | (Sesma-Martín, 2019) | 12.2 | 0.65 | 0.89 | 915 | 2.60 | 2.60 | 1.447 | 2.225 |
| **Combined Cycle** | | | | | | | | | |
| *Place* | Reference | T (ºC) | H (%) | P (bar) | Altitude (m) | Data (L/kWh) | Adj. Data (L/kWh) COC | | |
| | | | | | | | | No Drift | |
| *Andorra* | (Sesma-Martín, 2019) | 10.3 | 0.65 | 0.88 | 1023 | 0.68 | 0.68 | 1.11 | |
| *Castejon 1* | (Sesma-Martín, 2019) | 12.9 | 0.67 | 0.97 | 278 | 0.69 | 0.69 | 0.97 | |
| *Castejon 2* | (Sesma-Martín, 2019) | 12.9 | 0.67 | 0.97 | 278 | 0.69 | 0.69 | 0.97 | |
| *Castejon 3* | (Sesma-Martín, 2019) | 12.9 | 0.67 | 0.97 | 278 | 0.69 | 0.69 | 1 | |
| *Arrubal* | (Sesma-Martín, 2019) | 13.9 | 0.67 | 0.96 | 356 | 0.70 | 0.70 | 0.57 | |
| *Escatron Peaker* | (Sesma-Martín, 2019) | 21.0 | 0.61 | 0.98 | 143 | 0.80 | 0.80 | 0.78 | |
| *Escatron T2* | (Sesma-Martín, 2019) | 21.0 | 0.61 | 0.98 | 143 | 0.80 | 0.80 | 0.78 | |

## References

Delgado, A., Herzog, H.J., 2012. A simple model to help understand water use at power plants 21.

Ghobeity, A., Noone, C.J., Papanicolas, C.N., Mitsos, A., 2011. Optimal time-invariant operation of a power and water cogeneration solar-thermal plant. Solar Energy 85, 2295–2320. https://doi.org/10.1016/j.solener.2011.06.023

Jiang, D., Ramaswami, A., 2015. The `thirsty' water-electricity nexus: field data on the scale and seasonality of thermoelectric power generation's water intensity in China. Environmental Research Letters 10, 024015. https://doi.org/10.1088/1748-9326/10/2/024015

León, E., Martín, M., 2016. Optimal production of power in a combined cycle from manure based biogas. Energy Conversion and Management 89–99.

Martín, L., Martín, M., 2013. Optimal year-round operation of a concentrated solar energy plant in the south of Europe. Appl. Therm. Eng. 59, 627–633. https://doi.org/10.1016/j.applthermaleng.2013.06.031

Morin, G., Richter, P., Nitz, P., n.d. New method and software for multi-variable technoeconomic design optimization of CSF plants.

Palenzuela, P., Zaragoza, G., Alarcón-Padilla, D.C., Guillén, E., Ibarra, M., Blanco, J., 2011. Assessment of different configurations for combined parabolic-trough (PT) solar power and desalination plants in arid regions. Energy 36, 4950–4958. https://doi.org/10.1016/j.energy.2011.05.039

Sesma-Martín, D., 2019. The River's Light: Water Needs for Thermoelectric Power Generation in the Ebro River Basin, 1969–2015. Water 11. https://doi.org/10.3390/w11030441

Wallas, S.M., 1990. Chemical Process Equipment. Selection and Design, Series in Chemical Engineering. Butterworth-Heinemann, Boston.

Xia, L., Li, J., Ma, W., Gurgenci, H., Guan, Z., Wang, P., 2017. Water Consumption Comparison Between a Natural Draft Wet Cooling Tower and a Natural Draft Hybrid Cooling Tower—An Annual Simulation for Luoyang Conditions. Heat Transfer Engineering 38, 1034–1043. https://doi.org/10.1080/01457632.2016.1216975

Xu, C., Wang, Z., Li, X., Sun, F., 2011. Energy and exergy analysis of solar power tower plants. Applied Thermal Engineering 31, 3904–3913. https://doi.org/10.1016/j.applthermaleng.2011.07.038

# *Chapter 6*

# Multi-layer approach for product portfolio optimization: Waste to added-value products

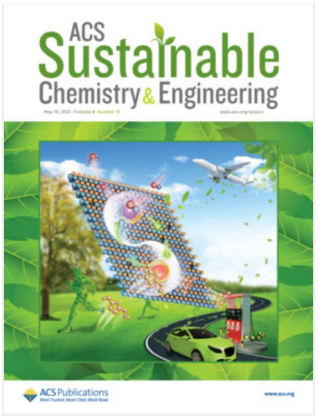


*Authors:* ***Lidia S. Guerras***, *Debalina Sengupta, Mariano Martín*, and Mahmoud M. El-Halwagi*

*DOI:* doi.org/10.1021/acssuschemeng.1c01284

## Abstract

A multistage multilayer systematic procedure has been developed for the selection of the optimal product portfolio from waste biomass as feedstock for systems involving water−energy−food nexus. It consists of a hybrid heuristic, metric-based, and optimization methodology that evaluates the economic and environmental performance of added-value products from a particular raw material. The first stage preselects the promising products. Next, a superstructure optimization problem is formulated to valorize or transform waste into the optimal set of products. The methodology has been applied within the waste to power and chemicals initiative to evaluate the best use of the biomass residue from the olive oil industry toward food, chemicals, and energy. The heuristic stage is based on the literature review to analyze the feasible products and techniques. Next, simple metrics have been developed and used to preselect products that are promising. Finally, a superstructure optimization approach is used to design the facility that processes leaves, wood chips, and olives into final products. The best technique to recover phenols from “alperujo”, a wet solid waste/byproduct of the process, consists of the use of membranes, while the adsorption technique is used for the recovery of phenols from olive leaves and branches. The investment required to process waste adds up to €110.2 million for a 100 kt/yr for the olive production facility, while the profit depends on the level of integration. If the facility is attached to an olive oil production, the generated profit ranges between 14.5 MM €/yr (when the waste is purchased at prices of €249 per ton of alperujo and €6 per ton of olive leaves and branches) and 34.3 MM €/yr when the waste material is obtained for free.

## 1. Introduction

The term water-energy-food (WEF) nexus was coined back in 2011 in the World Economic Forum to strengthen the links among different resources and to provide basic and universal rights to food, water, and energy security (Biggs et al., 2015). Since then, the WEF nexus has gained increasing attention globally from different perspectives (e.g., engineering, social sciences, policy) due to their critical importance toward sustainable development. A key challenge in addressing the WEF nexus is the need to consider the strong interactions among the various components. For example, zones of drought have food and energy security problems because of the high consumption of water supply involved in their production.(Zhang et al., 2018). The energy, food and water demand has increased in the world because of the rise in the population. The energy, food, and water demand has increased in the world because of the increase in the population. Therefore, there is a growing need for improving the efficient use of resources within the WEF nexus. One important point to promote and strengthen the WEF nexus is to employ the circular economy approach. One example is the case of the agricultural sector, in particular, the food industry, that generates a large amount of waste that can generate greenhouse gases or pollute water due to the decomposition of the residues. If such wastes were used as raw materials (RM) to produce added-value products or to generate energy, they become a valuable resource. Thus, the circular economy concept is a strategy that improves the economics and the environmental impact (Borghi et al., 2020) as it can be seen in previous cases in the orange (Criado and Martín, 2020) and coffee (Taifouris et al., 2021) industries and the production of biofuels (López-Díaz et al., 2018).

In the case of processing olives to produce olive oil, several wastes are produced including branches, leaves, and a wet solid lignocellulosic material called “alperujo”. Recently, 19-20 million tons of olives per year have been harvested around the world. Spain is the largest producer with estimated shares ranging between 25 and 40% of the world’s production and 41 and 72% of the total amount of olives produced in Europe. Greece and Italy follow Spain as major world producers representing 8-16% and 11-18%, respectively (“FAOSTAT,” 2019). In Europe, 50−70% of the olive production is used to obtaining olive oil, while the rest is used to develop different types of table olives. In Spain, 90−94% of the amount of olive harvesting is employed to produce olive oil (“EUROSTAT,” 2019).

Since ancient times, olive oil and diverse types of leaves and branches have been used to produce various types of foods, medicines, perfumes, and fuels. Recently, attention has been devoted to the valuable components contained in olive milling wastes including phenols, organic matter (nitrogen, phosphorus, potassium), and sugars, among other species. Several works have evaluated the recovery of phenols and compared alternative processing techniques for the different types of residues such as alperujo, leaves, and branches. These processes can be classified mainly into two groups, namely, conventional and modern techniques. The advantages of modern techniques include a lower time of extraction, easier scale-up to industrial scale, and less use of solvents among others (Romero-García et al., 2016). Most of the previous studies have evaluated the recovery of value-added products from an experimental point of view to determine the yield and operating conditions. In the case of membrane module, different combinations of membranes are used to recover distinct classes of phenols. Examples of such systems include microfiltration, nanofiltration, and osmotic distillation membrane to recover phenols in general (Bazzarelli et al., 2016) or the combination of microfiltration, ultrafiltration, and nanofiltration membranes for the recovery of oleuropein from olive leaves and branches (Khemakhem et al., 2017). Adsorption technique was employed using different types of resins and operation conditions. For instance, Yoon et al. (1997) studied the adsorption of flavonoids employing the XAD-7 resin, while Aehle et al. (2004) used XAD-7HP and XAD-16HP resins. Bayçin et al. (2007) used a silk fibroin to recover the antioxidants, analyzing different parameters like temperatures, pH, and solid/liquid ratios. The work of Li et al. (2011), evaluated eight types of resins to purify phenols and flavonoids from olive leaves. There are other studies that compare conventional and modern technologies in the recovery of phenols such as Lama-Muñoz et al. (2020). that compared the Soxhlet method to the pressurized liquid extractor (PLE) or optimized the phenolic compound extraction through the pressurized liquid extractor changing the operating conditions (Paze et al., 2019). Works by Serrano et al. presented several economic evaluation studies about different pretreatments and recuperation of phenols after biomethanization of the wastes.(Serrano et al., 2017a, 2017b, 2017c). Lama-Muñoz et al. (2019) optimized the operating conditions of pressurized liquid extraction, developing correlations to determine extraction yields, total phenol content, total flavonoid content, as well as oleuropein content as a function of moisture content, temperature, and ethanol concentration. Therefore, systematic methods for product selection and process design are still missing in the literature.

A systematic methodology is proposed for the selection of a set of promising products out of waste biomass to identify and select a subset and the techniques to recover them. It is applied to a particular case of study. This work aims at the development of a process for the recovery of a limited set of added-value compounds from diverse olive oil wastes, including leaves and branches. The rest of the paper is organized as follows. The next section presents the proposed methodology, followed by the general description of the formulated superstructure, associated modeling of the units, and the solution procedure for the problem are shown. Subsequently, the results are analyzed and finally the conclusions are drawn.

## 2. Methodology

The methodology consists of two stages. The first one deals with the prescreening of potential products. We define different indicators to be able to rank the high added-value products available within the biomass. Once a subset of chemicals is selected, a superstructure optimization approach is formulated to select the techniques and the optimal portfolio of products.

### *2.1. Product prescreening*

Four different metrics are developed to quickly identify potential promising products contained or extractable from the biomass. The indicators are ranked so that first the economic potential is evaluated. Next, the process conditions are evaluated. The larger the energy required to obtain a particular product, the higher is the associated operating cost. The third layer of decision-making is given by the operating conditions of the process. The more extreme conditions require processing units to withstand them and increase the capital investment of the process. Finally, at the same decision level are the safety and health issues of the species involved in the processing of the waste for sustainable decisions.

#### *2.1.1. Economic potential indicator*

From a benefit point of view, this indicator based on the metric for inspecting sales and reactants "MISR" (El-Halwagi, 2017) aims to identify the type of compound that is more promising from the economic perspective. This indicator is computed as the ratio between the benefit from a particular product (P) and the cost of the raw material (RM) (see eq 1)

$$\eta_{profit} = \frac{m_P \cdot Cost_P}{m_{RM} Cost_{RM}} \quad (1)$$

This indicator ranks chemicals as a function of their economic potential, where a value greater than 1 indicates economic feasibility of the product, while the greater the indicator is from 1, the more profitable the pathway is expected to be.

### 2.1.2.Energy and environment

The biomass may be converted into products. The smaller molecular size of the final product or required intermediates such as syngas require larger energy and number of units for processing. The ratio of the molecular size of the product versus that of the raw material is representative of the energy involved as well as the equipment required. Therefore, the energy indicator, η, is computed as the ratio between the molecular weights (eq 2)

$$\eta = \frac{MW_{RM}}{MW_{product}} \quad (2)$$

The particular case of biomass presents challenges to compute this indicator. Hemicellulose, cellulose, and lignin are mostly polymers. Therefore, to estimate the molecular weight of the initial raw material, the degree of polymerization (DP), by number, is used

$$MW_{RM} = DP \cdot MW_{Monomer} \quad (3)$$

Hemicellulose shows degree of polymerization (DP) values of 100−200,23 (Bajpai, 2018), Cellulose shows 700 (Wadsworth et al., 1973), and lignin shows a value of 60 (Petridis and Smith, 2016).

When dealing with lipids, the composition of the lipid as a mixture of them allows computing the average molecular weight from the distribution of fatty acids. The unit of measure is Da (= 1 g/mol). In some cases, the final product is already available as such within the raw material and only extraction is required. In that case, this indicator becomes 1.

The operating conditions to process the biomass into products can also be classified by high-, medium-, and lowtemperature processes such as gasification, pyrolysis, and biochemical pathways. Each of them has its own typical equipment and costs. Therefore, the maximum operating temperature and

pressure across the process are also metrics to indirectly evaluate the environmental impact and safety issues of the transformation process. Operating indicators $m_P$ and $m_T$ are defined as given in eq 4.

$$m_P = \max\{P_i\}$$
$$m_T = \max\{T_i\} \quad (4)$$

The maximum temperature can also be related to the emissions since various energy sources are required to provide high temperatures. Some examples are shown in Table 6.1.

***Table 6.1.*** Temperature of typical biomass processing routes, and the sources of energy

| Temperature (ºC) | Process type | Source of energy | Emissions |
|---|---|---|---|
| *1000* | gasification | Combustion | kg $CO_2$/kg Biomass |
| *500* | Pyrolysis | Combustion / CSP | |
| *250* | High temperature Biochem | HP steam | |
| *180* | Medium temperature. biochemical | MP steam | |
| *120* | Medium to low temperature biochemical | LP steam | |
| *<100* | Low temperature | LP steam/ energy integration | |

To further distinguish among processes operating at the same temperatures and pressures, for instance, among pretreatments in lower-temperature processes, the need for adding an acid, a base, or a solvent is an additional feature to characterize the process. Solvents can be flammable, explosive, and/or toxic. Martínez-Gomez et al. (2017) presented a study where the safety of a heat transfer fluid was analyzed. For quick and preliminary assessment of techniques, the processes that involved chemicals with the highest LC50 will be considered last or discarded. A safety analysis can be part of the detailed process design at the superstructure optimization stage if needed.optimization stage if needed.

### *2.2. Superstructure Design.*

Based on the subset of promising products, a superstructure of alternatives is formulated to design the production process capable of recovering them.

#### *2.2.1. Heuristic-Based Selection of Techniques.*

We consider different raw materials arising from the production of olive oil. On the one hand, during the harvest, leaves and branches can be collected. On the other hand, once the oil is extracted from the

olive, the alperujo or olive pomace is the second waste that becomes a raw material of the process. The superstructure will consider both processing lines.

Several methods to obtain olive oil are employed traditionally including pressing and centrifugation. Nowadays, centrifugation methods are employed more at the industrial scale because they can work in continuous processes (Shahidi and Kiritsakis, 2017). Lately, two-phase and three-phase centrifugation are the more widely used. The two-phase centrifugation process uses less water and generates the least residues compared to the threephase centrifugation process. Because of this, in Spain, 90% of the production of olive oil is carried out by the two-phase method (SCP/RAC, 2019). This will be the technique of choice in this work.

Alperujo is composed of a mix of biomass and water as well as a solid fraction consisting of bones, mesocarp, and skin. Alperujo has a high organic content, and it presents phytotoxic components. This fact generates environmental problems and makes it difficult to use (Rodríguez-Gutiérrez et al., 2012). One important feature of alperujo is that it is not possible to separate both phases by centrifugation, decantation, or another process from the beginning. To perform this separation, it is necessary to apply a preprocessing or pretreatment stage (Lama-Muñoz et al., 2019b).The main technique is thermal pretreatment and usually consists of steam explosion and hydrothermal treatment (Galanakis, 2017). Thermal pretreatment is necessary to solubilize the phenolic compounds in the liquid phase by means of their breakdown from complex molecules (Rubio-Senent et al., 2017). Next, it is possible to carry out the phase separation. In the case of industrial scale, the hydrothermal treatment is better than steam explosion because of the lower operating temperatures and pressures (Lama-Muñoz et al., 2019b). Sedimentation, centrifugation, or flocculation can be employed for the separation between the liquid phase and the solid phase. At industrial scale, the best process to achieve this separation is centrifugation due to fast splitting, avoiding the use of chemicals as in the case of flocculation (Ochando-Pulido et al., 2018). At this point, the liquid phase follows one path and the solid phase another. It should be noted that the liquid phase contains most of phenols within the alperujo. Due to this fact, the solid phase is not employed as a resource for phenols but it can be used to generate other chemicals such (Serrano et al., 2017a) or bioethane (Christoforou and Fokaides, 2016), power or heat (Christoforou and Fokaides, 2016), and compost (Fernández-Hernández et al., 2014). In some cases, the liquid phase can be used for irrigation. However, in this work, the target is to obtain

added-value compounds, the phenolic ones, due to their wide array of biological activities (Boskou, 2015). Different techniques exist for the recuperation of these phenols. The first technique, also called a conventional technique (Soxhlet and maceration), is based on the extraction of phenols using different solvents. Depending on the nature of the compound to be obtained, the type of solvent is employed (Ochando-Pulido et al., 2018). The main problem with these techniques is the time of extraction to obtain high yields of phenols. Advanced extraction techniques allow decreasing the time of extraction and energy consumption. These types of techniques can be classified into pressurized liquid extraction, high-pressure or high-temperature, subcritical water extraction or superheated water extraction, supercritical fluid extraction, molecular distillation or shortpath distillation, ultrasound-assisted extraction, microwave assisted extraction, chromatographic methods, or membranes (Boskou, 2015). In this case, use of membrane module is a good technique for recovering the phenols due to their low cost and low consumption of energy (Ochando-Pulido and Martinez-Ferez, 2017). Furthermore, this technique not only recovers the phenols but also produces them with the required degree of purity (Socaci et al., 2019). From the industrial point of view, there is another interesting technique to recover phenols, the adsorption technique or the chromatographic technique (Fernández-Prior et al., 2020). Based on the species-pathway representation of Pham and El-Halwagi (2012). Figure 6.1 shows the possibilities for the recovery of phenols from alperujo based on the above discussion.

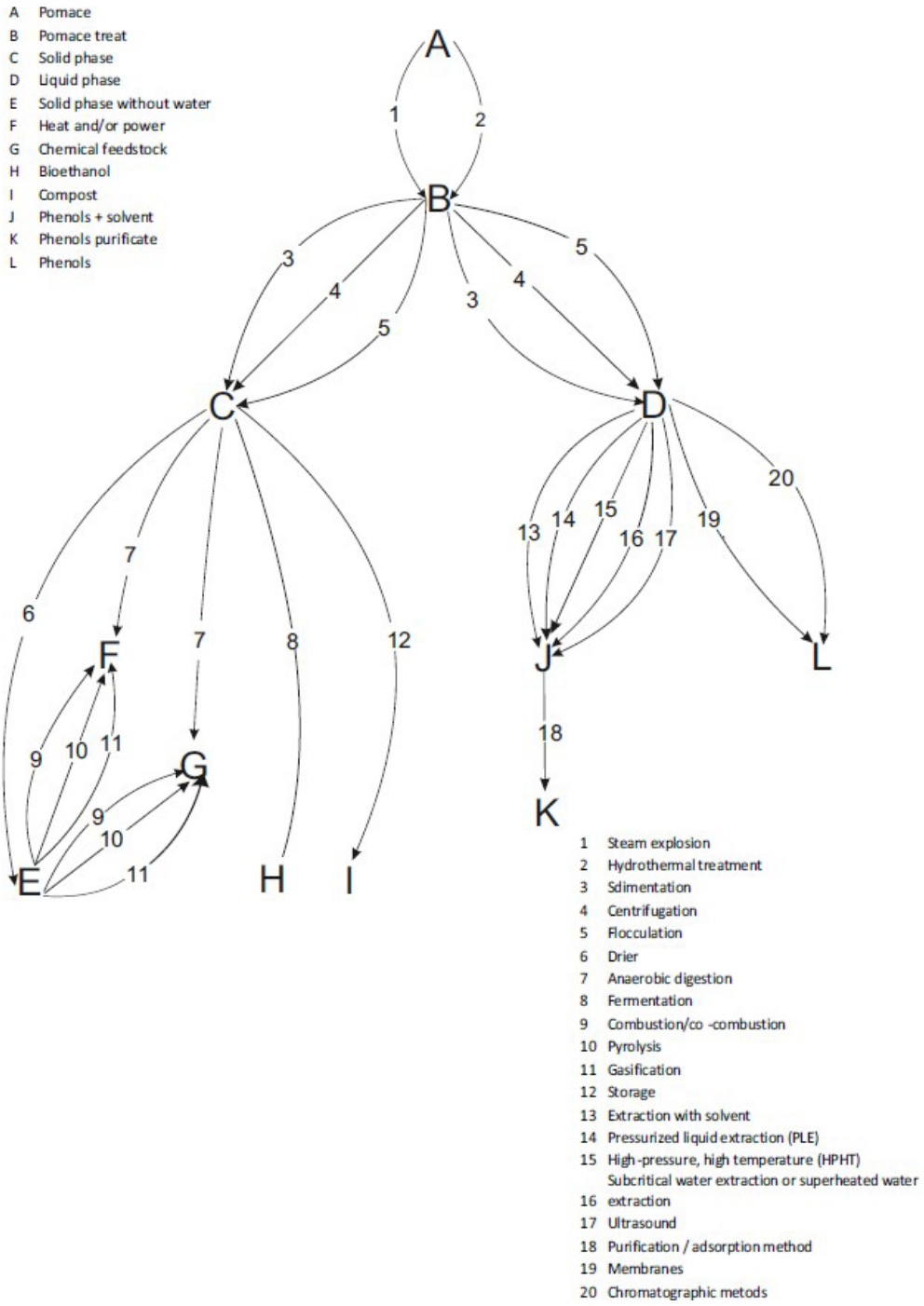


***Figure 6.1.*** Techniques to recover high added-value compounds from olive pomace.

Over the last years, different techniques have been developed to extract phenol compounds from olive leaves. Maceration and Soxhlet extraction are very popular ones but the main problem is that they are difficult to scale up to the industrial scale. They are used mainly at the laboratory scale (Romero-García et al., 2016). Other techniques such as pressurized liquid extraction, dynamic ultrasound-assisted extraction, supercritical fluid extraction, or microwave-assisted extraction have been evaluated (Castro and Priego-Capote, 2010). Among the modern techniques, the pressurized liquid extraction process is the more

promising technique for recovering polyphenols from olive leaves (Roselló-Soto et al., 2015) and it was also successful for phenol recovery from various plant matrices and can be used at the industrial scale (Barba et al., 2016). After applying this technique, product purification has to be carried out. Two alternatives can be used, either membrane modules or adsorption-desorption beds. Figure 6.2 shows processes that can be applied to recover added-value products from leaves and branches.

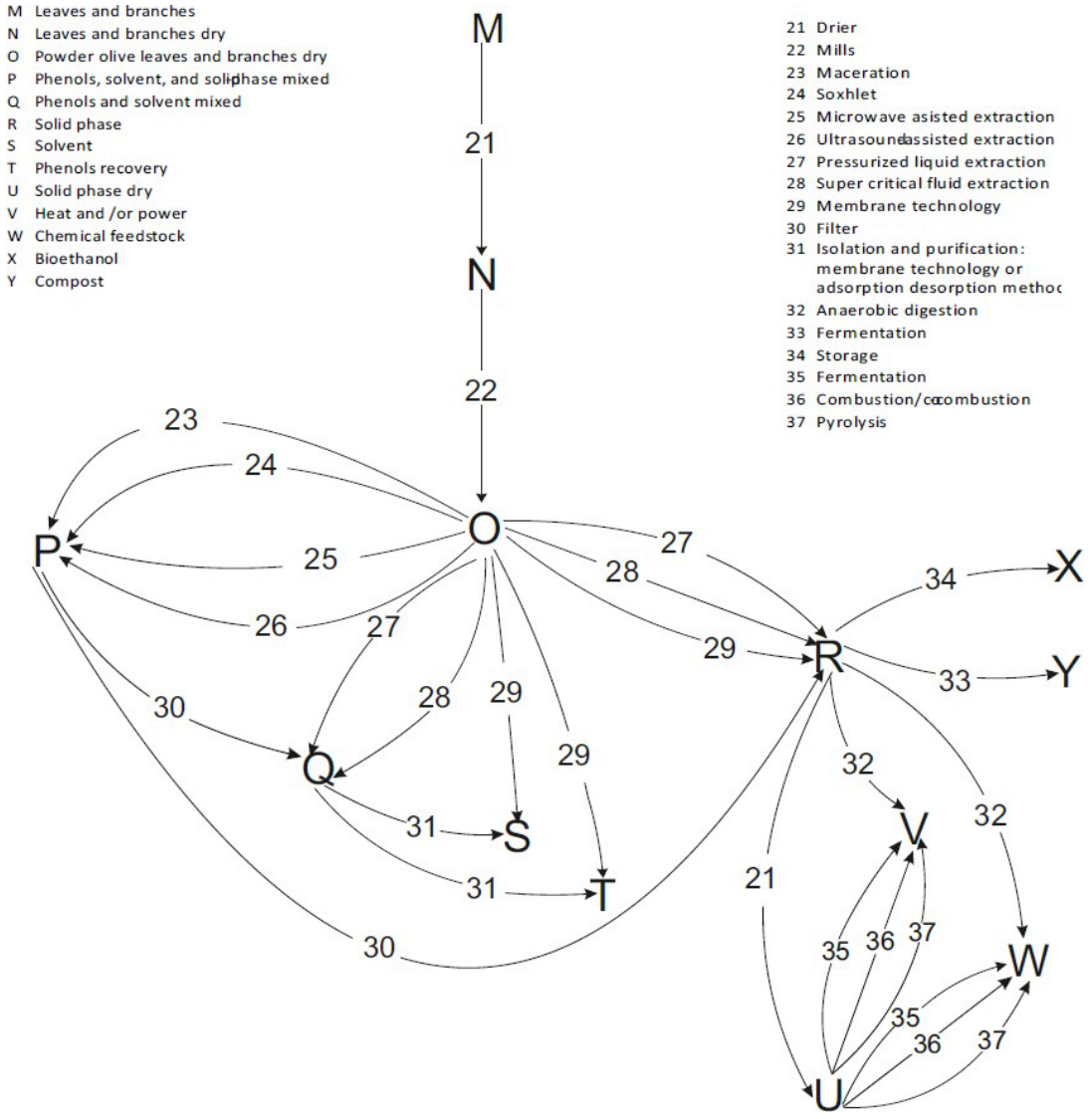


***Figure 6.2.*** Techniques to recover high added-value compounds from olive leaves and branches.

### *2.2.2. Superstructure Definition.*

As referenced above, after harvesting, cleaning, and production of olive oil, mainly two types of wastes are generated, alperujo (the liquid waste stream from oil extraction) and leaves and branches. These wastes are treated separately for the recovery of phenols. Figure 6.3 shows the superstructure including the

most promising techniques. The harvesting of olive and generation of olive oil are carried out for around 4 months. In this way, to develop the model of the facility, the olive leaves and branches are processed for 8 months, while the alperujo is processed for 4 months. During these 4 months, the olive leaves are dried, crushed, and stored. These treatments are necessary to avoid the degradation of olive leaves.

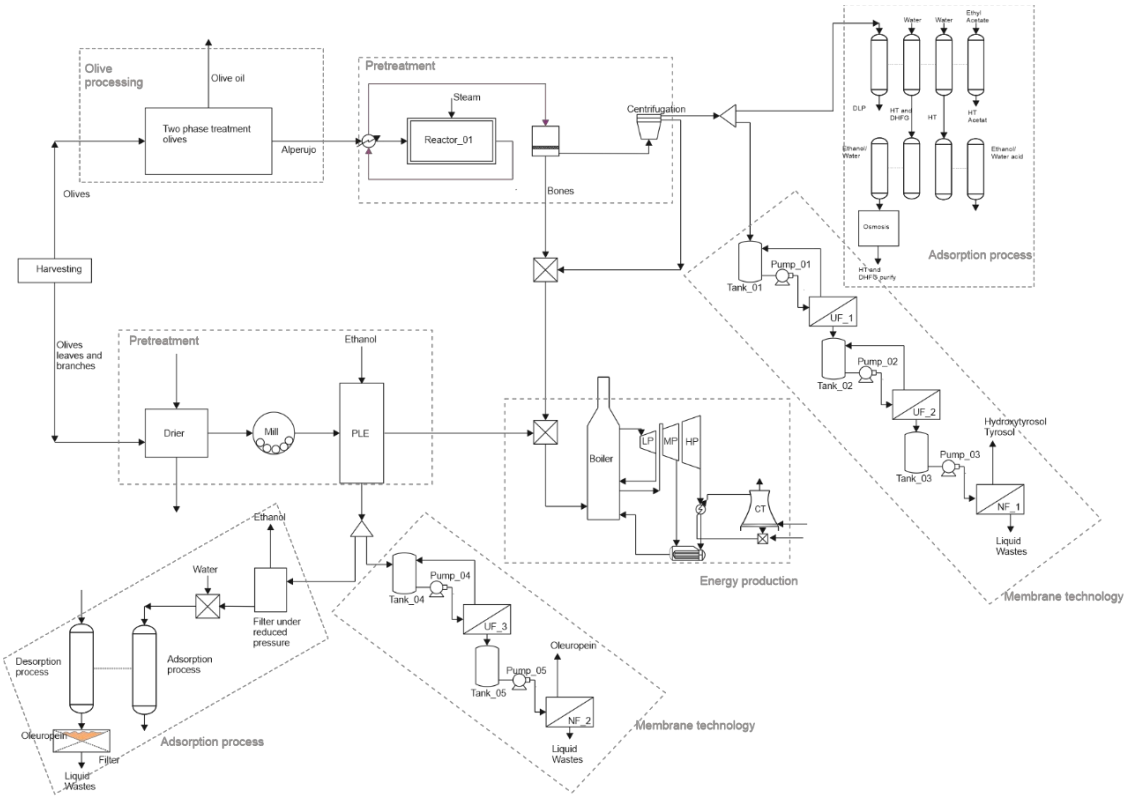


***Figure 6.3.*** Superstructure of alternative technologies for the recovery phenols from olive pomace, olive leaves and branches and recuperation of energy.

In the case of alperujo, the first step is the hydrothermal treatment. After the pretreatment, the liquid and the solid phases are separated. The solid phase is used for the generation of energy using a boiler and a steam turbine and the liquid phase is used to recover phenols. The recovery of phenols can be carried out through two techniques, either membrane modules or adsorption-desorption techniques.

In the case of leaves and branches, the first step consists of drying, milling, and storage. For the recuperation of phenols, the pressurized liquid extractor (PLE) is selected, using ethanol as a green solvent. In this process, liquid and solid phases are generated. Similar to the processing of alperujo, the phase solid is employed to generate energy, and the liquid phase is employed as a raw material for the recovery of phenols. To purify the phenols soluble in the solvent, either membranes or adsorption-desorption techniques are used.

The solid phase is burnt to generate energy through a regenerative Rankine cycle with reheating (Martín and Martín, 2013).

## 3. Superstructure model formulation

The superstructure described in the previous section, and presented in Figure 6.3, is modeled in this section. The modeling of the superstructure is developed unit by unit, considering mass and energy balances, thermodynamic properties, and experimental data in the appropriate unit. Surrogate models are developed from experimental data. To simplify the explanation of the superstructure, the selection of the products based on the indicator should be mentioned; for more information about this analysis, we refer to the Portfolio of Products section in this work. Therefore, the phenols recovered from alperujo are hydroxytyrosol and tyrosol, while from olive leaves and branches, it is oleuropein. In addition, the explanation of the superstructure is divided into three parts for the detailed presentation of the models developed. All of the units are modeled based on mass and energy balances using experimental yields from the literature, as will be explained in the following sections.

### *3.1. Recovery of Phenols from Alperujo.*

The composition of alperujo depends on the olive's variety, the fruit ripeness, among other parameters; in such a way, it is widely variable (Galanakis, 2017). Table 6.2 shows the composition of alperujo employed in this work.

***Table 6.2.*** Main compound of alperujo (Adapted (Fernández-Prior et al., 2020; Leite et al., 2016)) (WSC: Water soluble content)

| Component | %Wet weight |
|---|---|
| *Bones* | 5.062 |
| *Orujillo* | 17.084 |
| *WSC* | 0.028 |
| *Phenols* | 0.066 |
| *Hydroxytyrosol* | 0.120 |
| *Tyrosol* | 0.060 |
| *Oil* | 4.081 |
| *Water* | 73.500 |

### *3.1.1. Pretreatment of Alperujo.*

The first stage is the pretreatment of the alperujo (see the top line in Figure 6.3). The process used for the pretreatment is based on the patent number WO 2012/020159 A1. The process developed in this patent consists of one heat exchanger, a reactor, the split of bones, and a centrifugation process (see Figure 6.3). The first step of the pretreatment is preheating the alperujo in a heat exchanger, using the hot stream exiting the reactor. Therefore, with this type of preheating, heat integration is achieved minimizing the consumption of steam. The preheated alperujo is sent to the reactor heating with steam. To provide the heating, 1.1 L of steam per kg of fed alperujo (Serrano et al., 2017a) is used, assuming medium-pressure steam at 230 °C and 2.7 MPa. The reactor is equipped with a stirrer and a heating jacket. In the operation, the reactor operates around 170 °C and 0.85 MPa. The pretreatment increases the solubility of the organic compounds up to around 26.3% compared to the initial alperujo, and in the case of phenols, it reaches 60.4% (Serrano et al., 2017a).

Once it has passed through the reactor, the separation of the solids and liquid phases is easier. Two types of techniques are used for such a separation due to the presence of two to remove the bones broken in the process of crushing. Thus, two streams are generated, the bones with moisture and the rest of compounds. Generally, by the end of the process, the bones have an average of 13% moisture (Junta de Andalucía, 2010).

To perform the separation process, a centrifugation system is employed. The solid-phase content is mainly orujillo, defined as the residue remaining after oil extraction from the oil, but around 25% of organic-soluble compounds or in the case of phenols 11.5% are lost in the solid phase. Besides, the content of water is around 8.7% of the product obtained (Campoy et al., 2014). The liquid phase contains the majority of the organic-soluble compounds as well as phenols, so this stream continues the process of recovery of these phenols.

To compute the cost of this pretreatment, the data from Serrano et al. are employed and is under patent. In this study, 50,000 metric tons per year are treated, and the investment cost in the case of heat recovery reaches €330,000, while the operation and maintenance costs were estimated as 2% of the construction cost. Therefore, this investment cost is around $6.6 \times 10^{-3}$ €/(kg yr) (Serrano et al., 2017a). Therefore, the cost (eq 5) is calculated as follows

$$\left(Cost_{invest}\right)_{PT} = 6.6\cdot10^{-9}\cdot m_{treat}$$
$$\left(Cost_{OM}\right)_{PT} = 0.02\cdot\left(Cost_{invest}\right) \quad (5)$$

### 3.1.2. Techniques for Phenol Recovery.

In this work, two techniques to recover the phenols are considered, resin adsorption columns and membrane modules (see Figure 6.3); only one is to be used.

#### *3.1.2.1. Resin Adsorption Columns.*

One of the most popular alternatives to recover phenols is based on the patent WO 2013/007850 A1. This patent presents several adsorption and desorption steps through different columns of anionic and cationic resins. The liquid phase obtained in the previous separation is fed to the columns (see the top line in Figure 6.3). This process is carried out by floating or force of gravity. The phenols are retained in the bed of the columns, and to desorb them, different steps are followed. The first step consists of the discharge of the column with water, obtaining 3,4-dihydroxyphenylglycol and hydroxytyrosol. The second step is based on the discharge of the column with water at acidic pH, obtaining hydroxytyrosol with 30−70% of purity. In the end, the column is emptied, refilled with ethyl acetate, and closed. The temperature is increased with a heating jacket and then it is emptied; acetate hydroxytyrosol is obtained. According to Serrano et al. (2017a), using this process, the yields of hydroxytyrosol, tyrosol, 3,4-dihydroxyphenylglycol, and vanillic acid are about 77.8, 93.0, 75.9, and 92.5%, respectively. It should be noted that in this case, hydroxytyrosol and tyrosol are recovered separately.

As in the previous case, this process is under patent, and to compute the cost, the data of Serrano et al. are employed (Serrano et al., 2017a). In this way, the investment cost is around 0.42 €/kg and the operation and maintenance cost is 0.5 €/(kg yr) (Serrano et al., 2017a), as shown in eq 6

$$\left(Cost_{invest}\right)_{RA} = 0.42\cdot10^{-6}\cdot m_{trea}$$
$$\left(Cost_{OM}\right)_{R} = 0.5\cdot10^{-6}\, m_{trea} \quad (6)$$

#### *3.1.2.2. Membrane Techniques.*

Another alternative employed to recover phenols consists of the use of membrane modules (see the multistage membrane system on the right of Figure 6.3). This process is based on the purification of the olive pomace. The small area requirement and low-energy consumption of the operation make it popular in water treatment and it is feasible for olive pomace treatment (Mudimu et al., 2012). In this work, this technique is based on three types of membranes, two ultrafiltration membranes and one nanofiltration membrane.

The first step of the process is to increase the pressure until a transmembrane pressure of 0.5 bar is achieved. The yield considered for the pump is around 80%. Once it has passed through the membrane, the permeate is sent to the next membrane using another pump. In the second step, using a second pump, the transmembrane pressure (ΔP) must reach 9 bar. The final step consists of recovering the phenols using the nanofiltration membrane. The permeate obtained from the second membrane is sent to the nanofiltration membrane using a third pump, achieving a transmembrane pressure of 12 bar. The parameters employed to develop the mass balance like yields, permeate flux, transmembrane pressure, and water permeability are given in Table 6.3.

***Table 6.3.*** Properties of membranes (Cassano et al., 2013)

| | $J_p$ (l/m²·h) | $K_{water}$ (l/m²·bar) | $\eta_{Phenols}$ (%) | $\eta_{SCO}$ (%) |
|---|---|---|---|---|
| *UF 1* | 12 | 218.07 | 21 | 33.7 |
| *UF 2* | 150 | 22.47 | 17.6 | 72.1 |
| *NF* | 13.75 | 5.95 | 100 | 96.4 |

The temperature of operation employed in the process is the ambient temperature. It should be kept in mind that the membrane module does not recover phenols separately but a mix of phenols where the principal phenols are hydroxytyrosol and tyrosol.

In the case of membrane technique, three types of membranes are employed, two ultrafiltration membranes and one nanofiltration membrane. In the case of ultrafiltration membranes, the investment cost accounts for 5.37 €/m³ per year, while the operating costs are 0.54 €/m³ per year. The process to compute the nanofiltration membrane is the same as in the previous case; therefore, investment costs are 3.79 €/m³ and operating costs are 0.49 €/(m³ yr) (Stoller et al., 2015).

$$\begin{aligned}
\left(Cost_{invest}\right)_{U} &= 5.37\cdot10^{-6}\cdot m_{treat} \\
\left(Cost_{OM}\right)_{UF} &= 5.4\cdot10^{-7}\cdot m_{treat} \\
\left(Cost_{invest}\right)_{NF} &= 3.79\cdot10^{-6}\cdot m_{treat} \\
\left(Cost_{OM}\right)_{N} &= 4.9\cdot10^{-7}\cdot m_{treat}
\end{aligned} \tag{7}$$

*3.2. Recovery of Phenols from Leaves and Branches.*

During harvesting of olives, around 5% by weight of olive leaves, with respect to olives, are recollected (Galanakis, 2017). At this point, different treatments are described for the recovery of phenols from the olive leaves and branches. As mentioned above, the main phenol content in the olive leaves is oleuropein.

The typical composition of the olive leaves that is employed in the model is shown in Table 6.4. The addedvalue products are extracted from the carbohydrate and crude fiber. The second line of processes in Figure 6.3 shows the processing of leaves and branches.

***Table 6.4.*** Composition of olive leaves (Erbay and Icier, 2009)

| Component | Amount (g/100 g olive leaves) |
|---|---|
| *Protein* | 5.45 |
| *Oil* | 6.54 |
| *Carbohydrate* | 27.57 |
| *Crude fiber* | 7 |
| *Ash* | 3.61 |
| *Water* | 49.83 |

*3.2.1. Drying of Olive Leaves.*

After cleaning the olives and removing the olive leaves and branches, these are dried with hot air. This technique has a crucial role in the process because if the operating conditions are not optimal or appropriate, a huge loss of the total phenol content occurs. To model the process and minimize the losses of total phenols, the optimal operating conditions determined in Erbay et al.51 are employed. In this way, to obtain the moisture content below 6%, the dryer must operate at 53.43°C.51 In the model, it is assumed that the olive leaf temperature is constant across the dryer and the air temperature can decrease by 3 °C. Thus, it is possible to compute the airflow necessary to dry the olive leaves. The energy balance developed in the process of drying is presented below

$$G \cdot H_{G_{IN}} + L \cdot H_{L_{IN}} = G \cdot H_{G_{OUT}} + L \cdot H_{L_{OUT}} \tag{8}$$

where:

$$\begin{aligned} H_{G_i} &= Cp_{da}(\mathrm{T}_{G_i} - T_{ref}) + \lambda \cdot Y \\ Cp_{ad} &= 1.005 + 1.84 \cdot Y \\ H_{L_i} &= Cp_{ds}(\mathrm{T}_{L_i} - T_{ref}) + X \cdot Cp_{water}(\mathrm{T}_{L_i} - T_{ref}) \end{aligned} \tag{9}$$

To compute the heat capacity of the leaves, their composition and corresponding heat capacities are used (Singh, 2006).

$$Cp_{ds} = \sum_i Cp_i \cdot x_i^w \tag{10}$$

$$\begin{aligned} Cp_{protein} &= 2.0082 + 1.2089 \cdot 10^{-3} \cdot T - 1.3129 \cdot 10^{-6} \cdot T^2 \\ Cp_{fat} &= 1.9842 + 1.4733 \cdot 10^{-3} \cdot T - 4.8008 \cdot 10^{-6} \cdot T^2 \\ Cp_{carbohydrate} &= 1.5488 + 1.9625 \cdot 10^{-3} \cdot T - 5.9399 \cdot 10^{-6} \cdot T^2 \\ Cp_{fiber} &= 1.8459 + 1.8306 \cdot 10^{-3} \cdot T - 4.6509 \cdot 10^{-6} \cdot T^2 \\ Cp_{ash} &= 1.0926 + 1.8896 \cdot 10^{-3} \cdot T - 3.6817 \cdot 10^{-6} \cdot T^{-2} \end{aligned} \tag{11}$$

According to the information collected, for this operating capacity, the investment cost of the dryer is around \$15 000, while the operation and maintenance cost is a function of removed water in the leaves and takes a value around $9.82 \cdot 10^{-5}$ M€/(kg $H_2O$/h) (Alibaba, 2019a).

$$\begin{aligned} \left(Cost_{invest}\right)_{dryer} &= 15{,}000 \cdot \delta / 10^6 \\ \left(Cost_{OM}\right)_{drier} &= 9.82 \cdot 10^{5} \cdot \ _{waterremoved} \end{aligned} \tag{12}$$

After completing the drying process of the leaves, they are fed to the milling process and then the powder is stored. The cost of the crushing machine varies between \$60 000 and \$145 500. Due to the lack of information about this specific process, to be on the safer side, a higher cost is used. With regard to operation and maintenance cost, the cost of the energy consumed according to the specifications is assumed, taking a value of around 6.3 kW per ton of olive leaves milling per hour (t/h) (Made-in-China, 2019).

$$\begin{aligned} \left(Cost_{invest}\right)_{mill} &= 145{,}500 \cdot \delta / 10^6 \\ \left(Cost_{OM}\right)_{mill} &= 4.35 \cdot 10^{-6} \cdot m_{olives} \end{aligned} \tag{13}$$

*3.2.2. Pressurized Liquid Extraction (PLE) for Phenol Recovery.*

Lama-Muñoz et al. (2019a) developed correlations to compute the extraction yield of the soluble solid content from the liquid phase as well as the oleuropein content as a function of temperature, moisture, and ethanol concentration. The correlations shown in eq 14 are used to compute the extraction yield and the content of oleuropein in the olive leaves

$$\eta_s = 380.99 + 146.75 \cdot T^* + 12.98 \cdot MC^* - 3.52 \cdot E^* + 11.33 \cdot T^* \cdot E^* - 17.38 \cdot MC^* \cdot E^* + 25.85 \cdot \left(T^*\right)^2$$
$$m_{OC} = 40.75 + 7.59 \cdot T^* - 5.79 \cdot MC^* - 5.22 \cdot T^* \cdot MC^* - 6.14 \cdot \left(T^*\right)^2 + 10.13 \cdot \left(MC^*\right)^2 \quad (14)$$

The parameters T*, MC*, and E* take values between -1 and 1. To apply these values and boundaries in the model, a variable change is presented for the moisture content, temperature, and the ratio between ethanol and water. The boundaries applied in these correlations correspond to 60-80% of ethanol at 70-190 °C and 4.70-22.60% moisture contents, as given in eq 15.

$$MC^* = 0.10 \cdot MC\left(4.70 - 22.60\%\right) - 1.5$$
$$T^* = 0.0167 \cdot T\left(70 - 190^{\circ} C\right) - 2.167 \quad (15)$$
$$E^* = 0.10 \cdot E\left(60 - 80\%\right) - 7$$

In this technique, the ratio between the solvent and the olive leaves should be around 7 and is lower than the other techniques (Lama-Muñoz et al., 2019b). The losses of solvent in the process are considered to be around 2% of the solvent fed.

Based on the work of Osorio-Tobón et al. (2014)., a surrogate model is developed to calculate the investment cost of the pressurized liquid extractor as given by eq 16.

$$\left(Cost_{invest}\right)_{PLE} = 0.2833 \cdot \left(V_{leaves}\right)^2 + 0.4392 \cdot V_{leaves} + 0.0285 \quad (16)$$

To obtain a maximum range of extraction, the time and number of cycles in the process are 5 min and 1 cycle, respectively (Lama-Muñoz et al., 2019a). To obtain a continuous process, two extractors are used. While one extractor is operating, the other one is cleaned and refilled with powdered leaves. Taking into account these considerations, the extractor capacity is computed through eq 17

$$V_{leaves} = \frac{\left(m_{leaves}\right) \cdot t_{extraction} \cdot n_{cycle}}{\rho_{leaves}} \quad (17)$$

The density of the powdered olive leaves is considered to be around 1510 kg/m$^3$ (Canabarro et al., 2019).

The operation and maintenance cost are computed as a function of ethanol losses in the process, considering the cost of the ethanol to be around 0.42 €/kg (Galán et al., 2019).

### *3.2.3. Purification of Oleuropein Content.*

Two methods have been used to purify the oleuropein, membrane modules (Khemakhem et al., 2017) and adsorption resins (Şahin and Bilgin, 2017), and only one is used.

#### *3.2.3.1. Membrane Modules.*

The technique of membrane modules employed in the model consists of two membranes (to the right in the bottom of Figure 6.3): an ultrafiltration membrane and a nanofiltration membrane. The treatment of membranes to purify oleuropein is similar to that of alperujo.

The first step is to increase the pressure with a pump until the transmembrane pressure (ΔP) generated reaches 1 bar. Having reached that pressure, the solution is sent to the ultrafiltration membrane, whose characteristics are shown in Table 6.5. The permeate obtained from the ultrafiltration membrane is sent through another pump to the nanofiltration membrane. In this pump, the transmembrane pressure must reach 9 bar. The product obtained consists of other phenols, flavonoids, and carbohydrates. The process to compute the investment cost and the operation and maintenance cost are the same as in the previous case.

***Table 6.5.*** Properties of membranes (Khemakhem et al., 2017)

| | $J_p$ (l/m$^2$·h) | $\eta_{oleuropein}$ (%) | $\eta_{soluble}$ (%) |
|---|---|---|---|
| *Ultrafiltration Membrane* | 27.5 | 32.81 | 37 |
| *Nanofiltration membrane* | 50 | 100 | 95 |

#### *3.2.3.2. Selective Adsorption of Oleuropein.*

The extract obtained in the pressurized liquid extraction process is filtered through a filter under pressure to recover ethanol (see the units to the bottom left corner of Figure 6.3). Thus, ethanol is collected and recycled to the previous step. The ethanol losses are considered to be around 1%. The extract without ethanol is diluted with water, generating a ratio of (grams of extract per liter of water) around 100. After the

adsorption process is completed, the resins are washed with distilled water and subjected to the desorption process. To carry out the desorption process, 40% ethanol in water mix (Şahin and Bilgin, 2017) is added to the resins, promoting the desorption of oleuropein. To remove the water, the obtained extract is percolated through a 0.45 µm filter (Li et al., 2011; Şahin and Bilgin, 2017).The resin employed is Amberlite XAD-7HP, recommended by Şahin and Bilgin (2017) for the recovery of oleuropein from olive leaves. Table 6.6 shows the main characteristics of the resin employed in the process.

***Table 6.6.*** Properties of Amberlite XAD 7 HP resin

| | | References |
|---|---|---|
| Qe (mg /g resin) | 97.9 | (Şahin and Bilgin, 2017) |
| ρ (g/ml) | 1.05 | (Lookchem, 2019) |
| Price (€/kg) | 5.00 | (Lookchem, 2019) |

The yield of oleuropein recovery in the process of adsorption is 91%, while the process of desorption is 97%. The adsorption process runs for 180 min, whose adsorption capacity corresponds to 97.90 mg of oleuropein per g of resin (Şahin and Bilgin, 2017) and 17.50 mg per g of resin for the rest of phenols. The adsorption capacity is used to determine the amount of resin that is necessary for the operation of the process (eq 18)

$$m_{resin} = \frac{m_{OA}}{Q_e} \tag{18}$$

To compute the cost of the process, the filter under pressure and the pressurized liquid extractor are considered. The filter under pressure is assumed to be a vessel, and the cost is estimated as follows (Matches, 2020).

$$\left(Cost_{invest}\right)_{FUP} = \left(0.9635 \cdot (m_{steel}) + 103785\right) \cdot \delta / 10^6 \tag{19}$$

The weight of vessel is determined using the following equations (20) (Martín and Grossmann, 2011):

$$u_t = 0.07 \cdot \sqrt{\frac{\rho_l - \rho_v}{\rho_v}}$$
$$D_v = \sqrt{\frac{4 \cdot V}{\pi \cdot (0.15 \cdot u_t)}}$$
$$L_v = 3 \cdot D_v \quad (20)$$
$$e = 0.023 + 0.003 \cdot D_v$$
$$m_{steel} = \rho_{steel} \cdot \left[ \pi \left( \left( \frac{D_v}{2} + e \right)^2 - \left( \frac{D_v}{2} \right)^2 \right) \cdot L_v + \frac{4}{3} \pi \left( \left( \frac{D_v}{2} + e \right)^3 - \left( \frac{D_v}{2} \right)^3 \right) \right]$$

The cost of the adsorption−desorption process is estimated using the price of the XAD resin and vertical vessels. The mass of resin employed in the process is determined as a function of the adsorption capacity of the adsorbent and the amount of sorbent. The size of the vessel should be such that it has to be able to contain the bed of resins. An overdesign factor of 10% is used for safety reasons and in the case of bed expansion (eq 21) (Almena and Martín, 2016).

$$V_{vessel} = 1.1 \cdot V_{resin}$$
$$D_{vessel} = \sqrt[3]{\frac{V_{vessel}}{3 \cdot \pi}} \quad (21)$$
$$L_{vessel} = 3 \cdot D_{vessel}$$

The cost of resin XAD is considered to be 2000 €/t (Lookchem, 2019), and to estimate the cost of the vessel, a correlation obtained from Matches (2020) (eq 22) is used:

$$\left( Cost_{invest} \right)_{ads} = 2 \cdot \left( (0.1699 \cdot m_{steel} + 37.847) + 5 \cdot m_{resin} \right) \cdot \delta / 10^6 \quad (22)$$

The change of resin along the campaign is considered as operation and maintenance costs. One change per campaign is assumed to be on the safer side.

### *3.3. Energy Recovery.*

Two of the products obtained in the recovery of phenols are solid compounds made of cellulose or lignin. To improve the sustainability of the process, where the pretreatments are energy-intense, the solids obtained are employed to produce energy and generate the steam used in the pretreatment step.

The first aim is to generate the steam needed in the pretreatment stage and heat the air in the dryer; the rest of the wastes is used in the production of electricity. To compute the energy required to generate the steam, the type of pressure is defined. A medium-pressure steam (2.7 MPa and 503.15 K)

(Pérez-Uresti et al., 2019) is produced. Therefore, based on these parameters and the amount of steam needed, which was fixed by the characteristics of the pretreatment, the energy required is calculated using eq 23

$$Q_{SN} = m_{steam} \cdot \left( Cp_{water;l} \cdot (T_{boil,water} - T_{in,water}) + \lambda_{water} + Cp_{water;g} \cdot (T_{out,steam} - T_{boil,water}) \right) \quad (23)$$

Taking into account that the energy efficiency toward power in a Rankine cycle is around 40% ($\eta_{SN}$), the energy needed in this process is computed as eq 24

$$Q_{SN,real} = \frac{Q_{SN}}{\eta_{SN}} \quad (24)$$

As previously mentioned, the sources employed to generate thermal and electrical energies are bones and orujillo whose calorific values are 4400 and 4100 kcal/kg, respectively (Junta de Andalucía, 2015). The efficiency of the boiler to produce thermal energy is assumed to be 80%. The analysis of the energy produced from these wastes is carried out separately since alperujo is used for 4 months and olive leaves are used for the rest of the year. To compute the power generated, two boilers and two turbines are modeled with the characteristics of the wastes.

The process considered to produce electricity is a regenerative Rankine cycle with reheating. This cycle is modeled unit by unit like in the previous work, considering mass and energy balance and the detailed thermodynamics (Martín and Martín, 2013).

The cost of this section of the facility is computed through the following surrogate models (Caputo et al., 2005).

$$\begin{aligned} Cost_{turbine} &= 633000 \cdot \left( W_{NE} \right)^{0.398} \\ Cost_{boiler} &= 1340000 \cdot \left( W_{NE} \right)^{0.694} \end{aligned} \quad (25)$$

### *3.4. Solution Procedure.*

#### *3.4.1. Selection of Techniques: Superstructure Optimization.*

The aim of the process is the recovery of the added-value products together with the use of residues to produce power from the wastes of the olive oil production. Thus, the objective function is a simplified annual profit, considering a life cycle of 20 years, as presented in eq 26, where the annualized cost of the

units involved allowed for the fixed costs of selecting a unit to be considered, while the operating costs consider the use of utilities involved in the processing of the waste.

$$\text{Profit}_{anual} = \sum_{products} \left( m_{product} \cdot Cost_{product} \right) - \frac{1}{3} \sum_{j} \left( Cost_{invest\ j} \right) - \sum_{j} \left( Cost_{OM\ j} \right) \quad (26$$

Within the superstructure, the purity of the products depends on the selected technique. As a result, different prices are assigned to the products of each of the alternative path, as shown in Table 6.7.

***Table 6.7***. Price of different phenols obtained.

| | Obtained from | Price (€/kg) | Reference |
|---|---|---|---|
| *Hydroxytyrosol* | Adsorption | 300 | (Alibaba, 2019b) |
| *Tyrosol* | Adsorption | 100 | (Alibaba, 2019c) |
| *Hydroxytyrosol/Tyrosol* | Membrane | 85 | (Alibaba, 2019d) |
| *Oleuropein* | Adsorption | 850 | (Alibaba, 2019e) |
| *Oleuropein* | Membrane | 45 | (Alibaba, 2019f) |

Two operating periods are considered: the recovery phenols from alperujo operate for 4 months, while the recovery phenols from olive leaves and branches work along the rest of the year. The optimization is subjected to the models of all of the unis described in the Superstructure Model Formulation section representing an NLP problem that consists of around 1818 equations and 2508 variables. The model is formulated in GAMS and solved using a multistart optimization approach with CONOPT as the preferred solver. No global optimum is claimed.

### *3.5. Cost Estimation.*

After the optimization of the superstructure, the operation and maintenance costs are computed based on Sinnot and Towler's factorial method (Sinnott and Towler, 2016). The investment cost of the facility is based on the unit's costs, estimated using the equations presented along the text. The total investment is estimated using Lang factors for a facility that processes fluids and solids.

With regard to the production costs, the variable cost includes the cost of raw materials and utilities, while the fixed cost includes the cost of maintenance, operating labor, laboratory cost, supervision, plant overheads, capital charges, insurance, local taxes, and royalties. The methodology employed to develop this cost is described by Sinnott and Towler (2016).

## 4. Results and discussion

As a case study for the analysis, 99 227.4 tons of olives gathered per campaign are considered. In the oil production, 800 kg of alperujo is generated per ton of olives, and leaves and branches generated represent around 5% of the mass of the total amount harvested. Results obtained after the selection of products and the optimization process are shown in the next subsections.

### *4.1. Portfolio of Products.*

The first part of the results consists of the application of the indicators developed to select the product(s) to be obtained. In the case of study, only two indicators can be applied, on the one hand, the economic potential indicator and, on the other hand, the energy indicator regarding the rupture of the raw material in smaller parts. For the indicator concerning solvents, in the majority of the processes, ethanol is employed, which is considered as a green solvent (Capello et al., 2007). For developing the methodology, a particular composition of olive pomace and leaves and branches is taken, allowing the characterization and selection of these wastes.

### *4.2. Alperujo.*

The composition of phenols from alperujo is shown in kilograms per cubic meter (Table 6.8). To compute the fraction of each one in the alperujo, the density of the olive pomace density is assumed to be 1.63 g/cm$^3$ (Romero-Quiles, 2001). To estimate the energy indicator, it is necessary to determine the original source of the phenols. Two alternative sources are identified. We consider the natural source, the phenols already available within the waste. Alternatively, they can be produced from the breaking down of longer molecules. In this part of the study, only two phenols can be obtained from the different sources: hydroxytyrosol and tyrosol. Oleuropein, verbascoside, and hydroxytyrosol 4-β-D-glucoside can be broken down to form hydroxytyrosol. In the case of tyrosol, it can be obtained from oleuropein and natural sources. Without experimental data, it is not possible to determine the proportion of rupture of each molecule. To compute the energy indicator, we assume that each source can generate the same amount. In other words, to calculate the indicator for the hydroxytyrosol, we consider 25% of each source, and in the case of tyrosol,

we consider 50%. To consider the same source for the price of the products in all cases, the price at lab-scale from Sigma-Aldrich's web page is used (see Table 6.8).

***Table 6.8.*** Results of indicators applied in the main phenols of alperujo.

| | Amount of phenols ($kg/m^3$) | Amounts of phenols in alperujo (%) | Cost (€/mg) | Molecular weight (g/mol) | $\eta_{profit}$ | $\eta_{energy}$ | Standardization of $\eta_{profit}$ |
|---|---|---|---|---|---|---|---|
| *3,4-Dihydroxyphenylglycol* | 0.157 | 0.00963 | 10.26[a] | 170.16 | $1.39 \cdot 10^3$ | 1 | 0.12 |
| *Hydroxytyrosol* | 0.540 | 0.03313 | 25.41[b] | 154.16 | $1.18 \cdot 10^4$ | 2.652 | 1.00 |
| *Tyrosol* | 0.122 | 0.00748 | 13.1[c] | 138.16 | $1.62 \cdot 10^3$ | 2.456 | 0.14 |
| *Vanillin* | 0.076 | 0.00466 | 2.45[d] | 152.15 | $1.60 \cdot 10^2$ | 1 | 0.01 |
| *p-Coumaric acid* | 0.032 | 0.00196 | 6.90[e] | 164.16 | $1.90 \cdot 10^2$ | 1 | 0.02 |

a (Merck, 2019a) ; b (Merck, 2019b); c (Merck, 2019c); d (Merck, 2019d); e (Merck, 2019e)

Table 6.8 shows the results of the indicators that can be applied in this case of the study. To rank the products, the economic potential indicator shows that the best phenols to recover are hydroxytyrosol, tyrosol, 3,4-dihydroxyphenylglycol, p-coumaric acid, and vanillin. In this way, the best option for recovery is hydroxytyrosol.

Regarding the energy indicator, since there is a possibility to obtain hydroxytyrosol and the tyrosol from other phenols, their indicator shows higher values with respect to other phenols.

In the view of the above results, hydroxytyrosol is the best option for recuperation but the literature suggests considering both hydroxytyrosol and tyrosol.

### *4.3. Leaves and Branches.*

In the case of olive leaves and branches, the calculation procedure is the same as in the previous case (see Table 6.9 for the properties of the raw material). The main difference is that the composition of olive leaves is given on a dry basis. The amount of water is around 49.7% based on the literature and that is the value assumed for the residue (Lama-Muñoz et al., 2020).

***Table 6.9.*** Results of indicators applied in the main phenols of olive leaves and branches.

| | Amounts % (dry basis) | Amounts % | Cost ($/mg) | Mw (g/mol) | $\eta_{profit}$ | $\eta_{energy}$ | Standardization of $\eta_{profit}$ |
|---|---|---|---|---|---|---|---|
| *Oleuropein* | 11.5 | 5.78 | 18.5 | 540.51[79] | $1.36 \cdot 10^{8}$ | 1 | 1.00 |
| *Luteolin-7-glucoside* | 0.319 | 0.16 | 40.47 | 448.38[80] | $8.28 \cdot 10^{6}$ | 1 | 0.06 |
| *Apigenin-7-glucoside* | 0.134 | 0.07 | 31.4 | 432.38[81] | $2.70 \cdot 10^{6}$ | 1 | 0.02 |
| *Verbascoside* | 0.086 | 0.04 | 31.45 | 624.59[82] | $1.73 \cdot 10^{6}$ | 1 | 0.01 |
| *Quercetin* | 0.026 | 0.01 | 0.0051 | 302.24[83] | 8.49 | 1 | 0.00 |

In this case, it does not make sense to compute the energy indicator because all phenols are found in the waste. As a result, the compound selected for the extraction in olive leaves is oleuropein. In this case, only one compound is selected because it is the major compound in leaves and generates the larger economic potential indicator by comparison.

*4.4 Process Design: Selection of Techniques to Recover Phenols.*

The result of the optimization of the superstructure is presented in Figure 6.4. The use of membrane module is selected to recover phenols from alperujo, while for processing olive leaves and branches, the adsorption technique is one of the choices.

From the economic point of view, the recovery of phenols from alperujo should be done using the membrane module. The main reason behind this is the high cost of the resin employed to separate and recover hydroxytyrosol and tyrosol separately. It should be noted that in this case of using the membrane separation, the product generated is a mix of phenols composed mainly of hydroxytyrosol and tyrosol, but it is cheaper compared to the use of adsorption and the production of both separately does not compensate for the additional cost. The mix of phenols obtained through this process is around 62% of hydroxytyrosol, 26.7% of tyrosol, and the rest of soluble compounds like other phenols or carbohydrate-soluble. Nowadays, this type of mix of phenols has wide use in different sectors such as pharmaceuticals, food products, and cosmetics, among others.

In the case of olive leaves and branches, it is more profitable to use adsorption for the recovery of phenols. Since the phenol recovered is different from that of alperujo, the type of resin employed in the

process must also be different, resulting in a cheaper cost. The adsorption technique allows the production of oleuropein with 85.5% purity. The quantity of phenols per month is shown in Figure 6.5. Note that the production of olives lasts 4 months, which results in the production of alperujo from processing the waste, while the rest of the year, the leaves and branches are processed to obtain the oleuropein.

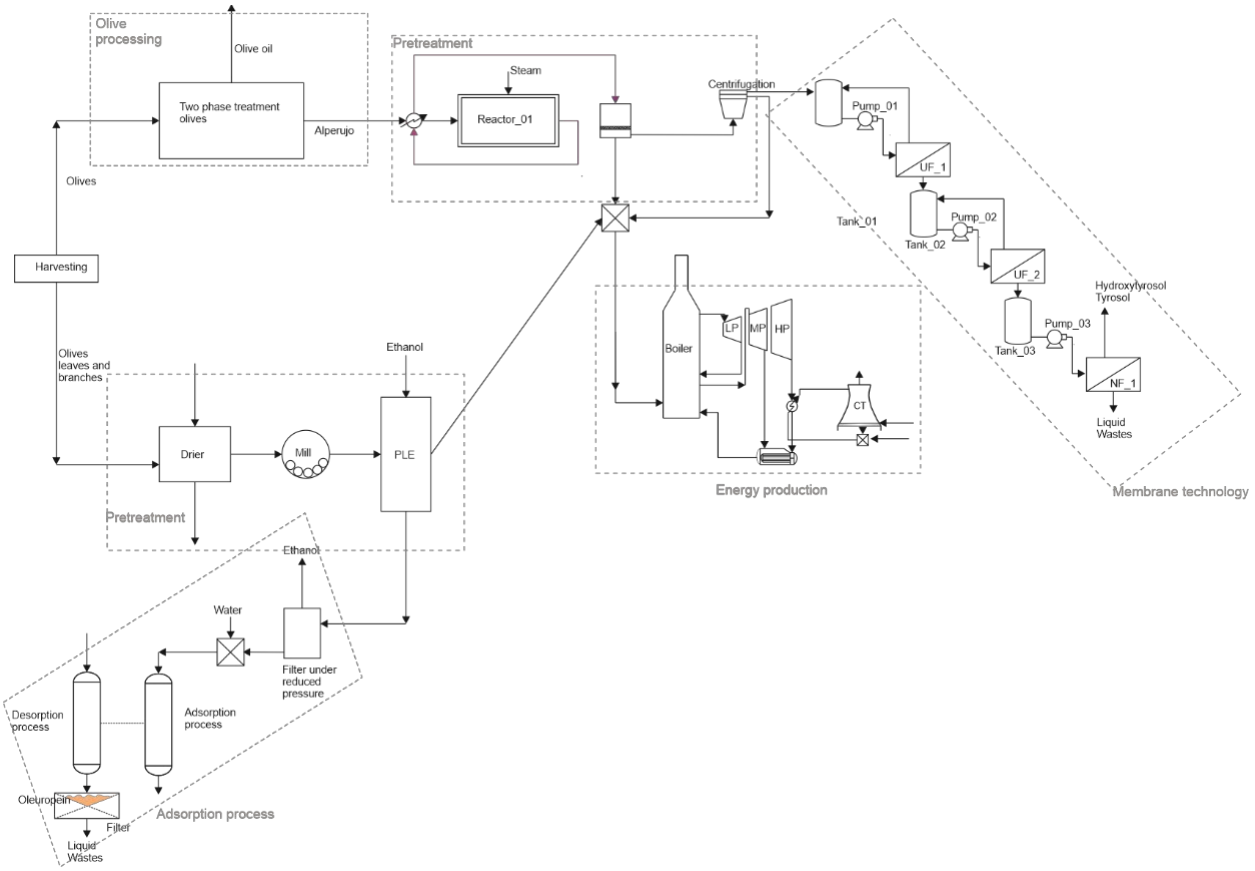


***Figure 6.4.*** Optimal flowsheet for the processing of olive's waste. Solution of the superstructure optimization.

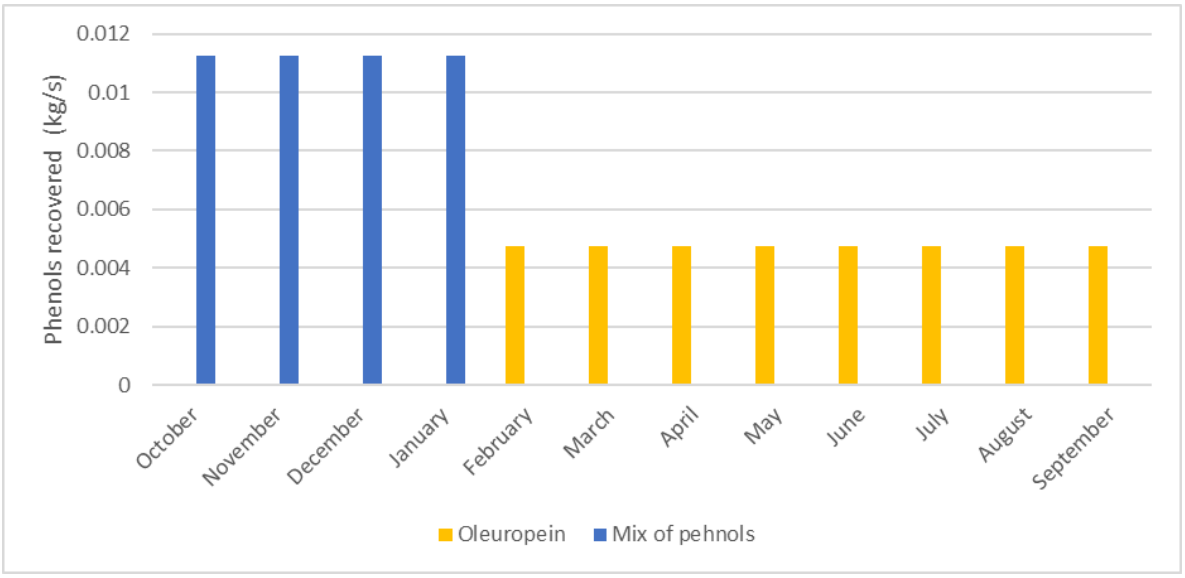


***Figure 6.5.*** Summary of the products obtained over a year of operation from alperujo and the leaves and branches.

*4.5. Economic Evaluation.*

Using the correlations developed for each one of the units as a function of their size, the cost of each unit is computed. The investment in units adds up to 18.22 M€. Table 6.10 shows the detail of the processing lines for alperujo and the leaves and branches. The total investment cost of the plant is around 110.23 M€.

***Table 6.10.*** Investment cost of units of alperujo and olive leaves and branches.

| | Treatments | | Investment cost (M€) |
|---|---|---|---|
| ALPERUJO | Pretreatment | | 0.524 |
| | Membrane Technology | | 0.597 |
| | | UF 1 | 0.306 |
| | | UF 2 | 0.276 |
| | | NF 1 | 0.014 |
| | Power Technology | | 9.919 |
| | | Turbine | 1.75 |
| | | Boiler | 7.93 |
| LEAVES AND BRANCHES | Dryer | | 0.01275 |
| | Mill | | 0.1455 |
| | Filter Under pressure | | 0.089 |
| | PLE | | 0.039 |
| | Resin Adsorption | | 6.319 |

As shown in Table 6.10, the share of the alperujo pretreatment used for the separation of the liquid and solid phases represents 46.74%, while the rest of the investment cost corresponds to the membrane module technology. In the case of olive leaves and branches, only around 3% correspond to the investment in the pretreatment. The investment costs for the turbine and the boiler are around 1.75 and 7.93 M€,

respectively. Note that the power plant represents more than half the investment in units. Note that because the larger solid production comes from the alperujo, there is a need to design the power island based on that production capacity.

The operation and maintenance costs are described in the Solution Procedure section. Typically, this methodology considers the cost of utilities like electricity and steam as variable costs. However, in this case, it has not been considered due to the fact that the facility has the capacity to generate them. Two alternative solutions are presented, whether the raw materials are received at a zero cost or if they are

purchased. In the latter case, prices of €249 per ton of alperujo84 and €6 per ton of olives and branches are considered. Figure 6.6a shows the first alternative, and Figure 6.6b shows the second one. The operation and maintenance costs without raw materials adds up to 33.75 M€/yr, while in the case where raw materials are considered, the costs reach a value of around 53.54 M€/yr. The cost increases by 61% in the case the raw materials do not belong to the facility. As shown in Figure 6.6a, the cost of raw materials reaches 37% of the operation and maintenance costs followed by capital changes and maintenance costs. In Figure 6.6b, costs have the same order, the capital changes being more expensive followed by maintenance and local tax costs.

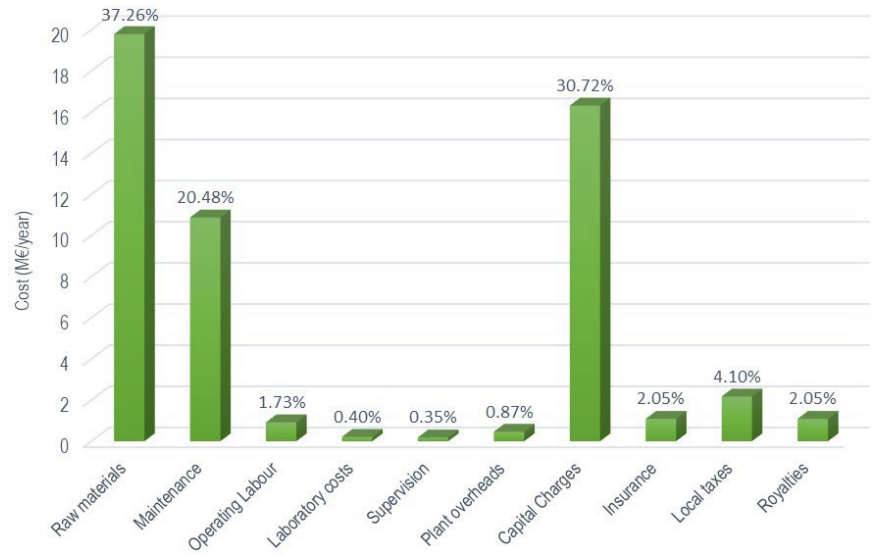


a

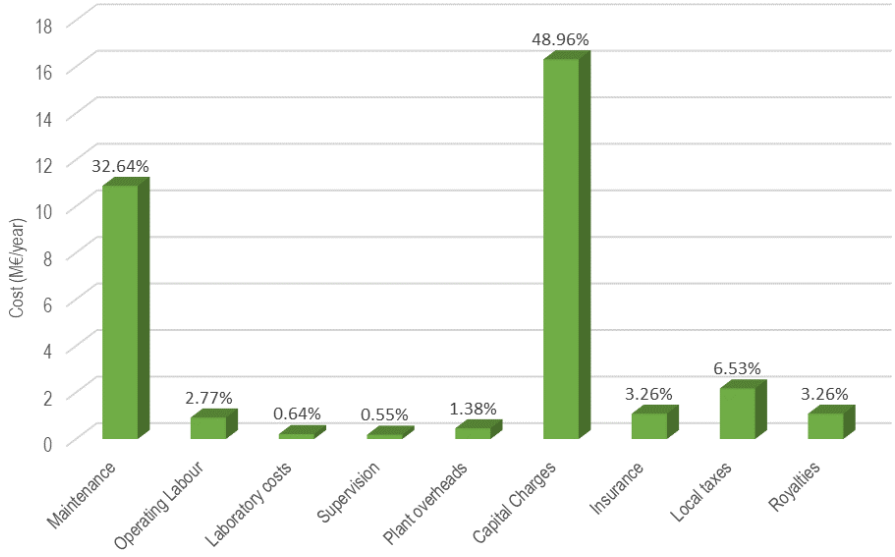


b

***Figure 6.6.*** Total operation and maintenance costs: (a) considering raw materials and (b) not considering raw materials.

Benefits from phenols correspond to around 104.7 M€/yr. Using eq 26, we compute profit, considering benefits from phenols, annualized investment cost, and the operation and maintenance cost defined in Figure 6.6. In the case of purchasing the raw materials, the profit reaches 14.5 M€/yr, while in the other case, the profit achieved is around 34.3 M €/yr. The return on investment in the case of raw materials accounted is around 16.02%, while in the case of raw materials not accounted, it is approximately 48.61%.

### *4.6. Energy Evaluation.*

Solid wastes are used to generate electric energy and thermal energy. Thermal and electrical energy requirements annually by the part of the facility to recover phenols from alperujo is around 140 kW on a monthly basis, of which 92.6% corresponding to thermal energy. While in the part of recovery, oleuropein from olive leaves and branches achieves 60 kW monthly, 95% corresponding to thermal energy. To better understand the operation of the facility, the monthly thermal and electrical energy requirements of alperujo and olive leaves and branches are shown in Figure 6.7.

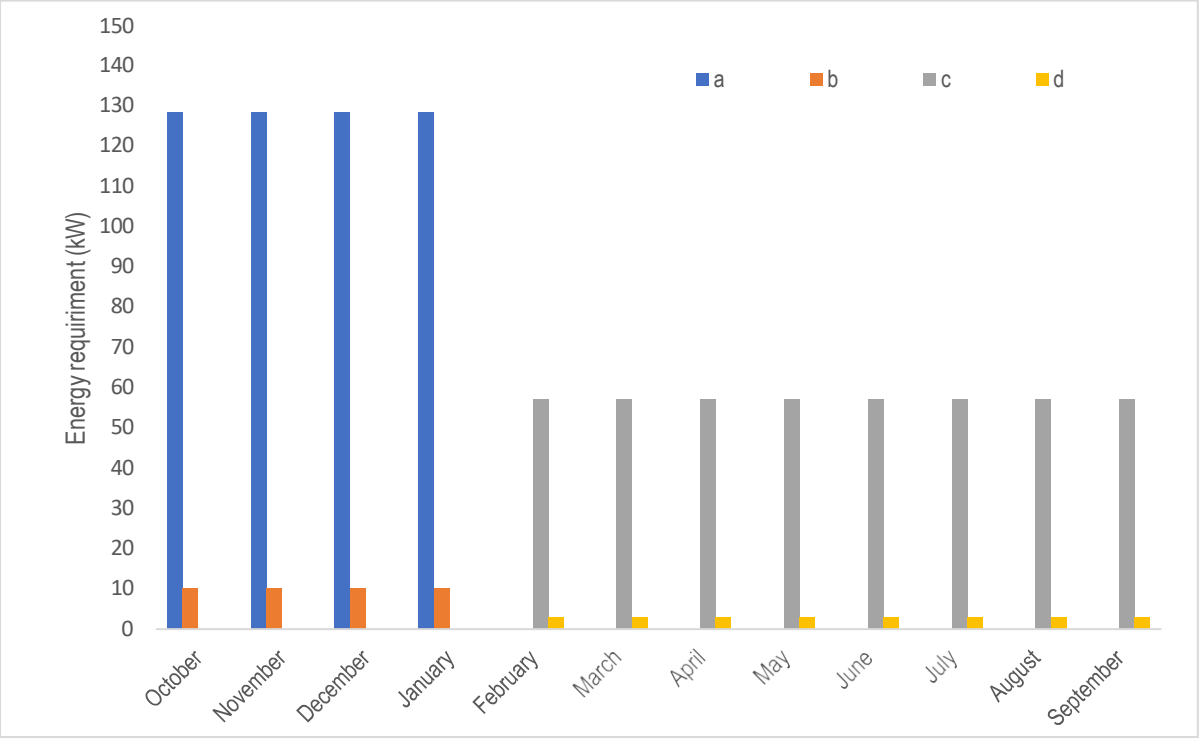


***Figure 6.7.*** Monthly energy requirements. (a) Thermal energy required by alperujo, (b) electric energy required by alperujo, (c) thermal energy required by olive leaves and branches, and (d) electric energy required by olive leaves and branches.

Once the thermal energy requirement is fulfilled, the rest of the solid wastes are transformed into electric energy by the power plant. Results show that from the alperujo residues, 12.95 MW can be produced, while from the leaves and branches, the power can only be 312 kW. In view of these results, the power plant may only operate for 4 months because, the rest of the months, the power island of the facility should operate at such a low load that it will cause a problem for the units.

The electric energy consumed by the units corresponds to 10.2 kW during the alperujo treatment (4 months) and 3 kW during the leaf and branch processing (8 months), a total of 46,711 kWh (see Figure 6.8). Since the power plant capacity installed in the facility is around 12.95 MW and 312 kW for each of the operating periods, it is not necessary to buy this type of utility. In this way, the facility, or the part of recovery phenols of the facility, is capable of supplying on its own.

In case the recovery of phenols becomes part of the olive oil generation facility, the energy consumption of the main section producing the olive oil should also be analyzed. Considering the production capacity of this facility and data from the literature, the annual energy consumed by the olive oil production is around 3920 MWh.85 Therefore, the power plant using the residue from the alperujo, with a total energy production of 37 296 MWh, would be able to supply energy at this part of the facility.

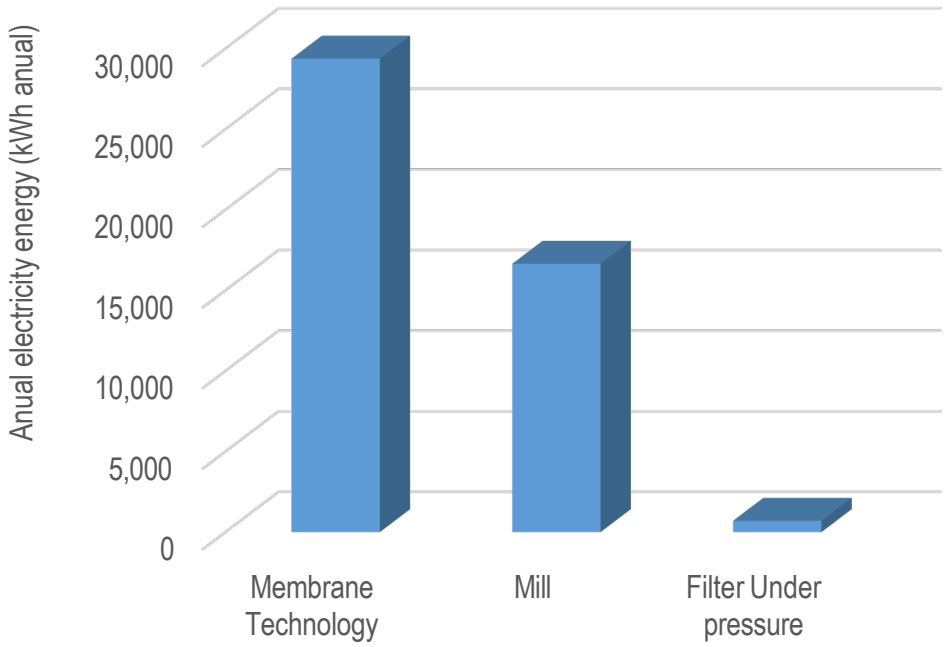


***Figure 6.8.*** Annual electric energy consumption by techniques.

## 5. Conclusions

In this work, a systematic methodology has been developed for the screening and designing of multiproduct facilities associated with the WEF nexus. It combines hybrid heuristicbased, metric-based, and superstructure optimization approaches to identify the promising high added-value products so as to put together a superstructure for the design of an integrated facility that makes the most of waste and valuable products toward a sustainable biorefinery. Novel indicators have been developed to identify value-added products. The methodology has been applied to the waste from olive trees, olive leaves and branches, and alperujo from olive oil production. Value-added products of these wastes include phenols that can be used in the pharmacy, cosmetic, or food industries.

The results show that the optimal portfolio of products corresponds to the recovery of phenols, hydroxytyrosol, and tyrosol from alperujo and oleuropein from olive leaves and branches based on the economic indicator, which is the largest. After the selection of the products to be obtained, a superstructure is formulated and optimized. As a result of the optimization, pretreatment and membrane module technique should be used from alperujo to recover a mix of phenols, while in the case of olive leaves and branches, a dryer followed by a mill, a pressurized liquid extractor, a filter under pressure, and resin adsorption are used. The final economic evaluation is carried out, wherein the profit comes to 14.5 M€ annually in case this process is integrated into an olive oil production facility and 34.3 M€ annually if the raw materials have to be purchased. Regarding energy, solid waste is used to generate the utilities employed in the recovery process. A power plant is integrated into the facility where the power is around 12.95 MW, which is sufficient for the recovery process.

## 6. List of acronyms and abbreviations.

$Cost_{boiler}$: Cost of boiler (€)
$(Cost_{invest})_{ads}$: Inversion cost of adsorption (M€)
$(Cost_{invest})_{dryer}$: Inversion cost of dryer process (M€)
$(Cost_{invest})_{FUP}$: Inversion cost of Filter under pressure (M€)
$(Cost_{invest})_{mill}$: Inversion cost of mill (M€)
$(Cost_{invest})_{PLE}$: Inversion cost of pressurized liquid extractor (M€)
$(Cost_{invest})_{PT}$: Inversion cost of pre-treatment (M€)

$(Cost_{invest})_{RA}$: Inversion cost of resin adsorption (M€)

$(Cost_{OM})_{dryer}$: Operation and maintenance cost of dryer (€)

$(Cost_{OM})_{Mill}$: Operation and maintenance cost of mill (M€)

$(Cost_{OM})_{PT}$: Operation and maintenance cost of pre-treatment (M€)

$(Cost_{OM})_{RA}$: Operation and maintenance cost of resin adsorption (M€)

$Cost_{turbine}$: Cost of turbine (€)

$Cp_{ash}$: Heat capacity of ash (kJ/kg·K)

$Cp_{carbohydrates}$: Heat capacity of carbohydrates (kJ/kg·K)

$Cp_{da}$: Heat capacity of dry air (kJ/kg·K)

$Cp_{ds}$: Heat capacity of dry leaves (kJ/kg·K)

$Cp_{fat}$: Heat capacity of fat (kJ/kg·K)

$Cp_{fiber}$: Heat capacity of fiber (kJ/kg·K)

$Cp_{protein}$: Heat capacity of protein (kJ/kg·K)

$D_v$: Diameter (m)

$D_{vessel}$: Diameter (m)

e: Thickness (m)

E: Ethanol concentration

E*: Ethanol concentration (-1;1)

G: Dry air flow (kg dry air/s)

$H_{Gi}$: Enthalpy of air under "i" conditions (kJ/kg)

$H_{Li}$: Enthalpy of solid under "i" conditions (kJ/kg)

L: Dry solid flow (kg dry leaves/s)

$L_v$: Tank length (m)

$L_{vessel}$: Tank length (m)

MC: Moisture content (%)

MC*: Moisture content (-1:1)

$m_{leaves}$: mass flow of leaves (kg/s)

$m_{resin}$: mass of resin (kg)

$m_{steel}$: mass of steel (kg)

$m_{steam}$: mass flow of steam (kg/s)

$m_{treat}$: treated mass (kg/year)

$m_t$: treated mass ($m^3$/year)

$m_{OC}$: Oleuropein content (kg oleuropein/kg dry leaves)

$m_{OA}$: mass of oleuropein adsorbed (kg soluble/kg dry leaves)

$m_{olives}$: mass flow of olives (kg/h)

$m_{waterremoved}$: mass flow of water removed (kg/h)

$n_{cycle}$: number of cycles.

T: temperature (ºC)

T*: temperature (ºC)

$t_{extraction}$: extraction time (s)

$u_t$: terminal velocity (m/s)

V: steam volume ($m^3$).

$V_{leaves}$: extraction vessel capacity ($m^3$).

$V_{resin}$: Volume of resin ($m^3$)

$V_{vessel}$: Volume of vessel ($m^3$)

$W_{NE}$: net electric energy power output (MW)

X: humidity of leaves (kg water/kg dry leaves)

$x_i^w$ : mass fraction of i component.

Y: Specific moisture (kg water/kg dry air)

δ: conversion euro dolar (0.85$/€)

$\rho_{leaves}$: Leaves density ($kg/m^3$)

$\rho_l$: Liquid density ($kg/m^3$)

$\rho_v$: Vapor density ($kg/m^3$)

$\rho_{steel}$ Steel density ($kg/m^3$)

## 7. References

Aehle, E., Grandic, S., Ralainirina, R., Baltora-Rosset, S., Mesnard, F., Prouillet, C., Mazière, J.C., Fliniaux, M.A., 2004. Development and Evaluation of an Enriched Natural Antioxidant Preparation Obtained from Aqueous Spinach (Spinacia oleracea) Extracts by an Adsorption Procedure. Food Chem. 86, 579–585. https://doi.org/10.1016/j.foodchem.2003.10.006

Alibaba, 2019a. Drying equipment. URL https://www.alibaba.com/product-detail/Food-industry-mesh-belt-dryer_62048155440.html?spm=a2700.galleryofferlist.normal_offer.d_title.70471248pYfXNM&s=p

Alibaba, 2019b. Hydroxytyrosol Price. URL https://spanish.alibaba.com/product-detail/natural-olive-leaf-extract-health-care-hydroxytyrosol-powder-62018947344.html?spm=a2700.galleryofferlist.0.0.11bf4d55p5mwjd&s=p

Alibaba, 2019c. Tyrosol Price. URL https://spanish.alibaba.com/product-detail/natural-high-quality-tyrosol-4-hydroxyphenethyl-alcohol-hot-selling-with-factory-price-cas-no-501-94-0-60723337558.html?spm=a2700.galleryofferlist.0.0.515a3098DH7xiA

Alibaba, 2019d. Mix of phenols price. URL https://spanish.alibaba.com/product-detail/organic-oleuropein-40-98-with-best-price-olive-leaf-extract-oleuropein-62554226616.html?spm=a2700.galleryofferlist.normal_offer.d_title.4010141cv1Oaj7

Alibaba, 2019e. Oleuropein Price. URL https://spanish.alibaba.com/product-detail/factory-price-bulk-oleuropein-98-olive-leaf-extract-in-bulk-60830276672.html?spm=a2700.galleryofferlist.0.0.35ab3839EmqQt2&s=p

Alibaba, 2019f. Oleuropein Price with impurities. URL https://spanish.alibaba.com/product-detail/quality-50-oleuropein-powder-olive-leaf-extract-1600068466360.html?spm=a2700.galleryofferlist.normal_offer.d_title.50e8e6128QLgus&s=p

Almena, A., Martín, M., 2016. Technoeconomic Analysis of the Production of Epichlorohydrin from Glycerol. Ind. Eng. Chem. Res. 55, 3226–3238. https://doi.org/10.1021/acs.iecr.5b02555

Bajpai, P., 2018. Biermann's Handbook of Pulp and Paper, 3rd ed. Elsevier.

Barba, F.J., Zhu, Z., Koubaa, M., Sant'Ana, A.S., Orlien, V., 2016. Green alternative methods for the extraction of antioxidant bioactive compounds from winery wastes and by-products: A review. Trends Food Sci. Technol. 49, 96–109. https://doi.org/10.1016/j.tifs.2016.01.006

Bayçin, D., Altiok, E., Ulku, S., Bayraktar, O., 2007. Adsorption of Olive Leaf ( Olea europaea L.) Antioxidants on Silk Fibroin. J. Agric. Food Chem. 55, 1227–36. https://doi.org/10.1021/jf062829o

Bazzarelli, F., Piacentini, E., Poerio, T., Mazzei, R., Cassano, A., Giorno, L., 2016. Advances in membrane operations for water purification and biophenols recovery/valorization from OMWWs. J. Membr. Sci. 497, 402–409.

Biggs, E.M., Bruce, E., Boruff, B., Duncan, J.M.A., Horsley, J., Pauli, N., McNeill, K., Neef, A., Van Ogtrop, F., Curnow, J., Haworth, B., Duce, S., Imanari, Y., 2015. Sustainable development and the water–energy–food nexus: A perspective on livelihoods. Environ. Sci. Policy. 54, 389–397. https://doi.org/10.1016/j.envsci.2015.08.002

Borghi, A.D., Moreschi, L., Gallo, M., 2020. Circular economy approach to reduce water–energy–food nexus. Curr Opin Environ Sci Health 13, 23–28. https://doi.org/10.1016/j.coesh.2019.10.002

Boskou, D. (Ed.), 2015. Olive and Olive Oil Bioactive Constituents, AOCS Press. ed.

Campoy, M., Gómez-Barea, A., Ollero, P., Nilsson, S., 2014. Gasification of wastes in a pilot fluidized bed gasifier. FPT, Fuel Processing Technology 121, 63–69. https://doi.org/10.1016/j.fuproc.2013.12.019

Canabarro, N.I., Mazutti, M.A., do Carmo Ferreira, M., 2019. Drying of olive (Olea europaea L.) leaves on a conveyor belt for supercritical extraction of bioactive compounds: Mathematical modeling of drying/extraction operations and analysis of extracts. Ind. Crop. Prod. 136, 140–151. https://doi.org/10.1016/j.indcrop.2019.05.004

Capello, C., Fischer, U., Hungerbuhler, K., 2007. What is a Green Solvent? A Comprehensive Framework for the Environmental Assessment of Solvents. Green Chem. 9. https://doi.org/10.1039/b617536h

Caputo, A.C., Palumbo, M., Pelagagge, P.M., Scacchia, F., 2005. Economics of biomass energy utilization in combustion and gasification plants: effects of logistic variables. Biomass Bioenergy 28, 35–51. https://doi.org/10.1016/j.biombioe.2004.04.009

Cassano, A., Conidi, C., Giorno, L., Drioli, E., 2013. Fractionation of olive mill wastewaters by membrane separation techniques. J. Hazard. Mater. 248–249, 185–193. https://doi.org/10.1016/j.jhazmat.2013.01.006

Castro, M., Priego-Capote, F., 2010. Extraction of Oleuropein and Related Phenols from Olive Leaves and Branches, in: Olives and Olive Oil in Health and Disease Prevention. pp. 259–273. https://doi.org/10.1016/B978-0-12-374420-3.00028-0

Christoforou, E., Fokaides, P.A., 2016. A review of olive mill solid wastes to energy utilization techniques. Waste Manage. 49, 346–363. https://doi.org/10.1016/j.wasman.2016.01.012

Criado, A., Martín, M., 2020. Integrated Multiproduct Facility for the Production of Chemicals, Food, and Utilities from Oranges. Ind. Eng. Chem. Res. 59, 7722–7731. https://doi.org/10.1021/acs.iecr.0c00476

El-Halwagi, M.M., 2017. Sustainable Design Through Process Integration Fundamentals and Applications to Industrial Pollution Prevention, Resource Conservation, and Profitability Enhancement. Butterworth-Heinemann. https://doi.org/10.1016/B978-0-12-809823-3.00026-6

Erbay, Z., Icier, F., 2009. Optimization of Drying of Olive Leaves in a Pilot-Scale Heat Pump Dryer. Dry. Technol. 27, 416–427. https://doi.org/10.1080/07373930802683021

EUROSTAT, 2019. Olive by production. URL https://ec.europa.eu/eurostat/databrowser/view/tag00122/default/table?lang=en

FAO, 2019. Organización de las naciones unidas para la alimentación y la agricultura. URL http://www.fao.org/faostat/es/?#data/QC

Fernández-Hernández, A., Roig, A., Serramiá, N., Civantos, C.G.-O., Sánchez-Monedero, M.A., 2014. Application of compost of two-phase olive mill waste on olive grove: Effects on soil, olive fruit and olive oil quality. J. Waste Manag. 34, 1139–1147. https://doi.org/10.1016/j.wasman.2014.03.027

Fernández-Prior, M.Á., Fatuarte, J.C., Oria, A.B., Viera-Alcaide, I., Fernández-Bolaños, J., Rodríguez-Gutiérrez, G., 2020. New Liquid Source of Antioxidant Phenolic Compounds in the Olive Oil Industry: Alperujo Water. Foods 9. https://doi.org/10.3390/foods9070962

Galán, G., Martín, M., Grossmann, I., 2019. Optimal Production of Renewable ETBE From Lignocellulosic Raw Materials, in: Muñoz, S.G., Laird, C.D., Realff, M.J. (Eds.), Computer Aided Chemical Engineering. Elsevier, pp. 391–396. https://doi.org/10.1016/B978-0-12-818597-1.50062-X

Galanakis, C.M. (Ed.), 2017. Olive Mill Waste. Recent Advances for the sustainable development of olive oil industry. Academic Press.

Junta de Andalucía, 2015. Evaluacion de la producction y usos de los subproductos de las agroindustrias del olivar en Andalucía. URL https://www.juntadeandalucia.es/agriculturaypesca/observatorio/servlet/FrontController?action=RecordContent&table=11031&element=1585171&

Junta de Andalucía, 2010. Potencial energético de los subproductos de la industria olivarera en Andalucía. URL https://www.juntadeandalucia.es/export/drupaljda/Potencial%20energ%C3%A9tico.pdf

Khemakhem, I., Gargouri, O.D., Dhouib, A., Ayadi, M.A., Bouaziz, M., 2017. Oleuropein rich extract from olive leaves by combining microfiltration, ultrafiltration and nanofiltration. Sep. Purif. Technol. 172, 310–317. https://doi.org/10.1016/j.seppur.2016.08.003

Lama-Muñoz, A., Contreras, M. del M., Espínola, F., Moya, M., Romero, I., Castro, E., 2020. Content of phenolic compounds and mannitol in olive leaves extracts from six Spanish cultivars: Extraction with the Soxhlet method and pressurized liquids. Food Chem. 320, 126626. https://doi.org/10.1016/j.foodchem.2020.126626

Lama-Muñoz, A., del Mar Contreras, M., Espínola, F., Moya, M., de Torres, A., Romero, I., Castro, E., 2019a. Extraction of oleuropein and luteolin-7-O-glucoside from olive leaves: Optimization of technique and operating conditions. Food Chem. 293, 161–168. https://doi.org/10.1016/j.foodchem.2019.04.075

Lama-Muñoz, A., Rubio-Senent, F., Bermúdez-Oria, A., Fernández-Bolaños, J., Prior, Á.F., Rodríguez-Gutiérrez, G., 2019b. The use of industrial thermal techniques to improve the bioactive compounds extraction and the olive oil solid waste utilization. Innov. Food. Sci. Emerg. Technol. 55, 11–17. https://doi.org/10.1016/j.ifset.2019.05.009

Leite, P., Salgado, J.M., Venâncio, A., Domínguez, J.M., Belo, I., 2016. Ultrasounds pretreatment of olive pomace to improve xylanase and cellulase production by solid-state fermentation. Bioresour. Technol. 214, 737–746. https://doi.org/10.1016/j.biortech.2016.05.028

Li, C., Zheng, Y., Wang, X., Feng, S., Di, D., 2011. Simultaneous separation and purification of flavonoids and oleuropein from Olea europaea L. (olive) leaves using macroporous resin. J. Sci. Food Agric. 91, 2826–34. https://doi.org/10.1002/jsfa.4528

Lookchem, 2019. Cost of Amberlite XAD7 High purity. URL https://www.lookchem.com/casno37380-43-1.html

López-Díaz, D.C., Lira-Barragán, L.F., Rubio-Castro, E., Serna-González, M., El-Halwagi, M.M., Ponce-Ortega, J.M., 2018. Optimization of biofuels production via a water–energy–food nexus framework. Clean Technol. Envir. 20, 1443–1466. https://doi.org/10.1007/s10098-017-1395-0

Made-in-China, 2019. Cost of crushing machine [WWW Document]. URL https://granulatormachine.en.made-in-china.com/product/HstJyThvZZWa/China-Wood-Tree-Leaves-Branch-Crushing-Machine-Suitable-for-Biomass-Power-Plant.html

Martín, L., Martín, M., 2013. Optimal year-round operation of a concentrated solar energy plant in the south of Europe. Appl. Therm. Eng. 59, 627–633. https://doi.org/10.1016/j.applthermaleng.2013.06.031

Martín, M., Grossmann, I.E., 2011. Energy optimization of bioethanol production via gasification of switchgrass. AIChE Journal 57, 3408–3428. https://doi.org/10.1002/aic.12544

Martínez-Gomez, J., Peña-Lamas, J., Martín, M., Ponce-Ortega, J.M., 2017. A multi-objective optimization approach for the selection of working fluids of geothermal facilities: Economic, environmental and social aspects. J. Environ. Manage. 203, 962—972. https://doi.org/10.1016/j.jenvman.2017.07.001

Matches, 2020. Cost of filter under pressure. Matches. URL https://www.matche.com/equipcost/Vessel.html (accessed 10.26.20).

Merck, 2019a. 3,4-Dihydroxyphenylglycol Price [WWW Document]. URL https://www.sigmaaldrich.com/catalog/product/sigma/d9753?lang=en&region=US

Merck, 2019b. Hydroxytyrosol Price. URL https://www.sigmaaldrich.com/catalog/product/supelco/phl80152?lang=en&region=US
Merck, 2019c. Tyrosol Price. URL https://www.sigmaaldrich.com/catalog/product/supelco/phl80166?lang=en&region=US
Merck, 2019d. Vanillin Price. URL https://www.sigmaaldrich.com/catalog/product/sial/30304?lang=en&region=US
Merck, 2019e. p-Coumaric acid Price [WWW Document]. URL https://www.sigmaaldrich.com/catalog/product/sial/03200595?lang=en&region=US
Mudimu, O., Peters, M., Brauner, F., Braun, G., 2012. Overview of Membrane Processes for the Recovery of Polyphenols from Olive Mill Wastewater. Am. J. Environ. Sci. 8, 195–201. https://doi.org/10.3844/ajessp.2012.195.201
Ochando-Pulido, J.M., Corpas-Martínez, J.R., Martinez-Ferez, A., 2018. About two-phase olive oil washing wastewater simultaneous phenols recovery and treatment by nanofiltration. PSEP 114, 159–168. https://doi.org/10.1016/j.psep.2017.12.005
Ochando-Pulido, J.M., Martinez-Ferez, A., 2017. On the Purification of Agro-Industrial Wastewater by Membrane Technologies: The Case of Olive Mill Effluents, in: Yonar, T. (Ed.), Desalination. IntechOpen, Rijeka. https://doi.org/10.5772/intechopen.68401
Osorio-Tobón, J.F., Carvalho, P.I.N., Rostagno, M.A., Petenate, A.J., Meireles, M.A.A., 2014. Extraction of curcuminoids from deflavored turmeric (Curcuma longa L.) using pressurized liquids: Process integration and economic evaluation. J. Supercrit. Fluid. 95, 167–174. https://doi.org/10.1016/j.supflu.2014.08.012
Paze, I., Lozano-Sánchez, J., Borrás, I., Nuñez, H., Robert, P., Segura Carretero, A., 2019. Obtaining an Extract Rich in Phenolic Compounds from Olive Pomace by Pressurized Liquid Extraction. Molecules 24, 3108. https://doi.org/10.3390/molecules24173108
Pérez-Uresti, S.I., Martín, M., Jiménez-Gutiérrez, A., 2019. Estimation of renewable-based steam costs. Appl. Energy 250, 1120–1131. https://doi.org/10.1016/j.apenergy.2019.04.189
Petridis, L., Smith, J.C., 2016. Conformations of Low-Molecular-Weight Lignin Polymers in Water. ChemSusChem 9, 289—295. https://doi.org/10.1002/cssc.201501350
Pham, V., El-Halwagi, M., 2012. Process synthesis and optimization of biorefinery configurations. AIChE Journal 58, 1212–1221. https://doi.org/10.1002/aic.12640
Rodríguez-Gutiérrez, G., Lama-Muñoz, A., Ruiz-Méndez, M.V., Rubio-Senent, F., Fernández-Bolaños, J., 2012. New Olive-Pomace Oil Improved by Hydrothermal Pre-Treatments, in: Dimitrios, B. (Ed.), Olive Oil. IntechOpen, Rijeka. https://doi.org/10.5772/28742
Romero-García, J.M., Lama-Muñoz, A., Rodríguez-Gutiérrez, G., Moya, M., Ruiz, E., Fernández-Bolaños, J., Castro, E., 2016. Obtaining sugars and natural antioxidants from olive leaves by steam-explosion. Food Chem. 210, 457–465. https://doi.org/10.1016/j.foodchem.2016.05.003
Romero-Quiles, A.S., 2001. Diagnóstico y estudio de los diferentes sistemas de gestión de alpechines, orujos y alperujos en las almazaras: Características de los residuos. CSIC -IRNAS.
Roselló-Soto, E., Koubaa, M., Moubarik, A., Lopes, R.P., Saraiva, J.A., Boussetta, N., Grimi, N., Barba, F.J., 2015. Emerging opportunities for the effective valorization of wastes and by-products generated during olive oil production process: Non-conventional methods for the recovery of high-added value compounds. Trends Food Sci. Technol. 45, 296–310. https://doi.org/10.1016/j.tifs.2015.07.003
Rubio-Senent, F., Fernández-Bolaños, J., García-Borrego, A., Lama-Muñoz, A., Rodríguez-Gutiérrez, G., 2017. Influence of pH on the antioxidant phenols solubilised from hydrothermally treated olive oil by-product (alperujo). Food Chem. 219, 339–345. https://doi.org/10.1016/j.foodchem.2016.09.141
Şahin, S., Bilgin, M., 2017. Selective adsorption of oleuropein from olive (Olea europaea) leaf extract using macroporous resin. Chemical Engineering Communications 204, 1391–1400. https://doi.org/10.1080/00986445.2017.1365062
SCP/RAC, 2019. Reginonal Activity Centre for sustainable consumption and production. Nº 11. Pollution prevention case studies: Integral treatment of the solid and liquid waste produced during the olive oil extraction process. URL http://www.cprac.org/es/mediateca/medclean
Serrano, A., Fermoso, F.G., Alonso-Fariñas, B., Rodríguez-Gutierrez, G., Fernandez-Bolaños, J., Borja, R., 2017a. Olive mill solid waste biorefinery: High-temperature thermal pre-treatment for phenol

recovery and biomethanization. Journal of Cleaner Production 148, 314–323. https://doi.org/10.1016/j.jclepro.2017.01.152
Serrano, A., Fermoso, F.G., Rodríguez-Gutierrez, G., Fernandez-Bolaños, J., Borja, R., 2017b. Biomethanization of olive mill solid waste after phenols recovery through low-temperature thermal pre-treatment. J. Waste Manag. 61, 229–235. https://doi.org/10.1016/j.wasman.2016.12.033
Serrano, A., G. Fermoso, F., Alonso-Fariñas, B., Rodríguez-Gutiérrez, G., Fernandez-Bolanos, J., Borja, R., 2017c. Phenols recovery after steam explosion of Olive Mill Solid Waste and its influence on a subsequent biomethanization process. Bioresour. Technol. 243. https://doi.org/10.1016/j.biortech.2017.06.093
Shahidi, F., Kiritsakis, A. (Eds.), 2017. Olives and Olive Oil as Functional Foods: Bioactivity, Chemistry and Processing, First Edition. ed. Wiley.
Singh, R.P., 2006. Heating and cooling processes for foods, in: Handbook of Food Engineering, Second Edition. pp. 397–426.
Sinnott, R., Towler, G., 2016. Chemical Engineering Design:Principles, practice and economics of plant and process design., Chemical Engineering Series. Elsevier, Butterworth-Heinemann, Oxford.
Socaci, S., Fărcaş, A., Galanakis, C., 2019. Introduction in Functional Components for Membrane Separations. pp. 31–77. https://doi.org/10.1016/B978-0-12-815056-6.00002-4
Stoller, M., Pulido, J.M.O., Saco, O., 2015. Optimized design of Wastewater stream treatment processes by membrane technologies. pp. 211–236. https://doi.org/10.3303/CET1647066
Taifouris, M., Corazza, M.L., Martín, M., 2021. Integrated Design of Biorefineries Based on Spent Coffee Grounds. Ind. Eng. Chem. Res. 60, 494–506. https://doi.org/10.1021/acs.iecr.0c05246
Wadsworth, J.I., Segal, L., Timpa, J.D., 1973. Average Degree of Polymerization of Cellulose by GPC without Viscosity Measurements, in: Polymer Molecular Weight Methods, Advances in Chemistry. AMERICAN CHEMICAL SOCIETY, pp. 178–186. https://doi.org/10.1021/ba-1973-0125.ch016
Yoon, S., Choi, W., Park, J., Yang, J.-W., 1997. Selective adsorption of flavonoid compounds from the leaf extract of Ginkgo bilobaL. Biotechnol. Tech. 11, 553–556. https://doi.org/10.1023/A:1018434704902
Zhang, C., Chen, X., Li, Y., Ding, W., Fu, G., 2018. Water-energy-food nexus: Concepts, questions and methodologies. J. Clean. Prod 195, 625–639. https://doi.org/10.1016/j.jclepro.2018.05.194

# *Chapter 7*

# Conclusions

One of the main problems in the energy industry is greenhouse gases. For this reason, the first two works were carried out (chapters 3 and 4), whose main objective is the reduction of these gases through different techniques. Another problem is the consumption of water within the plants, which is why the third work (chapter 5) was carried out. Since pulverized coal thermal plants are being closed, it is necessary to study other sources of energy, such as waste, to replace this energy generation. Since many wastes have value-added products, a study was carried out on this subject (chapter 6). Considering research carried out and described throughout this doctoral thesis, the following conclusions can be drawn:

- The optimal selection of flue gas treatment technologies was carried out for a pulverized coal-fired power plant in Spain to determine the optimal operating train to reduce pollutant emissions. For a specific mix of coals, the following order of technologies was obtained for catalytic NOx removal, an electrostatic precipitator, and $SO_2$ removal by LSD.
- Based on the above results, the blending problem was evaluated, but since the most commonly used technology for $SO_2$ is LFSO, it is included in the problem parameters. After analyzing the obtained results, it was obtained that LFSO is a more flexible technology than LSD and allows the removal of a larger amount of $SO_2$. The blending coals selected are 25% imported coal and the rest crude coal tar. Imported coal is the preferred feedstock due to its composition, but if its cost were to increase by 4% or if there were a 12.5% reduction in the cost of LFSO, national coal would be selected.
- The second work that was carried out dealt with the gas treatment of an oxy-combustion plant with different proportions of oxygen and carbon dioxide. With this work, the optimized treatment chain was determined, generating a superstructure based on heuristic methods and mathematical optimization. The result obtained was the dry desulfurizer for sulfur dioxide removal and zeolite beds for carbon dioxide cleaning. Regarding the cost of treatment increases as the oxygen concentration decreases.
- A blending problem was also conducted for coal selection based on the composition and price of three types of coal. The relationship between sulfur content, price, and energy yield results in no coal blend being chosen because of the low cost of raw coal tar, despite the higher increased flue gas treatment.

- A mathematical optimization framework was developed to calculate the wet cooling tower geometry as well as water consumption rates for the sustainable design of the new energy system where different energy sources and thermodynamic cycles are employed. The research was based in Spain since it is a country very sensitive to water stress problems especially in the south of the country.
- Different correlations were developed for water consumption, cooling tower size, and cost as a function of humidity, temperature, and atmospheric pressure. These correlations allow estimating the water stress and help the energy transition to determine an appropriate location for new renewable energy plants. Bigger towers are needed for southeastern of Spain.
- A methodology for the systematic design of multi-product facilities has been developed. New indicators have been developed to identify value-added products. A case study has been developed and applied to olive oil production residues (olive pomace, olive leaves, and branches). After the selection of the products to be obtained, a superstructure was built for each residue, based on heuristic methods and mathematical optimization.
- The rates obtained indicate that the phenols to be recovered are as follows hydroxytyrosol, and tyrosol from alperujo and oleuropein from olive leaves and branches. The result of the optimization of the superstructure is pretreatment and membrane module technique for alperujo treatment, while a dryer followed by a mill, a pressurized liquid extractor, a filter under pressure, and resin adsorption should be used for olive leaves and branches. The facility has an integrated power plant with a capacity of 12.95 MW, enough to be self-sufficient.

# *Chapter 8*

## List of contributions

## 1. Other publications: journal papers

Martín-Hernández, E; *Guerras LS* and Martín M. (2020) Optimal biogas upgrading to biomethane. Journal of Cleaner production, 267: 122032. https://doi.org/10.1016/j.jclepro.2020.122032.

Tovar-Facio J, *Guerras LS*, Ponce-Ortega JM and Martín M. (2021) Sustainable Energy Transition Considering the Water–Energy Nexus: A Multiobjective Optimization Framework. ACS Sustainable Chemistry & Engineering, 9-10: 3768–3780. https://doi.org/10.1021/acssuschemeng.0c08694

## 2. Books chapters

Pérez-Uresti,SI, *Guerras LS*, Martín M, Jiménez-Gutierrez A. Use of Lingo for product Design. Martin M. (Ed.) Introduction to Software for Chemical Engineers, Second Edition. 2019. ISBN: 9781138324213

## 3. International Conference

*Guerras LS*, Taifouris M, Sengupta D, Corazza M, Martín M and El-Halwagi MM. Methodology for the design of multiproduct facilities: Case of the olive tree. Nov. 2020. 14th Mediterranean Congress of Chemical Engineering (MeCCE14)

*Guerras, LS* and Martín M. Optimal gas treatment and coal blending for reduced emissions in power plants. Nov: 10-15, 2019. AICHE 2019.

*Guerras, LS* and Martín M. Cooling tower design for the water-Energy nexus: Effect of weather conditions on water consumptions and tower sizing. Nov: 10-15, 2019. AICHE 2019.

Martín-Hernández, E, *Guerras LS* and Martín M. Superstructure Optimization Approach for the Optimization of Biogas Upgrading into Biomethane. Nov: 10-15, 2019. AICHE 2019.

# Optimal biogas upgrading to biomethane. Journal of Cleaner production

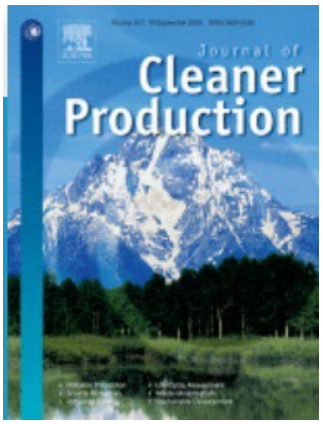


Authors: Edgar Martín-Hernández, ***Lidia S. Guerras*** and Mariano Martín

DOI: doi.org/10.1016/j.jclepro.2020.122032

# Sustainable Energy Transition Considering the Water–Energy Nexus: A Multiobjective Optimization Framework

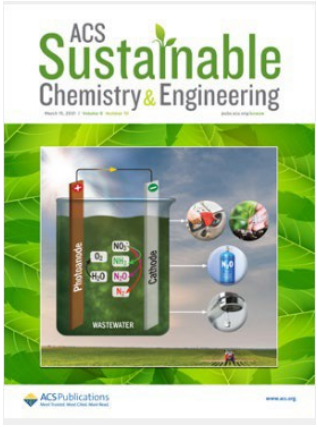


Authors: Javier Tovar-Facio, **Lidia S. Guerras**, José M. Ponce-Ortega, and Mariano Martín

DOI: doi.org/10.1021/acssuschemeng.0c08694